Ultrasound-triggered drug release from liposomes using nanoscale cavitation nuclei

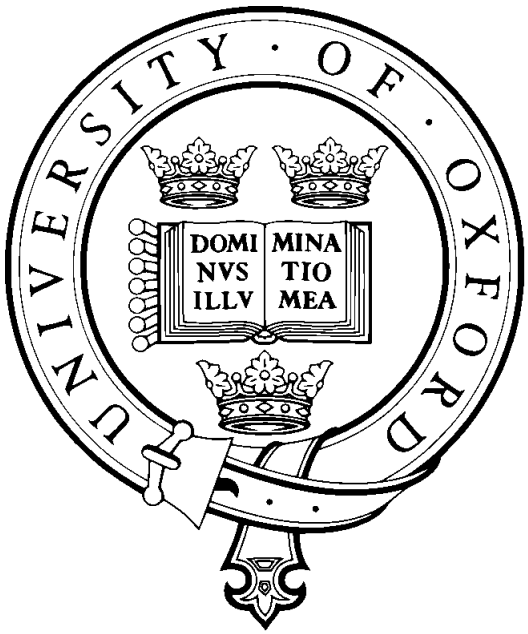

Susan M. Graham

Wolfson College

University of Oxford

Supervised by
Professor Constantin Coussios and Professor Robert Carlisle

Submitted: December 11, 2014

Submitted to the Department of Engineering Science, University of Oxford, in fulfilment of the requirements for the degree of Doctor of Philosophy

Declaration

I declare that this thesis is entirely my own work, and except where otherwise stated, describes my own research.

Susan M. Graham

Wolfson College

Dedication

This thesis is dedicated to the giants on whose shoulders I stand, and all the people who've supported me to keep me up there.

Abstract

Side effects of current chemotherapeutics limit their use in cancer therapy. Although many current drugs are highly toxic and potent, the effects they have on non-cancerous tissue are unbearable for patients. Targeting these drugs may provide a means to restrict their toxic effects to only cancer tissue while leaving healthy tissue unaffected. This approach requires that the drug is only available in cancer tissue, which has been achieved here by encapsulating drugs into liposomal nano-capsules which are capable of passively accumulating in cancerous tissue via the enhanced permeability and retention effect (EPR). In addition to localisation, a threshold dose must be achieved to deliver the desired toxic effect to the target tumour tissue. Previous strategies have relied on passive 'leaching' of the drug from liposomes, however this 'leaching' does not necessarily achieve the threshold dose required. In the present work, a new generation of liposomes has been developed whereby release is solely achieved in the presence of ultrasound triggered cavitation.

Instigation of such cavitation events would normally require the target tissue be exposed to high and possibly damaging ultrasound pressures. To remove the need for these high pressures, cavitation nuclei have been developed to lower the cavitation threshold of surrounding media. To allow for improved co-localisation and treatment deeper into cancer tissue, cavitation nuclei were developed to be in the nanoscale size range. Two types of novel cavitation nuclei were produced, a rough surfaced carbon nanoparticle (CNP, ∼180 nm) and smooth shaped polymeric nano-cup particle (NC, ∼150, 470, or 770 nm). Both types of particle are solid nanoparticles with gas entrapped on their surface which was capable of cavitating in response to ultrasound without greatly affecting the particle itself. These particles are classified as cavicatalytic nanoparticles due to their ability to reduce the cavitation threshold of their surrounding media without being destroyed themselves. Finally, an entirely nanoscale release system was developed and tested *in vitro* and *in vivo*. The drug carrier (the liposome) and effector agent (the cavicatalytic nanoparticle) were used to demonstrate ultrasound triggered drug release, specifically in response to the generation of cavitation events. These cavitation events could be non-invasively monitored and characterised, adding to the potential clinical utility of the technologies developed and described here.

Acknowledgements

I would like to acknowledge the significant support and guidance from my supervisors and my peers. In particular I would like to thank Prof. Constantin Coussios for initiating and overseeing this project and for his continued support; Prof. Eleanor Stride, Dr Jamie Collin, Dr James Kwan, and Dr Christian Coviello for imparting their wisdom; Dr Tracey King, Jim Fisk and David Salisbury for making things happen; Phil Jakeman, Richard Stebbing and Alex Clibbon for the tea breaks; Rachel Myers, my 'partner in crime', for her support; and Prof. Robert Carlisle for his guidance and mentorship.

I would also like to thank the support from my family and friends, with particular thanks to my husband, Matthew Ritchie, for his probing questions and unwavering encouragement and support.

My research was supported by the Clarendon Fund, RCUK (Digital Economy Programme grant number EP/G036861/1 Oxford Centre for Doctoral Training in Healthcare Innovation) and the Wellcome Trust & EPSRC under grant number WT088877/Z/09/Z.

Contents

List of Figures

List of Tables

Chapter 1

Introduction

1.1 Clinical perspective

Cancer Research UK estimates that more than one in three people will develop cancer during their lifetime [30]. Current oncological treatments have seen unacceptable levels of side effects from chemotherapy (for example doxorubicin [184]). To minimise side effects and maximise therapeutic benefit, oncological drug development is moving towards personalizing products and tests in terms of dosage, route of administration, and length of treatment for each patient [152]. Over 100 years ago Paul Ehrlich postulated that a magic bullet could be designed for any disease where the disease-causing organism (or target cells) could be identified [172]. The quest for this magic bullet still continues today, and the advances thus far are reviewed here.

Metastatic cancer poses a particular challenge for cancer therapy, as the 'target' for Paul Ehrlich's magic bullet is spread inside the patient. The high proportion of cancer patients presenting with metastatic disease and its high associated morbidity is why metastatic cancer remains one of the most important and intractable clinical challenges. Novel agents that are amenable to intravenous injection, have minimal side effects, and which are able to achieve specificity of accumulation in and action against all tumour deposits, have the potential to provide substantial therapeutic benefit.

1.2 Challenges in cancer drug delivery

The challenges in cancer drug delivery are posed both by the drugs which have been developed (dealt with in Section 1.2.1) as well as the tumour microenvironment which limits the use of these drugs (dealt with in Section 1.2.2). The drugs which have been developed for cancer therapy cover many drug classes, each with their own limitations. Many of the limitations faced are due to unacceptable levels of side effects on non-target, healthy tissues. These challenges are the driving motivation to develop a triggered, targeted drug release system to minimise side effects and limit drug action to only target tumour tissue which is discussed in the latter part of this Introduction.

1.2.1 Current oncological drug therapies and their limitations

Chemotherapeutics, such as anthracyclines, are used in many cancer therapies, relying on their high toxicity to kill cancer cells. As these drugs have such strong side effects, they are the main focus for this body of work. In addition to traditional chemotherapeutics however, novel oncological drugs are also being developed, such as antibodies, oncolytic viruses, siRNA and toxins, each with their own limitations, which might also benefit from a targeted, triggered release strategy for delivery to tumour tissue. Each of these drug types are discussed below.

1.2.1.1 Anthracyclines

Anthracyclines e.g. doxorubicin and daunorubicin, are some of the most common chemotherapeutic drugs used for cancer therapy [23]. Doxorubicin has been used for indications including: cancer of breast, ovary, prostate, stomach, and thyroid; small cell cancer of lung, and liver; squamous cell cancer of head and neck; multiple myeloma, Hodgkin's disease, and lymphomas. Daunorubicin has been used for acute myeloid leukemia and acute lymphocytic leukemia. Although these drugs have been successful in many cases, they also have a number of limitations [123].

One limiting factor effecting doxorubicin is that although highly effective in vitro, it often has poor local accumulation at a tumour site leading to limited efficacy in vivo. In addition

to poor drug localisation, chemotherapeutics are highly toxic with side effects including nausea, hair-loss and vomiting being the most distressing to the patient [48].

The reason these drugs have such severe side effects is that they are able to act on both healthy and tumour cells. These drugs act on replicating cells, taking advantage of the high replication rate of tumour cells. However some healthy tissues such as the stomach lining, and hair follicles also have high replication rates. These drugs intercalate with DNA and inhibit topoisomerase II enzyme from relaxing the supercoiling, a process which is necessary for replication of the DNA. This action ultimately halts replication thereby triggering the induction of apoptosis [132]. If these drugs could be targeted, healthy tissues might be spared from these toxic effects.

In addition to toxic side effects of these drugs, tumours are able build up a resistance to drugs such as doxorubicin. One method of drug resistance development is by increasing expression of drug transporters such as ATP-binding cassette (ABC) transporters leading to an increase in drug efflux from the cells [66]. Tumours are also able to acquire drug resistance through mutation or over expression of the drug target or inactivation of the drug [50]. Furthermore, as the mechanism of cell kill is ultimately apoptotic, a lack of efficacy may be linked to the mutation of the apoptosis pathways required. Each of these limitations discussed above has the potential to be addressed by employing a drug encapsulation and triggered release strategy.

1.2.1.2 Antibodies

The aberrant surface receptor expression profile of cancer cells provides the possibility of achieving selectivity by modifying therapeutics with ligands to target these receptors. A prime example is the utilisation of the highly selective binding of antibodies.

Trastuzumab (anti-ErbB2, Herceptin®) is an antibody targeted to the ErbB2 (HER2/neu) receptor which is over expressed on the surface of breast cancer cells [121] in up to up to 34% of breast cancers [151]. As the HER2 pathway promotes cell growth and division, antibody binding is able to reduce proliferation by interfering with cell signaling pathways [121], in addition to triggering antibody dependent cell-mediated cytotoxity and complement dependent cytotoxicity.

Another example is the programmed death 1 (PD-1) protein and one of its ligands, PD-L1, which play a critical role in tumour cells evading the immune system. Anti PD-L1 antibodies have been developed to target this pathway and have lead to durable tumour regression and prolonged disease stabilization in patients with metastatic non-small-cell lung cancer, melanoma, renal-cell cancer, and ovarian cancer. Adverse events during this trial were high for all severity levels considered (91%) but severe (grade 3), or life-threatening or disabling (grade 4) events were only seen in 9% of patients [26].

A limitation associated with therapeutic antibodies is that although they have long circulation half lives, due to their large size (approx. 70 kDa) avoiding clearance through kidney glomeruli, they also have low tumour penetration due to decreased diffusion with increasing molecular weight [35]. Antibody fragments have been developed to reduce the size of the molecule, for example Abciximab, a fragment antigen binding (Fab) fragment to address this issue. As a result of the reduced size, antibody fragments penetrate tumours much more rapidly and efficiently than full immunoglobulin G (IgG) antibodies, however they have a low serum half-life lowering the overall tumour uptake [35].

1.2.1.3 Viruses

Viruses have been used in cancer therapy to preferentially infect and replicate in tumour cells [142]. OncoVEX is an oncolytic herpes simplex virus expressing granulocyte macrophage colony-stimulating factor (GM-CSF). The virus infects and kills tumour cells, as well as secreting GM-CSF which recruits and activates dendritic cells to boost the anti-tumour immune response [165]. OncoVEX is currently in stage III clinical trials for melanoma tumours [106].

Both the innate and adaptive immune system have developed a defense against viruses capable of clearing the virus, and in this case, the therapeutic, from the body. Adenoviruses, including the 'common cold', are particularly affected, as most patients will have antibodies to the viral therapy based on previous exposure to the same virus type. This immune response limits the spread and restricts the replication of the oncolytic viruses thus ultimately limiting efficacy [142].

1.2.1.4 siRNA

Small interfering RNA (siRNA) are short double stranded oligonucleotides that are able to bind to messenger RNA (mRNA) preventing the translation of a target protein. The use of siRNA to target drug efflux transporters has shown promise both in vitro and in vivo [3]. The limitations to siRNA therapy however are that it is cleared from the body quickly, before it is able to act, and that the delivery rates are low [141].

1.2.1.5 Toxins

Bacterial vaccines, such as "Coley's toxins", a combination of Gram positive, heat-killed streptococcus plus Gram negative, heat-killed S. *marcescens*, have been shown to boost the immune system in some patients leading to inhibition of tumour growth and in some cases remission. These toxins however are only appropriate for approximately 10% of cancer patients, and even then have severe side effects of fever and chills [170]. In addition to the limitations specific to each drug class, the tumour microenvironment poses additional challenges, further limiting the efficacy of these drugs.

1.2.2 Adverse tumour microenvironment

Several aspects of the tumour environment hamper drug delivery: increased intratumoral pressure; dense disorganised extracellular matrix; decreased drainage into lymphatics; and leaky or absent vasculature. The intratumoral pressure is often higher than in normal tissue [178], which has been linked with poor drug penetration [88]. One of the features of tumours that contributes to the high intratumoral pressure [178] is the lack of functional lymphatics [118]. The combined impact of high interstitial pressure and aberrant lymphatics removes convective flow across the tumour, making the movement of drug an entirely diffusive process reliant on the drug concentration gradient [137,178]. Tumour neovascularisation, the process of forming new blood vessels, is thought to occur simply when there is a nutrient and oxygen demand in larger tumours that cannot rely on diffusion of nutrients alone to supply the whole tumour [22]. Tumours smaller than 2 mm in diameter are in an avascular phase where diffusion alone is sufficient to support the dormant state of the tumour [22]. Upon further growth, a vascular stage is necessary to support the rapid cell proliferation, which is known

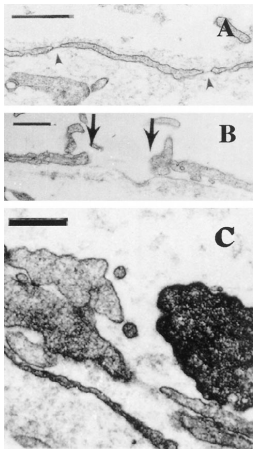

Figure 1.1: *Representative electron micrographs of MCa IV (murine mammary carcinoma) tumour vessels grown in the dorsal chamber. (A) Venular-sized vessel with fenestrated endothelium (arrowheads). (Bar = 500 nm.) (B) Tumour vessel with an open gap measuring 856 nm delineated by the arrows. (Bar = 500 nm.) (C) Open endothelial gap in tumour blood vessel from a long-circulating liposome-injected animal. What appear to be long circulating liposomes are shown traversing through the open junction. Serial sections (not shown) demonstrate that these are not transverse sections of cellular projections. (Bar = 300 nm.) Image taken from [90] (Hobbs et al. 1998).*

as the angiogenic switch. Rapid vessel growth leads to an often leaky and haemorrhagic vasculature. This irregular vasculature in turn can lead to slow and even oscillating blood flows, resulting in dysfunctional capillaries [22]. All of these features of the tumour microenvironment have the potential to impede the delivery of drugs.

1.3 Overcoming drug delivery challenges for cancer

1.3.1 Enhanced permeability and retention effect

Nanotechnology has been proposed as a method for encapsulating and targeting drugs to tumour sites before the drug is released. In cancer therapy, enhanced permeability and retention (EPR) is an effect whereby nanoparticles in the 100 nm to 780 nm size range [90] passively accumulate in tumours due to the uniquely disregulated and permeable nature of the vasculature that supports solid tumours (Figure 1.1). These vessels have poor pericyte coverage and inter-endothelial cell gaps of up to 800 nm, compared to 5-10 nm for most healthy tissue. Provided that extended blood circulation is able to be achieved, selective extravasation of nanoparticles into tumours is also able to be accomplished [124]. Using particles smaller than 1 μm has shown to increase the efficiency of intracellular uptake upon reaching a tumour site. Desai et al. [55] found that, *in vitro*, particles with a diameter of 100 nm had a 2.5-fold greater uptake than 1 μm particles, and 6-fold greater than the 10 μm particles. Desai et al. [54] also showed similar results *in vivo* with uptake of 100 nm particles being 6.7×10^3 fold higher than 1 μm particles in Peyer's patches in the rat intestine. By encapsulating or incorporating drugs into a nano-sized particle, the EPR effect

and the increased cellular uptake may be utilised to increase drug dosing at specific sites.

1.3.2 Overcoming drug limitations

To improve the efficacy of existing drugs, and to allow drugs which are currently too toxic, or are cleared too quickly from the body, to be therapeutically useful the following issues need to be addressed: increasing drug concentration in tumour, without increasing drug concentrations in other organs; reducing action in non-target sites to reduce side effects; using active release strategy when at the target site, overcoming the problem of stability of drug carriers in circulation as opposed to at the target site; and monitoring of drug release, to ensure lack of treatment efficacy is due to the drug not acting, rather than the drug not being available.

1.4 Drug delivery vehicles

1.4.1 Defining 'nano-' particle

It has been observed that drugs in nano-particulate form are able to achieve better accumulation and increased selectivity of anti-tumour activity than free drug [16, 138, 181]. This observation is based on the exploitation of the EPR effect mentioned above. Yet the term 'nanotechnology' still has no universally accepted definition [61]. 'Nano' refers to varying size ranges depending on the context from sub 100 nm in physics, which is now the recommended definition given by the European Commission [147], to up to 1000 nm in biology, which is consistent with the U.S. Food and Drug Administration's (FDA) scope for nano [70]. Taking advantage of the EPR effect, many particles for nano-medical applications are being designed as smaller than 300 nm (Figure 1.2) and so some people consider 300 nm a more relevant size limit. In the context of this thesis, 'nanoparticles' will be used to refer to particles with a diameter less than 1000 nm.

In addition to the added benefits of using nanoparticles as compared with free drugs, new toxicity issues are also introduced. Nanoparticles have potential for toxicity specific to their size, shape and charge, and may be able to penetrate into tissues, such as past the blood brain barrier or through the skin [43]. When deciding what should be classified as a

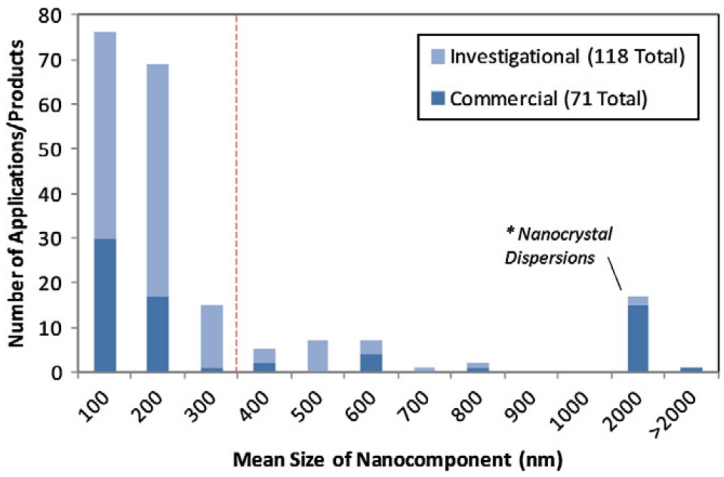

Figure 1.2: *Mean size of nanocomponents for all nanomedicine applications and products for which data were available. The dotted line indicates the cut-off for this study's definition of nanomedicine, below which a significant number of the products fall. The notable peak around 2000 nm consists of a number of 'nanocrystal dispersion' products. Image taken from [61] (Etheridge et al. 2013).*

Nanocomponent	Investigational			Commercial		
	Therapeutic	Device	Total	Therapeutic	Device	Total
Hard NP	3	12	15	0	28	28
Nanodispersion	5	0	5	1	1	2
Polymeric NP	23	0	23	9	0	9
Protein NP	4	0	4	2	0	2
Liposome	53	0	53	7	1	8
Emulsion	18	1	19	9	0	9
Micelle	8	0	8	3	1	4
Dendrimer / Fleximer	2	2	4	0	3	3
Virosome	6	0	6	2	0	2
Nanocomposite	0	0	0	0	18	18
NP Coating	0	2	2	0	6	6
Nanoporous Material	0	3	3	0	2	2
Nanopatterned	0	2	2	0	2	2
Quantum Dot	0	1	1	0	4	4
Fullerene	0	1	1	0	0	0
Hydrogel	0	0	0	0	1	1
Carbon Nanotube	0	1	1	0	0	0
Totals	122	25	147	33	67	100

Figure 1.3: *Type of nanostructure for confirmed and likely nanomedicine applications and products, by developmental status. Image taken from [61] (Etheridge et al. 2013).*

'nanoparticle' for regulatory purposes in medicine, both the advantageous features as well as the disadvantageous features of nanoparticles must be considered.

1.4.2 Drug delivery vehicle types

The majority of nanoparticles both under investigation and in commercial use are either 'soft' nanoparticles e.g. liposomes, or 'hard' nanoparticles e.g. polymeric or metallic in nature (Figure 1.3 [61]). Classification of particles into 'soft' and 'hard' is able to help in the assessment of toxicity and manufacturing considerations.

Liposomes are spherical structures formed by one or several concentric lipid bilayers

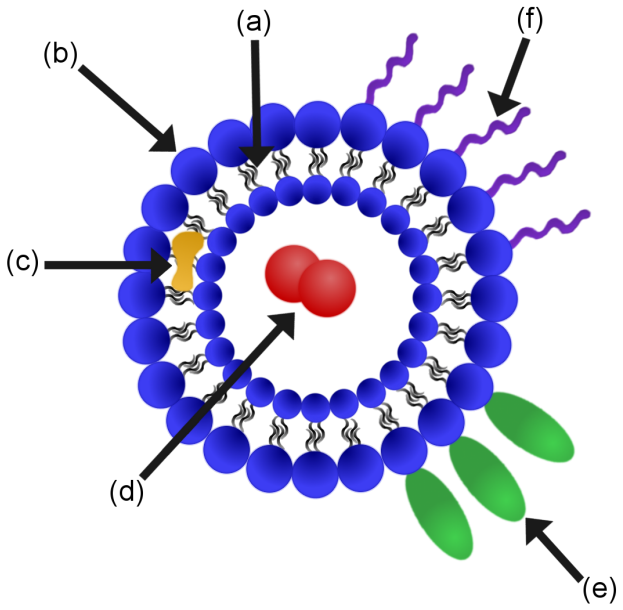

Figure 1.4: *A schematic diagram of a liposome showing a lipid bilayer comprised of phospholipids made up of a (a) hydrophobic tail and (b) hydrophilic head. Liposomes have been developed as potential drug carriers for (c) hydrophobic drugs or (d) hydrophilic drugs transported in the bilayer or in the aqueous core respectively. (e) Targeting ligands and (f) 'stealth' polymers such as polyethylene glycol (PEG) are able to be attached to the outer surface of the liposome. Note inside lipid head groups are represented as smaller for diagrammatic simplicity and PEG is only shown on the outside whereas experimentally it would be present on the inside as well.*

with inner aqueous phases. Liposomes have the ability to entrap both hydrophilic and hydrophobic drugs in the aqueous phase or in the lipid bilayer respectively, and be modified with targeting agents on the surface. In addition, a common modification to liposomes is to incorporate polyethylene glycol (PEG) in the surface to improve circulation time by stabilising and protecting liposomes from opsonization [143]. These features are shown diagrammatically in Figure 1.4.

Liposomes, with their proven non-toxic, biocompatible, biodegradable and non-immunogenic properties, have the potential to encapsulate drugs to protect the payload from degradation, and minimize unwanted drug toxicity [143]. Liposomes are further able to be functionalised with targeting ligands, or with gas, similar to a microbubble. Furthermore, by altering the composition of the lipid shell, liposomes may be tailored to be responsive to external stimuli such as heat, pH or ultrasound.

To improve local accumulation in vivo, and address the issues discussed in Section 1.2.1, a liposomal form of doxorubicin has been prepared under the name Doxil, approved by the FDA in 1995, and registered as Caelyx in Europe. *In vitro* and *in vivo* studies suggest however that even though there is increased localisation of the Doxil liposomes, only 0.4 % of the doxorubicin translocated to the nucleus, compared with 26 % when added as free drug [161]. Nonetheless, Vaage et al. [181] showed that in a murine model the mean tumour volume decreased significantly with the use of Doxil compared to free doxorubicin or a saline

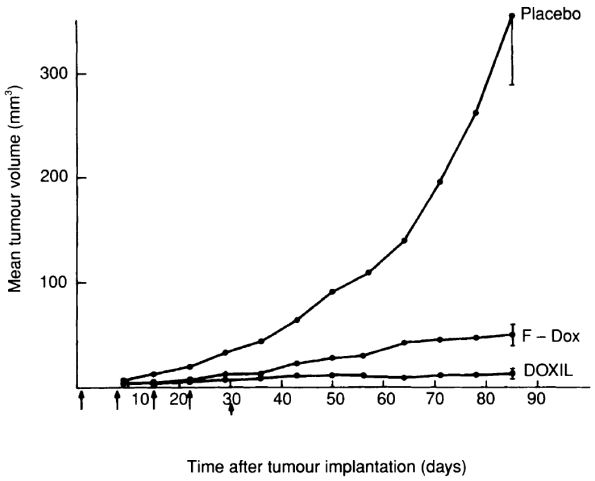

Figure 1.5: *The effects of treatments with saline (placebo), free doxorubicin in saline (F-Dox) and doxorubicin in polyethylene glycol-coated liposomes (DOXIL), on the growth of s.c. implants of tumour AsPC-1. Arrows indicate the time points of treatment. Each mouse carried two tumour pieces implanted s.c. in the right and left posterior flanks on day 0. The values are the mean volumes of all tumours in each group of ten mice. Image taken from [181] (Vaage et al. 1997).*

placebo (Figure 1.5).

Another common chemotherapeutic which has been made into particle form is Abraxane (paclitaxel protein-bound particles) and was approved by the FDA in 2005 [71]. Doxil and Abraxane, with sizes of 90 and 130 nm respectively, have been shown to have significant antitumoural activity in highly vascularised tumours such as Kaposi's sarcoma [139] and breast cancer [78]. However, when Doxil was tested in hypovascular and hypopermeable tumours, it showed limited penetration and accumulation [180] demonstrating that efficacy may suffer as a result of reduced EPR assisted accumulation.

Cabral *et al.* showed that a potent tumoricidal agent (1,2-diaminocyclohexane-platinum (II)) could be loaded into varying sized micelles and allowed to accumulate in tumours. Complete suppression of tumour growth in tumours with low permeability (subcutaneous hypopermeable human pancreatic adenocarcinoma BxPC3 in mice) was achieved using 30 nm DACHPt-loaded micelles. However as the size increased to 100 nm, there was no antitumour effect seen [29]. This accumulation was in comparison to the more permeable tumours (hyperpermeable murine colon adenocarcinoma (C26)) where the micelles from 30-100 nm all showed similar levels of accumulation [29]. This study shows how particle size can be tailored to suit different tumour targets and further direct nanoparticles to minimize side effects.

In addition to drug targeting, nanoparticle formulations have been developed to circumvent (e.g. bypassing the efflux pumps) or overcome (e.g. increasing accumulation) multiple drug resistance (MDR) which was discussed briefly in Section 1.2.1. Liposomes, polymeric

nanoparticles, polymeric micelles, polymer conjugates, solid lipid, magnetic, gold, and silica nanoparticles, and carbon nanotubes have all shown positive results in overcoming anthracycline MDR [123]. Although these particle formulations have been developed to reduce side effects and increase efficacy, they also introduce new health concerns which are discussed below.

1.4.3 Pharmacokinetics and toxicity

It has been demonstrated that particles on the nanoscale have several desired attributes, however they also have the potential to cause toxicity and trigger immune responses, resulting in clearance from the body and potential tissue damage. One important aspect of toxicity for solid nanoparticles is the protein adsorption that occurs after injection into the body, called the protein corona [33]. The protein corona alters the pharmacokinetics and biodistribution of the particle. Uptake by the mononuclear phagocyte system (MPS), also known as the reticuloendothelial system (RES), (consisting of dendritic cells, blood monocytes, and tissue resident macrophages in the liver, spleen and lymph nodes) following intravenous injection can limit the biodistribution and pharmacokinetics of nanoparticles [133]. Due to the importance of this clearnace pathway, assays have been developed in order to characterise protein adsorption to nanoparticles as an indicator of pharmacokinetics before in vivo testing [186].

Poly(ethylene glycol) (PEG) is widely used for surface modification to improve stability and circulation. PEG polymers have been approved by the FDA and have low toxicity and no immunogenicity [2]. PEG has been shown to decrease uptake of nanoparticles by monocytes and significantly increase the half-life of particles *in vivo*. These affects are attributed to the steric hindrance and the hydrophilicity of the surface [21]. The half life of pegylated liposomes is up to 24 hours in rodents and up to 45 hours in humans, however particles are eventually cleared by the macrophages of the RES after eventual displacement of polymers by plasma proteins [133].

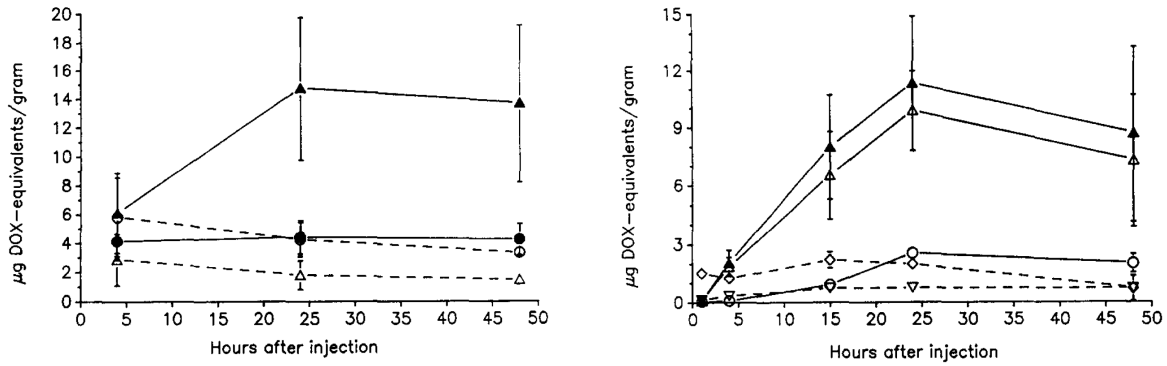

(a) *Solid lymphoma* **(b)** *Ascitic lymphoma*

Figure 1.6: *Uptake of liposomal doxorubicin by solid and ascitic mouse J6456 lymphoma. Doxorubicin (DOX) was encapsulated in HPI-HPC-Chol liposomes and injected intravenous into tumour-bearing BALB/c mice. (A) Mice bearing intramuscular implants of the J6456 lymphoma received free or liposomal DOX, 10mg/kg. black triangle = tumour after liposomal DOX; • = tumour after free DOX; △ = muscle after liposomal DOX; ∘ = muscle after free DOX. (B) Mice inoculated with ascitic J6456 lymphoma received free or liposomal DOX, 10mg/kg. Solid lines, drug levels in ascites after liposomal DOX (black triangle = total amount of drug in ascitic fluid; △ = liposome-associated drug in ascitic fluid; ∘ = drug associated to ascitic cells). Broken lines, drug levels in ascites after free DOX (▽ = drug in ascitic fluid; ♢ = drug associated to ascitic cells). Image taken from [73] (Gabizon 1995)*

1.5 Particle targeting

Particle targeting is traditionally thought of as passive targeting, where the drug accumulates due to non-specific diffusive processes, or active targeting, where there is some specific accumulation or binding mechanism involved.

1.5.1 Passive targeting

As mentioned in Section 1.4, the EPR effect may be utilised to allow selective passive accumulation of drugs at a tumour site. By simply using a particle compared to free drug, decreased tumour volume is able to be observed (Figure 1.5). A study of the circulation time and accumulation in murine tumours, showed that 24 -48 hours was required for maximum accumulation of liposomes in tumour tissue (Figure 1.6), findings similar to those of Laginha et al. [114]. Even at that time however, a majority of the drug was associated with liposome, not as free drug in ascitic fluid [73] (Figure 1.6 (b)). This compromise of stability in circulation to minimize side effects, and instability at the target site to allow for the drug to act is one that has not yet been adequately addressed.

Although the discovery of the EPR effect is significant, and has lead to an improvement

in therapy, it must be noted that the EPR effect only increased drug accumulation to 2% of the injected dose[1], and of that, a majority of the dose is still encapsulated. This limitation of dose being present in tumour tissue but not available to act could be overcome by a triggered release strategy as discussed in Section 1.6.

1.5.2 Active targeting

Antibodies specific to a tumour, as mentioned in section 1.2.1.2, are able to be used as a therapeutic molecule by themselves. To enhance antibody efficacy further, these targeting molecules have also been combined with drugs and drug carriers.

Marloes Kamphuis et al. [103] showed the highly specific targeting of layer-by-layer particles coated in monoclonal antibodies using click chemistry *in vitro*. Particles were targeted to a colorectal cell line (LIM2405) with and without expression of human A33 antigen, an antigen present in over 95% of human colon cancers [87]. These results were collected using fluorescence microscopy and flow cytometry. Highly specific targeting was achieved when antigen positive cells were present at less than 0.1% of the total cell population.

Although these *in vitro* studies have shown good targeting, the future of targeted therapy *in vivo* may be more complex than first presumed. Kirpotin et al. [108] showed that lipidic nanoparticles targeted to tumours using antibodies (anti-ErbB2) did not increase tumour localization compared to a control (Figure 1.7) but did increase internalization (Figure 1.7 inset) when tested *in vivo*. Indeed Bae [15] believes that active targeting cannot be separated from passive targeting as passive accumulation via the EPR effect is required before drugs 'stumble on' their target cancer cells in a probabilistic fashion and have the opportunity to bind in a selective manner.

Instead of using a one-step approach such as antibodies, von Maltzahn et al. [183] used a two-step targeting approach by utilizing the inflammatory pathways that exists in the body. The first nanoparticle (NP) when hit with electromagnetic radiation heated the local environment to disrupt tumour vessels and cause coagulation. The second nanoparticle had a peptide coating to recognise fibrin which acts as a substrate for the coagulation

[1]Calculation of EPR accumulation was based on data shown by Kirpotin et al. [108] using assumed values for tumour density of 1.05 g/ml and mouse weight of 25g

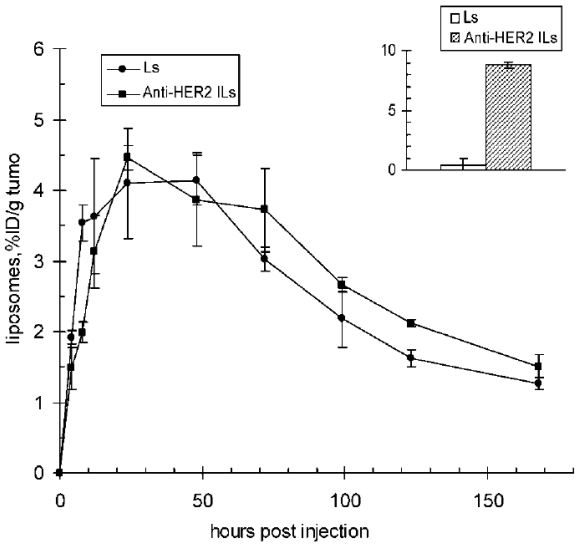

Figure 1.7: *Tumour pharmacokinetics of* ^{67}*Ga-labeled anti-HER2 immunoliposomes (Fab' targeted) versus control pegylated liposomes (Ls) in s.c. BT-474 breast cancer xenografts in nude mice. Liposomes/immunoliposomes were administered i.v. at 40 Amol phospholipid/kg. Points, mean; bars, FSD; three animals per group. Inset, uptake of anti-HER2 immunoliposomes (cross-hatched column) versus control liposomes (solid column) in HER2-overexpressing breast cancer cells (SK-Br-3)* in vitro. *Uptake units, nmol liposome phospholipid/106 cells (mean F SD; n = 4 experiments). Image taken from [108] (Kirpotin et al., 2006).*

transglutaminase factor XIII, used in the coagulation pathway. Using doxorubicin in the second nanoparticle (FX-III-liposome), von Maltzahn et al. found that the accumulation of doxorubicin in tumours was amplified by over 40-fold compared with liposomes (LP) alone and that this was an effective method in significantly restricting tumour growth *in vivo*. The first NP injected alone also reduced the tumour volume compared with liposomes alone due to the heat from irradiation, however not to the same extent as the dual particle system. This type of active targeting is straying from Bae's view of requiring probabilistic interactions and is coming closer to Enrich's magic bullet.

While limitations in the extravasation into, and penetration through, tumours may ultimately prevent a targeted particle reaching its cancer cell target, the tumour endothelium presents an attractive alternative target. A process during inflammation that is able to be mimicked is the natural rolling and accumulation of white blood cells in inflamed tissue. Carlisle et al. [31] have demonstrated that liposomes are able to be formulated such that they are monodisperse (polydispersity index (PDI) < 0.1) and in the size range to minimise hepatic capture (around 150 nm). Carlisle et al. modified the surface of the liposomes with a P-selecting glycoprotein ligand 1 (PSGL-1) to slow the flow of liposomes near tumour associated endothelium, in a similar way to leukocytes in blood vessels of inflamed tissue. The results showed that although there was no significant change in clearance or accumulation in the liver, spleen or lungs, there was a substantial (5-fold increase) and significant increase in the % injected dose in the tumour compared with non-modified control liposomes.

The successful active targeting and subsequent accumulation achieved using this method of functionalisation illustrates the potential of liposomes to enhance drug efficacy without modifying the drug itself.

1.6 Trigger mechanisms for release

It is notable that although passive EPR and in some cases active ligand-mediated targeting is able to greatly enhance accumulation of drug carrier in tumours, there is often little correlation to the level of ultimate therapeutic benefit observed. It is evident that carrier systems developed to be stable in the bloodstream are often too stable to give efficient release of payload upon reaching the target site [114, 175]. However this limitation also represents an opportunity to add further tumour selectivity to these agents by the incorporation of triggered release mechanisms that are responsive to the unique tumour environment or externally applied targeted stimuli.

Specific tumour conditions such as altered pH or enzyme levels [162] have been proposed as internal trigger mechanisms. A differential feature of the tumour extracellular environment is that it has a lower pH than normal tissues [46, 75]. The intracellular (alkalii) and extracellular (acidic) tumour pH values were reviewed by Gillies et al. [76] indicating an extracellular pH range of 6.4 to 7.3 (untreated human tumours). When normal tissue and cancerous tissue were compared within patients, with a range of cancer types, the tumour tissue always had an equal or lower extracellular pH than the normal tissue [75]. The pH differential between normal and cancerous tissue has been exploited as an endogenous active technique to release a drug at the target tumour site [16, 107, 146]. Poon et al. [146] designed layer-by-layer particles on quantum dots with a pH-sheddable layer to target the hypoxic tumour environment. *In vitro* studies showed that a sheddable PEG layer could be constructed using neutravidin iminobiotin which is susceptible to pH changes. Significant uptake was shown *in vivo*, however no data was provided to prove polymer shedding *in vivo*.

To increase control of the trigger, especially in cases where endogenous triggers are not present due to tumour variability, external triggers have been proposed. External energy sources such as radio frequency [144], heat [74, 134], lasers in conjunction with activated

nanoparticles [34], oscillating magnetic fields [127], or ultraviolet irradiation [159] have been suggested as possible strategies to release drug payloads and/or enhance uptake in a targeted manner. In contrast to these other modalities listed, ultrasound has the potential to treat [42, 94, 171], image and monitor tumours in real-time non-invasively, deep into the body, all using the one modality. Ultrasound will therefore be reviewed here in more detail.

1.7 Ultrasound in medicine

Ultrasound has been used routinely as an imaging modality for diagnosis and foetal imaging for decades, and more recently is showing promise in many therapeutic applications. Cavitation, the expansion and contraction of a bubble, is a phenomenon implicated in the observation of many ultrasound induced bioeffects. Ultrasound-triggered cavitation can be used to achieve therapeutic outcomes either alone, or in combination with drug therapies. Phenomena such as: heating following inertial bubble collapse [91]; sonoporation (transient cell membrane disruption) [156, 157, 169]; and enhanced extravasation of drugs [6, 19] due to microstreaming around cavitating bubbles acting as a nano-pump [82]; have all been observed as bioeffects involving cavitation.

To further improve cavitation-driven therapy, cavitation nuclei have been developed that allow the use of lower ultrasound pressures to avoid unnecessary side effects. One benefit of cavitation events for therapy is that cavitation is able to be monitored from outside the body. 'Sound signatures' of cavitation events may be monitored to better understand the bio-effects which take place. These sound signatures might therefore be used to monitor therapy in real time. For these reasons, ultrasound is of particular interest for drug release and delivery applications. Ultrasound alone, and cavitation events which are able to be instigated by ultrasound, have both thermal and mechanical effects which are able to be utilised for therapy in the body. The dominant mechanical effect in therapeutic applications is acoustic cavitation, and is discussed in greater detail below.

1.7.1 Cavitation dynamics

1.7.1.1 Classification of cavitation

One of the key features of ultrasound when used therapeutically is that it is able to cause cavitation of gas bubbles. Cavitation is the process whereby a small gas inclusion in a liquid will expand and contract with the negative and positive pressure cycles of the ultrasound. Cavitation may broadly be categorized into two groups: 'stable' and 'inertial'.

> **Stable cavitation** describes bubbles undergoing regular cyclic oscillations [189]. These oscillations, as is suggested by the name, are typically long lived, non-linear, and occur at lower pressure amplitudes.

> **Inertial cavitation** describes bubbles undergoing unstable expansion during the rarefactional half-cycle, before collapsing violently during the compressional half-cycle, typically instigated by higher pressure amplitudes than required for stable cavitation [189]. The term *inertial cavitation* is used to describe how the bubble collapse is dominated by the inertia of the surrounding liquid.

It is important to note that these terms 'stable cavitation' and 'inertial cavitation' are used to describe the extreme cases for simplicity of communication. In reality, the phenomena that exist span between these two definitions and in some cases would fit into both classes, or neither [117].

The type of cavitation, and whether it occurs or not, is determined by both the cavitation nuclei present and the ultrasound driving wave.

1.7.1.2 Cavitation thresholds

Some of the key factors which affect inertial cavitation have been outlined by Church: initial bubble size and content; acoustic frequency and pressure amplitude; the properties of the surrounding fluid; acoustic phase; and the nature of gas diffusion in the bubble [39], with some of these discussed below.

The theoretical inertial cavitation threshold has been broadly defined as satisfying one of these three criteria [117]:

- **Radius expansion threshold:** when R_{max} / R_o = 2; where R_{max} is the maximum radial expansion and R_o is the initial radius (Flynn, 1975 [67] and Church, 2005 [40]).

- **Collapse temperature threshold:** when the bubble attained a temperature of 5000 K during the adiabatic compression of the bubble below its initial radius (Apfel and Holland, 1991 [4]; Flynn, 1975 [67]).

- **Bubble wall velocity threshold:** when the maximum bubble wall velocity is greater than the speed of sound in air, approximately set to 330 m/sec (Church, 2002 [39]).

In addition to inertial cavitation thresholds, stable cavitation alone has the potential to promote beneficial bioeffects. Bader and Holland used bubble modelling to describe the stable cavitation threshold using a subharmonic threshold of -20 dB that of the fundamental spectral amplitude [14]. Here they propose a cavitation index (I_{CAV}) which is equal to the peak rarefaction pressure divided by the frequency. This index can then be used to estimate ultrasound contrast agent rupture, which increases for $I_{CAV} > 0.02$, or subharmonic emissions from stable cavitation, which increases for $I_{CAV} > 0.09$ [14].

Bubbles have been modelled in a sound field by many researchers, and have included varying assumptions and considered different variables. One of the most significant of these is the Rayleigh-Plesset equation (Equation 1.1) [187], which describes a single model undergoing radial oscillations in a sound field, where R = initial radius, $\dot{R}$ = radial velocity, $\ddot{R}$ = radial acceleration, ρ = density of the liquid, p_o = hydrostatic pressure, σ = surface tension of the liquid, R_o = bubble radius at equilibrium, p_v = liquid vapour pressure, κ = polytropic index of the gas, η = coefficient of viscosity of the liquid, p(t) = liquid pressure at t>0.

$$R\ddot{R} + \frac{3\dot{R}^2}{2} = \frac{1}{\rho}\{(p_o + \frac{2\sigma}{R_o} - p_v)(\frac{R_o}{R})^{3\kappa} + p_v - \frac{2\sigma}{R} - \frac{4\eta\dot{R}}{R} - p_o - p(t)\} \qquad (1.1)$$

Apfel and Holland showed the correlation between bubble size and frequency and their effect on inertial cavitation thresholds, for a single-pulse propagating through pure water assuming that all nuclei sizes exist *a priori* (Figure 1.8). The relationship shows that with decreasing driving ultrasound frequency, the cavitation threshold also decreases. This relationship is stronger for bubbles greater than 500 nm in diameter, which is particularly

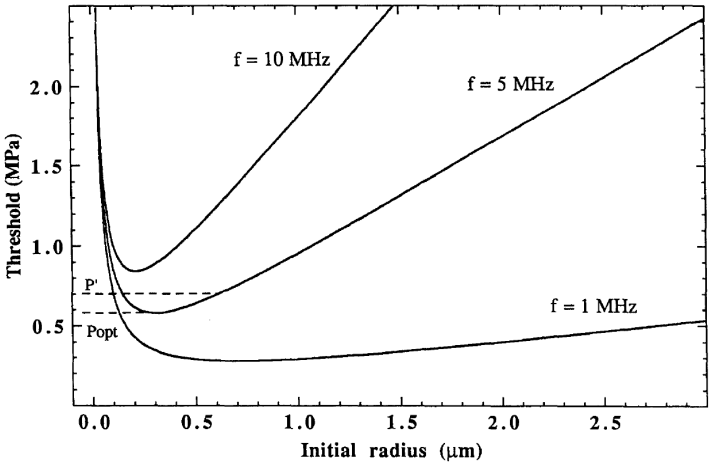

Figure 1.8: *Cavitation threshold of a single bubble in water as a function of initial nucleus radius for three frequencies of insonification 1, 5, and 10 MHz. Image taken from [4] (Apfel and Holland 1991).*

important for therapeutic ultrasound as most exogenous cavitation nuclei being developed also have a diameter greater than 500 nm.

There is a minimum bubble size, the Blake critical radius, which will exist in stable equilibrium unless the pressure is increased above a given threshold known as the Blake threshold pressure. At a given pressure, above the critical radius, R_C, bubbles will become unstable, grow explosively and cavitate; below that radius, bubbles will not [27]. Figure 1.9 shows the initial radius, R_S, and corresponding threshold, where the smaller the initial bubble, the greater the pressure required to cause cavitation, increasing with decreasing bubble size [7]. As the bubble radius decreases, the Laplace Pressure ($\frac{2\sigma}{R}$, the pressure difference between the inside and outside of the bubble, where σ = surface tension and R = radius) increases, increasing the pressure required to cause cavitation. This effect is also not greatly affected by frequency (Figure 3 in [68]). From Figure 1.9, the Blake threshold for a 100 nm-diameter bubble is just over 1 MPa (10 bar). As such, the limiting factor to instigating cavitation at the nanoscale is not the pressure threshold, but rather the stability of the bubble as discussed above is Section 1.7.2.

Although the initial bubble size is important, bubbles can grow with each ultrasound negative pressure peak (rarefaction), through a process known as rectified diffusion [89], until they reach a size which responds more to the ultrasound frequency being used. When combining rectified diffusion with a decrease in cavitation threshold at decreasing frequencies, endogenous cavitation nuclei in the body which may be small, are still able to respond to low pressure, low frequency ultrasound (e.g. 20 kHz). This issue is usually not realised clinically as ultrasound imaging probes use frequencies above 1 MHz to improve resolution

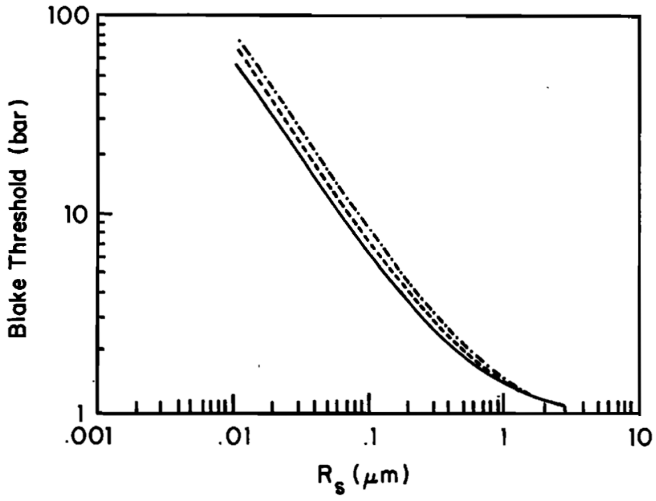

Figure 1.9: *Graph of the Blake threshold versus initial bubble radius R_s for the three cases examined. The solid line represents the constant surface tension case; the dashed line corresponds to $\alpha = 3$ (charged surfactant); the dash-dot line corresponds to $\alpha = 4$ (polar surfactant). Image taken from [7] (Atchley 1989).*

whilst retaining an acceptable attenuation.

1.7.2 Nucleation of cavitation

Nucleation (formation of a detectable cavity) rarely occurs (if at all) in homogeneous liquids [8]. To explain the results of experimental observations of cavitation in liquid and tissue, inhomogeneities in the liquid, on which nucleation is able to occur, must exist. It has been postulated that these cavitation nuclei have come in the form of inhomogeneities in liquid such as free bubbles, dirt particles, clusters of organic or ionic molecules, or due to cosmic rays or other radiation [8]. These inhomogeneities can be *endogenous* in a tissue or liquid or can be introduced artificially as *exogenous* nuclei.

Exogenous nuclei are necessary for medical applications to reduce the required ultrasound intensity to trigger cavitation. At high intensities, undesired side effects, pre-focally, such as skin burns may arise [131]. By introducing exogenous cavitation nuclei however, the input ultrasound intensity may be reduced while still achieving the same desired bio-effect at the target site. Of the various cavitation nuclei available, two main types of cavitation nuclei were considered in this thesis: shelled microbubbles; and solid particles.

1.7.2.1 Microbubbles as cavitation nuclei

Microbubbles have been used as ultrasound contrast agents (UCAs) in order to improve the quality of B-mode and Doppler ultrasound. As these microbubbles have been certified for clinical use, they are now being exploited for therapeutic applications as cavitation nuclei.

One commonly used microbubble is SonoVue® (SV). SV comprises a phospholipid monolayer shell encapsulating sulphur hexafluoride gas. The phospholipid shell gives SV its stability for *in vivo* applications. Several investigators have previously used this ultrasound contrast agent as a cavitation nucleation agent [6]. However, in the context of cavitation in tumours, SV microbubbles have been reported to be destroyed within 10 seconds following administration, requiring frequent re-injection [20]. Such frequent re-injection may not be possible in humans without exceeding the maximum tolerated dose.

Microbubbles have the advantage of clinical acceptance, however, for therapeutic applications, cavitation nuclei which are on the nanoscale might provide added benefit. Nanobubbles are not stable free in pure media and are predicted to diffuse within ~ 1 μsec [160] without lipid or surface stabilization. Adherence on a particle surface however might enable nanobubbles to be delivered in a stable form and to detach and cavitate when triggered by ultrasound.

1.7.2.2 Solid particle cavitation nuclei

Hydrophobic solid particles acting as cavitation nuclei are able to be explained by the crevice model [8]. This model assumes a small pocket of gas is able to be stabilized at the bottom of cracks or crevices found on hydrophobic solids dispersed in a liquid [8]. In this way, no initial bubble is required to be stabilised, but rather a bubble is able to grow out of the small pocket of gas.

These particles may be on any size scale as long as they are able to trap an amount of gas on the surface which can detach in response to ultrasound and cavitate, however of particular interest is entrapment on the nanoscale. Two methods for production of such particles are outlined in Section 2.1.

1.7.3 Safety of ultrasound

1.7.3.1 Diagnostic safety limits

Ultrasound has been used routinely as an imaging modality for diagnosis and foetal imaging. According to the FDA there are no known side effects of ultrasound imaging. There are however known biological effects of ultrasound which are being harnessed for treatment

methods such as High Intensity Focused Ultrasound (HIFU). These effects alone have the capability of killing cancer cells and healthy cells alike. Due to the potential risks, the British Medical Ultrasound Society (BMUS) have outlined the safety issues associated with the use of ultrasound in medicine, but have also noted that diagnostic ultrasound has caused no harm to patients in the four decades of its use [167].

The safety of ultrasound has been well established in imaging and the field has developed indices to restrict the use of ultrasound to a safe regime. The Thermal Index (TI) (equation 1.3) and Mechanical Index (MI) (equation 1.2) are used to help describe the potential for damage based on the thermal and mechanical effects of ultrasound [69]. The MI is defined by the FDA as: The spatial-peak value of the peak rarefactional pressure, derated by 0.3 dB/cm-MHz at each point along the beam axis, divided by the square root of the center frequency, that is:

$$MI = \frac{P_{r.3}(z_{sp})}{\sqrt{f_c}} \tag{1.2}$$

where $P_{r.3}(z_{sp})$ is the peak rarefactional pressure *in situ* in MPa derated by 0.3 dB/cm-MHz to the point on the beam axis, z_{sp}, where the pulse intensity integral ($\text{PII}_{.3}$) is maximum; and f_c is the center frequency in MHz.

The TI is defined by the FDA as: the ratio of total acoustic power, W_p, to the acoustic power required to raise tissue temperature by 1°C under defined assumptions, W_{deg}:

$$TI = \frac{W_p}{W_{deg}} \tag{1.3}$$

The MI and TI are only applicable in the case of ultrasound imaging, as these become both inaccurate and irrelevant when considering therapeutic ultrasound with or without the introduction of cavitation nuclei.

1.7.3.2 Therapeutic safety limits

Ultrasound intensities may be used to characterise an ultrasound exposure and the potential damage associated with it. Typical intensities calculated are: spatial peak, temporal peak $I_{SPTP} = \frac{p^2}{\rho c}$; spatial peak, pulse average $I_{SPPA} = \frac{p^2}{2\rho c}$; spatial average, temporal average I_{SATA}

$= \frac{p_{av}^2}{2\rho c}$; and spatial peak, temporal average $I_{SPTA} = \frac{p^2}{2\rho c} DC$ where the duty cycle (DC) is taken into account. Each of these equations refers to the peak pressure, p, the density of the medium, ρ, and the speed of sound in the medium, c [69], and where p_{av} is the pressure averaged over the area of interest.

The maximum allowed values when using **diagnostic** imaging of a peripheral vessel are as follows: MI= 1.9; I_{SPTA} (derated by 0.3 dB/cm-MHz) = 720 mWatts/cm^2; I_{SPPA} (derated by 0.3 dB/cm-MHz) = 190 Watts/cm^2 [69]. It should be noted that hemorrhage in rat lung has been observed using a diagnostic ultrasound probe below this reported MI limit [92]. For **therapy** however, ablative high intensity focused ultrasound (HIFU) uses focal peak intensities ranging from 2 to 20 kW/cm^2 [176]. The allowable intensities for therapy are necessarily higher than for imaging, to deposit sufficient energy to accomplish cell death. When considering therapeutic ultrasound, it is also important to remember the effect of the ultrasound in combination with any other drug (for example a chemotherapeutic), or device (such as a cavitation nuclei) that is used in conjunction with it.

1.7.4 Cavitation monitoring

Monitoring of cavitation is important in understanding safety as well as efficacy. Cavitation effects can be broadly divided into *thermal* and *mechanical* effects. Although these two effects are sometimes inextricably linked, they can be monitored independently.

1.7.4.1 Thermal monitoring

As thermal effects from cavitation can impact both biological tissues as well as drug carriers, thermal monitoring is important. Thermal monitoring can be achieved in an invasive, or non-invasive manner. Thermocouple needle probes are thin (200 μm) metallic needles which can be used *in vitro* or *in vivo* to measure temperatures directly in tissue. These devices have the advantage of being relatively cheap and simple, and the disadvantage of potentially initiating cavitation on the surfaces of the probe, leading to an artificially elevated temperature response. Non-invasively, magnetic resonance imaging (MRI) is used to measure temperature and is considered the 'gold standard' or thermometry *in vivo*. One disadvantage of MRI thermometry is its relatively high cost, which limits its use [100].

1.7.4.2 Mechanical monitoring

One key clinical feature of a successful treatment mechanism is having a real-time detection system [84]. Monitoring of the mechanical perturbations associated with cavitation itself can be achieved in real-time, in an 'active' or 'passive' manner, both using non-invasive, ultrasound devices.

B-mode imaging can be used 'actively' to monitor cavitation due to ultrasound, however as it is an active technique, the B-mode ultrasound probe can only be *on* when the HIFU is *off*, thus only recording hyperechogenic regions after the cavitation may have subsided and the bubbles dissolved [100], and thus may underestimate the amount of treatment [84].

Passive cavitation detection on the other hand has potential to provide a real time, accurate assessment of cavitation activity [153]. A cavitating bubble radiates pressure waves which are able to be detected passively by a single element or an array of receivers. Being a mechanical wave, ultrasound is able to mechanically move a detector which can be transformed into electrical energy and recorded remotely [117]. These signals can then be analysed in the frequency domain to characterise the cavitation activity. The energy associated with 'harmonic' or 'broadband' emissions can give indications of whether the cavitation occurring is 'stable' or 'inertial':

- **Harmonic emissions**, as well as subharmonics and ultraharmonics, are produced following cyclic contraction of a bubble. These emissions are typically associated with 'stable' cavitation. Harmonic emissions are defined as the energy within bands at multiples of the driving ultrasound frequency, the *fundamental*. For example if the *fundamental* frequency is 0.5 MHz, *harmonics* occur at 1, 1.5, 2, 2.5 MHz etc.

- **Broadband emissions** are produced following inertial cavitation of a bubble where during the rapid bubble wall collapse, a shock wave is generated, a short emission in time which has a corresponding 'broad' emission in the frequency domain. The chaotic nature of inertial bubble collapse dictates that energy is not concentrated in cyclic frequency bands but across all frequencies. Broadband emissions are observed as a rise in the 'noise floor' with no particular concentration of energy in frequency bands.

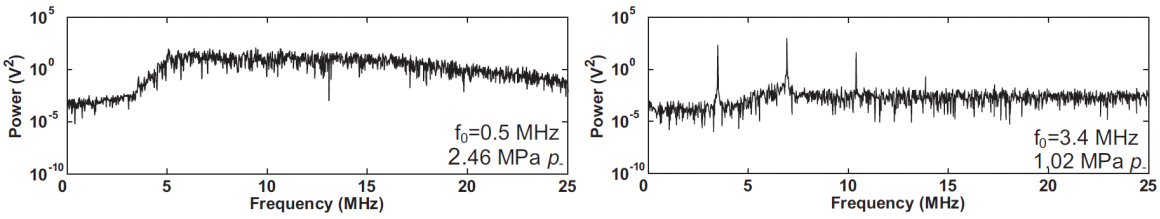

Figure 1.10: *The fast Fourier transforms (FFTs) of the received passive cavitation detector (PCD) signals further verifying the increased braodband noise emissions (left) and the presence of harmonics (right) and in particular the second and third harmonic. Exposure of 0.5 MHz and at a peak rarefactional pressure of 2.46 MPa when inertial cavitation is present at the acoustic focus (left) and at 3.4 MHz at 1.02 MPa peak rarefactional pressure when inertial cavitation is not present (right). Image taken from [112] (Kyriakou et al., 2011).*

The combination of the total power of cavitation as well as the frequency response may be used to determine the inertial cavitation threshold of a bubble [81]. Experimentally, the inertial cavitation threshold may be defined as the lowest rarefactional pressure amplitude that results in detectable broadband emissions. Detectable broadband emissions here were defined as those with a signal grater than 6 standard deviations above noise (an arbitrary threshold) [112]. Example traces showing 'harmonic' dominated and 'broadband' dominated emissions are given in Figure 1.10.

During cavitation, a shelled bubble, i.e. one which encapsulated in a lipid, protein or polymer, is assumed to be disrupted, either leading to lipid shedding or to complete bubble destruction. Chen et al. used passive cavitation detection to monitor inertial cavitation, correlating that with bubble fragmentation [36], thus validating the use of passive cavitation detection for assessing levels of inertial cavitation.

Development of detectors has transitioned from single element transducers (detecting in 1 dimension) to multi-element arrays (detecting in 2 or 3 dimensions) which are able to provide good spatial and temporal information as passive receivers [100]. Passive spatial mapping is a method developed by Gyongy and Coussios [84], and further developed for drug delivery monitoring by Haworth et al. [86], to record broadband emissions using an array of receivers. Beamforming (delay-and-sum) of the power of the signals received on each receiver then enables spatio-temporal reconstruction of the cavitation sources.

The original work [84] was done in a homogeneous agar phantom, and has since been demonstrated in murine models [38] mapping inertial cavitation events from microbubble

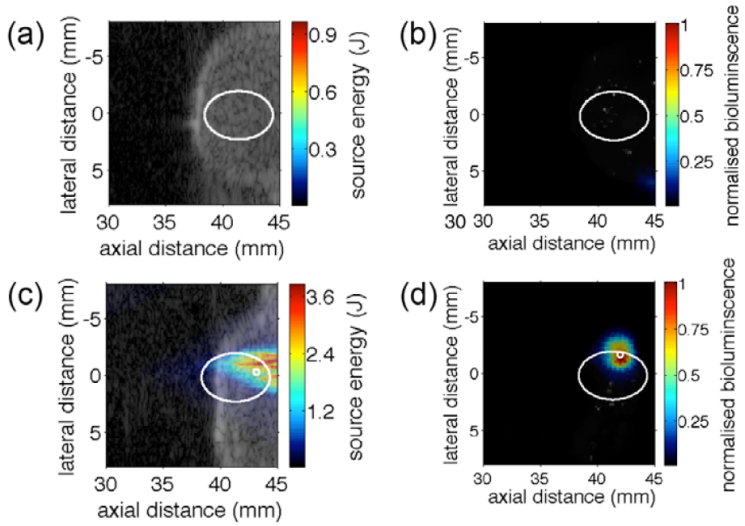

Figure 1.11: *Mapping of cavitation to luciferin release from liposomes. Focused ultrasound (FUS) was applied (white ellipsoid) within tumours in the presence of systemically administered cavitation-sensitive liposomes containing luciferin, but in the absence of SonoVue led to (a) no cavitation and (b) failed luciferin release. FUS applied in the presence of both liposomes and SonoVue generated (c) inertial cavitation activity, as indicated by the source energy of broadband noise, spatially correlated with (d) the location of luciferin release from liposomes. Image taken and modified from [38] (Choi et al. 2014).*

nuclei to liposomal drug release (Figure 1.11), discussed further in Section 1.8.

1.8 Ultrasound-enhanced drug delivery

Ultrasound is able to be used in isolation in the treatment of tumours using histotripsy and ablation [176] to kill cells without the use of drugs. High intensity focused ultrasound (HIFU) has been used primarily for tumour ablation purposes using the thermal and mechanical effects to kill tumour cells [136]. HIFU has also been used to perform non-invasive hemostasis [52, 95], thrombolysis [47, 148, 173] and opening of the blood brain barrier to improve drug uptake [93].

Although HIFU can be used alone to treat tumours, ultimately this approach is limited by damage to surrounding tissue and a requirement to know exactly where the tumour is, hence the use of ultrasound in conjunction with chemotherapy to reduce drug side effects and improve targeted delivery has been explored for over 20 years [194]. Initial investigations showed that low level ultrasound could be used synergistically with chemotherapy to increase cytotoxicity without any significant increase in temperature [85].

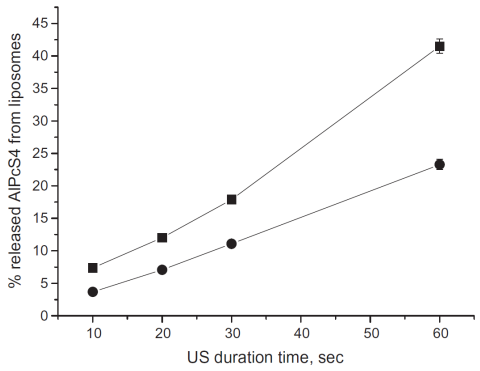

Figure 1.12: *In vitro US-mediated release profiles of $AlPcS_4$ (a fluorochrome) from DOPE-based liposomes (squares) and HSPC-based liposomes (circles). The mean and standard deviation of trpilicate measurements are given. Image taken from [62] (Evjen et al. 2013)*

1.8.1 Liposomes

The rationale for using liposomes is to shield the drug from the body to reduce drug breakdown, and shield the body from the drug to reduce toxic side effects of the drug. Once the liposome is at the site of action however, a release mechanism is required to allow the drug to act on the target cells. Ultrasound has been proposed as a method to trigger the release of drug from liposomes either mechanically or thermally as discussed below.

1.8.1.1 Sonosensitive liposomes

Sonosensitive liposomes, which only contain a drug without a gas bubble, are those which are broken by the mechanical perturbations of the ultrasound wave. Studies performed have typically been at high intensities which is associated with cavitation events (even though disruption by cavitation is not claimed in many of these studies as the mechanism of action) [62, 72].

Epitarget AS (http://www.epitarget.com/) is a therapeutics company that has developed a liposomal formulation which releases its payload, for example siRNA, in response to ultrasound [62]. The lipid composition has been shown to be important in determining the level of sonosensitivity of each liposomal formulation with DOPE based liposomes proving to be more sonosensitive than HSPC based liposomes shown both *in vitro* (Figure 1.12), and *in vivo* (Figure 1.13). These experiments were conducted using focused ultrasound with an I_{SPPA} of 10.5 kW/cm^2 at 1.1 MHz which corresponds to a PRFP of 17.6 MPa.

Similar release results have been achieved at 1.1 MHz using 25.7 MPa ultrasound with 1% duty cycle. At these conditions, cavitation was observed as transient hyperechogenic regions on B-mode images [72]. With increasing duty cycles, increasing tissue damage due

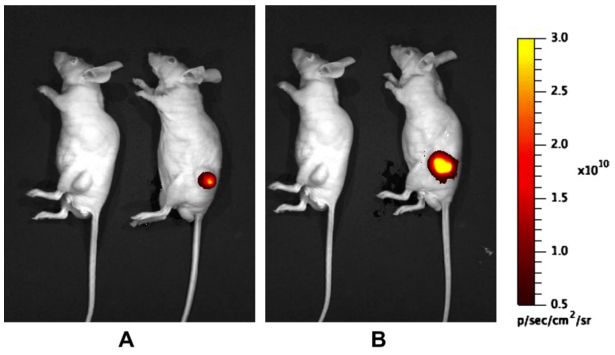

Figure 1.13: *Mice receiving intratumoural injection of $AlPcS_4$ (a fluorochrome)-containing DOPE-based liposomes before (A) and after US treatment (B). The mouse to the left in the images is an untreated control (no liposome or US treatment). Signal intensity reflects $AlPcS_4$ release. Imaging acquisition parameters were equal in all pictures. Image taken from [62] (Evjen et al. 2013)*

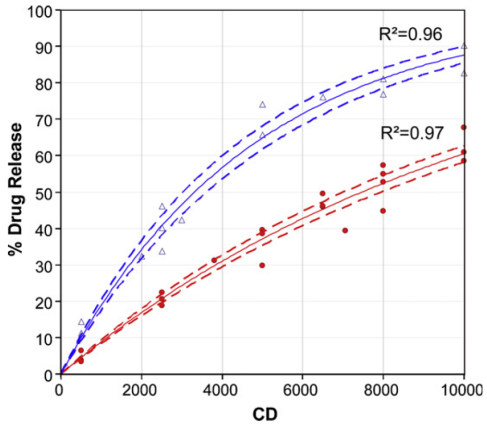

Figure 1.14: *Percentage of doxorubicin release versus cavitation dose for Caelyx® liposomes (circles) and DSPE-based liposomes from Epitarget (triangles). Image taken from [168] (Somaglino et al. 2011)*

to cavitation has been observed. Operating at high intensities, I_{SPTA} = 111 W/cm^2, at 2.5% DC, bruising and minor superficial damage was seen, while at 5% DC large amounts of necrosis occurred [128]. Mestas et al. developed cavitation sensitive liposomes releasing doxorubicin using HIFU (at 2.5% DC chosen based on the tissue damage seen) at the tumour site leading to a decrease in tumour size compared to the control in a murine model [128].

Drug release from liposomes has been correlated directly with cavitation dose by Somaglino et al. [168]. Cavitation dose was measured by amount of broadband noise received by a needle hydrophone and validated by the amount of hydroxyterephthalate (HTA, fluorescent) produced upon ultrasound exposure of terphthalate (TA, non-fluorescent) solution. A high correlation between cavitation dose and extent of doxorubicin release from liposomes was observed suggesting that inertial cavitation is at least participating in drug release from liposomes, if not the main mechanism for release (Figure 1.14) [168].

Duty cycles are deliberately kept low in these studies to minimise heating. Thermosensitive liposomes however require increased temperatures which can be achieved at high pressures and high duty cycles.

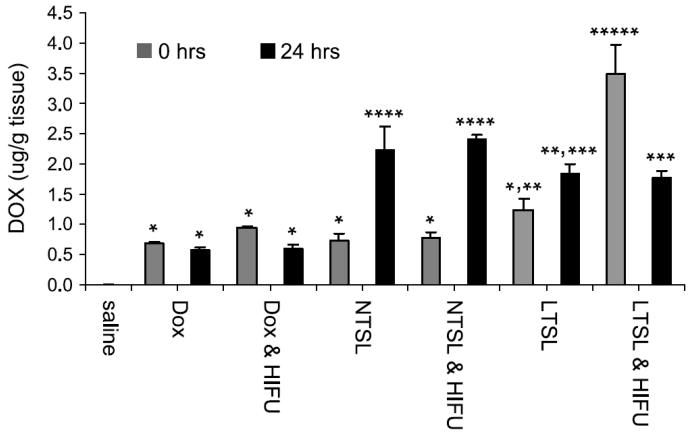

Figure 1.15: *Local drug delivery in murine adenocaricnoma tumours using free doxorubicin, NTSLs, or LTSLs, with or without pulsed-HIFU exposures. Liposomes or free doxorubicin (2mg/kg) were first injected i.v. followed by exposures in the tumours (400mm^3) at 0 and 24 h after administration. Immediately after the exposures, animals were sacrificed, and tumours were assayed for doxorubicin content. Significant differences were not found between exposed and unexposed tumours in mice receiving NTSLs at either exposure time point. The same occurred for free doxorubicin. Although accumulated doxorubicin was greatest in unexposed tumours receiving NTSLs (at 24h), the highest mean concentration of doxorubicin was found in tumours receiving LTSLs and pulsed-HIFU exposures. Differing lowercase letters between mean doxorubicin concentrations indicate a significant difference of at least P=0.05. Columns, mean (n=5); bars, SE. Image taken from [57] (Dromi et al. 2007)*

1.8.1.2 Thermally sensitive liposomes

Low temperature sensitive liposomes (LTSL) have been developed to release doxorubicin, and have been tested both in vitro and in vivo, using pulsed HIFU for heating [57]. Figure 1.15 shows the advantage of these liposomes over free drug and stable, non-temperature sensitive liposomes (NTSL) when used in conjunction with HIFU. Liposomes (or free drug) were delivered intravenously and exposed to HIFU at T=0 and T=24 hours. Doxorubicin (Dox) showed no enhanced drug delivery with HIFU. At T=0, NTSLs showed no enhanced drug delivery compared with no HIFU. At T=24, NTSLs showed enhanced drug delivery both with and without HIFU which is due to the passive accumulation via the EPR effect. LTSLs on the other hand showed significant increase in Dox concentration at T=0. This result illustrates the triggered response of LTSLs using ultrasound with a 10% DC, I_{SATA} = 1300 W/cm^2 for 15 to 20 mins over the tumour causing a temperature rise of 4 to 5 °C.

In vitro this affect has been quantified with 80% of a doxorubicin dose being released from dipalmitoylphosphatidylcholine (DPPC) based liposomes with a 20 second ultrasound

exposure at 1.6 MPa, 45% DC, 1.1 MHz focused ultrasound [125]. Mylonopoulou et al. [135] have shown that ThermoDox®, a thermally sensitive liposome developed by Celsion Corporation (celsion.com), is able to be disrupted by heating caused by HIFU exposure over short time periods. In contrast to Dromi et al. [57] where HIFU alone was used for heating, cavitation enhanced heating was used to further reduce the required exposure time for heating [134]. Six seconds continuous wave ultrasound at 4.4 MPa PRFP was sufficient to cause release of doxorubicin and significant cell death in vitro, whilst at 2.5 MPa PRFP no drug release or cell death was observed [135]. At lower duty cycles however significantly lower levels of release were seen [134].

The ultrasound intensity required to achieve release from sonosensitive or thermosensitive liposomes is however very high. In the absence of liposomes, ultrasound alone at these intensities can damage tissue and can therefore cause unwanted side effects. To lower the ultrasound intensity required for release, cavitation nuclei have been proposed and is discussed in the subsections below.

1.8.2 Cavitation nuclei for enhanced release from liposomes

1.8.2.1 Echogenic liposomes

To be able to visualise liposomes before using ultrasound for triggered release, liposomes have been developed to encapsulate both a drug and gas, making them both echogenic [45] and a drug carrier [174]. The drug is able to be loaded into the hydrophilic core or the hydrophobic bilayer, depending on the molecular structure of the drug (Figure 1.4). The gas component is stabilised using a lipid monolayer within the outer liposomal vesicle [109].

Ibsen et al. have developed liposomes with UCAs nested inside them [96] which is in contrast to Cochran et al. who encapsulated the drug into the UCA shell. The structure of these nested liposomes (1 μm bubble inside a 5 μm liposome) is hypothesised diagrammatically (Figure 1.16a) and shown under fluorescent microscopy (Figure 1.16 (b) and (c)) and has a higher loading capacity than microbubbles alone [96].

Triggered release from another formulation of echogenic liposomes was demonstrated by Huang et al. [94]. The liposomes produced ranged from 550 nm to several microns in diameter. Liposomes were imaged using 20 MHz ultrasound and triggered to release

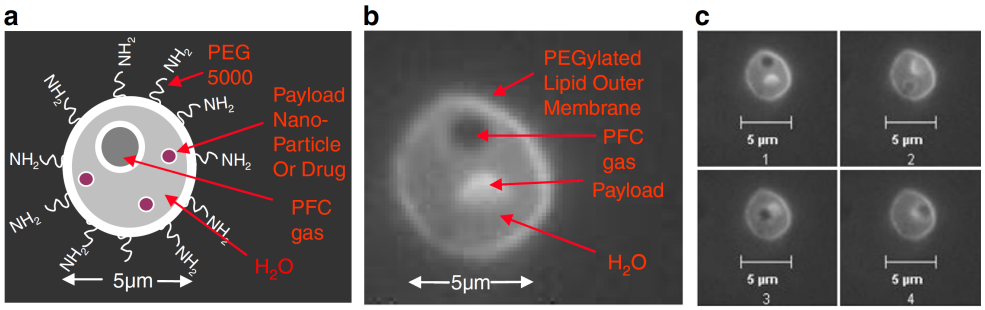

Figure 1.16: *Nested liposome structural design. (a) A schematic of the nested liposome. (b) Fluorescent image of a nested liposome and (c) a series of sequential images taken showing that the microbubble and fluorescent lipid payload moving around due to Brownian motion, confirming that the microbubble and payload were inside the outer membrane and not attached to the outside. Image taken from [96] (Ibsen et al. 2011).*

using 1 MHz ultrasound. Although some of these liposomes were on the nanoscale, the heterogeneous nature of the population produced makes it difficult to rule out the possibility that only the larger liposomes were visualised and their payload released during ultrasound exposure. Although unable to take advantage of the EPR effect, these liposomes, being larger, would have the benefit of carrying and delivery a larger payload. The liposomes demonstrated that up to 42% of the drug (calcein used as the model) was released using multiple ultrasound exposures. Huang et al. hypothesised that the rarefaction phase of the ultrasound causes expansion of the gas pocket in the liposome. When the peak negative pressure was sufficient to overcome the elastic limit of the liposomal wall, some or all of the contents were then released [94]. This technique is therefore potentially possible with stable cavitation rather than inertial cavitation if expansion of the bubble is sufficient to expand the liposome wall. A similar system was subsequently developed using recombinant tissue plasminogen activator as the payload demonstrating substantial clot lysis *in vitro* [163].

1.8.2.2 Microbubbles

Separation of the drug carrier and cavitation nuclei has been done to better control the system and the stability of both components. Microbubbles which have previously been used as UCAs have been proposed as cavitation nuclei for ultrasound triggered drug delivery and release. When tested in pre-clinical models, SV has been shown to increase extravasation of oncolytic adenoviruses into tumours when used in combination with a 0.5 MHz HIFU transducer at 1.2 MPa PRFP [20]. A PRF of 0.5 Hz was employed to ensure that the

bubbles were able to reperfuse the area between pulses as bubbles were destroyed with each pulse [20].

Cochran et al. [42] designed doxorubicin and paclitaxel loaded microbubbles which upon cavitation were destroyed, leaving sub - 400 nm drug loaded polymer fragments. It is hypothesised that these fragments are able to extravasate into tumours. *In vitro* cell viability decreased significantly in samples exposed to paclitaxel loaded ultrasound contrast agents in combination with HIFU compared with non-drug loaded and non-insonated controls [42]. In a similar way, Escoffre et al. [60] demonstrated an increase in cell kill using doxorubicin liposome-loaded microbubbles when exposed to 1 MHz, 0.6 MPa ultrasound compared to doxorubicin liposome-loaded microbubbles or free doxorubicin alone. Furthermore, Larina et al. showed that ultrasound in conjunction with Optison microbubbles could be used to improve cell uptake of macromolecules *in vitro* providing a good model for enhancing gene delivery to cancer cells [116]. Each of these methods however is limited by the size of the cavitation nuclei. Microbubbles are restricted to the tumour vasculature and are therefore not able to efficiently extravasate into tumours. To address this issue, cavitation nuclei at the nanoscale have been pursued.

1.8.2.3 Phase change droplets and vapour bubbles

To take advantage of the EPR effect, while also taking advantage of the interaction of ultrasound with microbubbles, phase change droplets have been developed. These vapour bubbles are able to be produced on the nanoscale and then when exposed to ultrasound or heat, expand to the micro-scale. Once expanded into a bubble, it has been proposed that they may be used as an ultrasound contrast agent, for drug release, or for ultrasound enhanced heating [150, 193].

Polymeric micelles (comprised of a hydrophilic shell and hydrophobic core) are able to be combined with perfluorocarbon (or similar liquid) and treated with a low frequency ultrasound probe to form nano- or micro-emulsions. Rapoport et al. [150] created such nano-emulsions for the purpose of drug delivery using ultrasound, however they found that at physiological temperatures (37°C) the particles grew from 428 nm (nanodroplets) to 1.03 mm (microbubbles) and at higher temperatures and over longer heating periods (longer than

5 minutes) bubbles coalesced to even larger sizes. This coalescence at physiological temperatures makes them ideal for ultrasound imaging but perhaps not for therapeutic applications such as systemic cancer therapy. These bubbles did however show good release and effective treatment of tumours in pre-clinical murine models when combined with ultrasound therapy.

Porter's group has developed sub-micron sized echogenic liposomes which have shown better stability when exposed to B-mode imaging than Optison®, an ultrasound contrast agent [166]. This opens up the possibility for such a liposome to be targeted to the sub-micron endothelial gaps of the tumour environment. Similar formulations have been developed for ablative therapies using HIFU where the ultrasound initially caused droplet vapourization followed by inertial cavitation for enhanced HIFU heating [193]. One issue that is associated with these vapour bubbles is stability at physiological temperatures. Vapour bubbles are designed to expand at elevated temperatures and so ensuring stability at physiological temperatures, and expansion at only a few degrees above that has proven difficult.

1.8.2.4 Solid particles as cavitation nuclei

To address the issue of stability of gas at the nanoscale, the author proposes solid nanoparticles to stabilise cavitation nuclei. Contrary to a bubble such as SV, it has been hypothesised that gas is able to be entrapped on the surface of a nanoparticle and used as the cavitation nuclei for ultrasound enhanced drug release [97]. The advantage of entrapping gas on a particle rather than developing free nanobubles, is that nanobubbles are more stable when entrapped in a surface crevice than as a free bubble [160]. Arora et al. [5] showed optically that microparticles (30 - 150 μm diameter) which had a corrugated surface were capable of acting as cavitation nuclei (tested between 5 - 7 MPa peak tensile stress), however smooth particles (30 μm diameter) were not. Neither showed cavitation at peak tensile stresses of 3 MPa or below. Figure 1.18 shows 3 solid microparticles in a) and one solid microparticle in b) in the top frame. The second frame, just after the tensile wave, shows 2 of the 3 in a) and the single particle in b) with a microbubble necking off the particle. The bubble then detaches from the particle completely. Although the particles shown in Figure 1.18 were relatively large particles, the roughness on the particles is in the order of the upper

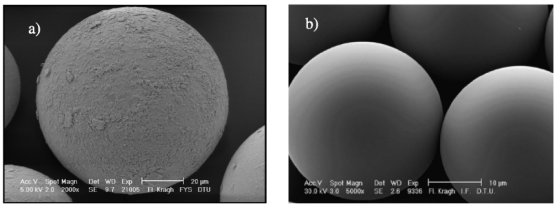

Figure 1.17: *Scanning electron microscope (SEM) images of the particles taken from batches where a) cavitation inception was observed (copolymer:divinylbenzol, diameter distribution 30 to 150 μm), and b) no inception was achievable (monodisperse 30 μm dynospheres EXP-SS-42.3-RSH. Please note the different magnifications. Image taken from [5] (Arora et al., 2004)*

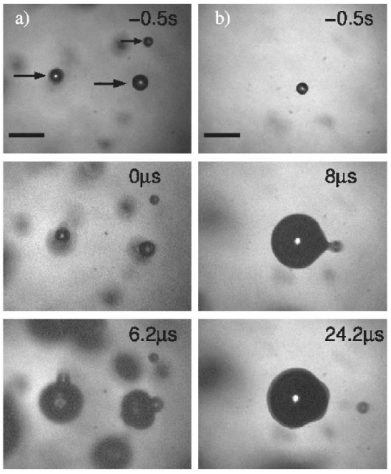

Figure 1.18: *Two three-frame sequences (a) and (b) depicting the explosive growth of cavitation bubbles from particles and their later separation. The timing of the individual frames relative to the start of the tensile wave (see Fig. 2) are indicated at the top of each frame (the length of the bar is 200 μm). Image taken from [5] (Arora et al., 2004)*

nano- to micro-scale. In addition to these findings, unmodified 0.1 μm polystyrene beads have also been shown to nucleate cavitation as demonstrated using passive cavitation detection [53] suggesting that gas stabilised on the surface of one smooth particle, or between agglomerations of multiple particles, can nucleate cavitation.

Enhanced drug delivery of a free drug has been demonstrated by Larina et al [115] in an athymic nude mice bearing human colon KM20 tumours using polystyrene nanoparticles as cavitation nuclei. Ultrasound was used to insonate tumours at 20 kHz, 0.5 MPa, with or without cavitation nuclei and/or the chemotherapeutic agent 5-fluorouracil (5-FU). Results showed that polystyrene particles alone, and ultrasound alone, caused no significant effect on tumour growth in the presence of 5-FU. Polystyrene particles exposed to ultrasound, in the absence of 5-FU, showed an initial reduction in tumour size followed by re-growth of the tumours. This initial decrease was attributed to mechanical damage to tumour blood vessels and tumour cells by cavitation. When the nano-cavitation nuclei were combined with 5-FU and exposed to ultrasound, a significant regression of all tumours was noted, with complete tumour regression without regrowth in two of the five tumours. These findings illustrate that delivery of free drug is able to be enhanced by cavitation nucleated from

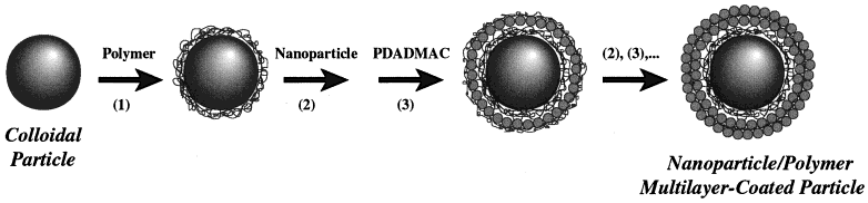

Figure 1.19: *Preparation of layer-by-layer nanoparticles. (Caruso et al. 1999)*

solid nanoparticles. The study's findings are limited as they were performed at a relatively low frequency (20 kHz) where focusing is difficult [115] and the cavitation threshold of native tissue is low. Liberman et al. detail hollow, silica and silica-boron, nano- and micro-particles developed that improve ultrasound contrast for imaging in tumours with the aim of improving imaging of smaller tumours that currently go undetected [119]. These particles could also have potential to be used as cavicatalytic particles for drug delivery in a similar way shown by Larina et al.

Preliminary work on layer-by-layer manufactured nanoparticles undertaken in the BUBBL group, University of Oxford, by Mike Molinari and Sarah Wagstaffe has indicated that solid particles in the nano-micro range are able to be formulated to decrease the cavitation threshold of water. Layer-by-layer assembled particles are of particular interest due to their varied templates [49, 65, 111], ability to use most inter-layer interactions [49], ease of surface functionalisation [102,103] and drug carrying capabilities [101] [1,102,188]. The pioneering work on multilayers of colloids and polymers was done by R Iler [98] followed by G. Decher et al. [51] who explored the layer-by-layer technique of alternating anionic and cationic polyelectrolytes on charged surfaces.

The particles used by Molinari and Wagstaffe were first produced by Frank Caruso and Helmuth Mohwald [32] and have a rough, hydrophobic surface. The particles are formed using a polystyrene core (PS) coated with alternating layers of poly(diallyldiamethylammonium chloride) (PDADMAC) and silica nanoparticles (SiO_2) (Figure 1.19) [32]. An initial layer had also been tried with poly(sodium 4-styrenesulfonate) (PSS) to improve the surface charge uniformity. This particle surface produced is hypothesised to be conducive to trapping air bubbles in the hydrophobic pockets between SiO_2 beads on the surface if they are dried and then resuspended in a solution.

One problem associated with this system, which has been identified by Schneider and

Decher [158], is particle agglomeration. They identified that the important parameters associated with agglomeration were the length of the polyelectrolyte, the particle concentration, the stoichiometric excess of either particles or polyelectrolyte chains and the salt concentration. Schneider and Decher [158] explored three possible regimes within the layer-by-layer assembly method. I) colloids in excess of polyelectrolytes, II) colloids and polyelectrolytes in approximately equal charge proportions, or III) polyelectrolytes in excess of colloids. In the third regime, they note that adsorption should be favoured over bridging flocculation if the individual nanoparticles are sufficiently separated from each other, i.e. the nanoparticle concentration is sufficiently low. Due to the issues of particle agglomeration, manufacturing complexity and lack of reproducibility, these LBL particles were not pursued in this research.

1.9 Overview of thesis

Current chemotherapeutics have shown unacceptable side effects and are often limited by low concentrations at the target tumour site. Nanoparticles have shown promise as drug delivery vehicles as they are able to take advantage of passive accumulation in tumours via the EPR effect. Although drug accumulates in the tumour via this method, it is typically still encased in the nanoparticle carrier due to the particle stability, and is not a sufficient dose to achieve the desired therapeutic effect. To release the drug from the nanoparticle, a triggered release mechanism is required. Ultrasound has been proposed as a possible mechanism by which to trigger drug release and has the benefits of being able to treat, image and monitor therapy in real-time, non-invasively, deep into the body. To minimise side effects of the ultrasound wave itself however, cavitation nuclei are necessary to reduce the required intensity. Most of these cavitation nuclei have been developed on the micro scale, which are constrained to the vasculature, and those which are on the nanoscale typically expand to the microscale at biological temperatures.

To take advantage of the potential accumulation and deeper tumour penetration via the EPR effect, while also utilising the ultrasound modality for triggered release, a nanoscale cavitation nuclei and cavitation sensitive liposome is required. Here, an ultrasound-triggered drug release system using nanoscale cavitation nuclei is proposed. A triggered release system

is necessary to ensure a sufficient drug dose is released in the target tumour tissue and to reduce potential side effect of drug not in the tumour.

The key aims of this thesis are to: develop nanoparticles capable of acting as cavitation nuclei under ultrasound exposure; develop ultrasound-stable liposomes sensitive to cavitation events; demonstrate drug release from liposomes using nano-scale cavitation nuclei; and show potential for use of nano cavitation nuclei for drug delivery *in vivo*.

Chapter 2 describes the methods used in the production and characterisation of cavitation nuclei and liposomal drug carriers both *in vitro* and *in vivo*.

Chapter 3 goes into detail into the development and characterisation of solid cavicatalytic nanoparticles. This chapter discusses one microbubble, SonoVue (SV); and two main solid particle types: carbon nanoparticles (CNPs) and polymeric nanocups (NCs) and their cavitation responses when exposed to varying ultrasound conditions.

Chapter 4 demonstrates how cavitation sensitive liposomes are able to be used for drug release using micro-scale cavitation nuclei. A large proportion of the work from this chapter was published in the Journal of Controlled Release [79].

Chapter 5 further develops the work in Chapter 4 to use nano-scale cavitation nuclei for liposomal drug release. The three particle types detailed in Chapter 3 are tested in this chapter.

Chapter 6 demonstrates the potential for nano-scale cavitation nuclei as triggers for drug release *in vivo*.

Chapter 2

Methods and materials

This thesis is focused around the development and testing of 1) cavitation inducing particles, in the form of an encapsulated microbubble and as gas-stabilizing solid nanoparticles, and 2) drug carrying liposomes sensitive to cavitation events. This chapter outlines the materials and methods used in the development and testing of these particles both *in vitro* and *in vivo*.

2.1 Production of cavitation inducing particles

2.1.1 SonoVue preparation

SonoVue® (SV) was prepared using the manufacturer's instructions and diluted in phosphate buffered saline (PBS) for use. Briefly, 25 mg lyophilised phospholipid powder was resuspended in 5 mL sodium chloride and shaken vigorously for 20 seconds. The suspension was allowed to stand for 10 minutes before dilution. The vial was rolled before dilution to disperse bubbles in the vial.

Shelled bubbles (gas and lipid) were sized using the same preparation as in ultrasound experiments described below matching concentration (300 μL SV in 7 mL PBS) and incubation (suspended in 37°C water-bath for 40 seconds). Samples were loaded onto a haemocytometer with cover slip before imaging using a 40 x objective microscope (Leica DM500, Microscope Services Limited, Woodstock, UK). Images were captured digitally (Image-Pro Insight 8.0.3, Media Cypernetics Inc.) and analysed using custom Matlab scripts. Size dis-

tributions were determined over 6 individual samples with 10 images per sample and plotted as percent distributions.

2.1.2 Carbon nanoparticle production

Carbon nanoparticles (CNPs) were developed over several cycles of experiments to determine the final formulation. This development process is outlined in Appendix A with the final procedure being outlined here. Mesoporous carbon at 0.2 mg/mL (699632-5G, Graphitized carbon black, Sigma, Lot MKBK34575) was prepared in 35 mL filter sterilised deionized water (Milli-Q, Merck, UK; 200 nm filtered, 18.2 MΩ.cm). Carbon suspensions were shaken vigorously to disperse and sonicated using a 22.5 kHz sonic probe (Microson™ Ultrasonic Cell Disrupter, Misonix) at 15 Watts for 30 seconds x 5 with 1 min rests, standing at room temperature. The sonication probe was centered and moved up and down every 5 seconds in 50 mL centrifuge tubes (polypropylene Falcon tubes, Fisher Scientific). Between sonications, solutions were shaken vigorously by hand for 5 seconds. Solutions were transferred to clean tubes before particle size separation by centrifugation. Samples were centrifuged at 2000 g for 5 minutes (acceleration = deceleration = 9; temperature = 25°C). The supernatant was transferred to clean tubes leaving 10 mL pellet and solution. The supernatant was centrifuged at 2000 g for 1 hour. Supernatant was removed and retained leaving 10 mL pellet and solution to be discarded. Carbon used for all experiments had a surface area of 216 m^2/ g (699632-5G, Sigma) except in the case of testing lower surface area of 80 m^2/ g (699624-5G, Sigma).

2.1.3 Polymeric cup nanoparticle production

Polymeric nanocups (NCs) were produced using a method first described by Lv et al. [122] and modified by James Kwan et al. 2015 (paper submitted for publication) to ensure cavitation nucleating properties. Polystyrene core beads, 100 nm diameter, (LB1-15ML, Sigma Aldrich), 300 nm diameter, (LB3-15ML, Sigma Aldrich), or 500 nm diameter, (LB5-15ML, Sigma Aldrich), were bubbled in water (4.89% vol/vol) with N_2 gas (for approximately 1 min per mL volume). Particles were heated in a water bath at 80°C and mixed with methyl methacrylate (M55909-500ML, Sigma Aldrich), hydroxyethyl methacrylate (477028-25ML,

Sigma Aldrich) and divinylbenzene (414656-250ML, Sigma Aldrich) to final concentrations of 2.29% vol/vol, 0.23% vol/vol and 1.43 % vol/vol respectively. N_2 bubbled potassium persulphate (216224-100G, Sigma Aldrich) solution was added (final concentration 0.153 mg/mL) to initiate the reaction to form the polymer cups. The reaction continued for 5 hours and thereafter the solution was cooled at room temperature. Particles were washed by centrifugation (30 min, 15 000 rpm) and resuspension in water three times to remove non-reacted polymer. Particles were allowed to air dry at 45°C over night in a petri dish. The powder was resuspended in the same starting volume of DI water using magnetic stirrers, entrapping air in the cups. Particles were sieved (106 μm then 32 μm, stainless steel sieve, Endecotts Ltd, London, UK) and filtered (1.6 μm syringe filter) to remove large agglomerates. A 1 in 10 dilution was used for ultrasound experiments (approximately 0.56 mg/mL).

2.2 Production of drug carrying liposomes

The method used for liposome production is as described by Graham et al. [79][1] and is given in more detail below.

Hydrogenated soy phosphocholine (HSPC, 840058, 88.6% 18:0 DSPC, 11.4% 16:0 DPPC (ratio represents carbon single:double bonds)), 1,2-distearoyl-snglycero-3-phosphoethanolamine (DSPE, 850715), and 1,2-distearoyl-snglycero-3-phosphoethanolamine-N-[methoxy(polyethylene glycol)-2000] (DSPE-PEG 880120) are shown diagramatically in Figure 2.1. The packing parameter (PP) of a lipid is defined as the ratio of the geometric area of the hydrophobic tail to the polar head. Lipids with PPs approximately equal to 1, for example HSPC, form tight, bilayer structures. Lipids with high PPs, for example DOPE (unsaturated), form inverted hexagonal structures in monolayers, making them less stable liposomal structures. At PPs in the middle, for example DSPE (saturated), lipids are able to form hexagonal structures at low pH (pH $<$ 9) and bilayers at high pH (pH $>$ 9), a feature that is able to be utilized when loading and releasing drugs. All lipids used in the production of liposomes were purchased from Avanti Polar Lipids.

Liposomes were prepared using the following method as described by Carlisle et al.

[1]The methods used to formulate liposomes are published in the Journal of Controlled Release

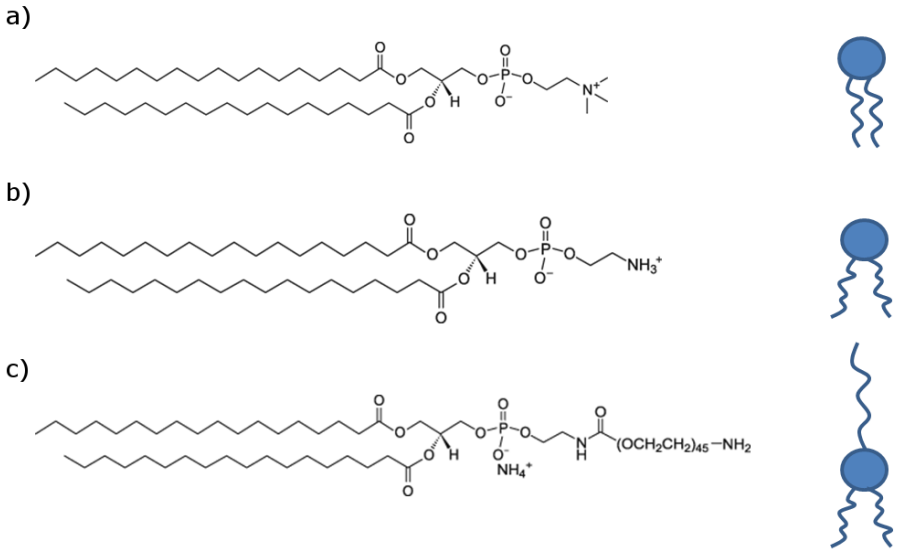

Figure 2.1: *Lipid chemical formula from Avanti Polar Lipids Inc (www.avantilipids.com) [9–11] and diagrammatic structures showing increasing packing parameters from (a) HSPC, (b) DSPE, and (c) DSPE - PEG.*

2013 [31]. Firstly a lipid layer was established. Lipid powders and cholesterol (C8667, Sigma, UK) were dissolved in methanol and chloroform under argon in a round bottomed flask at 55°C in a rotary evaporator. The formulations used are detailed in Table 2.1. Once dissolved, a 10 inHg vacuum was applied with a rotation speed of 60 rpm until a film had formed. The film was purged with argon and placed under a 10 Pa vacuum over night, until the film was dry. The film was resuspended in degassed Tris buffer (300 mM, pH 10) at a concentration of 41.9 mg/ mL and allowed to swell for 1 hour at 55°C on a rotary evapourator at 60 rpm. The solution was then allowed to stand for over 1 hour. Following hydration, the lipids were extruded. Extrusion of the lipids was done at 55°C for HSPC liposomes, and 75°C for DSPE liposomes. The temperature for extrusion is chosen such that it is above the phase transition temperature (T_m) of the lipid (Table 2.1). Lipids were extruded through 400 nm followed by 200 nm filters with 11 passes through each. Samples were stored in autoclaved glass vials purged with argon. Luciferin loading was conducted once liposomes were formed. Samples were passed through a PD10 column loaded with an acidic buffer (20 mM citric acid, 150 mM NaCl, pH 5) to exchange the basic suspending solution with an acidic solution creating a pH gradient across the lipid bilayer of the liposomes. D-Luciferin potassium salt (Gold Biotechnology, MO, USA) was dissolved in the acidic buffer

(pH 5) of citric acid (20 mM), NaCl (150 mM) to a concentration of 450 mg/mL. Luciferin solution was added to the liposomes to produce a final luciferin concentration of 15 mg/mL, and allowed to incubate for 24 hours. Luciferin has a neutral charge in the surrounding acidic buffer, and a positive charge in the internal basic buffer. When the luciferin passes through into the liposome and acquires a positive charge, it is more difficult for it to pass back through the membrane, thus remaining inside the liposome. Liposomes were purified to remove excess luciferin using a PBS loaded PD10 column. Liposomes were stored in sealed glass vials under argon at 4°C. Finally, the liposomes were tested for size distribution and encapsulation efficiency. Size and zeta potential were measured using dynamic light scattering (DLS). Luciferin loading was determined using the method described in Section 2.8.1.

Table 2.1: *Lipid ratios used to produce 'Doxil-like', and 'DSPE' liposomes. Phase transition temperatures (T_m) for each lipid are also shown (Avanti Polar Lipids and [105])*

	Doxil-like	**DSPE**	T_m
HSPC	56	3	55°C
DSPE		65	74°C
DSPE-PEG	5	7	12°C
Cholesterol	39	25	N/A

2.3 Characterisation of particles and liposomes

2.3.1 Particle size

Dynamic light scattering (DLS) also referred to as Photon Correlation Spectroscopy (PCS) relies on Brownian motion to measure the size of sub-micron particles, and electrophoretic mobility to measure the zeta potential of the particle [99].

When measuring size, the larger the particle, the slower the Brownian motion and vice versa [99]. The velocity of the Brownian motion is defined by a property known as the translational diffusion coefficient, D. This property is used to determine the hydrodynamic diameter ($d(H)$) as shown in the Stokes-Einstein equation (Equation 2.1) [99] where: k is the Boltzmann's constant; T is the temperature; η is the dynamic viscosity; and D is the translational diffusion coefficient. Parameters that are able to affect the particle diffusion

speed, and thus the apparent diameter, include the ionic concentration of the medium and the particle surface structure. Decreasing the conductivity of the medium will produce an extended electric double layer, called the Debye length, reducing the diffusion speed and resulting in a larger apparent particle size. If the adsorbed polymer is projecting out into the medium it will also reduce the diffusion speed making it appear larger [99].

$$d(H) = \frac{kT}{3\pi\eta D} \tag{2.1}$$

DLS uses the intensity of the scattered light received after hitting the particles. If the particles are moving quickly, the speckle pattern produced from the phase addition of the scattered light, will also change rapidly and vice versa. A correlator is used to compare the intensity of the scattered light at different time points. The correlation of the intensity decays over time until there is no correlation. Smaller particles, moving quickly, will have a short decay. However the correlation of larger particles, moving more slowly, will persist. The time at which the correlation starts to decay indicates the size of the particle. The steeper the correlation decay, the more monodisperse the sample is. Conversely, the more extended the decay, the more polydisperse the sample is [99]. The correlation function has a single exponential fitted to it giving a mean size and polydispersity or multiple exponentials fitted to obtain the distribution of the particles [99].

50 μL sample was diluted in 1 mL sterilize filtered deionized water and sized in lidded plastic cuvettes using dynamic light scattering (DLS) (ZetaSizerNano, Malvern, red laser, wavelength 633 nm, 3 measurements of approximately 10 runs, automatic run selection). Particles were deemed to be 'nanoparticles' if: the peak size by intensity was below 500 nm; the Z-average size matched peak size by intensity, that is, no larger peaks were present in solution; the polydispersity index lower than 0.3; and the above criteria were met for each of 3 measurement runs.

Sizing of larger particles was performed using laser light diffraction (Mastersizer, Malvern). Intensity of light scattered from particles in the range of 0.05 μm to 900 μm in flow was analysed using the Mastersizer software to calculate particle size and distributions.

2.3.2 Particle charge

Electrophoretic mobility measurements, also using DLS as described above were used to calculate zeta potential, a measure of the surface charge on a particle. When measuring zeta potential, a current is applied across the zeta cell and the electrophoretic mobility of the particles in solution is measured. Zeta potential measurements are highly dependent on pH, and a physiological pH, 7.4, is generally used when determining the stability of particles for *in vivo* applications. Zeta potential, z, is determined using the Henry equation (Equation 2.2) where: U_E is the electrophoretic mobility; ε is the dielectric constant; $F(Ka)$ is Henry's function; and η is viscosity.

$$U_E = \frac{2\varepsilon z F(Ka)}{3\eta} \tag{2.2}$$

Disposable zeta potential cells were washed with methanol and then DI (filtered) water before filling with 750 μL sample (particles diluted into aqueous buffer). The Smoluchowski approximation was used to give a F(Ka) value of 1.5 used in the Henry equation, as samples were diluted into moderate electrolyte concentrations (more than 10^{-3} molar salt). Samples were measured 3 times and analysed using the general purpose mode.

2.3.3 Particle morphology

Transmission electron microscopy (TEM), at Oxford Brookes (Hitachi A-7650, Berkshire, UK, HV=100.0 kV), was used for all TEM images. TEM grids (3.05 mm copper with Formvar support films, F233/025, TAAB) were initially treated with Alcian blue (1%) for 5 mins to remove the charge. The grids were washed with filtered (450 nm) DI water 3 to 5 times before allowing adhesion to the sample. Sample (8 μL) was pipetted onto a Parafilm (SPI Supplies) sheet and the TEM grid was placed onto the droplet. Each sample was allowed to adhere to the TEM grid for 15 mins before being air dried and stored until imaged.

2.4 Stability testing of cavitation inducing particles

Nanoparticle stability was tested in 7 solutions. Deionised water (DI H_2O) (Milli-Q, Merck, UK; 200 nm filtered, 18.2 MΩ.cm) was used as the basis for all sample solutions and used as a control. NaCl 1.8% (3 mM), glucose 5% (2.8 mM), Ringers solution (NaCl 147.2 mM, KCl 4 mM, $CaCl_2 \bullet 2\ H_2O$ 2.2 mM), lactated Ringers solution (NaCl 102.7 mM, KCl 5.4 mM, $CaCl_2 \bullet\ H_2O$ 1.8 mM, sodium lactate 28.6 mM), plasma lysate (NaCl 90 mM, KCl 5 mM, $MgCl \bullet 6H_2O$ 1.5 mM, sodium acetate trihydrate 26.5 mM, sodium gluconate 23 mM) and mannitol 10% (548.9 mM) were all prepared and filtered (220 nm) within two days of use.

Nanoparticles were diluted 50:50 into 2 x concentrated injectable solutions to produce final concentrations of solutions allowable for injection. Samples were incubated at room temperature, mixed, and sized immediately in their respective solutions by DLS and cavitation was confirmed in 1% agar flow phantom.

CNP solutions were primed for 2 minutes at 0.5 MHz driving frequency, 0.5 pulse repetition frequency (PRF), 1.2 MPa peak rarefactional focal pressure (PRFP), 5% duty cycle (DC) before mixing with injectables. Priming was carried out as an initial increase in power of cavitation was observed when CNPs were exposed to therapeutic ultrasound. This effect was not observed for NC or SV. Solutions were observed visually and sized repeatedly using DLS over several weeks. When particle sizes exceeded the detection limit of the DLS (max 10 microns diameter) or had a polydispersity index nearing 1, samples were discarded.

2.4.1 Effect of salt concentration

The role of salt in a charged particle suspension varies depending on the concentration. At low concentrations (1 mM) like charged particles repel by electrostatic forces, however at high concentrations (100 mM) these forces are screened until attractive van der Waals forces dominate [58]. Carbon black with a quaternary group was tested for stability at varying ionic strengths. The coagulation rate increased with increasing ionic strength of NaCl (Figure 2.2) which was explained by a decrease in the Debye length (a measure of the double layer thickness around each particle) with increasing ionic strength [192].

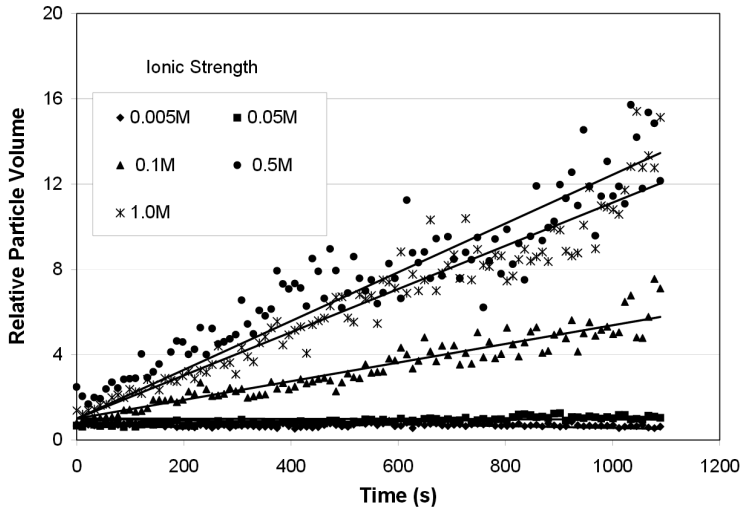

Figure 2.2: *Coagulation of cationic carbon black (BP700) as a function of ionic strength (NaCl). Image taken from [192] (Yu et al., 2002).*

2.4.2 Effect of surface charge

The charge of the outermost layer of a nanoparticle is critical in determining the particle stability in solution. Generally particles with a zeta potential greater than +30 mV or less than -30 mV are considered to be stable in solution [65] unless they have another form of stabilisation such as steric stabilisation.

2.5 Stability testing of drug carrying liposomes

Temperature stability of the liposomes was tested by immersion in a waterbath at 37°C and 43°C for 15 minutes. Low temperature sensitive liposomes have been previously developed by Dromi et al. [57] to respond to temperature rises of 5 °C, which is why the temperature of 43°C was chosen as a comparison. Samples were removed from the waterbath and assessed for luciferin release according to the luciferin - luciferase assay described in Section 2.8.1.

2.6 Ultrasound exposure

2.6.1 Experimental setup

A 0.5 MHz spherically focused, single element focused transducer (H-107D SN13; Sonic Concepts, Bothell, Washington, USA) was used as the driving transducer to insonate samples at its fundamental, 0.5 MHz, or third harmonic, 1.614 MHz. The elliptical focal zone at -6dB measured 4 x 4 x 37 mm^3 equivalent to 310 μL at 0.5 MHz (Figure 2.3). A circular cut-out

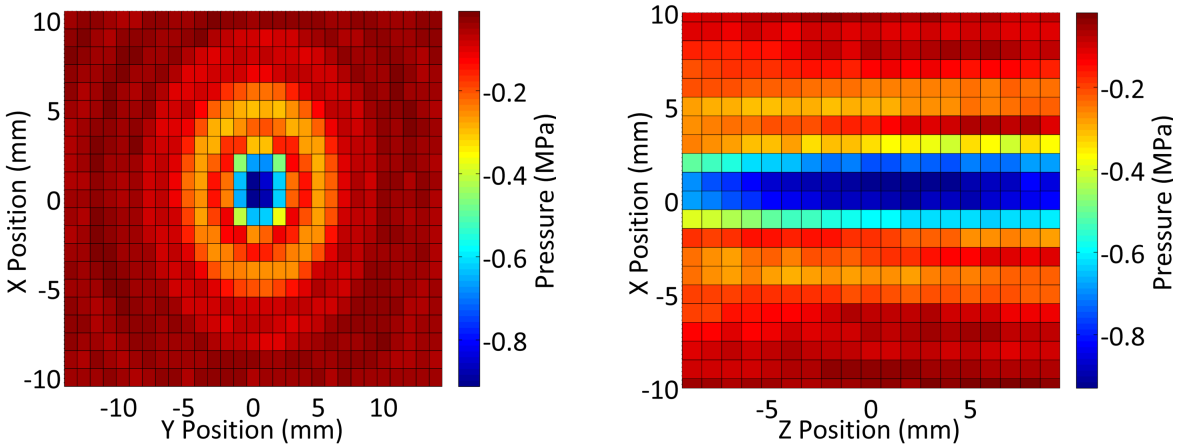

(a) *XY Beam Profile* **(b)** *XZ Beam Profile*

Figure 2.3: *Beam profile of the 0.5 MHz transducer in the (a) XY plane and (b) XZ plane. A 22 cycle pulse, burst period of 10 msec and function generator input of 50 mV was used. A 0.4 mm needle hydrophone (ONDA 1056) was used for both scans.*

in the transducer allowed for the alignment of a smaller transducer to be used as a passive cavitation detector (PCD) as discussed below (Figure 2.6). Custom made software using LabView 8.5 (National Instruments) was used to control and collect ultrasound signals. Voltage pulses from a function generator (33250A, Agilent Technologies, Santa Clara, CA, USA) were amplified using a 55 dB, 300 Watt, RF power amplifier (A300 Power Amplifier, 017098, Electronics and Innovation, Rochester, NY, USA), and passed through its matching network to the driving transducer. An absolute pressure calibration at the fundamental frequency (Figure 2.4) and third harmonic (Figure 2.5) and beam profile characterization (Figure 2.3) were performed using a 0.4 mm diameter needle hydrophone (ONDA 1056, Onda Corporation, Sunnyvale, CA, USA) and a 0.075 mm diameter needle hydrophone (PA 1594, Precision Acoustics, Dorset, UK). The average of the two measurements at the fundamental frequency was used to calculate input voltages to the function generator (Figure 2.4). All pressures reported throughout the present study are peak rarefactional focal pressures (PRFPs) in MPa.

All ultrasound exposures were conducted in a water tank heated to 37°C unless otherwise stated. Water from a Flexeon 300 (GAPS, Lancashire, UK) water system was filtered (400 μm) and degassed in the tank for at least 1 hour before experiments were conducted.

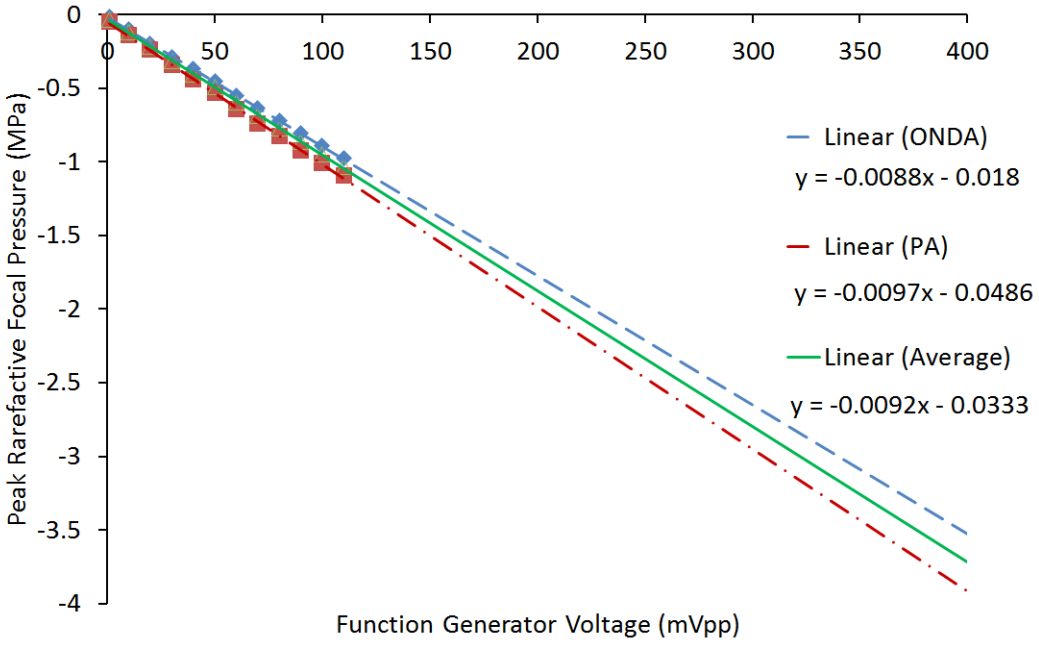

Figure 2.4: *Absolute pressure calibration of 0.5 MHz transducer (H107D13) using ONDA 1056 and PA 1594 extrapolated to 400 mV. Linear trend-lines and equations shown of ONDA (blue dashed), PA (red dot dashed) and the average of the two (green solid).*

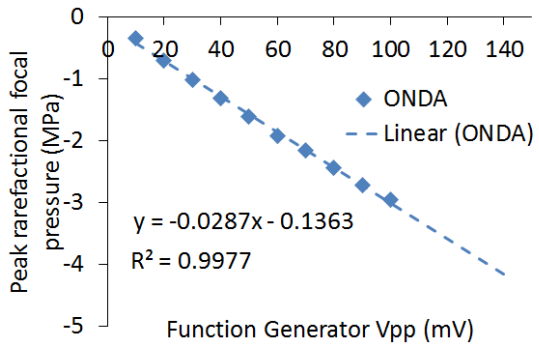

Figure 2.5: *Absolute pressure calibration of 0.5 MHz transducer at its third harmonic, 1.614 MHz, (H107D13) using ONDA 1056 extrapolated to 150 mV. Linear trend-line used for interpolation and extrapolation shown.*

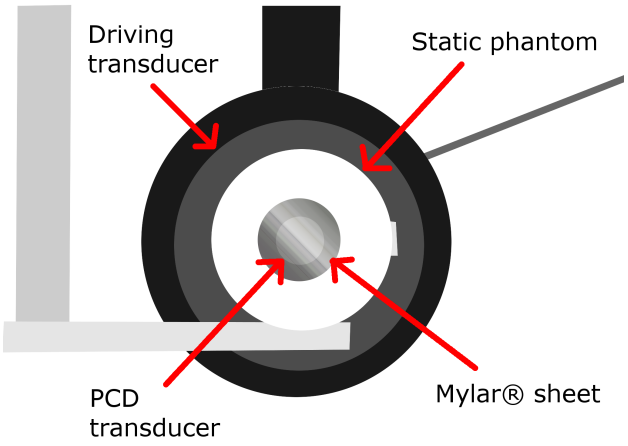

Figure 2.6: *Diagramatic representation of static phantom aligned with driving transducer and PCD transducer (behind).*

2.6.1.1 Static phantom

A Delrin® cylindrical phantom (diameter = 20 mm, width = 20 mm, volume = 6.8 mL) with Mylar® sheets on the front and back face was used to hold each sample (Figure 2.6). The front face of the holder had bevelled inner edges and the front screws holding the Delrin piece to the holder were ground down to minimise reflections from the driving transducer. The holder had a hole drilled into the side to allow sample loading through a needle. A 3D positioning system was used to immerse the phantom in the water tank, aligned with the driving transducer focus (-6 dB focal volume = 167 μL) and PCD focus (-6 dB focal volume = 6.6 μL).

2.6.1.2 Agarose flow phantom

A 1% agarose (UltraPure™ Agarose 1000, 16550-100, Invitrogen) flow phantom was prepared by filling OptiCells™ (155331, Nunc, Thermo Scientific) with in-house channel space savers in place. Two steel 2 mm diameter rods were inserted through drilled holes at each end of the OptiCell, 25 mm apart. The agarose phantoms were stored at 4°C to allow the agarose to set. Rods were removed creating two hollow channels. Double ended blood collection needles (21G, 368609, BD Vacutainer) were attached to polyvinyl chloride tubing (1mm inner diameter, 2 mm outer diameter, 8001-0102, Nalgene, Thermo Scientific) connected to syringe pumps (NE-1000, World Precision Instruments, Hertfordshire, UK) in series. Flow phantom channels were aligned to the focus of the driving US transducer (-6 dB focal volume

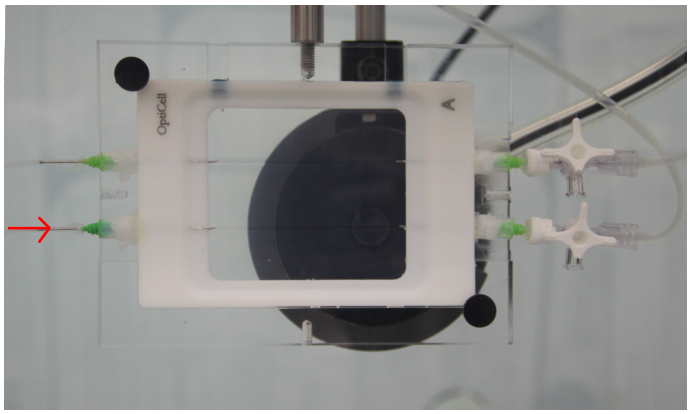

Figure 2.7: *Flow phantom aligned with transducer on bottom channel at the right most position. Red arrow indicates direction of flow.*

= 12.57 μL in channel volume) and PCD (-6 dB focal volume = 2.7 μL) and moved 10 mm horizontally to expose different regions along the channel (Figure 2.7). Flow rate was set to 1 mL/min for each experiment which corresponds to the approximate blood flow rate in a 1-2 g tumour [182]. This phantom was used to more closely simulate *in vivo* conditions and was able to be used for cell culture and fluorescence measurements. The pore size of 1% agarose is estimated to be 485 nm [145] where pores are measured within a gel matrix.

2.6.2 Ultrasound parameters

Several variables were tested when characterising both cavitation behaviour and dynamics as well as drug release. Ultrasound exposure time was varied between 30 sec and 10 min in cavitation dynamic studies. Peak rarefactional focal pressure (PRFP) was varied between 0 MPa and 4 MPa to test cavitation thresholds. Ultrasound driving frequency was set to 0.5 MHz or 1.614 MHz with responses at the higher frequency giving an indication of response at frequencies obtained with a diagnostic probe. Pulse repetition frequency (PRF) was varied between 0.5 Hz and 5,000 Hz allowing for number of cycles to vary correspondingly. Acquisition of PCD data was either 1 trace of duration 250 μsec synchronized with the therapeutic ultrasound pulse repetition frequency, or continuous trace collection of duration 250 μsec every 15 ms. Unless otherwise stated, the duty cycle was kept constant at 5% and the therapeutic ultrasound focus was positioned at the central position of each phantom.

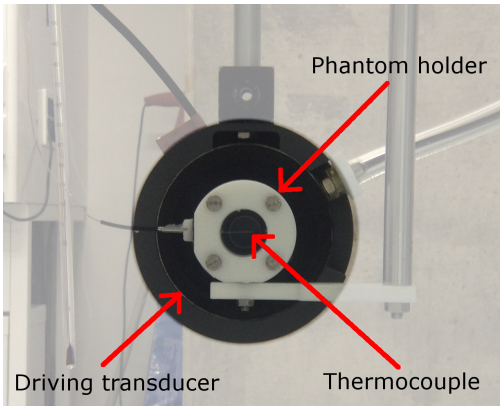

Figure 2.8: *Temperature monitoring during ultrasound exposure.*

2.6.3 Temperature monitoring

The influence of ultrasound exposure on temperature increase was assessed by placing a thermocouple (Type T, Omega Thermocouple) connected to a thermocouple reader (TC-08, Pico Technology Ltd) within the phantom during exposure, with a 100 msec sampling interval, as shown in Figure 2.8. The thermocouple diameter was 0.2 mm which is substantially smaller than the driving ultrasound wavelength to avoid heating artefacts. The study was conducted in a tank at room temperature and in a tank pre-heated to 37°C. The sample was at room temperature before immersion in the tank in both cases.

2.7 Cavitation detection

2.7.1 Experimental setup

Acoustic emissions were detected passively using a 7.5 MHz single element focused transducer (SN 671678, Panametrics, Waltham, MA, USA) referred to as the passive cavitation detector (PCD). The PCD frequency (7.5 MHz) is at least 10 times the therapeutic ultrasound (US) fundamental frequency (0.5 MHz) to enable preferential detection of high-frequency emissions whilst avoiding saturation from the therapeutic ultrasound fundamental and its harmonics. The -6 dB focal zone of the PCD is 0.866 x 0.866 x 16.9 mm^3, i.e. 6.636 μL at 7.5 MHz. It should be noted that the -6 dB beamwidth on receive will be approximately three times larger (3.2 mm) at the lowest receive frequency of 2 MHz, but is in all cases smaller than the -6 dB beam-width of the therapeutic ultrasound transducer (4

mm). The PCD was inserted through a central opening in the driving transducer and was confocally and coaxially aligned with the driving transducer. Voltage signals were filtered using a 2 MHz analogue high pass filter (FILT-HP2-A, Allen Avionics Inc., NY, USA) to exclude reflections of the driving frequency, amplified by a factor of 5 (SR445A, Stanford Research Systems, Sunnyvale, CA, USA), and acquired using a DAQ card with a sampling frequency of 100 samples per microsecond and trace length of 250 microseconds. Traces were either taken every 15 milliseconds (continuous acquisition) or taken at the beginning of each pulse, timed to the trigger (1 trace per pulse mode). The traces were saved on a computer before data analysis. Deionised water (Milli-Q, Merck, UK; 200 nm filtered, 18.2 MΩ.cm) was used as a background control in each phantom holder for all experiments and was not degassed prior to use unless otherwise stated.

2.7.2 Data analysis

Voltage data from ultrasound exposure experiments was acquired with Labview 8.5 and post processed using custom code in Matlab® (MathWorks). The main file used to analyse all data was analyse_smg_autoget.m which called three main functions detailed in Appendix B.

A flow chart outlining the data post processing is shown in Figure 2.9. Briefly, voltage data was collected from the DAQ and then divided by the SRS amplification used (5 or 25 times amplification). The DC bias was removed and a Hamming window applied. A Fast Fourier Transform (FFT) was applied to convert the data from the time domain to the frequency domain. The output was adjusted for the Hamming window with a weighting factor and the magnitude of the FFT was taken. The frequency data was truncated to 0 to 15 MHz to save on computational memory. The single sided Power Spectral Density (PSD) was calculated by: taking the square of the magnitude of the FFT (in V^2); taking half the data (already truncated to 0-15 MHz, and assumed 0 power between 15 MHz and 50 MHz); multiplying by 2 because only taking the single sided PSD; scaling the FFT by dividing by length and sampling frequency (mathematically, the FFT divided by the length is squared, and then scaled by multiplying by length and dividing by sampling frequency); and dividing by the impedance of the transducer (assumed to be 50 Ω) to convert from

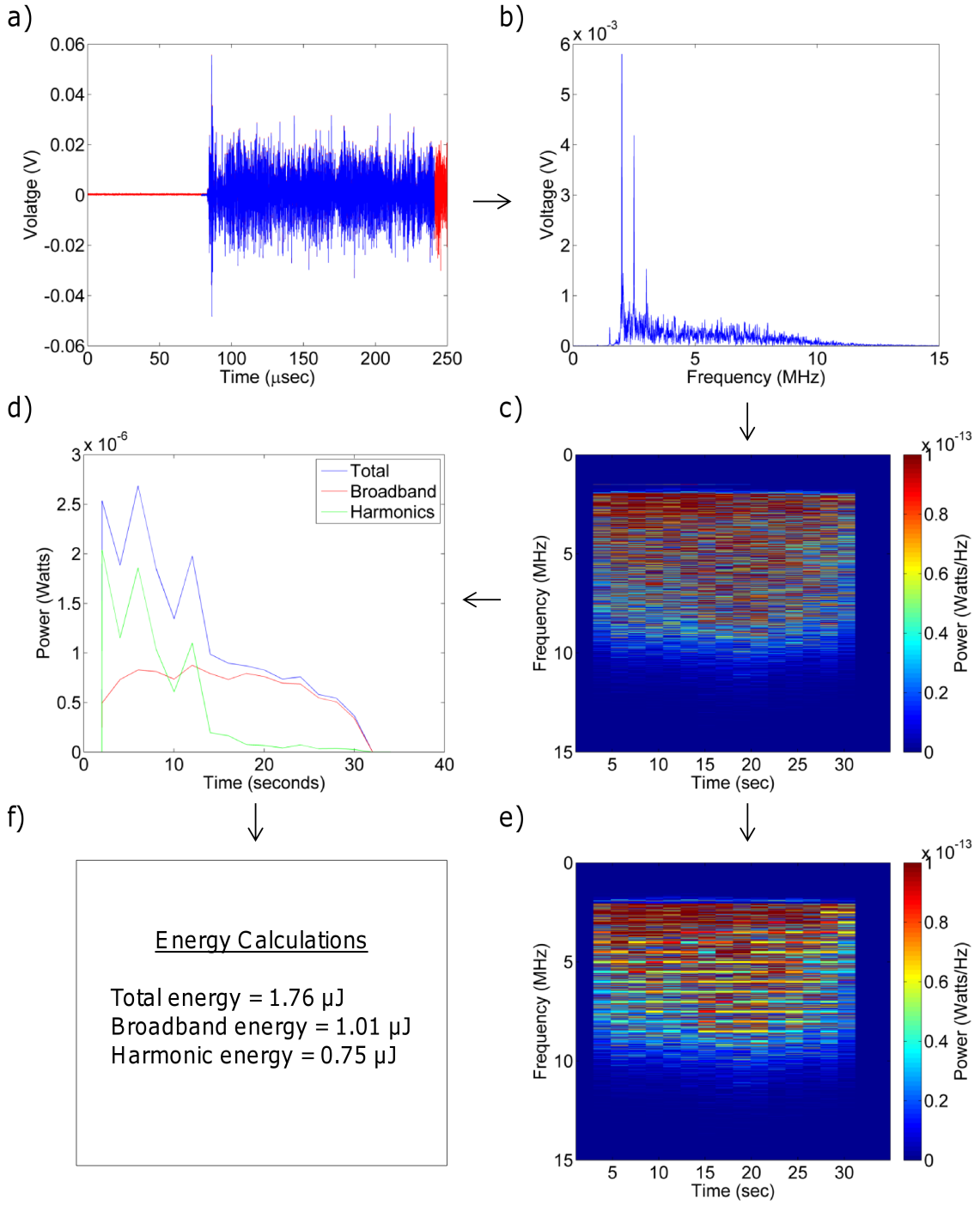

Figure 2.9: *Flow chart outlining the data post processing used to analyse cavitation signals using SonoVue insonated at 1.5 MPa PRFP, 0.5 MHz driving frequency and 0.5 Hz PRF as an example. (a) Raw voltage trace (red) and voltage segment used for analysis (blue) (DC bias removed, clipped to earliest possible sample signal). (b) Fast Fourier Transform of the voltage segment carried out for each trace and converted into a (c) single sided Power Spectral Density (PSD) plot which was integrated over frequency and displayed as (d) power over the exposure time. (e) Harmonic energy was removed displaying the broadband-only PSD. (f) The final energies were calculated by integrating the PSD over frequency and time.*

V^2/Hz to Watts/Hz.

The 'broadband PSD' was calculated by removing energy in 'harmonic bands' from the truncated FFT by comb filtering 96 kHz bands at multiples of the driving frequency. The energy was replaced with an average of the energy in the 'non harmonic band' (404 kHz bands between the harmonic bands) before it. The PSD was calculated as before.

Power was calculated by integrating over the frequency. Total and broadband power were calculated and harmonic power was calculated as the total power minus the broadband power. Energy was calculated by integrating over time. Total and broadband energy were calculated and harmonic energy was calculated as the total energy minus the broadband energy.

2.8 Monitoring drug release in vitro

Liposomal samples (50 to 100 μL) were diluted in PBS (approx 6.5 mL) and mixed with or without SV microbubbles (300 μL), or diluted directly in the nano cavitation nuclei solution of either NC or CNPs, in the static phantom. In some studies, a magnetic PTFE stir bar with a stir plate (Variomag Compact, Thermo Electron Corporation) was used to mix samples for 15 seconds, 1 minute before ultrasound exposure (Figure 2.10[2]). Samples were insonated at PRFPs of 0.14, 0.5, 0.8, 1.2 and 1.5 MPa with corresponding intensities shown in Table 2.2[3]. A pulse length of 100 millisecond and burst period of 2 seconds (i.e. 5% DC) was used to insonate each sample for 30 seconds unless otherwise stated. Samples were removed from the phantom holder immediately and stored in tubes in racks on ice in a lidded container. Importantly, the tubes were not submerged in the ice as this resulted in increased drug release. Disruption of echogenic liposomes has also been observed upon cooling which may follow a similar mechanism [110].

[2]Ultrasound setup is published in the Journal of Controlled Release, Supplimentary Figure 1

[3]Ultrasound exposure conditions are published in the Journal of Controlled Release, Supplimentary Figure 2a

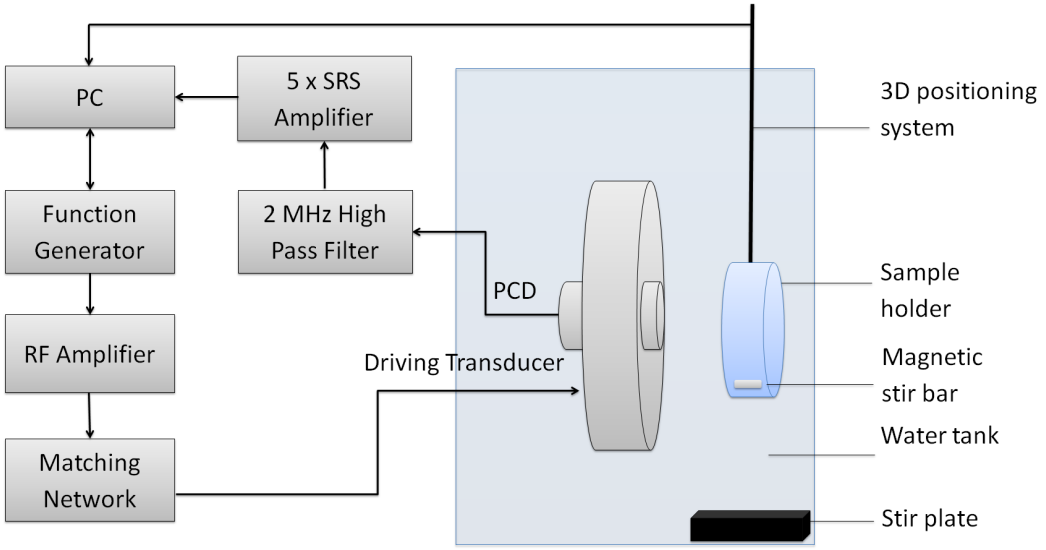

Figure 2.10: *Schematic diagram of the in vitro ultrasound exposure setup used for testing drug release (not to scale). Samples were loaded into the phantom holder and stirred before insonation. The passive cavitation detector (PCD) and driving transducer were coaxially and confocally aligned with the centre of the sample holder. The amplified signal from the function generator was impedance matched before pulsing through the driving transducer. Acoustic emissions were captured using the PCD and the electrical signal was filtered, amplified and then saved on the computer. Image taken from [79] (Graham et al., 2014) with permission from Elsevier.*

Table 2.2: *Pressures used in vitro with corresponding ultrasound exposure intensities. Table taken from [79] (Graham et al., 2014) with permission from Elsevier. MI should strictly speaking not be used for pulses of ultrasound longer than a single cycle, and is included here for reference only.*

PRFP	I_{SPTP}	I_{SPTA}	I_{SPPA}	**MI**
MPa	**kW/cm^2**	**kW/cm^2**	**kW/cm2**	
0	0	0	0	-
0.14	0.001323	3.31E-05	0.000662	0.198
0.5	0.01688	0.000422	0.00844	0.707
0.8	0.043214	0.00108	0.021607	1.131
1.2	0.097232	0.002431	0.048616	1.697
1.5	0.151924	0.003798	0.075962	2.121

2.8.1 Luciferase model

A luciferin - luciferase model was used to quantify drug release from liposomes. Solutions were prepared as follows: Luciferase (L9506 from Photinus pyralis (firefly), Sigma) was disolved in a pH 7.5 buffer of 4-(2-hydroxyethyl)-1-piperazineethanesulfonic acid (HEPES) (25mM), ethylenediaminetetraacetic acid (EDTA) (2mM), magnesium chloride (MgCl) (24mM), bovine serum albumin (BSA) (60 μg/mL), dithiolthreitol (DTT) (40 μg/mL) to a concentration of 20 μg/mL. Adenosine triphosphate (ATP) was dissolved in pH 7.5 buffer of HEPES (4-(2-hydroxyethyl)-1-piperazineethanesulfonic acid, 25 nM) and EDTA (2 mM) to a concentration of 1 mM.

Luciferin was encapsulated into liposomes as described in Section 2.2. Exposed liposomal samples and non liposomal controls were divided into two portions. 200 μL sample was heated to 100°C for 30 seconds in 0.5 mL microcentrifuge tubes (10458312, amber, Fisher Scientific). Note that the size of the Eppendorf tube affected the heating rate and thus the quality of results. Subsequently, both unheated and heated samples were stored at 4°C to reach the same temperature. Samples were assayed in white 96 well plates with final volumes of 25 μL 1mM buffered ATP, 25 μL 20 μg/mL buffered luciferase, 90 μL PBS and 10 μL sample per well. A luciferin standard curve was prepared and assayed in the same way to ensure the samples tested were in the linear range of luminescence of the plate reader (FLUOstar Omega, BMG Labtech, Aulesbury, UK).

Luminescence was measured in a plate reader (FLUOstar Omega, BMG Labtech, Aulesbury, UK) with an orbital shake at 500 rpm before measurements. **Percentage release** was calculated as the luminescence of non heated sample divided by luminescence of the corresponding heated sample, multiplied by 100. **Percent increase in release** was calculated as the luminescence of the sample, Lum_{sample}, minus the average luminescence of the corresponding no-ultrasound control samples, $AvLum_{noUS}$, divided by the luminescence of the heated sample, $Lum_{sample100C}$, minus the average luminescence of the corresponding no-ultrasound control samples. Equation 2.3 is provided for clarity:

$$\% \text{ Increase in release} = \frac{Lum_{sample} - AvLum_{noUS}}{Lum_{sample100C} - AvLum_{noUS}} x100 \tag{2.3}$$

2.8.2 Doxorubicin model drug

Doxorubicin was loaded into liposomes as a model drug. Release was measured in a plate reader (FLUOstar Omega, BMG Labtech, Aulesbury, UK) with an orbital shake at 500 rpm before measurements. Liposomes were stored at room temperature (test sample) or heated to 100°C for 30 seconds in 0.5 mL microcentrifuge tubes. Note: temperature disruption was used instead of Triton-X disruption to avoid any chemical reaction with the doxorubicin (personal communication, Prof. Robert Carlisle, 2013). Release was measured in a black 96 well plate in a plate reader by the increase in fluorescence at excitation of 490 nm and emission at 590 nm.

2.9 Monitoring particle delivery and drug release in vivo

2.9.1 Animals

All animals were handled in accordance with Home Office regulations. In both mouse models used, tumours were allowed to grow until a maximum size of 1200 mm^3 above which animals were euthanized.

2.9.1.1 Preliminary cavitation and pharmacokinetics experiments *in vivo*

For preliminary ultrasound experiments and for pharmacokinetic studies, female BALB/C mice were used. Mice were subcutaneously implanted with 200,000 CT-26 cells in 100 μL of PBS.

2.9.1.2 Drug delivery experiments *in vivo*

For drug delivery experiments, female C57Bl/6 mice were used. Mice were subcutaneously implanted with 500, 000 B16 F10 - LUC cells in 100 μL of PBS.

2.9.2 Pharmacokinetics

Pharmacokinetics of NC particles was assessed using fluorescently labelled, FITC, LB3 NCs. Particles were injected at 4 different concentrations from lowest to highest to ensure early

identification of any potential unpredictable toxic side effects. Particles were injected (100 μL) as a single bolus into the tail vein at concentrations of 0.49, 1.23, 3.07, and 6.14 mg/mL. One mouse was injected with 0.05 mg NC with blood samples taken at 5, 15, 30 and 60 minutes. One mouse was injected with 0.12 mg NC with blood samples taken at 2, 5, 15, and 30 minutes. Four mice were injected with 0.31 mg NC with blood samples taken at 5, 15, 30, and 120 minutes. Four mice were injected with 0.61 mg NC with blood samples taken at 5, 15, 30 and 120 minutes. A further 3 mice were injected with 0.61 mg NC with a blood sample taken at 5 minutes. All mice were culled immediately following the last blood sample taken.

2.9.2.1 Sample collection

Blood samples (20 μL) were taken at 4 time points, mixed with 5% glucose (180 μL), and centrifuged at 2000 rpm for 3 minutes. The plasma supernatant (190 μL) was removed and frozen for analysis, whilst the pellet was resuspended in 5% glucose (190 μL), re-centrifuged and the washed supernatant was frozen at -4°C for analysis. Urine and faeces samples were collected if the animals urinated or defecated within 2 minutes before or after blood samples were taken. Samples were frozen at -4°C for analysis. All samples were stored in amber Eppendorf tubes to minimize light exposure. Mice were euthanized at the final time point, and dissected, keeping the following organs: heart, kidneys, liver, lungs, spleen, and tumour. Organs were immediately frozen at -4°C and stored frozen in the dark for analysis.

2.9.2.2 Fluorescence analysis

Plasma samples and washed supernatant samples were thawed and assayed directly. Organs were thawed, lysis buffer (E397A, Promega, Madison, WI, USA) was added to each organ (300 mg organ/mL for tumour and liver; 100 mg organ/mL for heart, lungs spleen and kidney), and homogenized (Homogenizer, Workcenter, IKA T10 Basic, Germany). Control organs were prepared in the same way, and concentration curves were prepared by adding known volumes of cups to aliquots of homogenised organ covering the concentration range of 0% to 100% accumulation in the organ. The standard curves were incubated at 37°C for 30 minutes to mimic circulation in vivo, frozen and thawed before assaying. Samples were

assayed for fluorescence using a plate reader (FLUOstar Omega, BMG Labtech, Aulesbury, UK) with excitation wavelength of 490 nm and emission wavelength of 520 nm. Fluorescence measurements were converted to amount of cups, either as % injected dose, or mg/organ, using the standard curves prepared for each organ.

2.9.2.3 Fluorescent particle analysis

Urine samples were found to be fluorescent. Based on these measurements, further analysis was conducted to determine whether the fluorescence was associated with broken down polymer chains, or intact particles. Urine samples were diluted and analysed using FACS (FACS Calibur^{TM}, E5008, Becton Dickinson, Oxford, UK). The detection range for this machine is 500 nm to 50 μm, and the LB3 NC particles used in this experiment had a diameter of 501 nm as measured by DLS, which is at the lower edge of the detection limit. Although literature suggests that particles greater than 9 nm in size cannot be cleared through the glomerulus of the kidney [37,120], samples were analysed nonetheless. Concentration curves were prepared in the urine and analysed in the same fashion as the sample urine accounting for the dilution required for each urine sample.

2.9.3 In vivo ultrasound experimental setup

2.9.3.1 Preliminary cavitation experimental setup *in vivo*

The experimental setup used for preliminary animal experiments was almost identical to that used in vitro. In addition to the *in vitro* setup, alignment of the transducers was performed using a B-mode diagnostic ultrasound probe (L14-5w linear array, 55 mm wide field of view, Zonare Medical Systems, Inc., CA, USA) and imaging system (17367, Z.One Engine, Zonare Medical Systems, Inc., CA, USA). The image depth used for alignment and image capture was 8 cm. The ONDA hydrophone needle was aligned to the therapeutic ultrasound and PCD foci, and used to align the Zonare probe to the focus. The hydrophone was removed and the mouse tumour was aligned to the driving transducer focus using the Zonare B-mode probe. The focus was aligned to the centre of the tumour, and multiple positions were chosen laterally for ultrasound exposure. Tumours were imaged when aligned, and the B-mode probe was turned off during therapeutic ultrasound exposure.

2.9.3.2 Drug delivery experimental setup *in vivo*

To assess cavitation activity and drug release, mice were separated into 8 groups: (1) no cavitation nuclei control with ultrasound; (2) SV and ultrasound; (3) NC low concentration (6.14 mg/ml) no ultrasound; (4) NC high concentration (25.75 mg/ml) with ultrasound; and (5) NC high concentration (25.75 mg/mL) with ultrasound. Each group contained 4 mice. In addition, 2 mice were injected with NC at the low concentration (6.14 mg/ml) and exposed to pressure ramps to determin the cavitation threshold of the tumour. Every group was also injected with DSPE liposomes. In total, 22 mice were used for this study.

The experimental setup for drug delivery experiments utilised a passive acoustic mapping (PAM) set-up developed by Dr Christian Coviello and Calum Crake, to acquire 2D maps of cavitation events for improved spacial resolution compared with a single element PCD. A diagrammatic representation of the transducer and mouse configuration is shown in Figure 2.11. A 0.5 MHz driving transducer (H-107-B-10; Sonic Concepts, Bothell, Washington, USA) with rectangular cut-out to fit a broadband linear array (L-11-4v, 128 element linear array, Verasonics, WA, USA) was used to insonate tumours. Both transducers were coaxially aligned using a 75 μm needle hydrophone (PA 06022, S/N 1947; Precision Acoustics, Dorset, UK). A host PC, linked to the Verasonics system (Verasonics Vantage 256 research ultrasound system, Kirkland, WA, USA), was used to control a function generator (Agilent Technologies, Santa Clara, CA, USA), which generated pulses amplified by a 55 dB power amplifier (1040L Power Amplifier, SN 1054, Electronics and Innovation/Precision Acoustics, Rochester, NY, USA), before passing through the matching network to the driving transducer.

The focus of the transducer was aligned to at least 2 mm inside the skin along the longitudinal axis of the transducer and moved to 3 positions approximately 3 mm apart. The first position was chosen at the cranial end of the tumour, and moved 3 mm between each position caudally down the tumour, remaining in the same longitudinal and lateral plane relative to the transducer. The driving transducer had an approximate 4 x 4 mm, -6 dB focal region which ensured an approximate overlap of 1 mm when moving the focus caudally down the tumour.

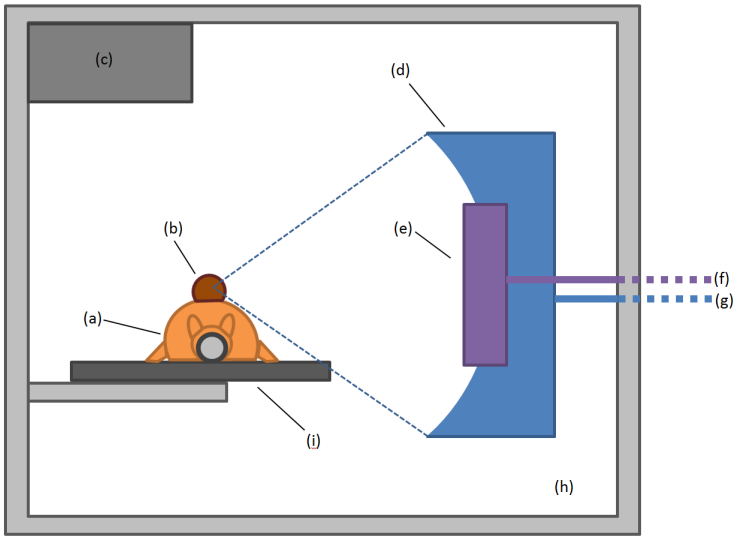

Figure 2.11: *Transducer and mouse configuration for drug delivery experiments in vivo. (a) C57Bl/6 mice bearing (b) B16F10-luc tumours were anaesthetised and secured to a (i) planar mount. Mice were suspended in a (h) water tank heated to 37°C using (c) an immersion water heater. (d) A 0.5 MHz driving transducer was coaxially aligned with (e) a linear array for B-mode imaging and passive acoustic mapping. (g) a function generator was used to drive the 0.5 MHz transducer and (f) a Verasonics system was used to record B-mode images and passive maps.*

2.9.4 Ultrasound exposure protocol

2.9.4.1 Preliminary cavitation protocol *in vivo*

During preliminary cavitation studies, protocols were adapted between animal experiments to make them more robust. The first protocol used (Table 2.3) was designed to minimize error due to tumour heterogeneity by using two positions. The first minute of passive cavitation data was recorded and analysed immediately to determine the tank water cavitation background energy, then the rest of the exposure was continued. If the background energy was too high (at levels expected upon injection of nuclei), steps were taken to reduce the nuclei in the tank (including filtering out organic matter).

Table 2.3: *Preliminary protocol for ultrasound exposure of tumours for detection of cavitation after injection of cavitation nuclei in vivo.*

Time (min):	0	1	3	5
US:	ON			OFF
Mouse:	Pos 1		Pos 2	out
Injection:		75 μL	75 μL	

The second protocol was developed to minimize the effect of the increased background

noise after moving the mouse (Table 2.4), which was presumably due to variations in the tumour. This decoupling of effects was achieved by including a 1 minute delay between moving the mouse and injecting the mouse.

Table 2.4: *Adjusted preliminary protocol for ultrasound exposure of tumours for detection of cavitation after injection of cavitation nuclei in vivo. Delay between moving positions and injections was introduced to de-couple effects from each action.*

Time (min):	0		0	2	3	5
US:	ON	check data				OFF
Mouse:	Pos 1			Pos 2		out
Injection:			75 μL		75 μL	

2.9.4.2 Drug delivery protocol *in vivo*

Two mice were used for preliminary pressure ramp studies to determine the background cavitation level in the tumour without cavitation nuclei injections. The pressure of 1.75 MPa was the highest pressure tested before substantial cavitation events were observed. Tumours were exposed to 9 minutes of 0.5 MHz ultrasound at 1.75 MPa PRFP, 0.5 Hz PRF, with injections of DSPE liposomes and cavitation nuclei, as well as alignment of the transducer at different positions according to the protocol given in Table 2.5. Therapeutic ultrasound was turned on before any injection to record the cavitation response (if any) of the untreated mouse tumour. Liposomes were injected before cavitation nuclei injections to ensure that any effect seen from cavitation nuclei could be solely attributed to the cavitation nuclei and not due to the liposomes. Moving the ultrasound focus within the tumour was off-set in time from any injections to assess the affect of moving the focus with no other change. The linear array was used for B-mode imaging (receiving at 9 MHz on all 128 elements, using harmonic imaging and pulse inversion) to align the transducer focus within the tumour both initially and when moving the transducer to expose a new region of the tumour, and to image in-between driving ultrasound pulses. During 0.5 MHz exposure, a B-mode image was taken before the driving pulse was generated and subsequently interleaved between driving pulses. Pulse generation was used as a trigger for PAM acquisition (250 μsec recording length). PAM reconstruction and B-mode registration were conducted using code developed by Dr Carl Jensen, and modified by Calum Crake.

The linear array used has not been calibrated on receive and as such, all data is shown as arbitrary units. It should be noted that the power and energy of acoustic emissions acquired using passive acoustic mapping cannot be directly compared to the values obtained using single-element passive cavitation detectors. This weakness of the setup was justified by the added advantage of ease of alignment and two dimensional cavitation information.

Table 2.5: *Protocol used for drug delivery testing in vivo. Tumours were exposed to 0.5 MHz, 1.75 MPa PRFP, 0.5 Hz ultrasound for a total of 9 minutes. DSPE liposome injections, cavitation nuclei injections, reposition of the focus and measurements taken are all shown.*

Time (min)	US	DSPE injection	Cavitation nuclei injection	Move	Measurement
-1					Photo
0	ON			Position 1	
0:10		100 μL			
1			33.3 μL		
3				Position 2	
4			33.3 μL		
6				Position 3	
7			33.3 μL		
9	OFF				
10					Photo
11					Whole mouse IVIS
15					Blood sample
16					Tumour IVIS (dorsal)
16					Tumour IVIS (frontal)

2.9.5 Drug delivery monitoring

Drug delivery was monitored by luminescence. Luminescent signal is only present if free luciferin interacts with luciferase enzyme, produced by the B16 F10 - LUC tumour cells. In this way, luminescence was used to monitor drug delivery to the tumour, and did not measure the amount of luciferin that was still encapsulated in liposomes *in vivo*.

All animals were imaged using IVIS (IVIS 100 system; Caliper Life Sciences, USA) 11 minutes after treatment began to show total payload delivery to the tumour. Animals were euthanized, tumours removed, and imaged using IVIS with the dorsal side upwards and then frontal side upwards.

Tumours were frozen before homogenization as described above at a concentration of

200 mg tumour per mL lysis buffer. Samples were assayed for luciferin using the luciferin-luciferase assay, as well as for NC-FITC by fluorescence.

Additionally, blood was taken before animals were euthanised, and plasma was separated by centrifugation, 2000 g for 3 minutes, in glucose 5%. Half the plasma was stored at 4°C for luciferin detection, and half was stored at -20°C for NC-FITC detection.

Chapter 3

Development and characterisation of cavicatalytic nanoparticles

Cavitation events have the potential to be used as a 'trigger' for drug release from liposomes. Cavitation can be nucleated from a bubble, for example a shelled bubble such as SonoVue®, or from gas entrapped on a solid surface which is then able to be removed from the surface to become a free bubble. Commercially available shelled bubbles are on the micron size scale and are constrained to the vasculature supplying the tumour. Solid particles on the other hand are able to be fabricated in the 'nano' size range, and may therefore be able to extravasate through the leaky tumour vasculature and penetrate deeper into tumour tissue. By entrapping gas on the surface of the particle, the particle may then be able to be carried into a tumour to nucleate cavitation deeper within the tumour. Furthermore, shelled bubbles have been developed as diagnostic ultrasound contrast agents (UCA). When attempting to use UCAs as inertial cavitation nuclei during ultrasound therapy, they are rapidly destroyed over time-scales of tens of seconds. A highly desirable property of solid cavitation-inducing particles would be sustained cavitation response on the order of minutes during prolonged ultrasound excitation.

In this chapter, the development of cavicatalytic nanoparticles is discussed. Firstly, the multiple 'failed' particles, which were either micron sized or were non-cavitation-responsive particles, are outlined. Insights from these studies were used in the development of particles that satisfied the criteria of being on the 'nano' scale and also decreased the pressure

threshold for instigation of cavitation of surrounding media. These 'successful' particles are analysed in detail below.

The different cavitation inducing particles studied (SonoVue® microbubbles (SV), Carbon Nanoparticles (CNP), and Polymeric Nano Cups (NC)) are described in terms of their physical characteristics, and then analysed in detail with respect to their cavitation response to varying ultrasound conditions.

3.1 Defining 'cavicatalytic'

As this field is still developing, various terms have been used in the literature and in scientific discussions to describe ultrasound responsive particles. The term 'sonosensitive', literally meaning sensitive to sound, has been used to describe liposomes which release a payload when exposed to high intensity ultrasound [62–64, 113], and also to describe solid particles which nucleate cavitation [185]. For the latter, the particle is not affected by ultrasound exposure and therefore is not 'sensitive' to it. It is apparent that a new adjective is required for this case.

For cases in which particles are found to decrease the cavitation threshold of a medium, and the particle itself is relatively unaffected by the cavitation event, the author proposes to use the term 'cavicatalytic'. This word is able to be broken down to it's derivative parts, 'cavi' from cavitation and 'catalytic' relating to catalysis. The Oxford English dictionary [140] defines 'cavitation' as "the formation of bubbles or cavities in a fluid"; and the word 'catalytic' as an adjective meaning "of the nature of, or pertaining to, catalysis", where 'catalysis' is defined as "the effect produced in facilitating a chemical reaction, by the presence of a substance, which itself undergoes no permanent change". Derived from these definitions, 'cavicatalytic' is an adjective meaning "Of particles, surfaces, structures etc.: capable of facilitating cavitation events in the surrounding liquid media without being greatly affected by the cavitation event(s) that ensue." Although the Oxford English dictionary uses the word "chemical" in the description of 'catalysis', here, 'cavicatalytic' makes no reference to a chemical reaction and indeed only refers to cavitation, a mechanical event.

To give examples using this definition, the microparticles described by Arora et al [5]

and the layer-by-layer particles described by Wagstaffe et al. [185] are both cavicatalytic as they both facilitate cavitation events in the surrounding media. The term 'cavicatalytic' was first used publicly at the Conference of the Acoustical Society of America in San Francisco in 2013 [80].

In this thesis, the term 'cavicatalytic' will be used as defined above. More specifically, a particle is deemed to be cavicatalytic if, when suspended in a particular medium and exposed to ultrasound, it instigates the production of acoustic emissions as detected by a passive cavitation detector at peak rarefactional pressures which are substantially lower than those required to instigate cavitation in the medium without that particle.

3.2 Preliminary findings

A preliminary study (Appendix A) showed that cavicatalytic particles could be produced as monodisperse suspensions on the nano-scale. This finding lead to the further characterisation of SV (as free bubbles), CNPs (as irregular rough structured cavicatalytic nanoparticles) and NCs (as uniform cavicatalytic nanoparticles with a single cavity) as candidates for therapeutic use. The production methods for these three particles is outlined in Section 2.1. These three particle types are characterised and analysed in detail in the remainder of this chapter.

3.3 Physical characterisation of cavitation inducing particles

3.3.1 Size

SV was sized using light microscopy as described in Section 2.1. Representative photos are shown in Figure 3.5. These images show that the bubbles are all spherical in nature and span a large size range with a majority of bubbles in the size range of 0.5 μm and 5 μm. In practice, the limit of resolution in these images is 0.5 μm. As such, bubbles may exist that are smaller than 500nm which can not be observed optically. It is likely however that these bubbles would be unstable and dissolve quickly [160]. Figure 3.1 shows the bubble

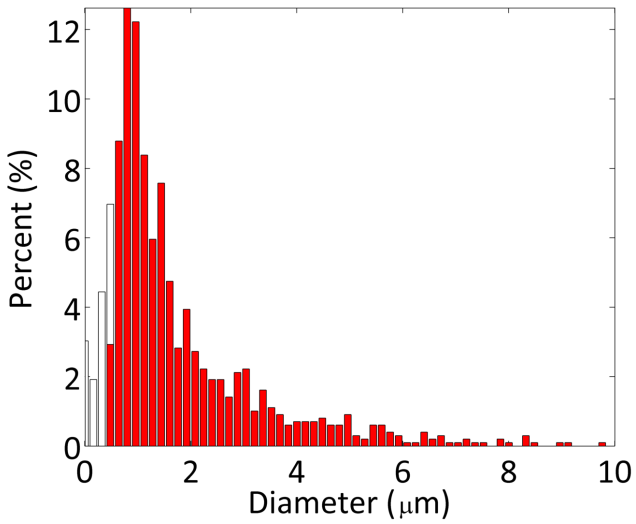

Figure 3.1: *Microbubble percent size distribution of SonoVue diluted in PBS (300 μL in 7 mL) and incubated in a water bath for 40 seconds at 37° C. Red bars show size range used for calculations shown in Table 3.1, white bars were not included due to higher error rate associated with smaller particle size in this measurement. Measurements taken using an optical microscope (see methods in Section 2.1*

size distribution with a peak at 0.896 μm and a maximum bubble size recorded of nearly 10 μm. A summary of bubble characteristics are shown in Table 3.1.

Table 3.1: *SonoVue size and concentration for bubbles subjected to 40 seconds at 37° C at diluted concentrations (300 μL in 7 mL PBS).*

	Concentration (bubbles/mL)		Bubble Diameter (μm)		
	Diluted	Initial	Mean	Mode	Median
Average	2.00E+07	4.67E+08	1.866	0.896	1.346
σ	1.54E+06	3.59E+07	0.296	0.088	0.170

A shift in bubble size was observed one day after resuspension of SV microbubbles. A 1.2-fold increase in mean diameter and a 2-fold decrease in bubble concentration (Figure 3.2) was observed suggesting Ostwald ripening had occurred [155]. Based on these results, SonoVue was used within the first 2 hours after resuspension for all experiments.

In developing a particle intended for injection into humans, it is essential that the particle retains its stability and size in solutions that are approved as vehicles for injection into humans. The size stability of CNPs was measured in 7 FDA approved injectate solutions. Hydrodynamic diameter by Z-average (Table 3.2) along with polydispersity index (PDI) (Table 3.3) were used as indicators of agglomeration using DLS. CNP suspensions

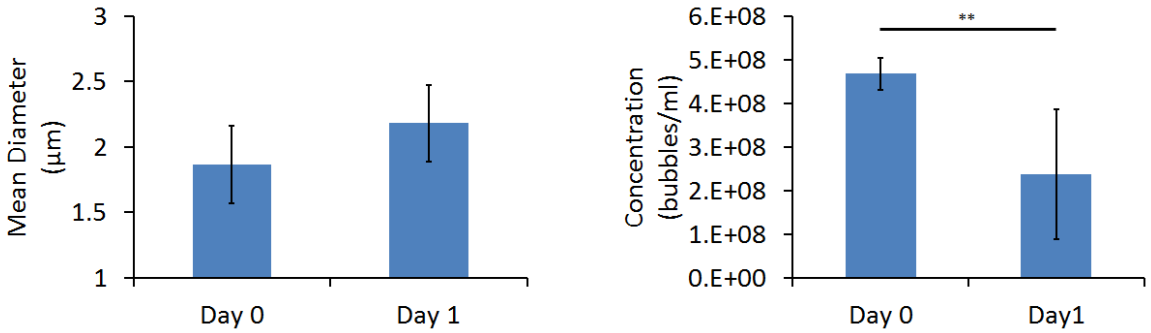

(a) *SonoVue diameter over time* **(b)** *SonoVue concentration over time*

Figure 3.2: *(a) Diameter and (b) concentration (plotted as original suspension concentration) of SV bubbles were measured immediately after resuspension, and 24 hours after resuspension. An increase in bubble diameter and a decrease in bubble concentration was observed with time. Student's t-test for significance, ** $p < 0.01$, $N = 3$, standard deviation shown.*

were homogeneous when formulated in water with each particle having a strong negative surface charge (-29.3 mV) by zeta potential, and so it was predicted that electrostatic repulsion would prevent agglomeration of particles in water. CNPs agglomerated in all solutions tested containing salt (NaCl, Ringers, Ringers lactate and plasma lysate). Sizes and polydispersities increased over incubation time, even in the few minutes between runs on the DLS during measurements when salt was present in solutions. The salt in solution could be acting to screen electrostatic repulsive forces [58, 192] allowing Van der Waals forces to dominate and cause agglomeration. Observing increased agglomeration in solutions with ionic strengths as low as 3 mM NaCl suggests that only a low level of charge screening is required to cause agglomeration of CNP particles.

Table 3.2: *Stability of CNPs in injectates. Particle Z-average, n=3, average values shown. Particles were not sized after they were deemed to be fully agglomerated and values are left as N/A.*

Z-average (nm)				
Injectate	**Days after production**			
	0	5	9	21
5% Glucose	223.7	272.2	224.6	225.1
DI water	148.8	162.0	238.2	4909.7
Mannitol	358.1	266.6	1332.1	2190.6
NaCl	1094.3	25280.0	N/A	N/A
Ringers	1016.2	24746.3	N/A	N/A
Ringers Lactate	1026.1	27179.0	N/A	N/A
Plasma Lysate	951.7	3512.7	N/A	N/A

After 5 days, the particles which had agglomerated could be seen with the naked eye,

Table 3.3: *Stability of CNPs in FDA approved injectates. Particle polydispersity index, n=3, average values shown. Particles were not sized after they were deemed to be fully agglomerated and values are left as N/A.*

Polydispersity Index				
Injectate	**Days after production**			
	0	5	9	21
5% Glucose	0.172	0.242	0.280	0.211
DI water	0.136	0.166	0.280	0.984
Mannitol	0.240	0.208	0.661	0.741
NaCl	0.338	0.665	N/A	N/A
Ringers	0.363	1.000	N/A	N/A
Ringers Lactate	0.317	0.785	N/A	N/A
Plasma Lysate	0.299	1.000	N/A	N/A

and had settled to the bottom of the tubes (Figure 3.3). CNPs in salt containing solutions all had Z-average values above 2 μm and PDI values above 0.5 and were eliminated from the study. CNPs in mannitol showed similar stability to those in DI water and 5% glucose over 5 days, however showed increasing agglomeration after 9 days. Particle distributions in water and 5% glucose remained similar from the first day to the 9th day with Z average of 238.2 nm and 224.6 nm, and PDI values of 0.28 and 0.28 respectively after 9 days. The intensity of the CNP peak in water after 9 days had reduced suggesting that some agglomeration had occurred resulting in a lower particle concentration. After 21 days however CNPs in glucose were the only particle suspensions tested which had remained stable, with Z average of 225.1 nm and PDI value of 0.21 (Table 3.2), and as such, glucose was chosen as the injectate for animal studies.

The NCs were produced in three monodisperse particle populations as shown by DLS in Figure 3.4 by the blue (NC LB1), green (NC LB3) and purple (NC LB5) solid lines. The smallest cup particle, NC LB1, had a mean diameter of 187 nm and PDI of 0.073; the medium sized cup particle, NC LB3, had a mean diameter of 475 nm and PDI of 0.195; The largest cup particle, NC LB5, had a mean diameter of 706 nm and PDI of 0.236 which according to the classification in section 2.3.1, is too large to be considered a 'nano'-particle. However, the term 'nanoparticle' is often used in the literature to mean any particle under 1000 nm.

Similar to CNPs, NCs were not stable in salt containing solutions (personal communi-

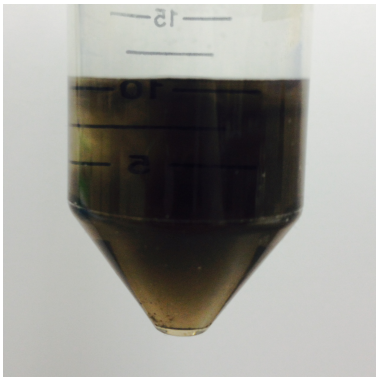

(a) *No dilution*

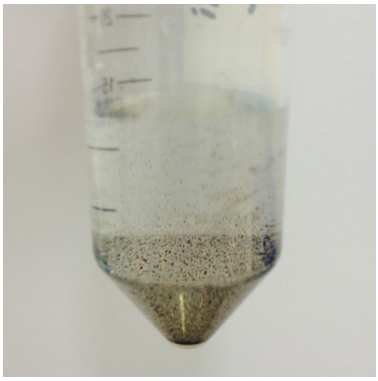

(e) *NaCl*

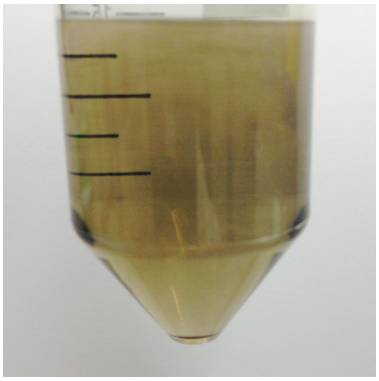

(b) *DI water*

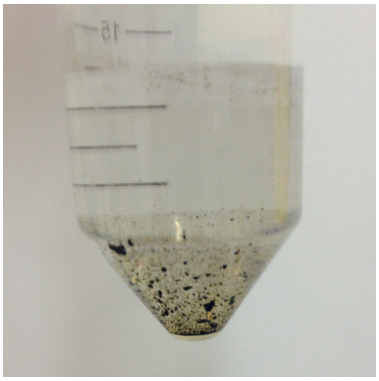

(f) *Ringers*

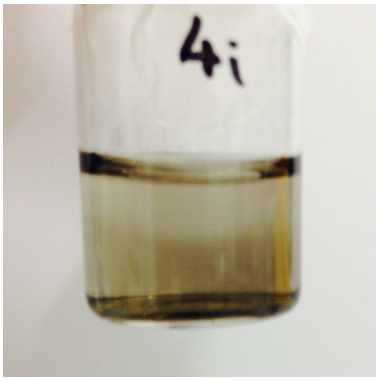

(c) *5% Glucose*

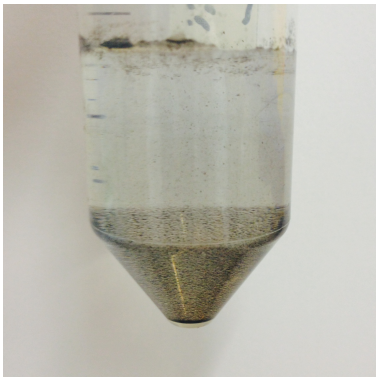

(g) *Ringers Lactate*

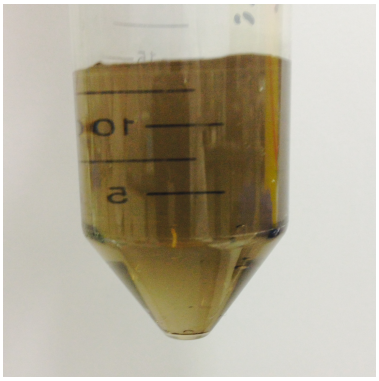

(d) *Mannitol*

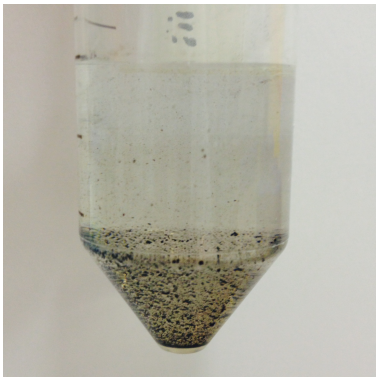

(h) *Plasma Lysate*

Figure 3.3: *Carbon nanoparticle stability in injectates after 5 days.*

cation, Rachel Myers, 2014). NCs were stable in DI water and glucose. Unlike CNPs which started to agglomerate in both water and glucose after 21 days, NCs were stable when stored at 4°C for up to 17 months. After 17 months NC LB3 were sized showing a monodisperse population with a size peak by intensity of 558.9 nm and polydispersity index of 0.067.

In summary, both CNPs and NCs are stable in DI water and in 5% glucose, an FDA approved injectate suitable for injection. NC however are stable over substantially longer time periods than CNPs making NCs more appropriate for clinical use.

The effect of therapeutic ultrasound on particle size was studied using the static phantom. Particles were exposed for 10 minutes using 0.5 MHz, 1.2 MPa PRFP, 0.5 Hz PRF ultrasound. Particle distributions shifted slightly to smaller sizes after therapeutic ultrasound exposure. CNP, NC LB1, NC LB3, and NC LB5 decreased in size by 7.5 nm, 1.0 nm, 2.8 nm and 74.7 nm respectively over the 10 minute exposure period (n=1). The size shifts observed could not be accounted for by particles being destroyed as the distribution shape is maintained, and the size shifts were not substantial. If particles were being destroyed, multiple size peaks would be expected as some particles would remain in tact, while others would break into smaller fragment populations, which was not observed. This result further points to each of these nanoparticles, CNP, NC LB1, NC LB3 and NC LB5, showing 'catalytic' properties, where the particles themselves are not greatly affected by the cavitation events, thus classifying them as cavicatalytic.

3.3.2 Morphology

The morphology of the different cavitation nuclei varies markedly. SV microbubbles are spherical shelled bubbles which varying in size (Figure 3.5). CNPs in contrast vary markedly in shape but are consistent in size (Figure 3.6) and finally NC particles are both uniform in shape and size (Figure 3.7).

Transmission electron microscopy (TEM) images were in accordance with DLS data for both CNPs and NCs. Approximate CNP diameters were on the order of 150-300 nm, as seen in Figure 3.6. The CNPs are rough in appearance with varying lengths and widths. Some particles appear longer in one dimension and shorter in the other (Figure 3.6 (a) and (b)), whereas other appear more spherical in structure (Figure 3.6 (c) and (d)). As the

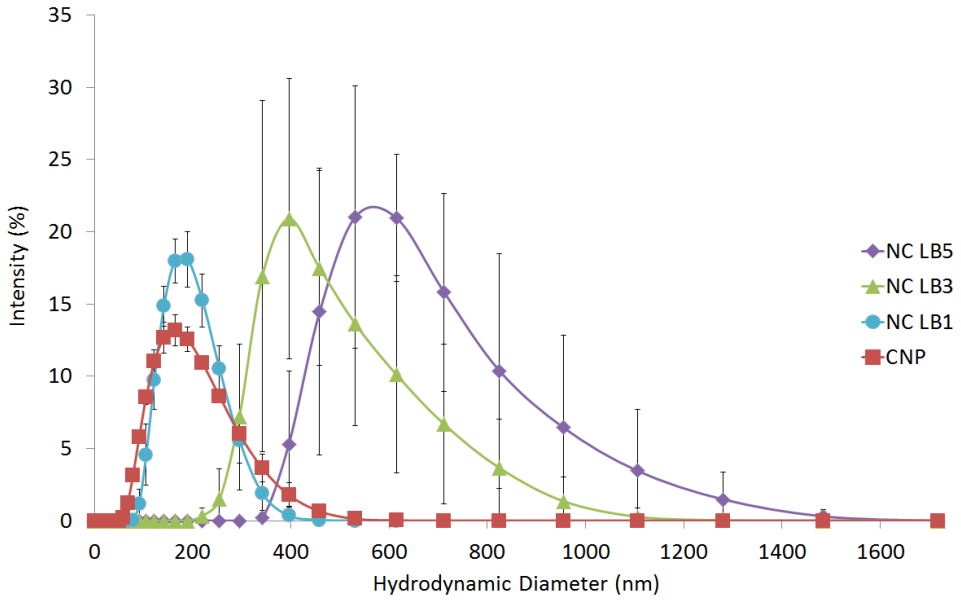

Figure 3.4: *Nanoparticle size distribution of CNP and NCs. Particle hydrodynamic diameter measurements by DLS of CNPs (red), NC LB1 (blue), NC LB3 (green), and NC LB5 (purple) are shown. N=3 batches, standard deviation shown.*

DLS technique makes the assumption that all particles are spherical, it is not able to discern between particles that are longer and thinner to those which are more globular, however it is apparent that there is a mix of particle morphologies when viewed under TEM. The surface characteristics of each particle however share the common feature of being 'rough'. Some areas on the surface have crevices on the 20 to 50 nm size scale, while others have pockets on the 100 to 200 nm size scale. Each particle has multiple crevices and pockets of varying shape and size over its surface. It is hypothesised that gas is able to be stabilised onto the surface of the CNPs either into the smaller crevices or larger pockets or in a combination of areas over each particle.

In contrast to the rough CNPs, NCs are smooth in appearance with typically a single cavity per particle (Figure 3.7). The size of the cavity for each particle is approximately the same size as the starting bead. NC LB1 has a cavity of approximately 100 nm, NC LB3 has a cavity of approximately 300 nm, and NC LB5 has a cavity of approximately 500 nm. The cup wall thickness in each case is approximately 100 nm. Tomographic modelling showed that the pale areas on the TEM that indicate less material present, are indeed open cavities in the particles (personal communication, Dr James Kwan, 2013).

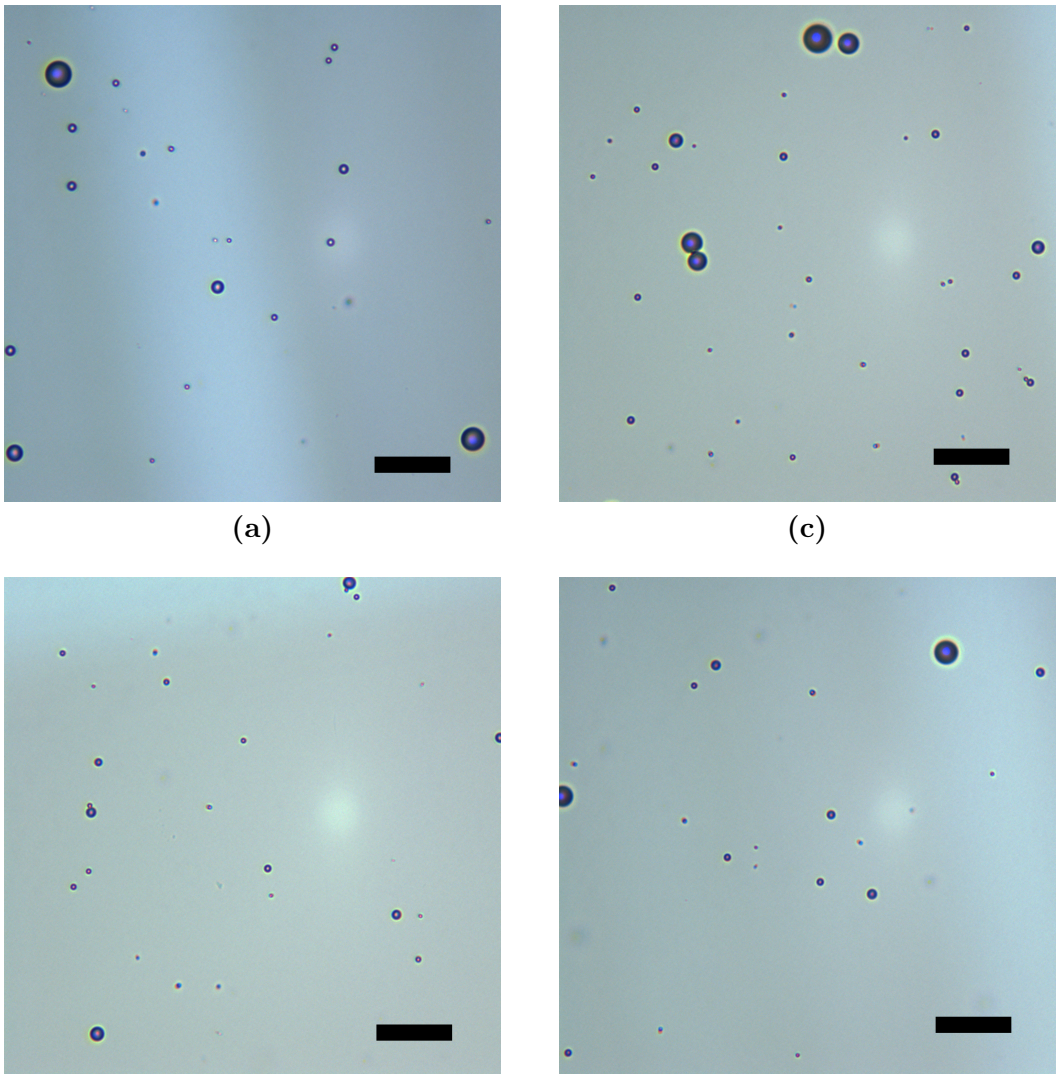

Figure 3.5: *Light microscope images of SV microbubbles heated at 37°C for 30 seconds before imaging. Images taken from separate bubble samples. These images were then processed using in-house Matlab code to measure the size distribution of bubbles in solution. 40 x objective, scale bar = 20 μm.*

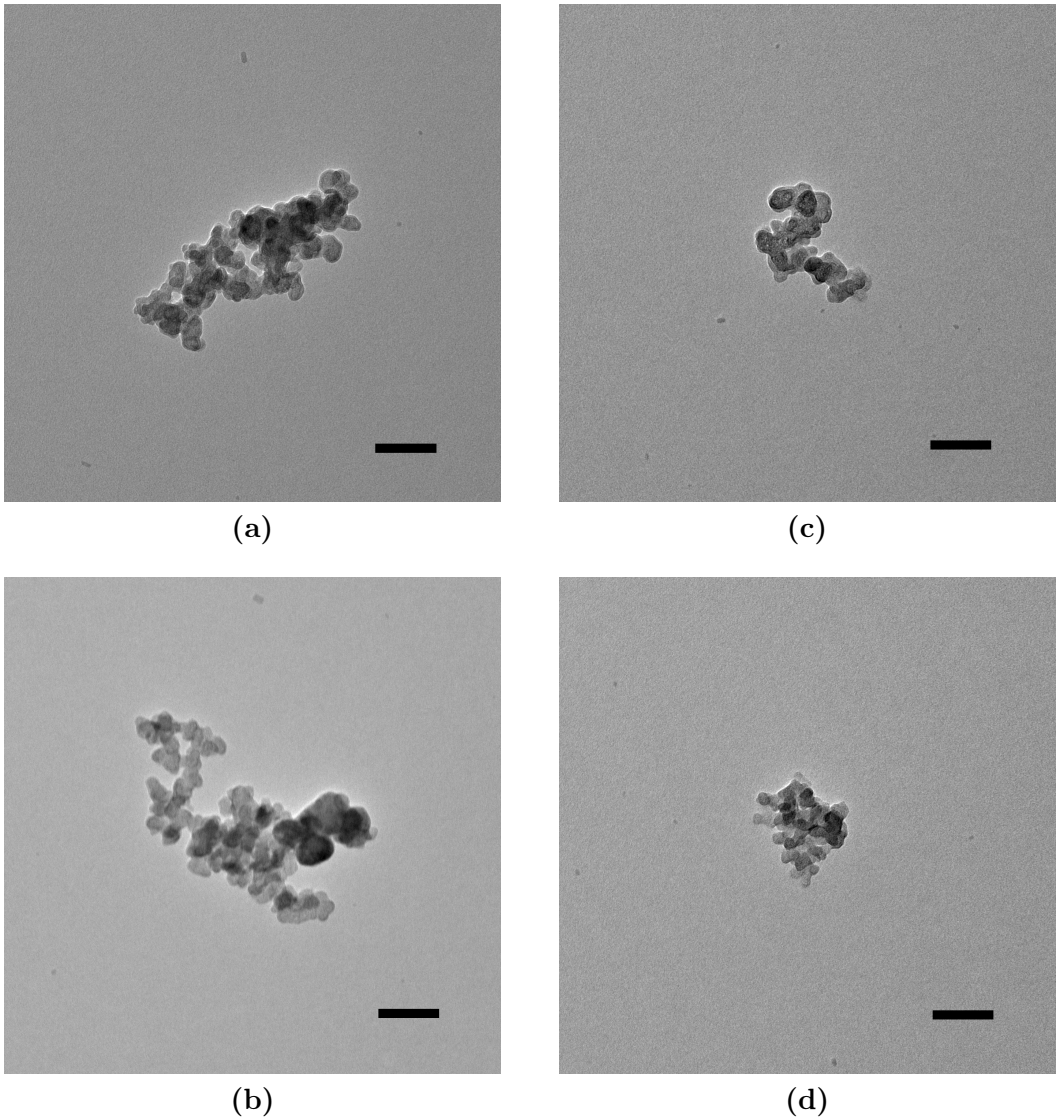

Figure 3.6: *TEM images of CNPs prepared in DI water. Images show rough surfaced particles varying in morphology, with each image (a, b, c, d) representing a different single particle. Images were selected to represent the variability in particle morphology between particles. Each single particle appears to be an agglomeration of 'smaller particles', however these possible 'smaller particles' were not observed individually. Particles were prepared in DI water before drying on Formvar-coated, copper TEM grids. Bar = 100 nm.*

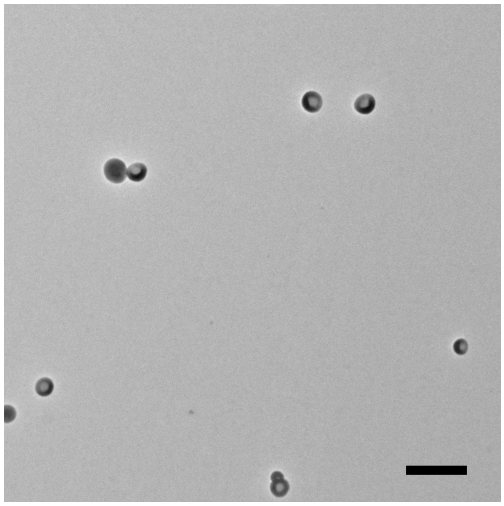

(a) *NC LB1*

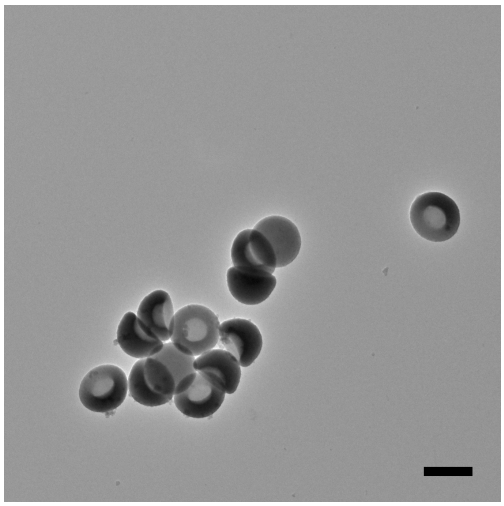

(b) *NC LB3*

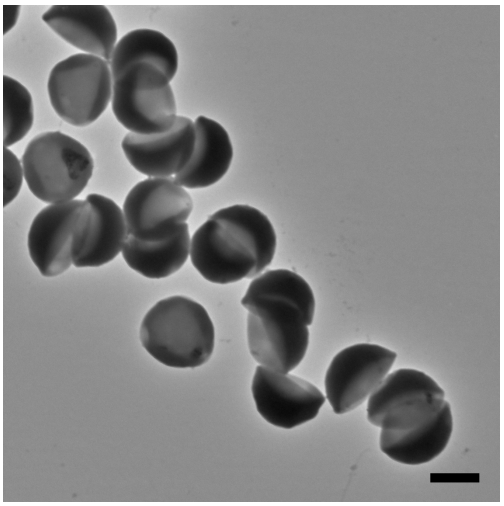

(c) *NC LB5*

Figure 3.7: *TEM images of NCs showing a range of particle sizes produced: (a) NC LB1, (b) NC LB3, (c) NC LB5 scale bars = 500 nm. All NC particles prepared and imaged by Dr. James Kwan.*

3.3.3 Concentration

When considering particle concentration, both weight concentration and number concentration are important for clinical applicability and mechanistic effect respectively. The number concentration of cavitation nuclei was determined using a haemocytometer for SV microbubbles, and was mathematically determined based on weight concentration for the two cavicatalytic nanoparticles. These concentrations are compared below.

SV had a number concentration of 4.67 x 10^8 microbubbles/mL (Table 3.1) when prepared using the manufacturer's instructions (5 mg/mL) and was diluted for experiments. CNPs were produced as a stock at 0.2 mg/mL (0.02 wt%). The density of mesoporous carbon, as given by the supplier, Sigma, is 1.886 g/cm^3. Assuming a spherical morphology (V = 4/3 π r^3) with diameter of 180 nm that gives a number concentration of 3.47 x 10^{10} particles/mL. This concentration is two orders of magnitude higher than the stock concentration of SV.

NCs were produced as a stock at approximately 30 mg/mL (3 wt%) and diluted to approximately 0.6 mg/mL for most experiments. The density of the two main constituents were considered. Polystyrene is 1.05 g/cm^3 and methyl methacrylate is 0.94 g/cm^3, giving a weighted average density of 1.01 g/cm^3. Assuming a spherical morphology and a diameter of 500 nm, that gives a stock number concentration of 4.52 x 10^{11} particles/mL which when diluted to 0.6 mg/mL gives a number concentration of 9.03 x 10^9 particles/mL. Again, this concentration is an order of magnitude higher than the stock SV.

3.3.4 Zeta potential

Zeta potential of CNPs and NCs LB3 in 12.5 mM HEPES buffer was -29.3 $\pm$ 2.1 mV and -41.0 $\pm$ 3.1 mV respectively. The zeta potential distributions of CNPs and NC LB3 are shown in Figure 3.8. Based on the 'rule of thumb' measure of stability, particles with zeta potentials of more than +/- 30 mV are considered stable [65], these zeta potentials of -29 mV and -41 mV would suggest that these particles would be stable in solution, with the NCs having a stronger charge and likely to have stronger inter-particle repulsion. This was shown to be true in certain solutions in Section 3.3.1.

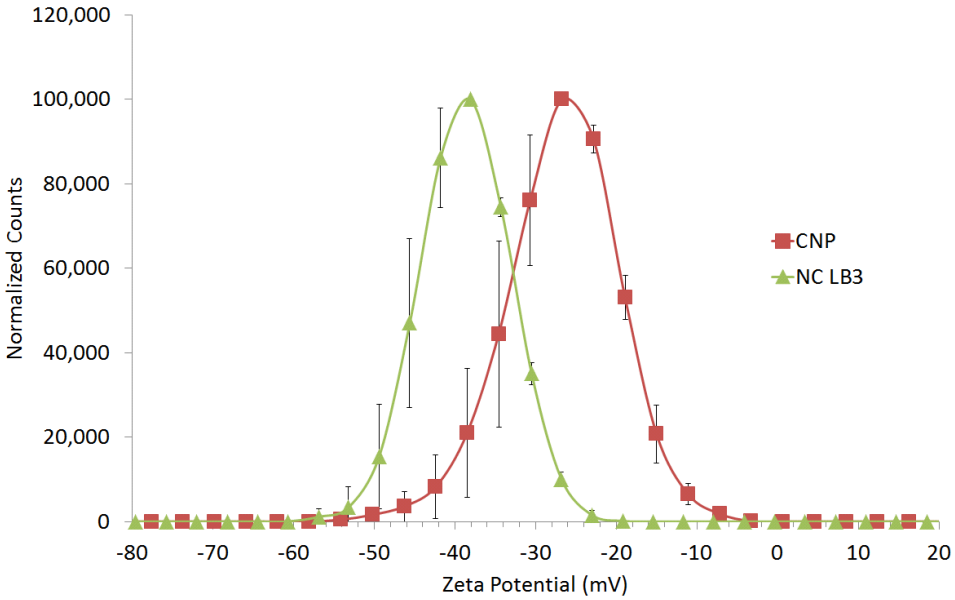

Figure 3.8: *Zeta potential of CNPs and NCs LB3 in 12.5 mM HEPES buffer. Mean zeta potential peak was -29.3 ± 2.1 mV and -41.0 ± 3.1 mV. Samples were diluted 50 µL into 1 mL buffer, 5 runs per sample, N=3 samples, standard deviation shown.*

3.4 Ultrasound characterisation of cavitation inducing particles

Cavitation dynamics and cavitation thresholds of CNPs and NCs were tested both in static and in flow phantoms and were modelled and verified experimentally with a selection of results in a paper under review by ACS Nano[1]. In this paper, experimental work using the static phantom was conducted by myself, S. M. Graham, experimental work using the flow phantom and mathematical modelling was conducted by J. J. Kwan. Results included in this paper, and additional findings are discussed below.

The cavitation nuclei chosen for the majority of studies were: SonoVue® (**SV**) (produced commercially), carbon nanoparticles (**CNPs**), and polymeric nano cup particles (**NCs**) with core beads of 100 ('**LB1**'), 300 ('**LB3**') and 500 nm ('**LB5**') diameter. An overview of the response of these cavitation nuclei to 0.5 MHz ultrasound with a PRF of 0.5 Hz and at 1.2 MPa PRFP is shown in Figure 3.9 when exposed in a static phantom.

[1] "Ultrasound-responsive gas-stabilizing nanocups for tumour mapping and enhancement of drug delivery" submitted to ACS Nano

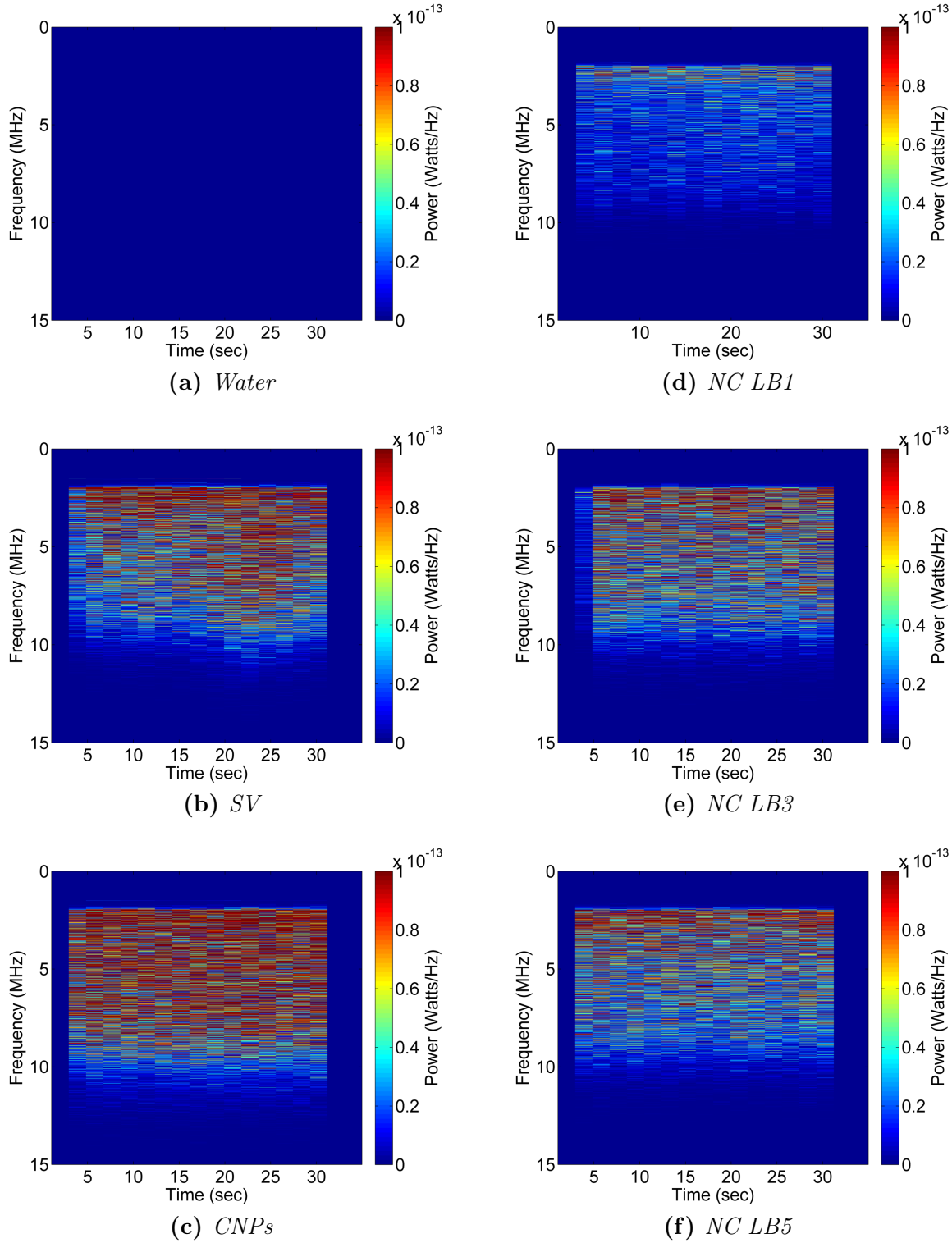

(a) *Water* **(d)** *NC LB1*

(b) *SV* **(e)** *NC LB3*

(c) *CNPs* **(f)** *NC LB5*

Figure 3.9: *Summary of cavitation responses from particles. Power spectral density plots of cavitation received from the PCD from cavitation nuclei insonated at 0.5 MHz, 5% DC, 1.2 MPa PRFP, 0.5 Hz PRF. (a) De-ionised water; (b) SV (20 x* 10^6 *microbubbles/mL); (c) CNPs (0.2 mg/mL) pre-primed; NC particles with starting bead diameter of (d) 100 nm (LB1)(0.43 mg/mL), (e) 300 nm (LB3) (0.46 mg/mL) and (f) 500 nm (LB5) (0.71 mg/mL). Representative PSDs shown of 3 repeats.*

3.4.1 Cavitation thresholds and pressure responses

The cavitation threshold may be broadly defined as the pressure for a given set of ultrasound parameters at which cavitation occurs, and below which cavitation does not occur. This definition however is not practical experimentally due to the potential presence of other nuclei and variation in the population of nuclei being tested. Instead, the increase in signal over the background noise from media is set to an arbitrary limit which we define as the cavitation threshold. Additionally, the cavitation threshold alone does not encompass the violence of cavitation, whether it is classified as 'stable' or 'inertial', nor the amount of energy associated with cavitation with increasing pressure. Each of these features are predicted to be important in drug delivery applications. As such, each of these features are included in the discussion below.

For therapeutic applications, lowering cavitation thresholds of surrounding media is desired. By lowering the cavitation threshold of a tissue, lower ultrasound pressures may be used to yield a particular physical response. As ultrasound alone at sufficiently high pressures is able to cause tissue destruction, using artificial nuclei to lower cavitation thresholds may allow for lower ultrasound intensities to be used thus minimising damage to non-target tissues.

Cavitation thresholds were determined by exposing samples to increasing ultrasound pressures and quantifying the acoustic emissions at each pressure. Three samples were used for each cavitation nuclei, and average values are shown. At 1.614 MHz, 2.8 MPa, in the NC LB3 sample, data acquisition failed for one sample and so that data point is only the average of 2 samples.

Total energy of cavitation at 0.5 MHz and 1.6 MHz exposure is shown in Figure 3.10. For standardisation, results have been plotted as an increase in energy over the energy signal from water at the corresponding pressure, expressed as gain ($10 \times log_{10}(\frac{E_{sample}}{E_{water}})$, where E = energy), in Figure 3.11. Setting a gain of 20 dB higher than water (arbitrary threshold), and a linear interpolation between the closest points tested, the approximate cavitation threshold was calculated. The cavitation threshold at 0.5 MHz for SV (0.17 MPa), CNPs (0.38 MPa), NC LB1 (0.76 MPa), NC LB3 (0.72 MPa), and NC LB5 (0.34 MPa) were all lower than the cavitation thresholds for the same particles at 1.614 MHz: SV (0.45 MPa),

CNP (2.33 MPa), NC LB1 (greater than 2.4 MPa (max pressure tested for NC LB1)), NC LB3 (1.30 MPa), and NC LB5 (1.14 MPa).

The cavitation threshold of SV is lower than all other cavicatalytic particles tested. Being a bubble on the micron scale, the cavitation threshold is lower than smaller bubbles, as predicted by Apfel and Holland [4]. In addition, SV bubbles are suspended as bubbles in the media whereas gas adsorbed on a surface requires energy input to overcome the surface tension forces to become free bubbles. The energy required to overcome the surface tensions forces to detach the gas pockets adds to the amount of energy required for cavitation to occur [117].

At both frequencies tested, the cavitation threshold increases with decreasing cavity sizes for the NCs. The smallest NCs, with the smallest gas pocket available, have the highest pressure threshold before cavitation is initiated. The largest NCs, on the other hand have the lowest cavitation threshold of the three NC sizes.

The cavitation threshold of the CNPs lies between NC LB3 and NC LB5 at 0.5 MHz, and lies between NC LB3 and NC LB1 at 1.614 MHz. The response of the CNPs is therefore frequency dependent, with a higher cavitation threshold at 1.614 MHz compared with 0.5 MHz relative to NC particles. At the lower frequency, the CNP cavitation threshold between that of NC LB3 and NC LB5 suggests that the cavity sizes also lie between 300 - 500 nm. Characterisation by DLS and TEM however show that the CNP measure a maximum of 300 nm in one dimension. Additionally, the CNP cavitation threshold at 0.5 MHz is closer to that of NC LB5 than NC LB3 suggesting that the cavities on the CNPs are closer to 500 nm rather than 300 nm. These data might therefore indicate that the gas entrapped in the crevices and pockets on the CNPs might coalesce over the first pulses of an ultrasound exposure, forming a larger bubble. This larger bubble is then able to respond to the subsequent ultrasound bursts with more energy at lower pressures.

This phenomenon is also supported by the 'priming' effect observed. At 0.5 MHz, CNPs show an increase in energy over the first 30 to 90 seconds of exposure. A coalescence of bubbles from different areas on the surface of the CNPs is hypothesized to explain the increasing energy associated with cavitation with each successive pulse. The point at which a maximum in energy is reached would therefore occur when the bubble size is at an optimum

for the ultrasound exposure conditions. As the CNPs were all 'primed' for 90 seconds before cavitation threshold experiments were conducted, we are able to assume that the gas stabilised on the surface was already at this enlarged bubble size, thus resulting in a cavitation threshold comparable to a cavity between 300 and 500 nm.

The energy associated with cavitation increases for all particles with increasing pressure as seen in Figure 3.10, relative to water, which they are all suspended in. At 0.5 MHz there is a point beyond which no further relative increase in energy associated with introduced cavitation nuclei is observed (Figure 3.11 (a)). At 1.614 MHz this point is only observed for SV, CNPs and NC LB3. This point of maximum gain at 0.5 MHz for SV (1.5 MPa), CNPs (1.7 MPa), NC LB1 (1 MPa), NC LB3 (1.7 MPa), and NC LB5 (1.7 MPa) occurs at a lower pressure than at 1.614 MHz. At 1.614 MHz the point of maximum gain for SV (3.2 MPa), CNP (3.6 MPa), and NC LB3 (2.8 MPa), could be measured, however the point of maximum gain for NC LB1 and NC LB5 was not reached at 1.614 MHz as they were only tested up to 2.5 MPa due to limited sample.

The point of maximum gain is important experimentally when looking at therapeutic effects. At pressures higher than this point, the effect due to the background will be increasing relative to the effect due to the particle. Experimentally, exposing above this pressure reduces the relative effect of the cavitation inducing particle. Clinically, the ability to limit side effects may be impacted. If the therapy relies on treatments only occurring where the cavitation inducing particles are present, beyond this pressure point there will be increasing background effects outside regions where the particles exist. This reduces the ability to target the therapy and minimize side effects. The energy associated with cavitation of the background media may not be high enough to see any effects clinically, but is a factor that needs to be considered.

Another notable difference between 0.5 MHz exposure (Figure 3.11 (a)) and 1.614 MHz exposure (Figure 3.11 (b)) is that CNPs produce relatively less energy associated with cavitation at 1.614 MHz than at 0.5 MHz compared with the other particles tested. Not only does the cavitation threshold shift, as discussed above, but the energy associated with cavitation also decreases.

The frequency decomposition of energy associated with cavitation may give insights

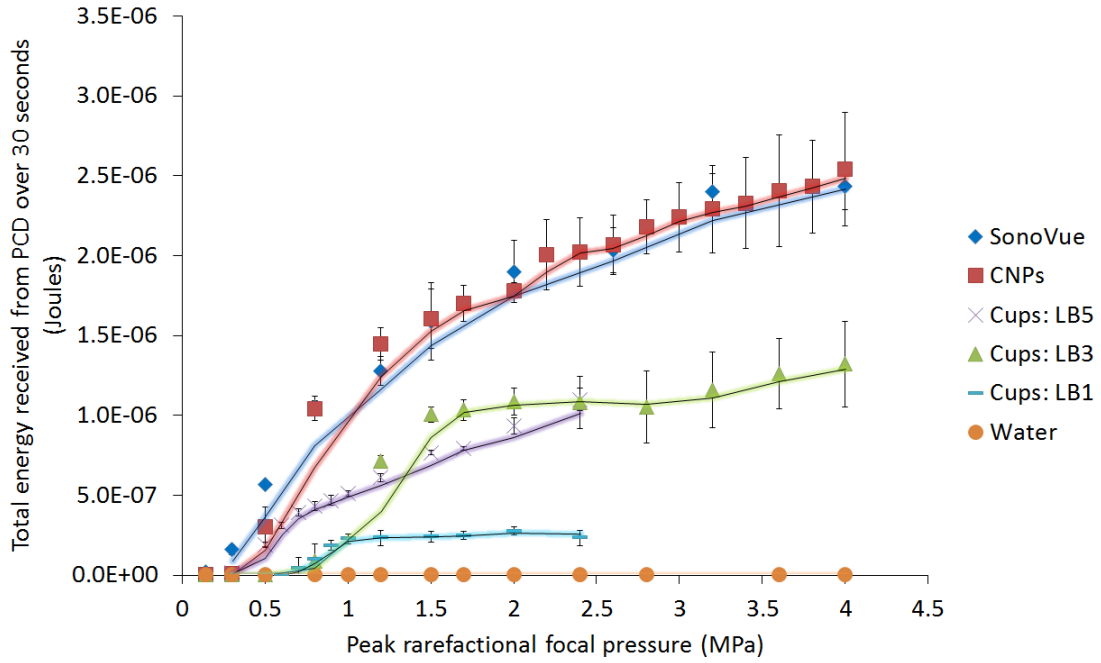

(a) *0.5 MHz*

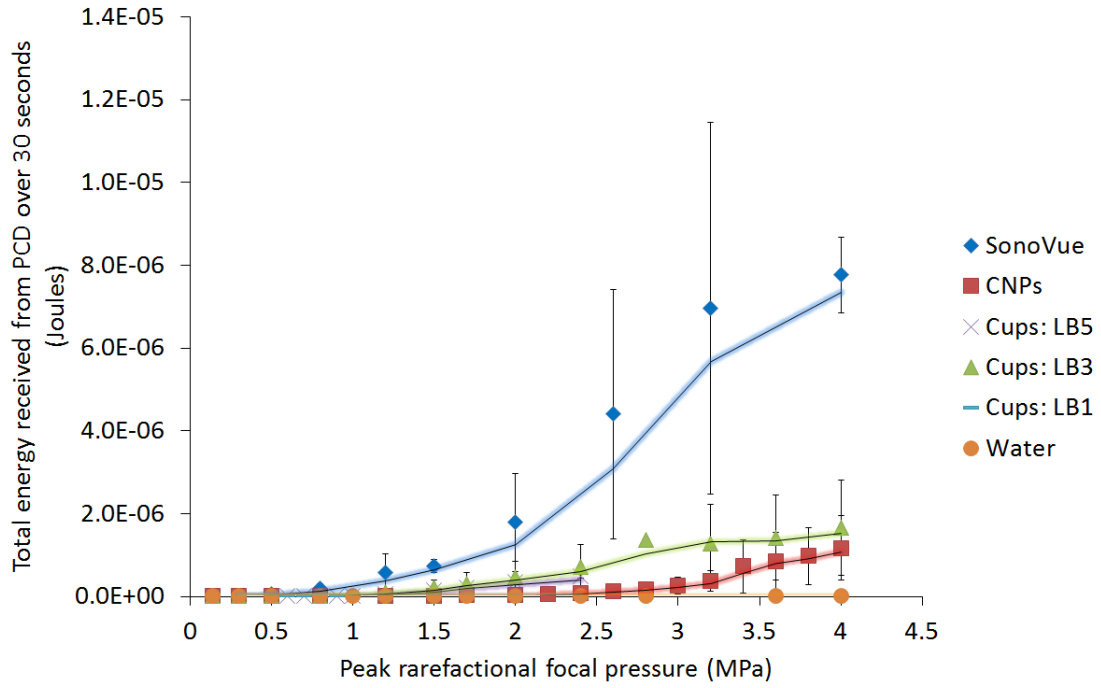

(b) *1.614 MHz*

Figure 3.10: ***Total energy response associated with cavitation*** *as received from the PCD of SV (4.3%), CNPs (0.2 mg/mL), NCs (LB5 (0.71 mg/mL), LB3 (0.46 mg/mL) and LB1 (0.43 mg/mL)) and DI water insonated at (a) 0.5 MHz or (b) 1.614 MHz, 0.5 Hz PRF, 5% DC, 30 second exposure. Tested in the static phantom holder; n=3; standard deviation shown; moving average trend-lines shown. SV and water were replenished at each pressure tested. One sample was tested over the full pressure range (ramping up) for CNPs and NCs and was replenished between repeats. NC LB1 and NC LB5 were not tested over the full pressure range due to limited sample. NC LB3, at 1.614 MHz, 2.8 MPa, n=2 due to data acquisition failure.*

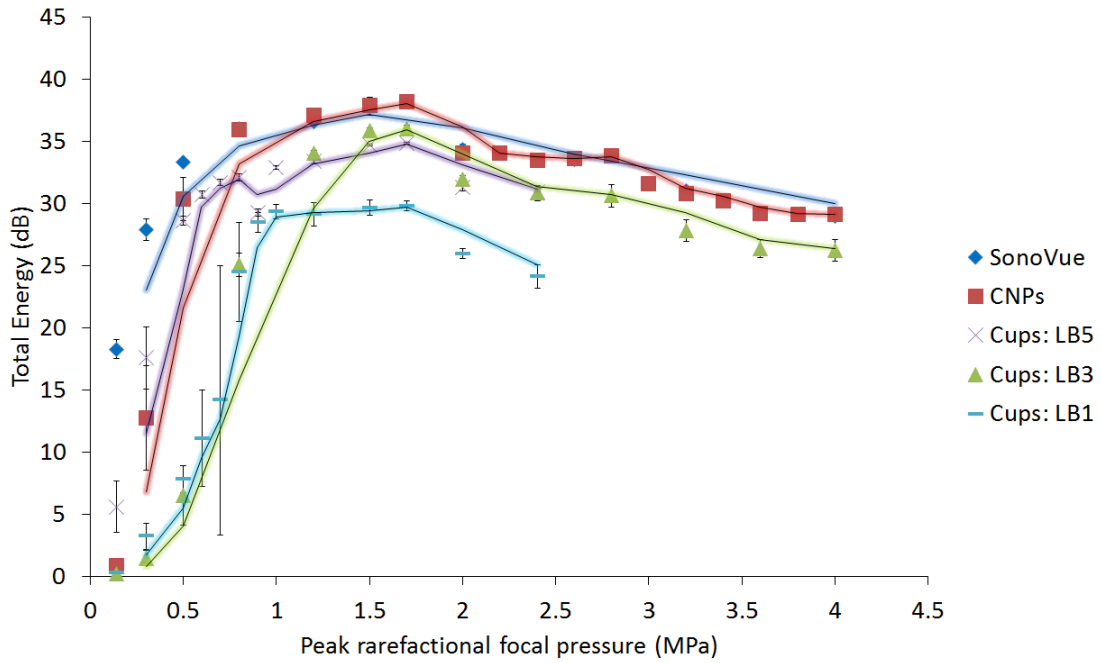

(a) *0.5 MHz*

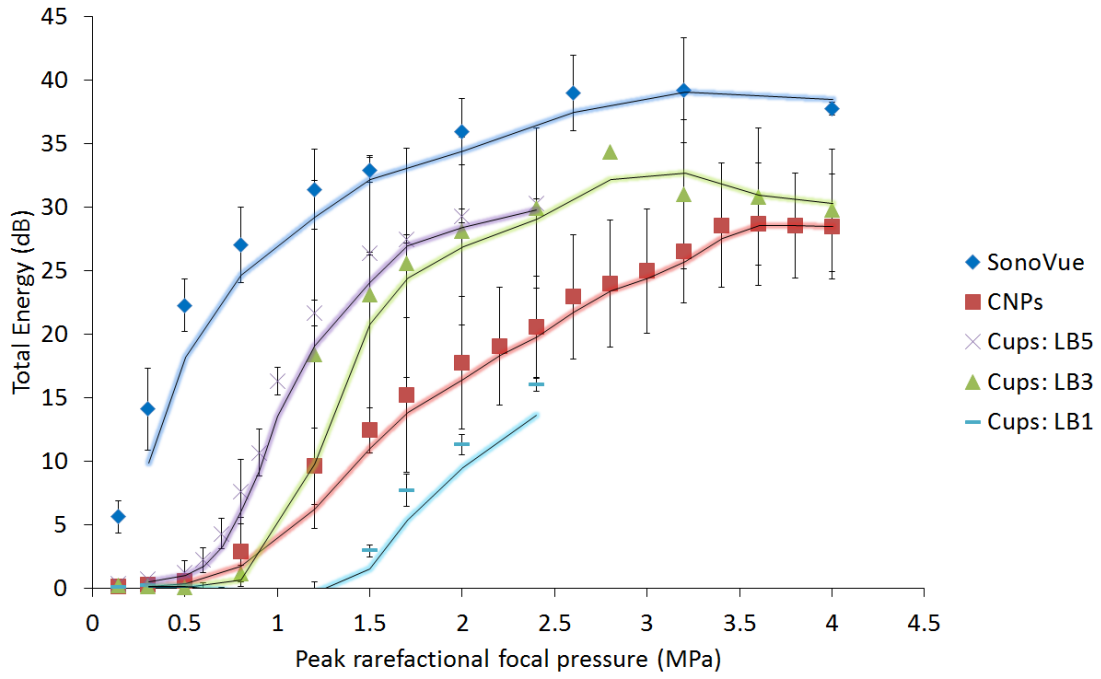

(b) *1.614 MHz*

Figure 3.11: ***Total energy response associated with cavitation plotted as gain over water*** *of SV (4.3%), CNPs (0.2 mg/mL), NCs (LB5 (0.71 mg/mL), LB3 (0.46 mg/mL) and LB1 (0.43 mg/mL)) and DI water insonated at (a) 0.5 MHz or (b) 1.614 MHz, 0.5 Hz PRF, 5% DC, 30 second exposure. Tested in the static phantom holder; n=3; standard deviation shown; moving average trend-lines shown. SV and water were replenished at each pressure tested. One sample was tested over the full pressure range (ramping up) for CNPs and NCs and was replenished between repeats. NC LB3, at 1.614 MHz, 2.8 MPa, n=2 due to data acquisition failure.*

into the type of cavitation occurring. As discussed in Section 1.7.1, stable cavitation, is generally associated with harmonic energy, while inertial cavitation, is generally associated with broadband energy. High energy inertial cavitation is predicted to be important for potential therapeutic responses where maximum bubble expansion and collapse may be able to be used to effect drug release and/or drug delivery. It should also be noted however that inertial collapse has the potential to cause negative bioeffects such as increasing tumour metastasis [130] or hemorrhage [92].

When comparing the total energy associated with acoustic emissions with broadband energy alone (Figure 3.11 compared with Figure 3.12), the total energy emissions are mainly comprised of broadband emissions for each cavicatalytic particle, whereas the broadband emissions from SV are substantially lower compared with the total energy, especially at 1.6 MHz.

This effect is more obvious when the broadband emissions are plotted as a percent of the total emissions. Figure 3.13 shows that at both 0.5 MHz and 1.614 MHz, all cavicatalytic nanoparticles have much higher broadband response as a percent of total emissions than SV at each pressure tested. At 0.5 MHz (Figure 3.13 (a)), cavicatalytic particles reach a maximum broadband response at pressures around 0.5 MPa PRFP, while SV shows increasing broadband energy as a percent of total up to around 3 MPa. A similar trend is observed at 1.614 MHz (Figure 3.13 (b)) where the broadband energy is dominant and peaks at around 1.5 MPa for the cavicatalytic particles however the broadband percent is increasing for all pressures tested for SV.

It is notable that there is no statistical difference in percent of broadband energy between the cavicatlytic nanoparticles, even with variation in cavity size between NC LB1, LB3 and LB5. This similarity suggests that where no free bubbles exist, the energy required to pull the gas entrapped from the surface of the particle such that it can cavitate, is also sufficient to cause inertial collapse of the bubble once detached from the surface. The exception to this observation is for NC LB5 where at low pressures, cavitation is present which has harmonic energy dominating the signal. This observation suggests that the energy required to remove these larger gas pockets from the surface is lower (indicated by the lower cavitation threshold) and therefore is at a pressure where the gas bubble once removed will cavitate

stably.

Power spectral density plots may be used to visualise the frequency content of the signal from cavitating bubbles at different pressures. Figure 3.14 shows SV microbubbles emitting harmonic energy when exposed to 0.5 MHz, 0.14 MPa without any broadband emissions detected (note: this was only observed at the lowest pressure tested). Increasing the pressure to 0.3 MPa then shows broadband energy emissions. Both CNPs and NCs however do not generate harmonic emissions at low pressures. There is a step change with increasing pressure, from PSDs where no cavitation energy emissions are observed to PSDs where broadband-only emissions are observed. This observation further confirms that peak rarefactional pressures required to pull bubbles from the surface such that they can cavitate, are above the inertial cavitation threshold for that bubble ensuring that these cavicatalytic particles only display broadband emissions characteristic of inertial cavitation.

3.4.2 Comparison of cavitation thresholds with mathematical model

Blake's threshold was developed to mathematically predict the cavitation threshold of a free bubble in a medium. It predicts that with decreasing initial bubble size, the pressure required to initiate cavitation increases. These calculations however were not applied to a bubble in a crevice, or on a surface.

To account for the size and morphology of the cavicatalytic particles used in these experiments, Kwan et al. (paper submitted for publication), developed a modified Raleigh-Plesset crevice model (Equation 3.1, where R, $\dot{R}$, and $\ddot{R}$ are the radius, velocity and acceleration of the radius of curvature for the bubble wall, ρ_L is the density of the liquid medium, P_L is the liquid side pressure at the bubble wall, P_{ac} is the acoustic pressure, which is a function of time (t), and P_H is the hydrostatic pressure) of a bubble constrained by a cavity. In this model the bubble is able to exist in 3 locations: 1) constrained within the cavity; 2) pinned to the cavity opening, and 3) detached from the cavity as indicated diagrammatically in Figure 3.15 at (a), (b) and (c) respectively.

$$R\ddot{R} + \frac{3}{2}\dot{R}^2 = \frac{1}{\rho_L}(P_L(R) - P_{ac}(t) - P_H) \tag{3.1}$$

The model predicted that in general there is a decreasing cavitation pressure threshold

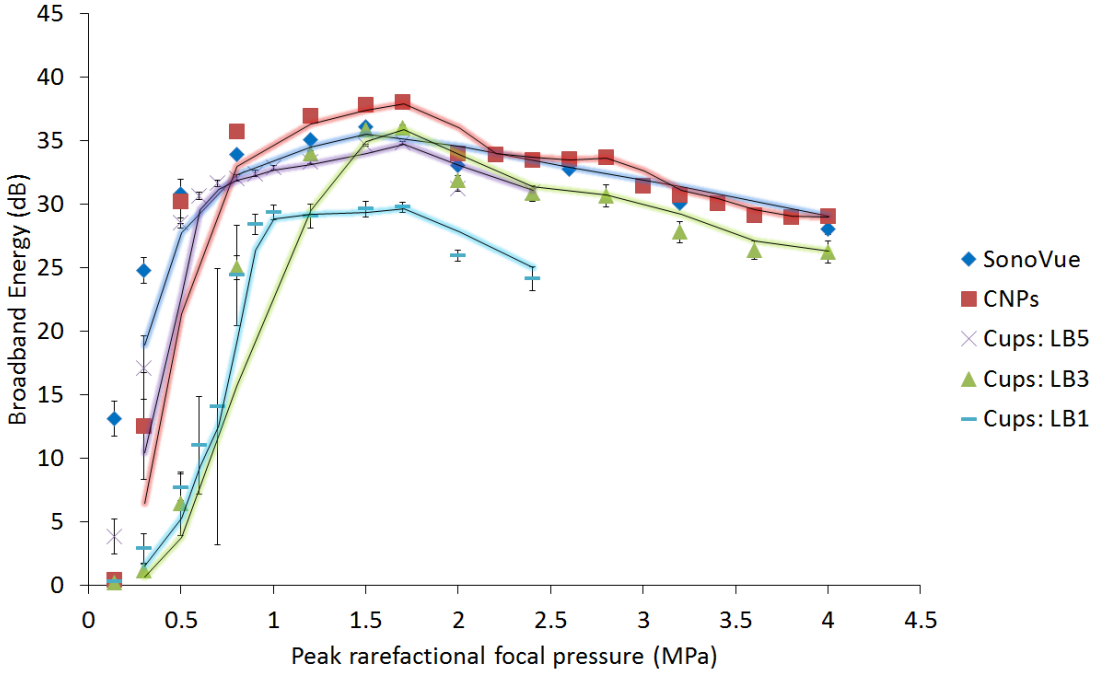

(a) *0.5 MHz*

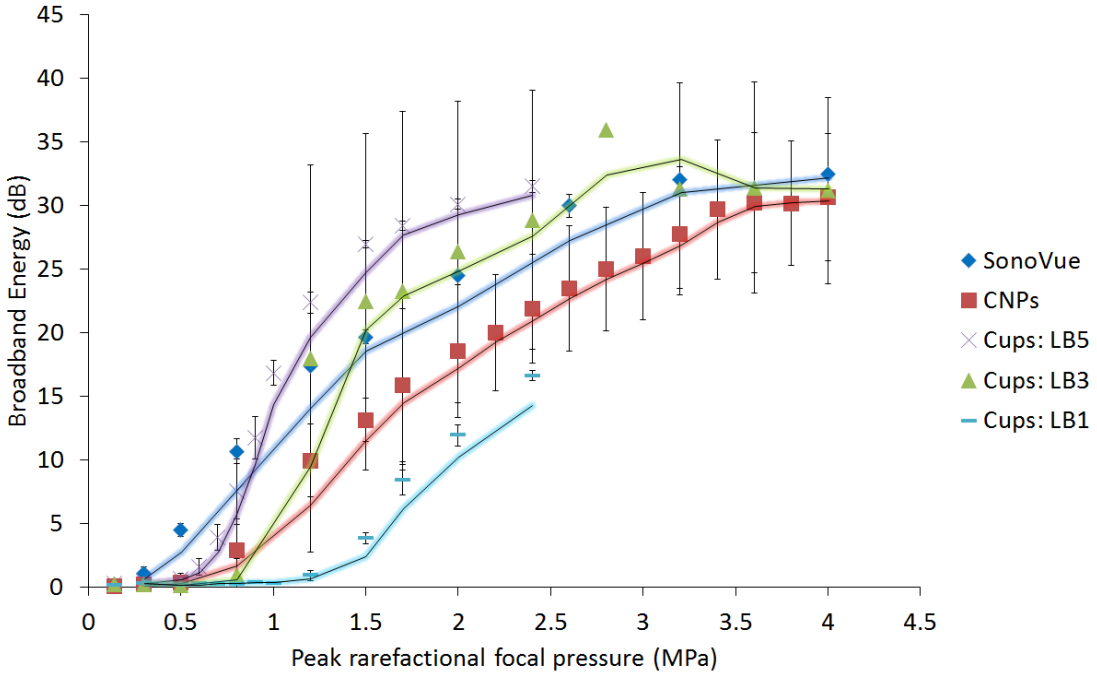

(b) *1.614 MHz*

Figure 3.12: ***Broadband energy response associated with cavitation plotted as gain over water*** *of SV (4.3%), CNPs (0.2 mg/mL), NCs (LB5 (0.71 mg/mL), LB3 (0.46 mg/mL) and LB1 (0.43 mg/mL)) and DI water insonated at (a) 0.5 MHz or (b) 1.614 MHz, 0.5 Hz PRF, 5% DC, 30 second exposure. Tested in the static phantom holder; n=3; standard deviation shown; moving average trend-lines shown. SV and water were replenished at each pressure tested. One sample was tested over the full pressure range (ramping up) for CNPs and NCs and was replenished between repeats. NC LB3, at 1.614 MHz, 2.8 MPa, n=2 due to data acquisition failure.*

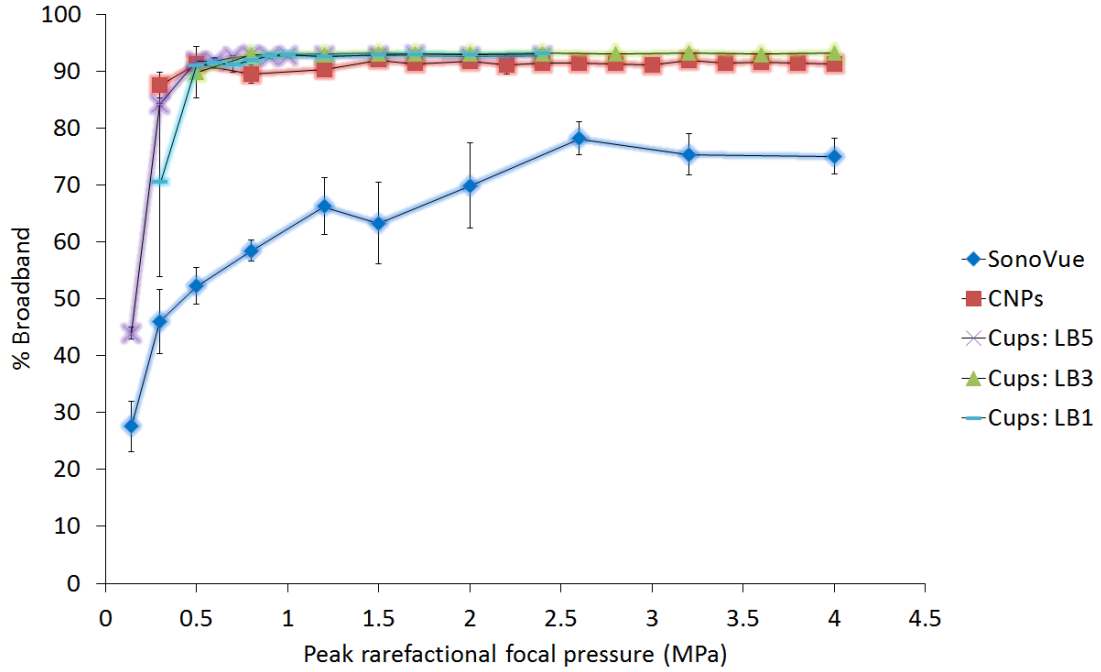

(a) *0.5 MHz*

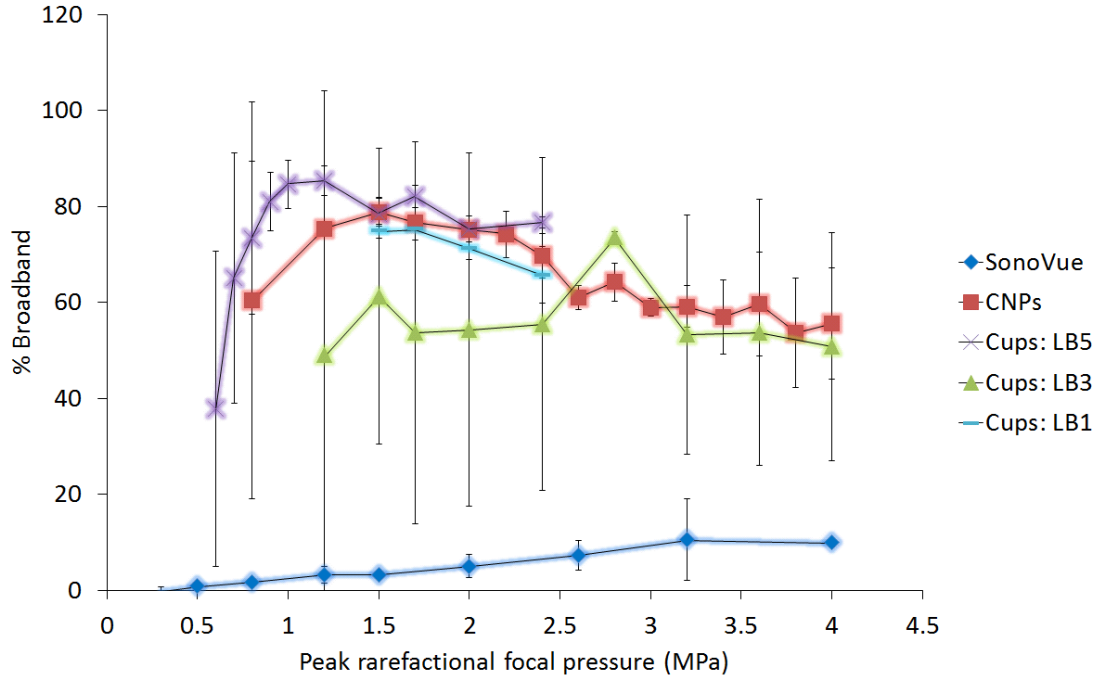

(b) *1.614 MHz*

Figure 3.13: ***Broadband energy response as a percent of total energy*** *received from the PCD of SV (4.3%), CNPs (0.2 mg/mL), and NCs (LB5 (0.71 mg/mL), LB3 (0.46 mg/mL) and LB1 (0.43 mg/mL)) insonated at (a) 0.5 MHz or (b) 1.614 MHz, 0.5 Hz PRF, 5% DC, 30 second exposure. Tested in the static phantom holder; n=3; standard deviation shown. Data points are only shown if total cavitation energy was at least 50% higher than water background. Data points below this threshold are nonsensical and dominated by broadband electrical energy. NC LB3, at 1.614 MHz, 2.8 MPa, n=2 due to data acquisition failure.*

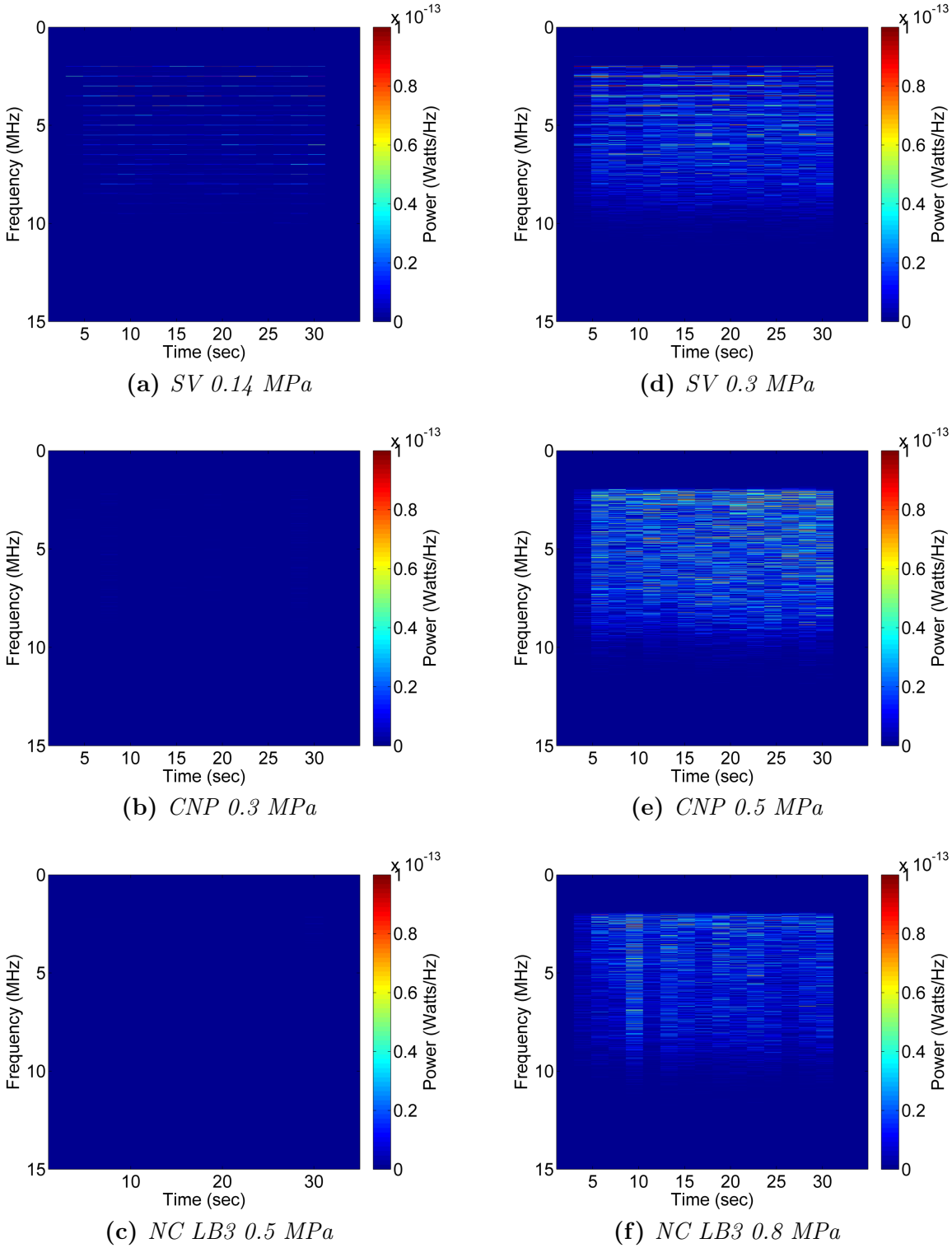

(a) *SV 0.14 MPa* **(d)** *SV 0.3 MPa*

(b) *CNP 0.3 MPa* **(e)** *CNP 0.5 MPa*

(c) *NC LB3 0.5 MPa* **(f)** *NC LB3 0.8 MPa*

Figure 3.14: *Power spectral density plots contrasting emissions from SV, CNPs and NCs. Samples were insonated at 0.5 MHz, 5% DC, 0.5 Hz PRF. Representative traces of 3 repeats shown at one pressure measurement lower than (a, b, c), and at the pressure required for inertial cavitation (d, e, f).*

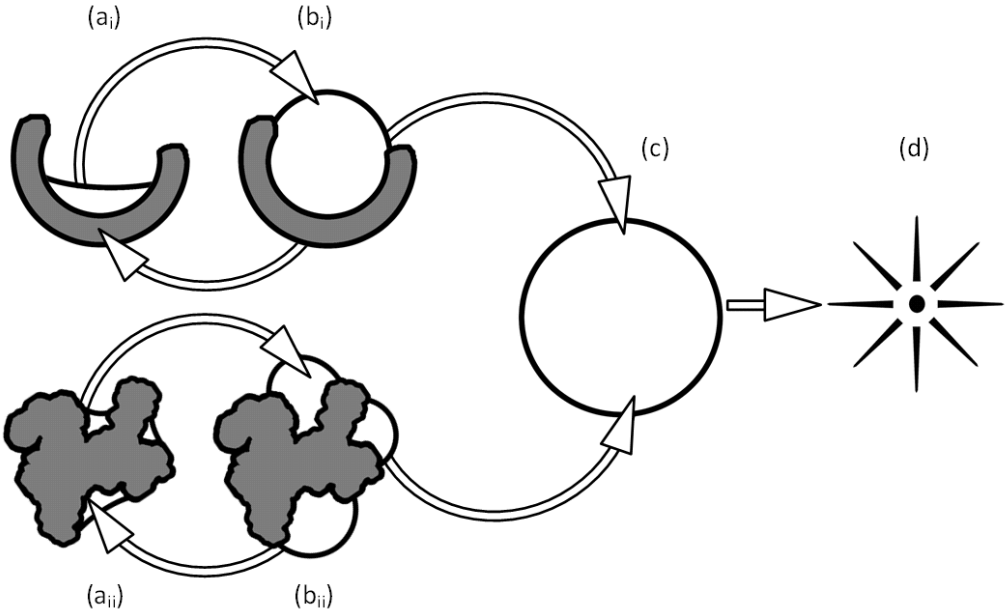

Figure 3.15: *Diagrammatic representation of the proposed mechanism for inertial cavitation for cavicatalytic nanoparticles. The positive pressure cycle of ultrasound compresses gas within the (a_i) NC cavity or (a_{ii}) CNP cavities followed by a rarefactional pressure cycle which expands the gas extending out of the (b_i) NC cavity or (b_{ii}) CNP cavities. With sufficient negative pressure, gas is pulled out of the cavity and grows unstably into a larger (c) free bubble. Unstable growth then leads to (d) inertial collapse of the bubble.*

with increasing cavity size and with decreasing ultrasound frequency. The model was validated using the experimental data collected in this chapter using NC particles, which have uniformly sized cavities that are able to be used to estimate gas pocket size, and also in a flow phantom designed by Dr. James Kwan (Figure 3.16). The model was then compared to CNPs which at 1.614 MHz coincided with the model but at 0.5 MHz did not coincide with the model. At 0.5 MHz, the cavitation threshold of 0.38 MPa is much lower than predicted by the model for a particle of maximum possible gas pocket size of 200 nm. This result suggests that the nucleation of inertial cavitation from the CNPs is likely to come from multiple gas pockets or a gas layer over the rough surface of the particle, rather than from a single cavity.

Simulations suggest that bubbles will only inertially cavitate when they are removed from the crevice and form a free bubble. If the inertial cavitation threshold is reached, inertial cavitation is predicted to be within the first negative to positive pressure amplitude cycle. During physical experimentation however there is a 'ring up' time of approximately 3 cycles, over which the pressure is increasing to the stated peak rarefactional focal pressure.

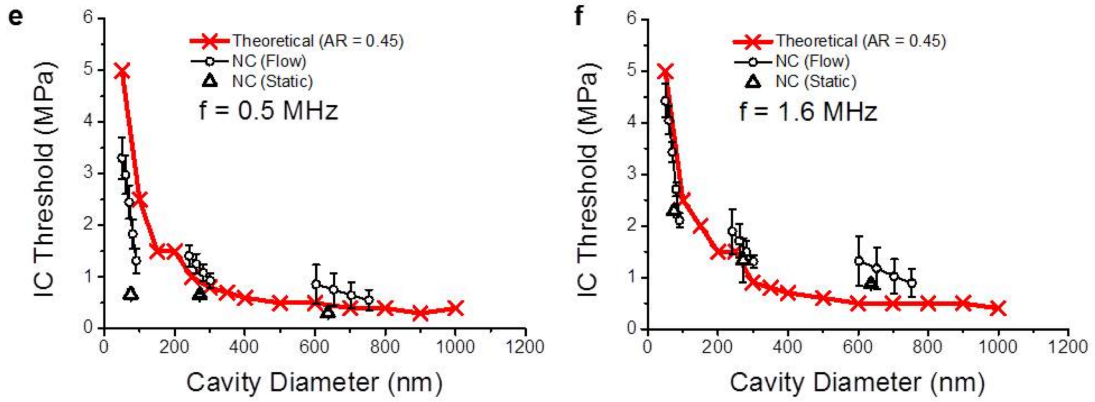

Figure 3.16: *Acoustic activation and characterization of nanoparticles. Inertial cavitation thresholds of NCs were determined experimentally and predicted numerically at (e) 0.5 MHz and (f) 1.614 MHz. Experimentally determined inertial cavitation thresholds for the flow through setup (open black circles) and static bulk setup (open black triangles) are shown to agree. The red crosses represent the predicted inertial cavitation thresholds of a hemispherical cavity with an aspect ration of 0.45 and coincide with measured values. For all experiment points, n=3 and standard deviations are shown. Data constructed in part by figure from Kwan et al., paper submitted for publication*

Due to this ring up, although the model predicts cavitation will occur on the first cycle, in practice cavitation is more likely between the first and fourth cycle dependent on initial bubble size.

The model predicts that the pressure required to detach the bubble from the nanoparticle surface is also sufficient to cause inertial collapse of the bubble after it has grown unstably in the media. This prediction was validated *in vitro* (Figure 3.14) and discussed above with a comparison between SV microbubbles and cavicatalytic nanoparticles.

3.4.3 Cavitation dynamics

Cavitation dynamics describe how the cavitation events change over time with continued ultrasound exposure. Here the cavitation dynamics are tested in the static phantom, ensuring that the same particle volume is exposed over time. Note that the pressure profile over the static phantom (Figure 2.3) means that not all particles are responding to the same pressure, and that the volume is large enough to allow for potential mixing within and between pulses.

When testing the effect of pulse repetition frequency, the duty cycle was kept constant at 5%, the exposure time was kept constant at 30 seconds, the pressure was kept constant at 1.2 MPa PRFP, and the number of cycles per pulse were allowed to vary. In this way, the

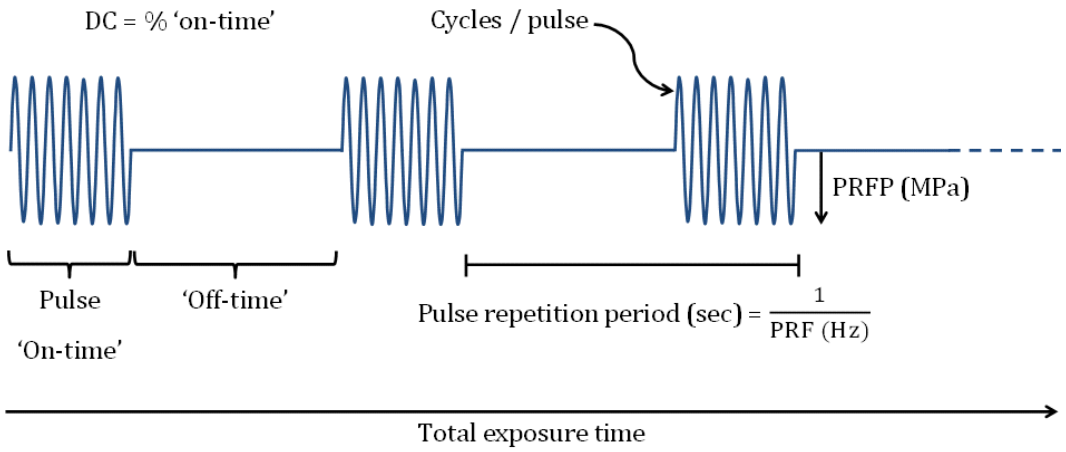

Figure 3.17: *Diagrammatic representation of ultrasound parameters. Duty cycle (DC) is calculated as the percentage of pulse 'on-time' with respect to pulse repetition period. The pulse 'on-time' is equal to the number of cycles per pulse divided by the ultrasound driving frequency. The pulse repetition period is the time between pulses and is the inverse of the pulse repetition frequency (PRF). Total exposure time is defined as the total time of exposure independent of duty cycle. Pressure is measured as the peak rarefactive pressure focal pressure (PRFP) in MPa.*

total 'on-time', or total number of cycles, was kept constant between sample groups. The relationship between these variables is shown diagrammatically in Figure 3.17.

Upon ultrasound exposure, SV bubbles are destroyed after cavitation, in accordance with the literature [149] and shown here over a range of PRFs (Figure 3.18). The cavitation decay time of SV, being the time at which the PCD power drops to below 1% maximum power, decreases with increasing PRF (Figure 3.19) from 30 seconds at 0.5 Hz PRF to 4 seconds at 500 Hz PRF where it reaches a minimum, with no further decrease even at 5000 Hz. By analysing the energy components associated with SV cavitation at each PRF it was observed that harmonic energy dominated early on in the exposure, while broadband emissions remained fairly constant throughout the exposure and dominated for the latter part. Two exceptions were observed at 2500 Hz and 5000 Hz where broadband emissions dominated throughout the exposure. This observation suggests that at these higher PRFs, either bubbles scattering energy at the harmonics are destroyed before the bubbles that are emitting broadband energy, or that the bubbles required a higher number of cycles to grow through rectified diffusion to a size that emitted more harmonics than broadband which was not possible at these high PRFs (low number of cycles per pulse).

It was also noted, that at a given PRF, cavitation power from SonoVue decayed more quickly at higher pressures (Figure 3.20). This observation demonstrates that bubble de-

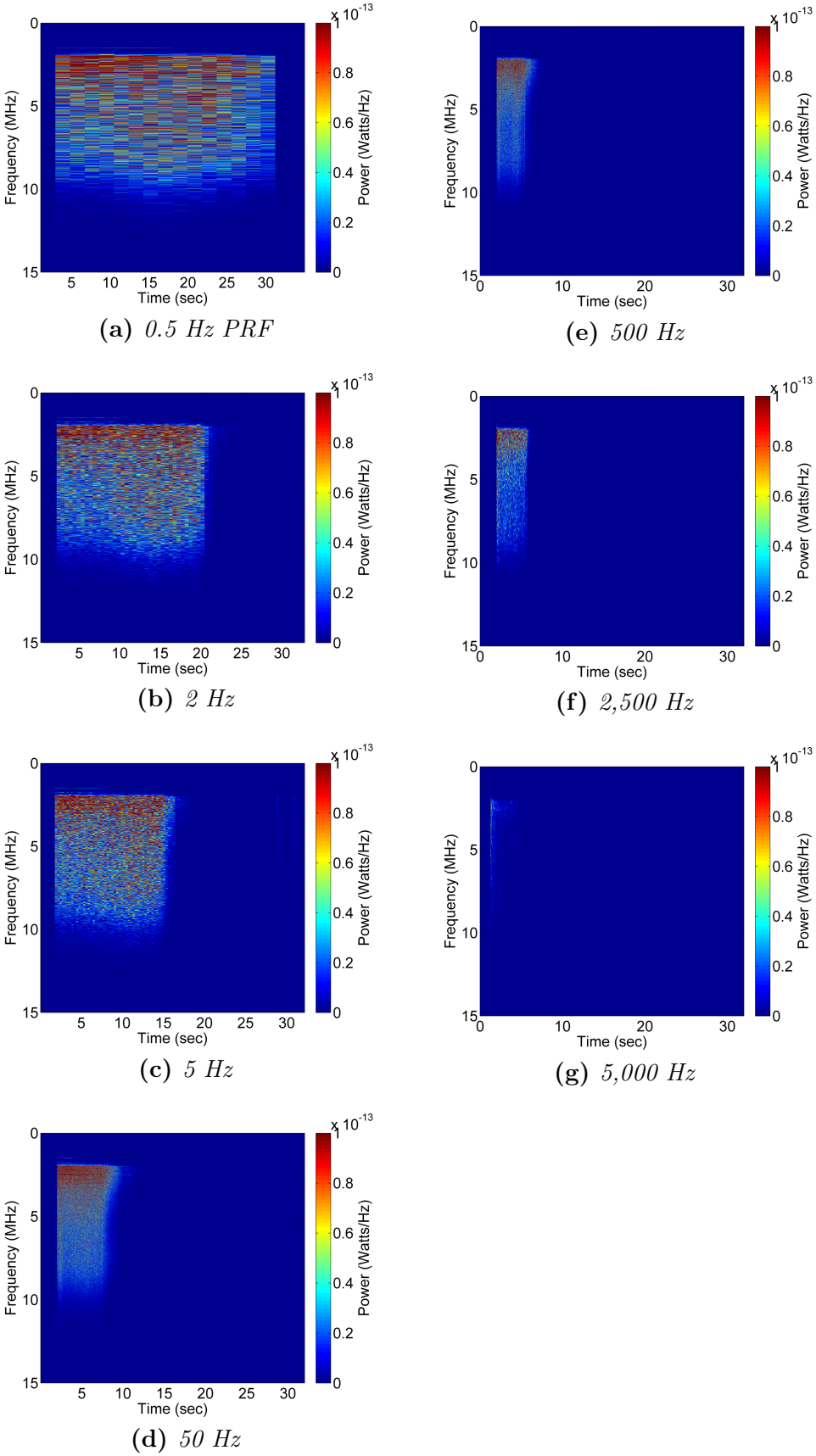

(a) *0.5 Hz PRF*

(e) *500 Hz*

(b) *2 Hz*

(f) *2,500 Hz*

(c) *5 Hz*

(g) *5,000 Hz*

(d) *50 Hz*

Figure 3.18: *Effect of varying PRF on cavitation dynamics of SonoVue. Power spectral density plots of cavitation received from the PCD from SonoVue insonated at 0.5 MHz, 5% DC, with varying PRF in the static phantom. Representative PSDs shown.*

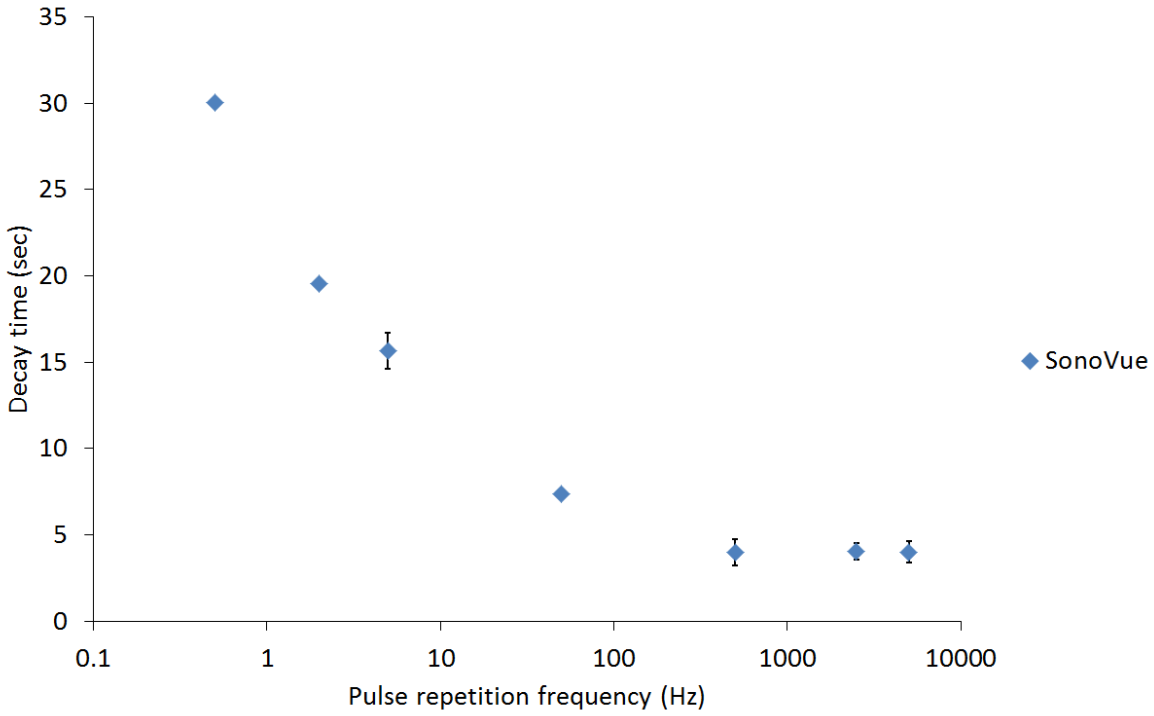

Figure 3.19: *SonoVue bubble destruction with varying PRF. SonoVue was exposed in the static phantom at 1.2 MPa PRFP, 5% DC, over a range of PRFs. Cavitation decay time, the amount of time before power dropped to below 1% maximum power, decreases in a log linear fashion with increasing PRF until 500 Hz where it reaches a minimum. N=3, standard deviation shown.*

struction rate is dependent both on the number of pulses (i.e. PRF) as well as the ultrasound pressure. This bubble destruction was observed visually in each sample and is discussed in Section 4.0.3.1.

In contrast, CNPs did not show a decay of cavitation with time at any PRF (Figure 3.21). As PRF was increased above 50 Hz, the response from CNPs became more sporadic, but remained sustained throughout the exposure period. This behaviour could suggest that a critical number of cycles is required for bubbles to be removed from the particle surface and respond to the driving ultrasound. This observation is however in contrast to the model developed by Kwan et al. (paper submitted for publication) where the bubble is assumed to be removed from the surface within the first negative - positive pressure cycle. Additionally, the power signal is dominated by broadband emissions throughout the exposure at all PRFs, in contrast to SV where harmonics dominated in the first part of each exposure at most PRFs tested. This observation suggests that if a response is observed, the energy required to remove the bubble from the surface was also sufficient to cause inertial collapse, and if the energy was not sufficient to remove the bubble from the surface, no cavitation event was

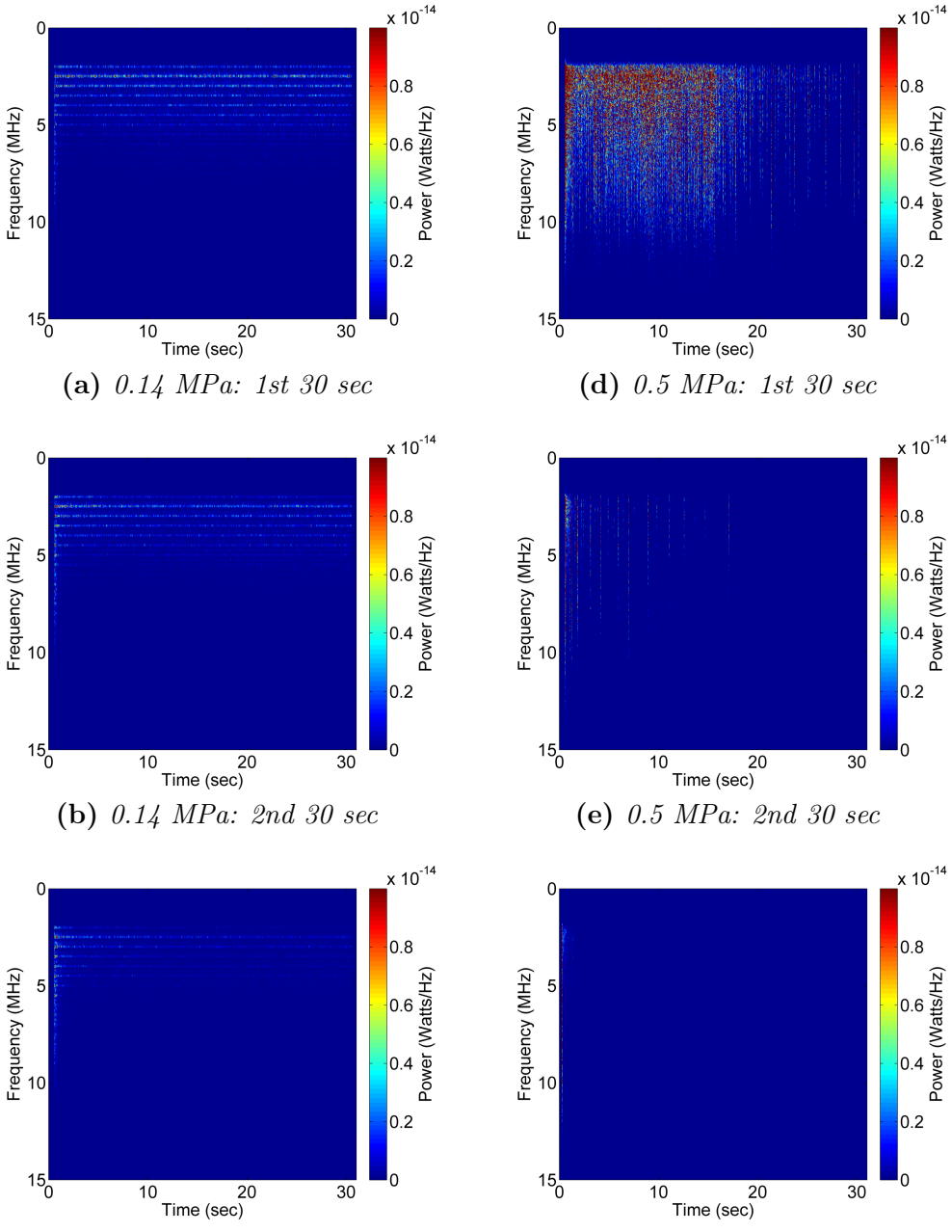

(a) *0.14 MPa: 1st 30 sec* **(d)** *0.5 MPa: 1st 30 sec*

(b) *0.14 MPa: 2nd 30 sec* **(e)** *0.5 MPa: 2nd 30 sec*

(c) *0.14 MPa: 3rd 30 sec* **(f)** *0.5 MPa: 3rd 30 sec*

Figure 3.20: *Effect of increased pressure on cavitation dynamics of SonoVue. Power spectral density plots of cavitation received from the PCD from SV (mixed with liposomes) insonated at 0.5 MHz, 5% DC, 2500 Hz PRF, in the static phantom. Samples were exposed for 30 seconds three times with 30 second mixing and 1 minute wait between each exposure. PRFP of 0.14 MPa in (a), (b), and (c) or 0.5 MPa in (d), (e), and (f) were used. Representative PSDs shown. Note: the colour scale is different from other Figures.*

observed.

The maximum power received from the bubble expansion and collapse remained fairly constant from 0.5 Hz to 500 Hz but reduced substantially at 2,500 Hz and further at 5,000 Hz for both SV and CNPs (Figure 3.22). This result suggests that the maximum violence of collapse and/or number of bubbles cavitating remained similar at lower PRFs but reduced at higher PRFs.

Although maximum power remained relatively constant for SV across the PRF range tested, the bubbles were destroyed more quickly with increasing PRF and so the total energy of cavitation over the set time period decreased (Figure 3.23). At 0.5 Hz PRF, the bubbles were only just destroyed over the 30 seconds tested at 1.2 MPa (Figure 3.18 (a)), at 50 Hz, the cavitation signal drops to background after about 10 seconds (Figure 3.18 d) and at 5,000 Hz the cavitation signal lasts for less than 10 seconds (Figure 3.18 g). The cavitation signal decay is able to be broken up into the decay in harmonic component, followed by decay in broadband component. At each PRF tested, in the initial exposure period, the harmonic power dominates the signal. The harmonic signal decays rapidly, and the remainder of the signal is dominated by broadband power.

There is a notable reduction in both maximum power and total energy at 5,000 Hz PRF for SV and CNPs in the static phantom (Figures 3.22 and 3.23). At very high PRFs, the acquired window is long relative to the pulse length, and as such also captures some noise segments before the first cavitation event, which reduces the power reported which could explain the lower power at 5,000 Hz.

Over longer exposure periods of cavicatalytic nanoparticles in water, for example 10 minutes, CNPs maintained the energy of cavitation, and NCs show a maintained response that decayed slowly over time (Figure 3.24). One explanation for this continued cavitation response over long time periods of both particle types is that gas bubbles which are pulled from the particle surface are able to then re-stabilize back onto the particle after the pulse has finished. When the bubble is stabilised it is then able to respond to the subsequent pulses. If the bubble is left free in the surrounding water, and not stabilised in any other way for example encapsulated in a lipid, it would dissolve or coalesce with other bubbles. In addition, the number concentration is substantially higher compared with weight concentration of

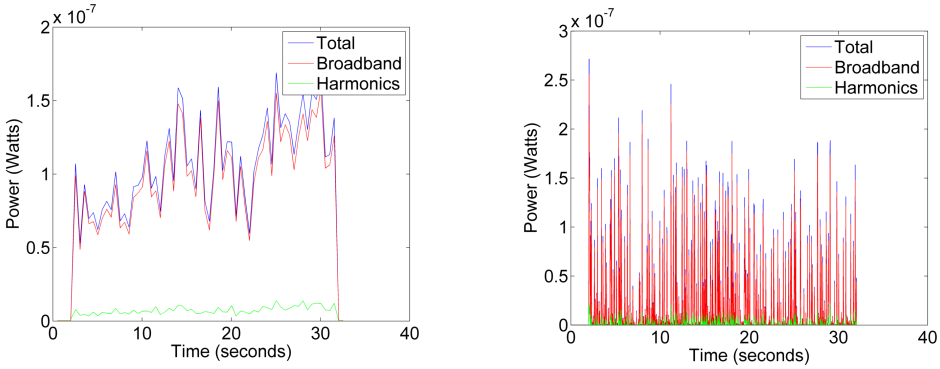

(a) *0.5 Hz*

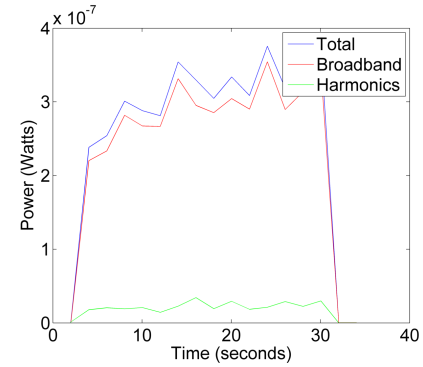

(b) *2 Hz*

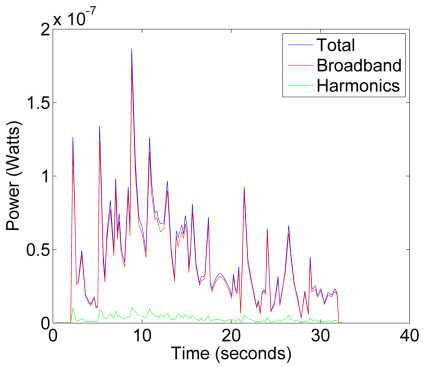

(c) *5 Hz*

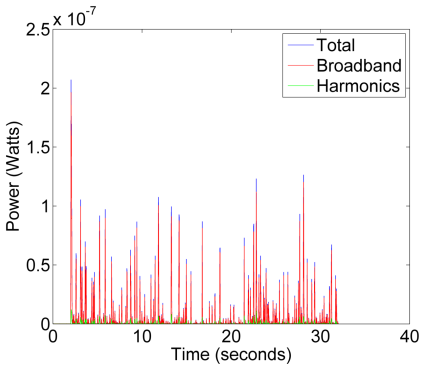

(d) *50 Hz*

(e) *500 Hz*

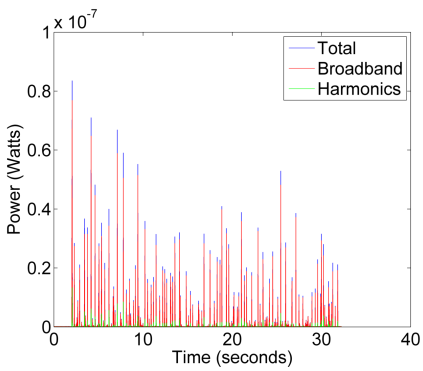

(f) *2,500 Hz*

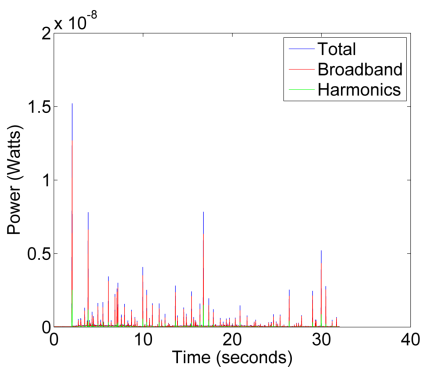

(g) *5,000 Hz*

Figure 3.21: *Power plots of cavitation received from the PCD from CNPs insonated at 1.2 MPa, 0.5 MHz, 5% DC, with varying PRF in the static phantom. Total (blue), broadband (red) and harmonic (green) power are plotted over the 30 second exposure period. Representative traces from each sample set are shown.*

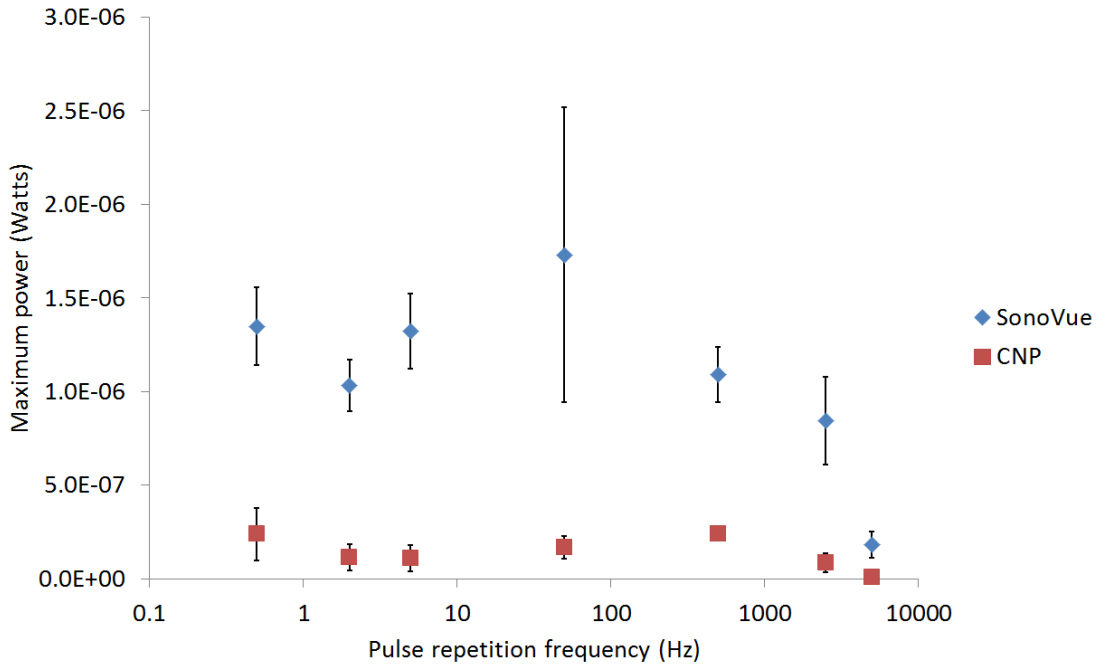

Figure 3.22: *The **maximum power** received over 30 seconds exposure was recorded over a range of PRFs for both SV and CNPs measured in the static phantom at 0.5 MHz. There doesn't seem to be a particular trend between maximum power and PRF. N=3, standard deviation shown.*

cavitation nuclei due to the small particle size. Extended cavitation activity may therefore also be explained by the high number of particles present in the phantom holder. The surface of the CNPs (Figure 3.6) compared with the NCs (Figure 3.7) shows a more 'open' surface where gas bubbles may more easily attach and stabilize. The NC particles on the other hand have a more 'protected' and 'closed' cavity which stabilises the gas once entrapped but is more difficult to re-stabilize once removed. This structure could explain why there is a slightly faster decay of the cavitation response from NCs compared with the CNPs.

In addition to the location of the gas relative to the particle type, and the shape of the particle, gas type also varies between cavitation nuclei tested. SV contains sulfur hexafluoride gas, which is poorly soluble in water. CNPs and NCs on the other hand trap atmospheric air on their surface which is mainly composed of nitrogen and oxygen. This difference in gas composition could also account for differences in cavitation energy and dynamics. Variation of gas composition on the particle surface could be explored further in future work.

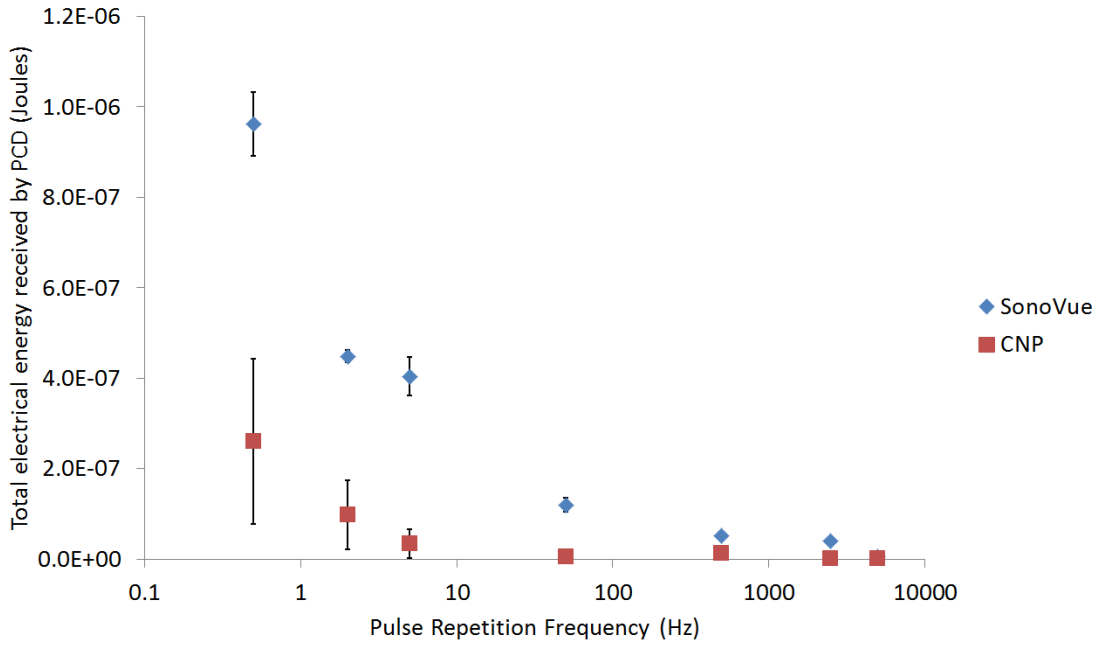

Figure 3.23: *The **total energy** over the 30 second exposure period was recorded over a range of PRFs for both SV and CNPs measured in the phantom holder at 0.5 MHz. There is a decrease in energy with increasing PRF for both SV and CNPs however this is attributed to different reasons as discussed in the text. N=3, standard deviation shown.*

3.4.4 Cavitation energy

3.4.4.1 Particle concentration

The concentration of cavitation nuclei (SV, CNPs and NC LB3s) is directly proportional to the energy received from cavitation events at low concentrations before reaching a plateau in energies at higher concentrations (Figure 3.25). This plateau may be explained by several theories: 1) a limit in the number of events which are able to be instigated in a given volume; 2) a limit in the violence of cavitation at a certain concentration; 3) shielding of ultrasound by the higher concentration of particles and gas bubbles between both the driving transducer and the sample and between the cavitation events and the PCD.

In the first two hypothetical cases, there is a decrease in the energy associated with cavitation events, even if it could be measured at the source. In the third case however, there are two possibilities. The first is that the nuclei are shielding the driving ultrasound pulse, and so the ultrasound energy at the nuclei is lower and the energy of cavitation events is reduced; the second is that the nuclei are shielding the ultrasound signal from the cavitation events that are produced, in that case the energy of cavitation events is still

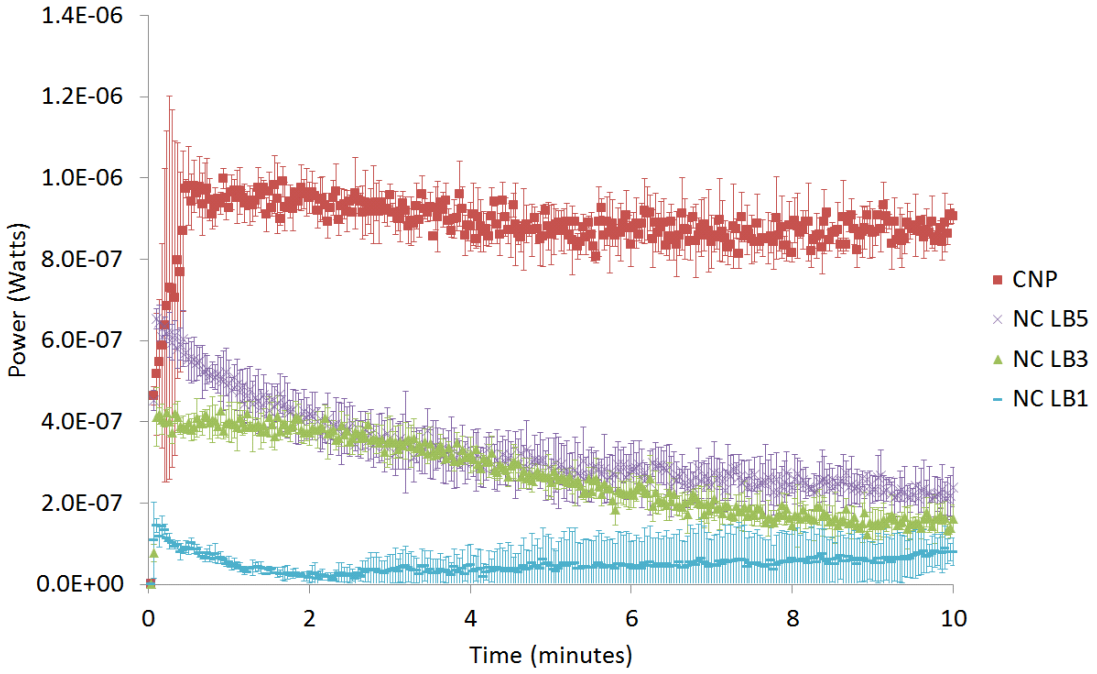

Figure 3.24: *Cavitation dynamics of cavicatalytic nanoparticles. Average and standard deviation of total power of cavitation instigated by CNPs (red), NC LB5 (purple), NC LB3 (green), NC LB1 (blue) over a ten minute period insonated at 0.5 MHz and 1.2 MPa PRFP is shown. N=3.*

increasing, it is just not possible to observe. It is likely that a combination of these two factors is contributing to the observed plateau in energy.

Given that SonoVue, a free microbubble, and the two cavicatalytic nanoparticles show the same response, it seems less likely that shielding of ultrasound is a dominating factor given the size difference between the cavitation nuclei, especially before the gas pockets have been exposed to the rarefactional pressure cycle. After the bubbles have expanded however, in each case, the gas from the cavicatalytic nanoparticles could reasonably shield in a similar way to the free microbubbles.

Clinically, this outcome suggests that at high concentrations, increasing the concentration of cavitation nuclei further will only marginally increase therapeutic outcomes compared with potential side effects of the increased concentration in the blood stream. This point however is heavily dependent on the pharmacokinetics of the cavitation nucleating particles.

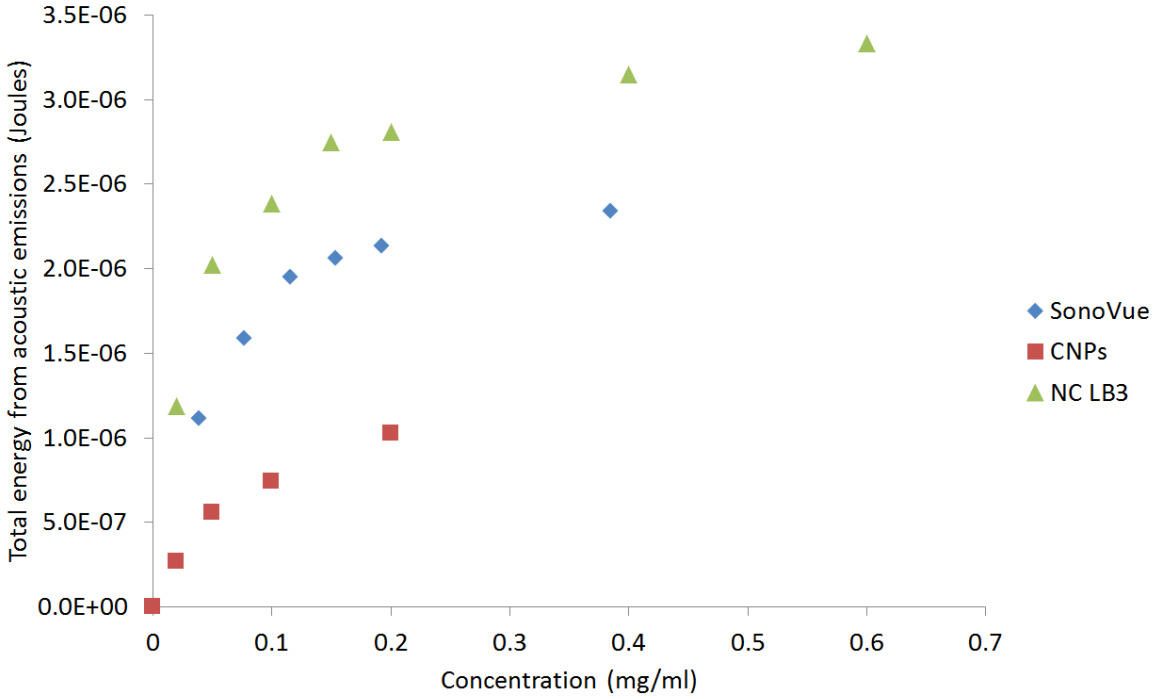

Figure 3.25: *Energy of cavitation with varying concentration of cavitation nuclei. SV (1.2 MPa), primed CNPs (1.5 MPa), and NC LB3 (1.5 MPa) in water were insonated in the static phantom holder at 0.5 MHz, 0.5 Hz PRF for 30 seconds. Total energy received from the PCD increases with increasing concentration in linear fashion at lower concentrations followed by a plateau at higher concentrations. N=1, previously un-exposed sample per concentration tested.*

3.5 Conclusions

Cavitation nuclei at the micro and nano scale both have potential to be used to enhance cancer therapy. Developing nuclei at the nano scale is important when considering the tumour microenvironment. At the nano-scale, particles are able to take advantage of the EPR effect as well as potentially penetrating deeper within the tumour.

The results presented and discussed in this chapter allow the following conclusions to be drawn. Firstly, cavicatalytic particles have been developed on the nano scale. These have been produced in two forms, rough and irregular CNPs; and smooth, regular particles with a single cavity, NCs. Both particle types were produced in monodisperse particle solutions. Each particle type was shown to instigate cavitation at thresholds dependent on the cavity sizes on the particle, with a signature broadband signal indicative of inertial cavitation. Secondly, the three particle types explored here, SV, CNPs and NCs, have thresholds useful for in vivo applications. The gain in signal above water is substantial over a wide range of pressures tested. Thirdly, cavitation thresholds for each particle type were frequency de-

pendent with a trend of increasing cavitation thresholds with increasing frequency for each particle type tested. Fourthly, cavitation dynamics were explored showing a decreasing time of cavitation decay with increasing PRF or increasing pressure for SV microbubbles, with no apparent cavitation decay with increasing PRFs observed for CNPs. Additionally, each of the cavicatalytic nanoparticles exposed to ultrasound showed a maintained cavitation signal over a 10 minute exposure. Fifthly, the stability of cavicatalytic particles was shown in clinically relevant injectable solutions (glucose 5%), over several weeks, with NCs showing good stability in water for up to 17 months. Finally, energy associated with cavitation showed a concentration dependence for each cavitation nuclei tested with a plateau in energies reached at high concentrations.

Chapter 4

Drug release using micro- scale cavitation nuclei

The motivation for this chapter's work is that the powerful cytotoxicity of low molecular weight chemotherapeutics could provide far greater anticancer efficacy if dosing was not restricted by severe adverse effects in non-target tissues [79].

To address this issue, liposomal delivery systems have been developed to take advantage of the EPR effect [124]. Doxil, a Food and Drug Administration (FDA) approved, HSPC-based liposomal form of doxorubicin, has shown clinical benefit in cancers such as Kaposi's sarcoma [17, 44], but has not been used more widely. Clinical efficacy of such systems has been limited by two main factors: poor penetration into non-vascularised tumour regions and poor release of payload within the tumour [114, 175].

Triggered drug release, as opposed to passive drug release as used in the case of Doxil, is critical in ensuring an effective dose is delivered to the tumour. Previous liposomes designed for triggered release have been formulated to be either heat sensitive or ultrasound sensitive as discussed in Section 1.8 or to respond to the distinct tumour environment [77, 104]. Here the development of cavitation sensitive liposomes, that are stable in the presence of heat or ultrasound alone, and rupture in the presence of cavitation, is discussed. These liposomes are distinct from those currently available commercially, and have the potential to deliver targeted and triggered drug release with minimal side effects due to the triggering mechanism. This chapter outlines the liposomal drug carriers and release

profiles in response to cavitation nucleated from microbubbles. Throughout this chapter, the 'stability' of liposomes is referring to their encapsulation and release profiles, where 'stable' liposomes do not release any drug when exposed to a stimulus. For clarification, this term is not being used to refer to 'stable cavitation' with regard to liposomes, unless otherwise stated.

Drug release from cavitation sensitive liposomes was tested using a luciferin - luciferase model as well as a model drug, doxorubicin. The main findings from this work are published by S. M. Graham et al. in the Journal of Controlled Release [79][1] and are described in more detail with greater analysis below.

4.0.1 Physical characterisation of liposomes

Liposomes used in these experiments were prepared either by the author or by Dr Robert Carlisle. The two liposomal formulations tested here were HSPC- and DSPE-based liposomes as described in Section 2.2. After formulation, liposomes were cloudy and coloured with the colour of the drug loaded e.g. yellow when loaded with luciferin and red when loaded with doxorubicin.

DSPE was incorporated into liposomes to confer the property of cavitation triggered destabilisation upon the liposomes. DSPE has a packing parameter above 1 which is why it has a propensity to form inverted hexagonal structures at pH <9 when the head phosphate group and amine group carry opposing charges. This lipid structure allows destabilisation of the lipid bilayer when compared with lipids with lower packing parameters.

During production, size and polydispersity of DSPE liposomes decreased to a final monodisperse liposomal population with hydrodynamic diameter 159 nm and PDI of 0.059 (Figure 4.1 (a)) and Table 4.1). Fenestrations in the sinusoidal epithelium of the liver are 99 $\pm$ 18.0 nm wide in the mouse and 50 - 300 nm wide in the human [25]. These liposomes have been designed to have a size just larger than the gaps in the sinusoidal epithelium of the mouse to improve circulation during *in vivo* studies. Zeta potential measurements of liposomes showed a slight negative surface charge (Figure 4.1 (b)) of -8.43 mV, most likely

[1]Drug release from cavitation sensitive liposomes using SonoVue as the cavitation nucleating particle has been published in the Journal of Controlled Release with permission from Elsevier [79]

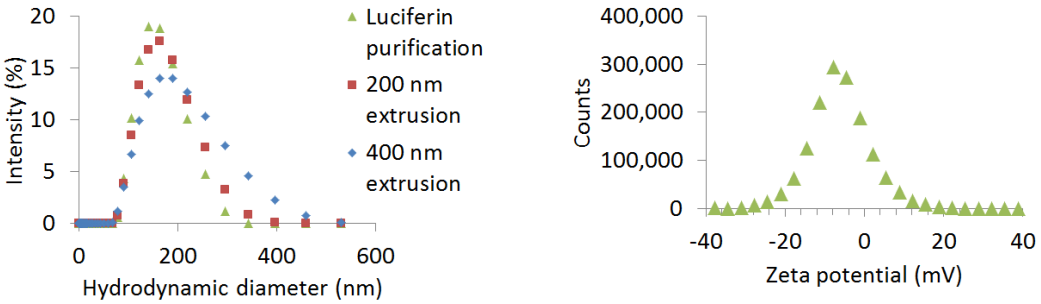

(a) *Size* **(b)** *Zeta potential*

Figure 4.1: *Characterisation of DSPE liposomes during and after production. (a) After 400 nm extrusion (blue diamond), 200 nm extrusion (red square), and luciferin encapsulation and purification (green triangle), DSPE liposomes were sized using DLS, 3 runs, showing a decrease in both hydrodynamic diameter and PDI during production; (b) After luciferin purification liposomes had a zeta potential of -8.43 mV in 12.5 mM HEPES, 10 mM NaCl buffer, pH 7.5, n=1.*

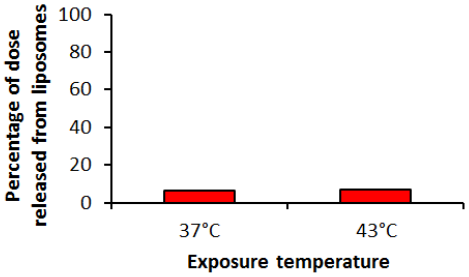

Figure 4.2: *Temperature stability of luciferin loaded liposomes, no increased release was observed at physiological temperature (37°C) or under mild hyperthermia conditions (43°C) over 15 minutes. N=3, SD shown. Image taken from [79] (Graham et al., 2014) with permission from Elsevier.*

due to the negative charge of DSPE-PEG [12]. As these liposomes are pegylated, the steric hindrance afforded to the liposomes by the PEG molecules provides stability whilst charge plays a minimal role.

Table 4.1: *Size characteristics of DSPE liposomes throughout production. Polydispersity index (PDI) and hydrodynamic diameter measured by Z-average (Z-ave) and Intensity (Int) distributions decrease with each step in production.*

After stage:	PDI	Z-ave (nm)	Int (nm)
400 nm extrusion	0.133	170.7	195.4
200 nm extrusion	0.082	155.0	169.7
Luciferin purification	0.059	147.9	159.1

Luciferin encapsulation was confirmed by the luciferin-luciferase assay which showed a low concentration of free luciferin background signal of 14.7%. DSPE liposomes were stable to both 37°C and 43°C temperatures over 15 minutes of incubation 4.2. This result suggests that the liposomes will be stable *in vivo* at physiological temperatures, and will not be affected by mild hyperthermia, unlike the thermosensitive liposomes produced by Dromi et al. [57].

4.0.2 Monitoring drug release from liposomes

In the presence or absence of SV microbubbles, liposomes not exposed to ultrasound were stable over the treatment period. These samples were used as background controls for all ultrasound treated samples.

The two formulations of liposomes tested, HSPC- and DSPE-based, were both stable to ultrasound exposure in the absence of SV cavitation nuclei, at each pressure tested (Figures 4.3 and 4.4). Without microbubbles present, no cavitation signal was detected, confirming that the liposomes were stable to non-cavitation inducing ultrasound conditions.

In the presence of SV and when exposed to increasing ultrasound pressures, cavitation signals were recorded (Figure 4.7) with increasing broadband energy while harmonic energy plateaued (Figure 4.8). HSPC liposomes were stable at each of the pressures tested, up to 1.5 MPa PRFP, in the presence of SV. DSPE liposomes were stable at the lower pressures tested, 0.14, 0.5 and 0.8 MPa, but were unstable to 1.2 and 1.5 MPa in the presence of SonoVue. The lowest ultrasound conditions used which showed drug release was 1.2 MPa, 0.5 MHz, which has a corresponding mechanical index (MI) of 1.697 and I_{SPPA} of 0.0486 kW/cm^2. Previously reported drug release had only been seen at 10.5 kW/cm^2 [62] in the absence of SV cavitation nuclei, showing how important reducing the cavitation threshold of the media is.

The same liposomal formulation of DSPE was prepared and loaded with doxorubicin and showed similar release results to the luciferin loaded liposomes. In the absence of SV, no increase in release was observed at any pressure. In the presence of SV, at 0.14, 0.5 and 0.8 MPa, no increase in release was observed. However at 1.2 MPa and 1.5 MPa, 49% and 100% drug release was detected respectively.

Cells were incubated with the liposomal samples after ultrasound exposure to determine the effect of this concentration of drug release on cells *in vitro*[2]. At conditions where no release was observed, there was no significant increase in cell death. At conditions where doxorubicin release was observed (1.2MPa and 1.5 MPa in the presence of SV), significant increase in cell death was also observed. This finding, shows that ultrasound is able to be used to release drug from liposomes when in the presence of SV, which in turn is capable

[2]Rachel Myers and Dr Apurva Shah conducted the cell death assays

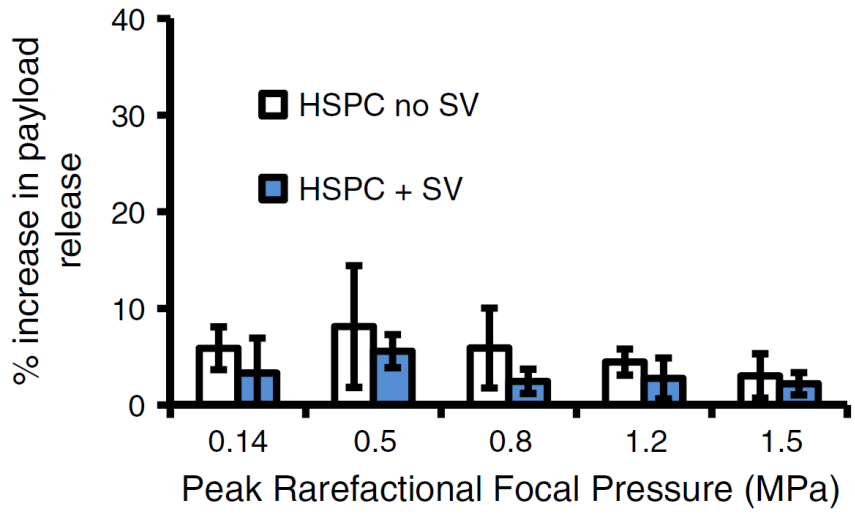

Figure 4.3: *In vitro assessment of inertial cavitation induced drug release. The 0.5-MHz ultrasound was used to expose samples at 5% duty cycle with 50,000 cycle pulses with a pulse repetition frequency of 0.5 Hz for 30 sec. Luciferin release from HSPC liposomes is shown as percentage increase from background (non-exposed) samples over the pressure range tested. Two-way ANOVA for significance, ***p<0.001, n=3, standard deviation shown. Image taken from [79] (Graham et al., 2014) with permission from Elsevier.*

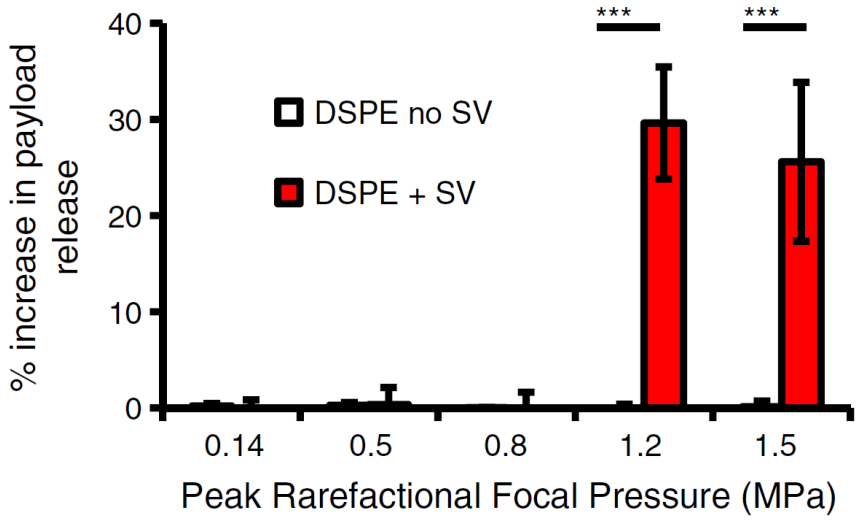

Figure 4.4: *In vitro assessment of inertial cavitation induced drug release. The 0.5-MHz ultrasound was used to expose samples at 5% duty cycle with 50,000 cycle pulses with a pulse repetition frequency of 0.5 Hz for 30 sec. Luciferin release from DSPE liposomes is shown as percentage increase from background (non-exposed) samples over the pressure range tested. Two-way ANOVA for significance, ***p<0.001, n=3, standard deviation shown. Image taken from [79] (Graham et al., 2014) with permission from Elsevier.*

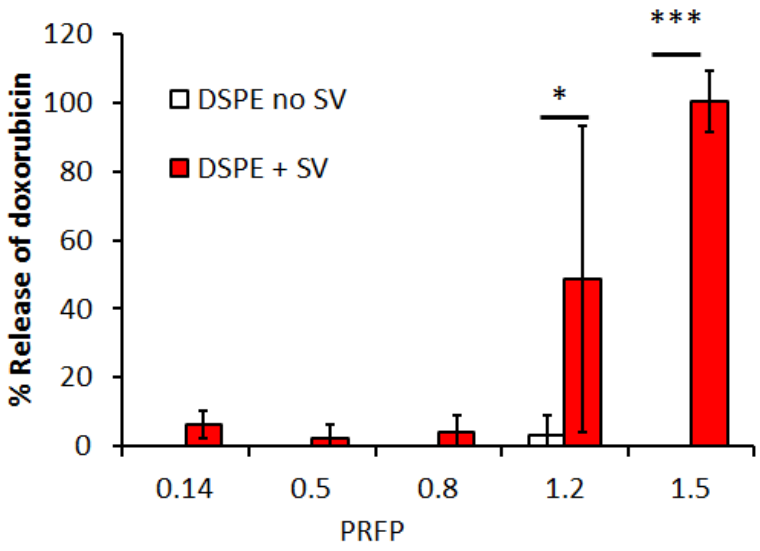

Figure 4.5: *Cavitation mediated release of doxorubicin from liposomes. Liposomes were formulated as in methods with the exception of the inclusion of doxorubicin instead of luciferin and exposed to a range of pressures creating no, stable, or inertial cavitation. Release was assayed by measuring increase in fluorescence signal at 490 ex/ 590 em. N=3, SD shown, analysis by ANOVA with Tukey compare all columns post test using PRISM software. Image taken from [79] (Graham et al., 2014) with permission from Elsevier.*

of eliciting a positive effect of cell death *in vitro*.

The factors associated with release from these liposomes are discussed below.

4.0.3 Variables affecting drug release

4.0.3.1 Level of cavitation activity

The activity of cavitation events is able to be measured in various ways: total energy of acoustic emissions arising from cavitation events; harmonic or broadband energy; maximum power of acoustic emissions over the exposure period; and indirectly by measuring the rate of bubble destruction observed visually. These measures are evaluated for their correlation with drug release below.

In the absence of SV, no acoustic emissions were observed at any exposure pressure, indicating that pressures tested were insufficient to instigate cavitation in a liposome and PBS mixture without additional cavitation nuclei. Figure 4.7 shows that over the full pressure range tested, acoustic emissions are able to be observed. At 0.14 MPa, low-energy harmonics are able to be observed (panel (i)), indicated by a red arrow as an example at 2.5

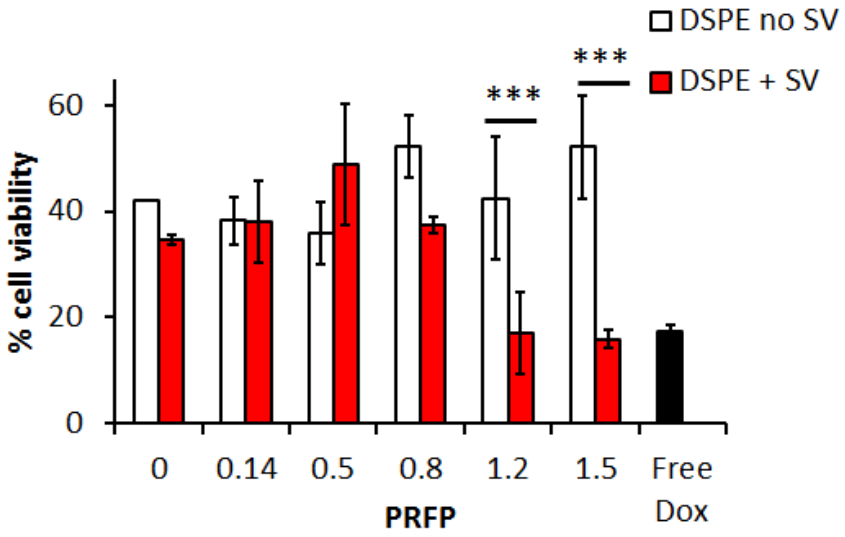

Figure 4.6: *Cavitation mediated release of doxorubicin from liposomes. Liposomes were formulated as in methods with the exception of the inclusion of doxorubicin instead of luciferin and exposed to a range of pressures creating no, stable, or inertial cavitation. Release was assayed by measuring kill of cancer cell line B16F10-luc by MTS assay, and plotted as a percentage of that achieved by heating to 100 degrees for 1 min. N=3, SD shown, analysis by ANOVA with Tukey compare all columns post test using PRISM software. 'Free Dox' = the equivalent concentration of doxorubicin added as free drug. Image taken from [79] (Graham et al., 2014) with permission from Elsevier.*

MHz, and repeated at multiples of 0.5 Mhz. With increasing pressure, the energy of broadband emissions (indicated by a black arrow in panel (ii)), also increases. These broadband emissions are associated with shock waves created when unstable bubble oscillations lead to inertial cavitation.

The cavitation energy in the harmonic bands increases to 0.5 MPa and then plateaus with increasing pressure. The broadband cavitation energy however increases in a near linear fashion with increasing pressure (Figure 4.8). This result suggests that the increasing broadband energy is what explains the liposomal release, and not the harmonic energy.

Figure 4.9 shows a total cavitation energy threshold, below which no release from cavitation sensitive liposomes is observed. The lowest energy of broadband acoustic emissions at which release was observed was 1.68 μJ over the 30 second exposure. Above this total energy threshold, release was seen from every DSPE sample, and below this threshold, no release was seen. This observation shows that these DSPE- based liposomes are sensitive to high energy inertial cavitation and stable to ultrasound alone, at the pressures tested.

In contrast however, there was no increase in payload release from HSPC- based liposomes, either in the absence or presence of SV, even when the total energy associated with

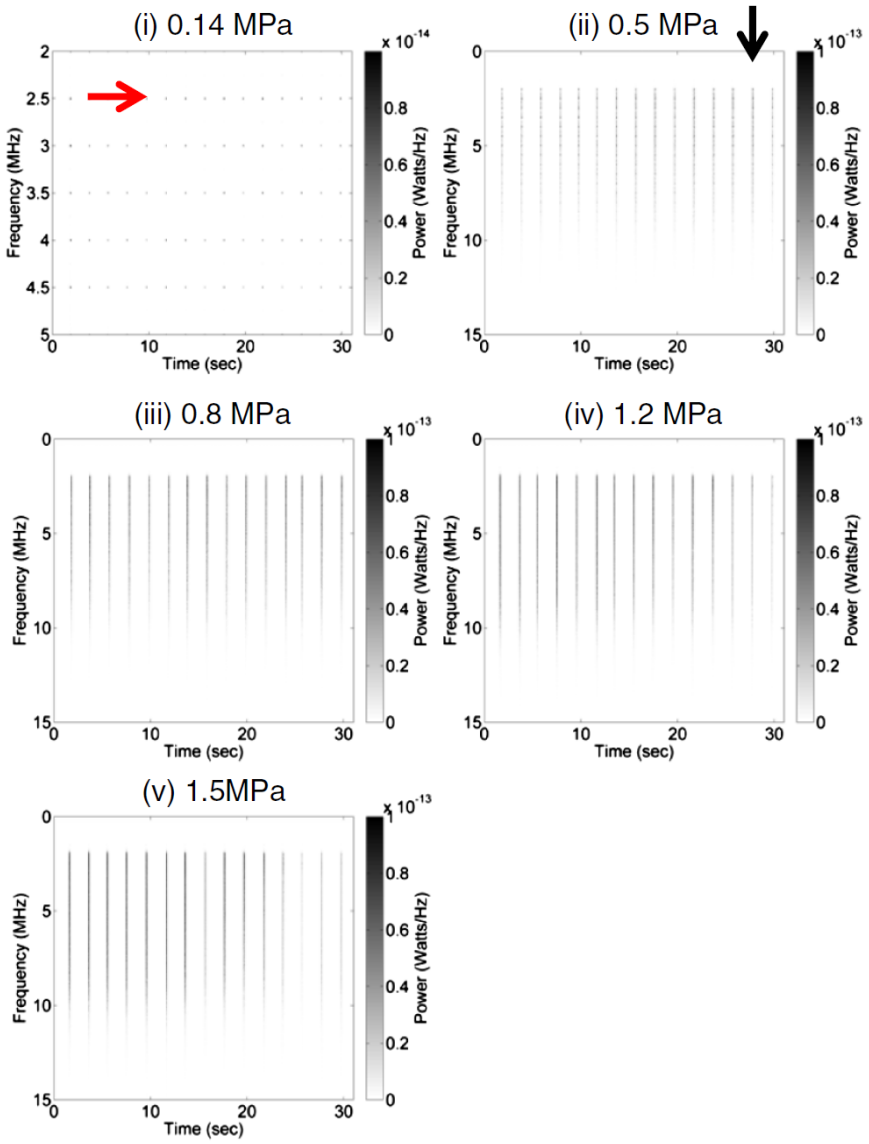

Figure 4.7: *In vitro assessment of inertial cavitation induced drug release. The 0.5-MHz ultrasound was used to expose samples at 5% duty cycle with 50,000 cycle pulses with a pulse repetition frequency of 0.5 Hz for 30 s. Representative power spectral densities of DSPE liposomes in the presence of SV at (i) 0.14 MPa, (ii) 0.5 MPa, (iii) 0.8 MPa, (iv) 1.2 MPa, (v) 1.5 MPa. Image taken from [79] (Graham et al., 2014) with permission from Elsevier.*

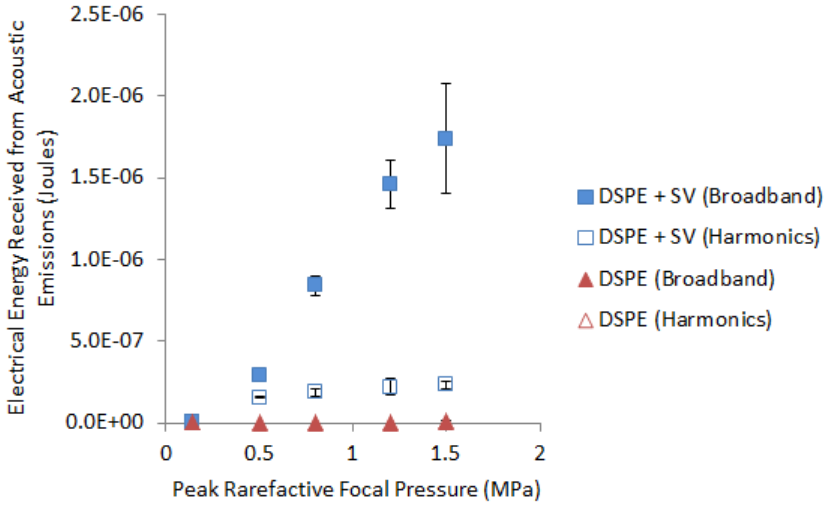

Figure 4.8: *Energy associated with cavitation from samples with and without SV, divided into harmonics and broadband emissions. At 1.5 MPa, rapid bubble destruction results in a decreased energy of emissions over exposure time resulting in higher variation between samples. Harmonic energy of acoustic emissions plateaus with increasing pressure, n=3, SD shown. Image taken from [79] (Graham et al., 2014) with permission from Elsevier.*

cavitation surpassed that seen in DSPE + SV samples insonated in a similar way.

The correlation between doxorubicin release and broadband energy emissions detected is much stronger than the correlation with maximum power of cavitation events. Similar to total energy, there is a 'broadband energy threshold' above which, there is doxorubicin release, and below which, there is not (Figure 4.11(a)). The correlation with maximum power however is weak with high maximum powers yielding both low and high release of doxorubicin from DSPE liposomes (Figure 4.11(b)).

When SV is exposed to ultrasound, bubble destruction is able to be observed in real time by eye. Still images from videos taken (Supplementary Video 1) of each sample are shown in Figure 4.12. Before ultrasound exposure begins (Figure 4.12 (a)), doxorubicin loaded, liposomal samples appear red and opaque. At 0.14 MPa, after 30 seconds of exposure, bubbles are still able to be seen in the sample (Figure 4.12 (b)), however some bubble destruction is able to be observed. Complete bubble destruction, as determined visually by total loss of opacity in the solution, occurs after 10 pulses, 8 pulses, 7 pulses and 6 pulses when exposed to 0.5 MPa, 0.8 MPa, 1.2 MPa and 1.5 MPa respectively (Figure 4.12 (c), (d), (e), and (f)). SV destruction is not necessarily correlated with liposome destruction, as the gas filled SV microbubbles are destroyed by the ultrasound expanding and collapsing that

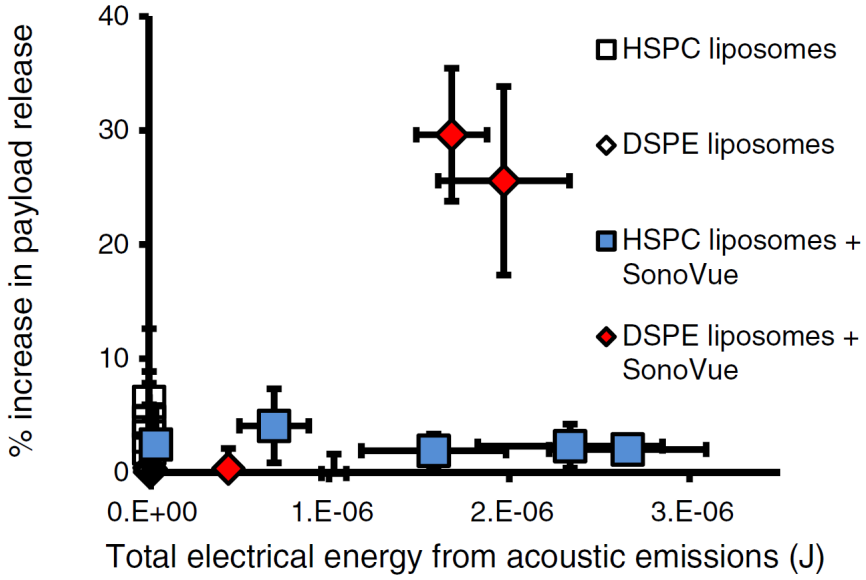

Figure 4.9: *In vitro assessment of inertial cavitation induced drug release. The 0.5-MHz ultrasound was used to expose samples at 5% duty cycle with 50,000 cycle pulses with a pulse repetition frequency of 0.5 Hz for 30 sec. Correlation between energy of acoustic emissions and liposomal release is shown for each sample set of HSPC liposomes and DSPE liposomes in the absence and presence of SV. n=3, standard deviation for both energy and release is shown. Image taken from [79] (Graham et al., 2014) with permission from Elsevier.*

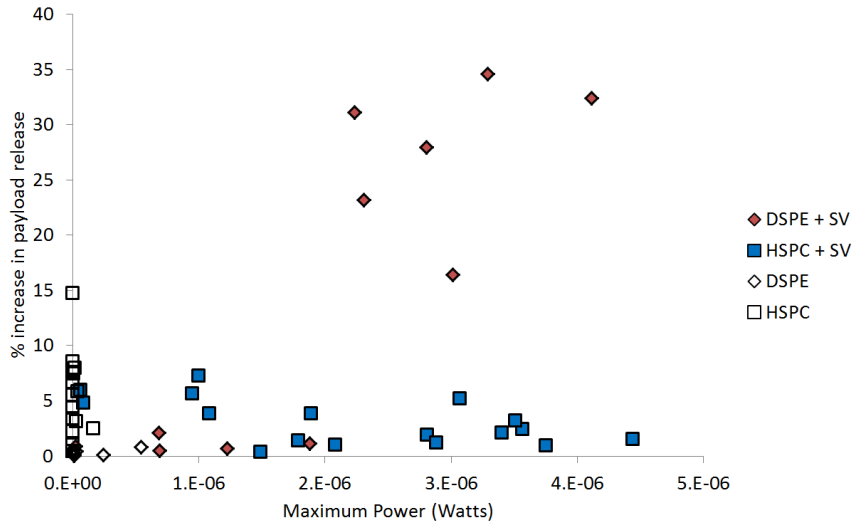

Figure 4.10: *Correlation between maximum power associated with cavitation over 30 second exposure and drug release. The 0.5 MHz ultrasound was used to expose samples at 5% duty cycle with 50,000 cycle pulse with a pule repetition frequency of 0.5 Hz for 30 seconds. Maximum power for each sample plotted against corresponding drug release for each of DSPE and HSPC liposomes in the absence and presence of SonoVue.*

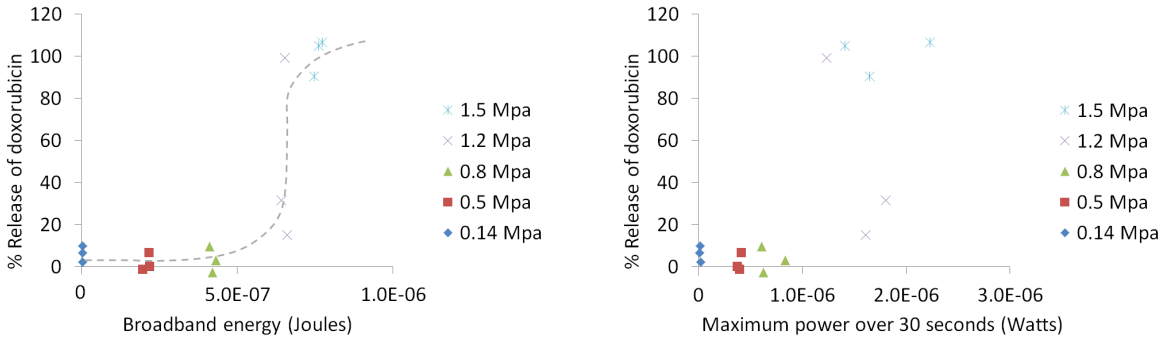

(a) *Broadband energy* **(b)** *Maximum power*

Figure 4.11: *Liposomal release compared to broadband energy and maximum power. Percent doxorubicin release from DSPE- based liposomes for each sample (n=3) plotted against (a) broadband energy shows a sharp threshold, where above that threshold, 100% release is observed (grey dashed line proposed as threshold). Release plotted against (b) maximum power does not show a clear threshold with low and high release observed with similar maximum powers. Maximum power was calculated over the 30 second exposure period.*

gas cavity, whereas the liposomes do not have gas inside them to expand and collapse. The liposomes are broken via mechanical disruption of their lipid bilayer from cavitation events of nearby bubbles. The rate of bubble destruction however is most likely proportional to the magnitude of the cavitation events. With increasing energy of cavitation emissions, the bubbles are destroyed faster. High destruction rates therefore likely correlate with more violent and more numerous cavitation events and therefore liposomal destruction leading to drug release.

4.0.3.2 Temperature

Temperature changes during ultrasound exposure were measured with and without SV cavitation nuclei present. The samples were immersed in a water tank either at room temperature or at 37°C.

In a tank at room temperature, slight fluctuations in temperature were seen every 2 seconds (equivalent to the pulse period) (Figure 4.13). The temperature increase at 1.2 MPa compared to 0.14 MPa and 0.5 MPa and the increase at 1.5 MPa compared to 0 MPa, 0.14 MPa, 0.5 MPa and 0.8 MPa in the presence of SonoVue was significant ($p<0.05$, One-way ANOVA). However, there was no overall increase in temperature of more than 0.11°C (Figure 4.14) which implies that temperature does not play any role in release from the liposomes.

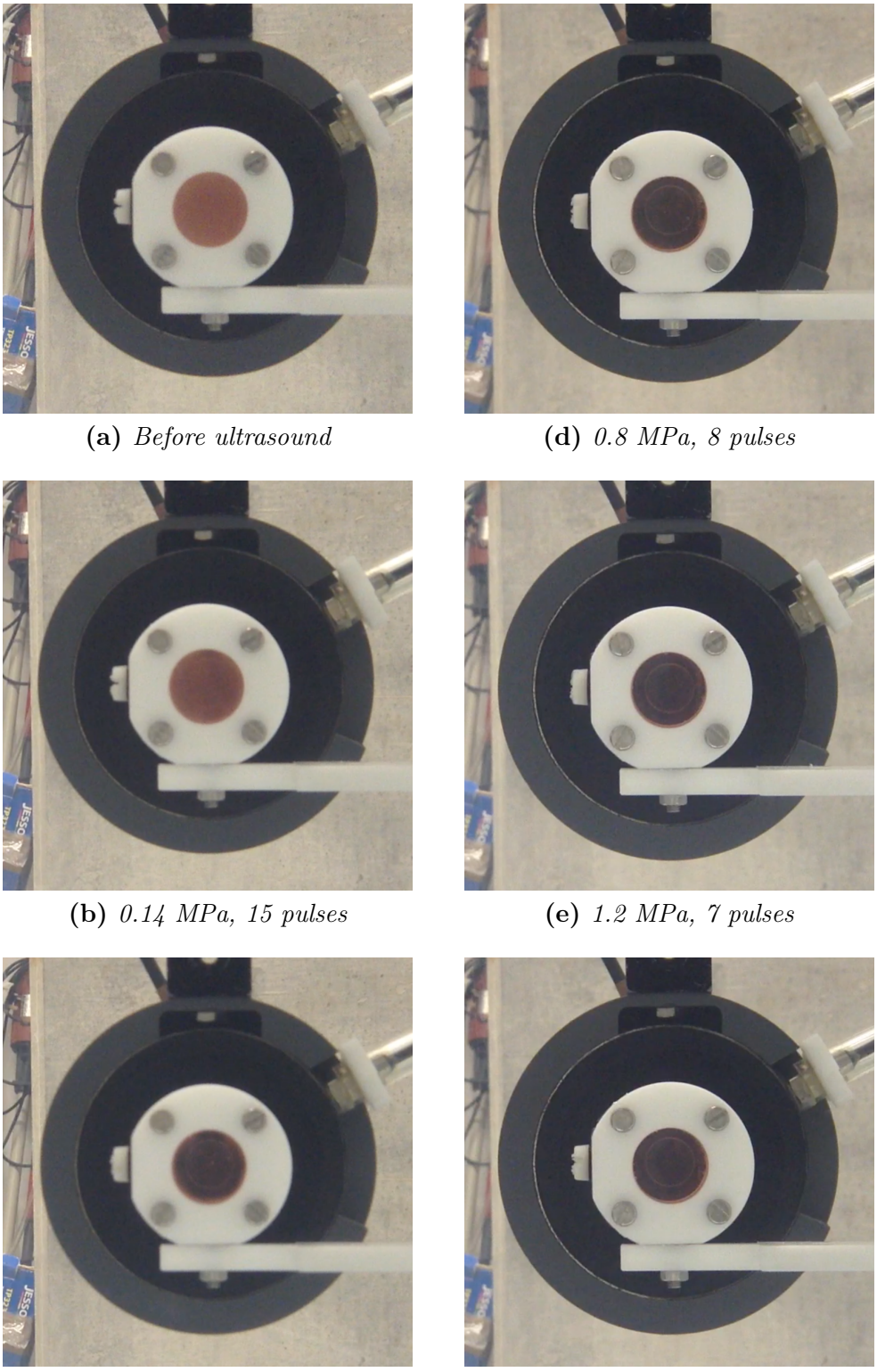

(a) *Before ultrasound*

(d) *0.8 MPa, 8 pulses*

(b) *0.14 MPa, 15 pulses*

(e) *1.2 MPa, 7 pulses*

(c) *0.5 MPa, 10 pulses*

(f) *1.5 MPa, 6 pulses*

Figure 4.12: *SonoVue microbubble destruction when exposed to ultrasound. DSPE liposomes, loaded with doxorubicin, exposed to ultrasound at 0.5 MHz, 5% DC, 0.5 Hz PRF for 30 seconds. a) Before insonation, samples were cloudy and showed the red from the doxorubicin loaded liposomes. b) 0.14 MPa did not destroy all the SonoVue over the exposure period. At 0.5 MPa and higher, complete SonoVue destruction was observed visually after c) 10 pulses at 0.5 MPa, d) 8 pulses at 0.8 MPa, e) 7 pulses at 1.2 MPa and f) 6 pulses at 1.5 MPa. Images taken after the pulse when no further bubble destruction was observed in each video.*

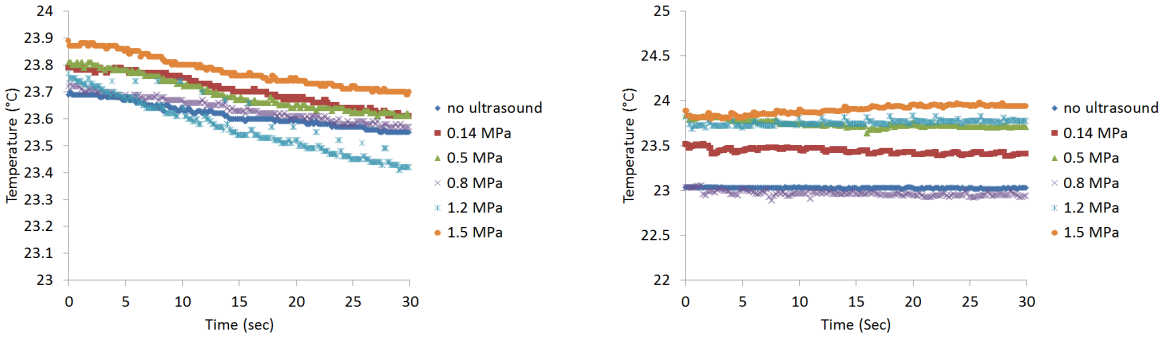

(a) *No SonoVue* **(b)** *With SonoVue*

Figure 4.13: *Temperature changes during ultrasound exposure. Samples were exposed to 0.5 MHz, 0.5 Hz PRF, 5% DC ultrasound at a range of PRFPs. Sample chambers either contained a) PBS alone or b) PBS with SonoVue, with a thermocouple aligned to the middle of the sample chamber, prepared at room temperature, and submerged in a water tank at room temperature. Representative thermocouple traces are shown of n=3.*

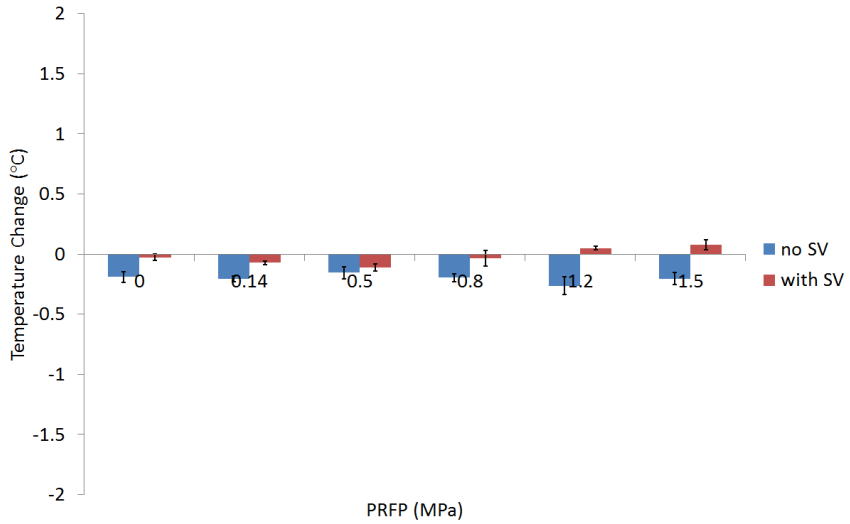

Figure 4.14: *Overall temperature change of samples exposed to ultrasound for 30 seconds with and without SonoVue. Samples were prepared at room temperature, submerged in a water tank at room temperature and exposed to 0.5 MHz, 0.5 Hz PRF, 5% DC for 30 seconds. Thermocouple measurements were taken in the centre of the phantom holder. N=3, standard deviation shown.*

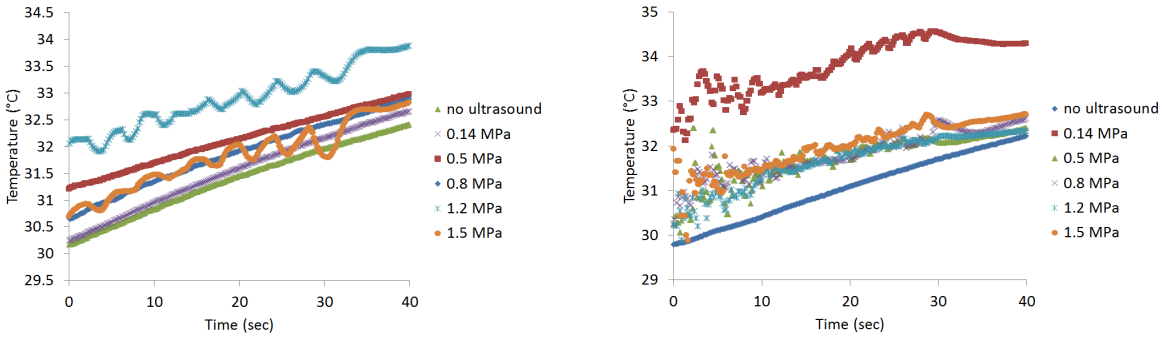

(a) *No SonoVue* **(b)** *With SonoVue*

Figure 4.15: *Temperature changes during ultrasound exposure. Samples were exposed to 0.5 MHz, 0.5 Hz PRF, 5% DC ultrasound at a range of PRFPs. Sample chambers either contained a) PBS alone or b) PBS with SonoVue, with a thermocouple aligned to the middle of the sample chamber, prepared at room temperature, and submerged in a water tank at 37° C. Representative thermocouple traces are shown of n=3.*

With samples prepared at room temperature and the tank heated to 37°C, the temperature at which release studies were performed, more pronounced fluctuations were observed, shown in Figure 4.15. The sample is gradually being heated from room temperature to the tank temperature (37°C) as seen with the 'no ultrasound' sample both with and without SV. The fluctuations occurring every 2 seconds however are far greater in magnitude when compared with those in the tank at room temperature. The fluctuations that occur may be due to a mixing effect in the sample chamber. The sample near the edge of the holder (nearest the 37°C tank water) is heating faster than in the middle and so upon each pulse, as the solution is mixed, the heated sample is pushed into the middle where the thermocouple probe is. This mixing, and not heating due to cavitation, explains why no significant increase ($p>0.05$, One-way ANOVA) in temperature is seen with increasing pressure (Figure 4.16). It is notable that temperature fluctuations are larger in the presence of SV (Figure 4.15 (b)) at each pressure tested than without (Figure 4.15 (a)), indicating that, in accordance with literature on microstreaming and bubbles [82], SV, when exposed to ultrasound, enhances mixing of the sample.

In summary, the results show that temperature fluctuations cannot account for the increase in release seen when exposed to ultrasound in the presence of SV. Although there is an increase in temperature of 0.11°C when performed at room temperature, and an increase of 2.28°C when performed at 37°C, the liposomes have been shown to be stable at elevated temperatures (Figure 4.2). Therefore, cavitation-induced heating does not play a

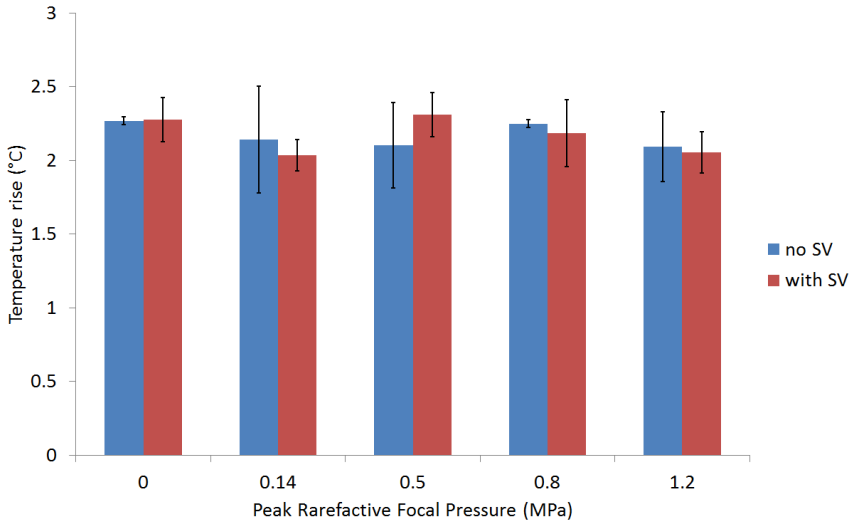

Figure 4.16: *Overall temperature change of samples exposed to ultrasound for 30 seconds with and without SonoVue. Samples were prepared at room temperature, submerged in a water tank at 37°C and exposed to 0.5 MHz, 0.5 Hz PRF, 5% DC for 30 seconds with a 10 second wait after exposure. Thermocouple measurements were taken in the centre of the phantom holder. N=3, standard deviation shown.*

role in release from these cavitation-sensitive liposomes.

4.1 Conclusions

Triggered drug delivery requires that drug carriers are stable in the blood stream, and are capable of being ruptured only in the presence of a given trigger. For practical applications, monitoring of drug release is important for delineating between failed drug delivery, and failed drug potency. In this chapter a triggered system for drug delivery, with corresponding cavitation monitoring system which correlates cavitation with drug release has been demonstrated. This system, although only demonstrated here with a single liposomal formulation and two payload types, has the potential to be developed for multiple drug payloads, and optimised for different ultrasound driving parameters.

The *in vitro* studies conducted here demonstrate that a DSPE-based liposome is able to be formulated to be cavitation-responsive. These studies showed that the property of cavitation sensitivity was dependent on liposome composition, where Doxil-like, HSPC-based liposomes were stable to cavitation events, where as DSPE-based liposomes were cavitation sensitive. In addition, this liposome formulation is stable to ultrasound alone,

only releasing their payload when in the presence of high energy inertial cavitation.

Using passive cavitation detection, the release seen from liposomes could be correlated with total energy and maximum power of the acoustic emissions arising from cavitation activity. Both metrics show that, in the absence of substantial energy associated with cavitation activity, release from liposomes is not observed. However, above a minimum threshold of either the energy or the maximum power substantial and significant ($p < 0.001$) release is observed.

To summarise, the following conclusions can be drawn. Firstly, liposomes have been formulated to be stable to conditions experienced *in vivo*. Secondly, liposomes are able to be formulated to be cavitation stable or cavitation sensitive depending on lipid composition. Thirdly, there is a strong correlation between broadband energy and maximum power from cavitation and drug release from DSPE-based liposomes which may be suitable for use in monitoring drug release. Finally, heating associated with cavitation cannot explain the drug release seen from DSPE-based liposomes indicating that cavitation in the absence of heating is sufficient for triggered drug release.

Chapter 5

Drug release using cavicatalytic nanoparticles

Drug release using cavitation events enables a triggered and targeted drug delivery strategy for tumours. In Chapter 4, cavitation using micro-scale cavitation nuclei, i.e. SonoVue, was shown to be effective in causing drug release from liposomes. It is also known however that in an *in vivo* environment, SV microbubbles are constrained to the vasculature, whereas nanoparticles (including drug carrying liposomes) have the potential to accumulate deeper into the tumour via the EPR effect as a result of their size. Based on this rationale, cavitation nuclei at the nano-scale could potentially provide a drug delivery stimulus over a larger volume of the tumour mass, and potentially closer to the drug carrying liposome. In this chapter, drug release studies using cavitation nuclei at the micro- and nano-scale are shown with varying ultrasound parameters, thus developing a system whereby both the drug carrier (liposome) and effector agent (cavicatalytic nanoparticle) are both at the nano-scale.

5.1 Method and materials adjustments

In a similar fashion to experiments conducted in Chapter 4, drug release from liposomes, when exposed to ultrasound and cavitation nuclei, was assessed *in vitro* in a static phantom. The liposomal formulation used for the study was the DSPE liposome developed in Chatper 4 using the luciferin - luciferase assay for assessing drug release. Expanding on the work of Chapter 4 however, both 0.5 MHz and 1.614 MHz ultrasound exposure was used to assess

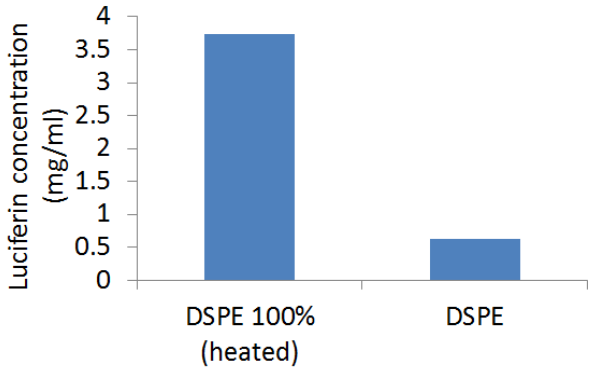

Figure 5.1: *Encapsulation of luciferin into undiluted DSPE liposomes. Background free luciferin of 21.6% with total loading (total in sample minus free luciferin) of 2.92 mg/mL was measured using the luciferase assay.*

the applicability of this system at frequencies more similar to those used clinically.

Based on the stability study findings in Chapter 3, particle solutions were prepared in 5% glucose solutions. CNPs were prepared as in Chapter 3 at 0.2 mg/mL in water and then diluted 50:50 into 10% glucose solutions to a final concentration of 5% glucose. CNPs were primed with 0.5 MHz, 5% DC at 1.5 MPa PRFP for 90 seconds before use. NC particles were prepared as in Chapter 3 and diluted 1:10 into 5% glucose. SonoVue® (SV) was prepared according to manufacturer's instructions and diluted 300 μL into 7ml PBS. Liposomal samples (50 μL) were added directly to 7 mL CNP or NC particle solution with no further dilution.

Liposomal encapsulation was tested using the luciferin-luciferase assay confirming a background free luciferin percentage of 21.6% with a total luciferin concentration of 3.73 mg/mL and a total encapsulated luciferin concentration of 2.92 mg/mL (Figure 5.1).

SV, CNPs and NC LB3s, were chosen as cavitation nuclei for liposomal release studies to test multiple criteria. SV was used as a known control particle based on results from Chapter 4. CNPs and NC LB3s were chosen as cavitation nuclei to prove the same concept as in Chapter 4 but at the nano-scale. CNPs were the smallest cavitation nuclei chosen and also exhibited a rough surface. The method of bubble action as proposed in Chapter 3 is that multiple smaller gas pockets join to form one larger bubble, or that a gas layer around the particle is detached to form one bubble. In contrast, NC LB3 were chosen as a morphologically uniform particle with an approximate 300 nm gas pocket and 500 nm particle diameter. NC LB3 was chosen over NC LB1 or NC LB5 as NC LB1 was more difficult to manufacture, and NC LB5 is unlikely to be able to take advantage of the EPR effect due to its size being close to the micron size range.

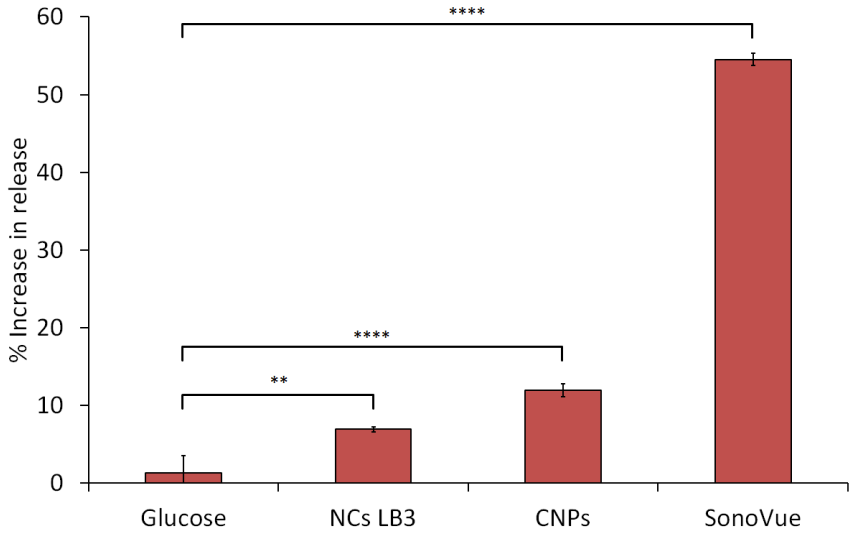

Figure 5.2: *Luciferin release from DSPE liposomes using a 0.5 MHz therapeutic ultrasound exposure of 90 seconds at 1.5 MPa with or without the addition of SV, CNPs or NCs (LB3). One-way ANOVA with Tukey for significance, **** $p < 0.0001$, ** $p < 0.01$, n=3, standard deviation shown.*

5.2 Achieving drug release using nanoscale cavitation nuclei

The work in this chapter expands on the *in vitro* work in Chapter 4 with further experiments *in vitro* using cavicatalytic nanoparticles as cavitation nuclei. Initial studies were conducted over a 90 second exposure period, similar to those in Chapter 4, using a 0.5 MHz ultrasound driving wave, at 1.5 MPa PRFP and 0.5 Hz PRF. Similar results were yielded for DSPE liposomes mixed with SV microbubbles, as seen in Chapter 4, showing an increase in payload release of over 50% (Figure 5.2).

SV, CNPs and NC LB3 particles mixed with liposomes in the absence of ultrasound showed no release, indicating that over a 90 second incubation period, no particle-particle interactions without cavitation events were able to destabilise the liposomal bilayer.

In contrast to SV microbubbles which yielded a 41-fold increase compared with glucose, NC LB3 and CNP particles only yielded a modest 5- and 9-fold increase in release compared to glucose alone when samples were exposed to ultrasound for 90 seconds ($p < 0.0001$, $p < 0.0001$, and $p < 0.001$) (Figure 5.2).

A correlation between maximum power over the exposure period, and payload release is able to be observed in Figure 5.3. Cavitation events as detected by a 7.5 MHz PCD show

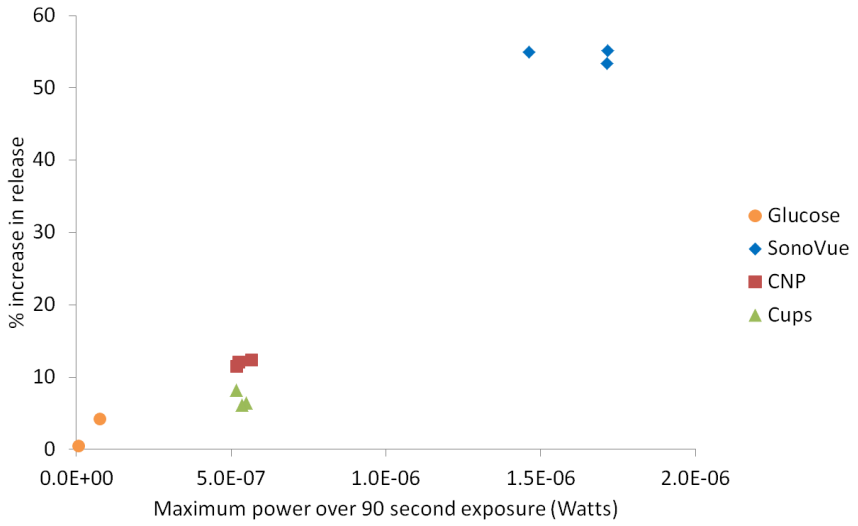

Figure 5.3: *Luciferin release from DSPE liposomes using a 0.5 MHz therapeutic ultrasound exposure of 90 seconds at 1.5 MPa with or without the addition of SV, CNPs or NCs (LB3) increases with increasing maximum power over the 90 sec exposure. n=3 shown.*

a maximum power of acoustic emissions of approximately 1.5 μWatts from exposed SV + liposome samples, compared to 0.5 μWatts from CNPs and NC LB3 particles. Maximum power of broadband-only emissions however are more comparable between sample groups with mean values of 0.48 μWatts, 0.50 μWatts, and 0.49 μWatts from liposomal samples containing SV, CNP and NC LB3 respectively. This difference in total maximum power from cavitation events, as discussed in Chapter 3 is a likely indicator of the violence (i.e. maximum bubble wall speed) and number of cavitation events occurring in the sample volume. In the case of SV, this maximum power of emissions accounts for both stable and inertial cavitation, where as for CNP and NC LB3, cavitation is almost purely inertial cavitation. Here, regardless of the type of cavitation nuclei used, maximum power correlates with payload release, where low maximum power yields only modest release, and high maximum power yields substantial release.

These initial results of low liposomal release in the presence of cavitation from cavicatalytic nanoparticles is able to be explained in different ways. Given these ultrasound parameters, either only 10% of liposomes in the solution are sensitive to cavitation from cavicatalytic nanoparticles, or the cavitation events were only sufficient to release 10% of the drug given this exposure period (90 seconds). Additionally, the ultrasound parameters which had been found to be optimal for release using SV may not be appropriate for initiat-

ing cavitation events from cavicatalytic nanoparticles suited for drug release from liposomes. To test these hypotheses, the same experiment was repeated over a longer time period (10 minutes), and at two different driving frequencies (0.5 MHz and 1.614 MHz).

Higher driving frequencies are of particular importance for the clinical applicability of this system. Diagnostic arrays typically operate at frequencies above 2 MHz, and as such, a drug release system which can operate at frequencies similar to those used currently would potentially allow for a dual use transducer, being able to both image and treat with the one device. To investigate cavitation triggered release at higher frequencies, the transducer was used at its fundamental frequency, 0.5 MHz, as well as at its third harmonic, 1.614 MHz.

Cavitation threshold studies conducted in Chapter 3 outlined the pressures required to achieve substantial increases in cavitation above background energy with each cavitation nuclei tested at both 0.5 MHz and 1.614 MHz. As was discussed, the maximum gain at 0.5 MHz was reached at 1.5 MPa for SV and at 1.7 MPa for CNP and NC LB3, however at 1.614 MHz, the maximum gain was reached at 3.2 MPa for SV, 3.6 MPa for CNP, and 2.8 MPa for NC LB3. To maximise the energy associated with cavitation at 1.614 MHz, the highest pressure tested, 4 MPa, at 1.614 MHz was chosen for drug release. Note, another difference between these two treatment conditions is the focal volume at 1.614 MHz is approximately a third the size of that at 0.5 MHz.

Over 10 minute exposures using PRFPs of 1.5 MPa at 0.5 MHz and 4 MPa at 1.614 MHz, release from DSPE liposomes increased substantially in the presence of SV and NCs. This release can be observed by the concentration of free luciferin measured in samples treated with and without ultrasound in the presence or absence of cavitation nuclei (Figure 5.4). For clarity, this value was then converted to a percentage increase in release above the no-ultrasound individual sample controls (Figure 5.5).

Similar to drug release experiments discussed in Chapter 3, no release was observed in the absence of ultrasound when suspended in any of the three cavitation nuclei tested. Additionally, ultrasound in the absence of cavitation nuclei did not cause an increase in release, even over an extended exposure period of 10 minutes.

In the presence of SV, increase in payload release at 0.5 MHz was 91.5% and at 1.614 MHz was at 83.1%. Payload release in the presence of NC particles was similar to that of SV at

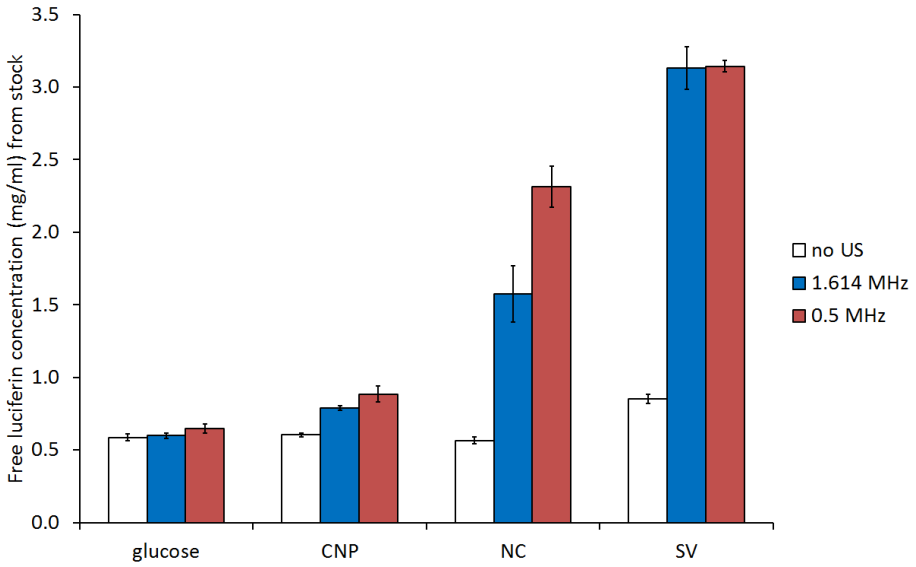

Figure 5.4: *Luciferin release from DSPE liposomes measured using the luciferin - luciferase assay. Samples were exposed to 0.5 MHz, 1.5 MPa, and 1.614 MHz, 4 MPa, therapeutic ultrasound for 10 minutes with or without the addition of CNP, NC LB3 or SV. Concentration of free luciferin is shown, calibrated using standard curves prepared in each cavitation nuclei solution. Concentrations of luciferin is adjusted for dilutions used in the experiment and the assay to concentration of luciferin in stock liposomal solution (mg/mL). n=3, standard deviation shown.*

0.5 MHz (86.6%), however at 1.614 MHz was only 47.5% which although substantially lower (1.7-fold decrease) was still substantially and significantly higher (94.6-fold increase) than in the absence of cavitation nuclei ($p < 0.0001$). In contrast however, CNPs yielded only a 4.6 fold increase in release above glucose alone at 0.5 MHz ($p < 0.05$), and a non-significant increase at 1.614 MHz.

A trend between increasing frequency and decreasing payload release can be observed across each cavitation nuclei group. SV, NC, and CNP particles have a 1.1-, 1.8-, and 1.6-fold decrease in release at 1.614 MHz as compared with 0.5 MHz (ns, $p < 0.01$, and $p < 0.05$). This effect of decreasing release with increasing frequency, although small, does appear to be present in each cavitation nuclei group tested. Future developments using this release strategy may use clinical ultrasound probes which operate at higher frequencies than those tested here. This higher frequency would offer the potential to initiate drug release and image using a single transducer system. The frequency dependence observed here should be taken into consideration when choosing or designing clinical transducers for this purpose.

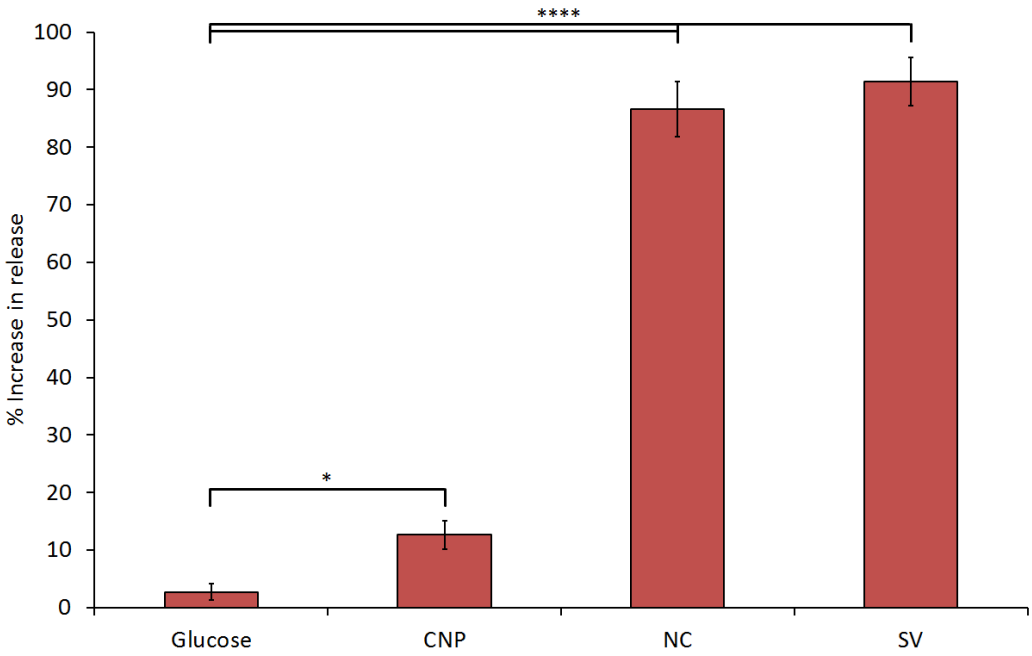

(a) *0.5 MHz*

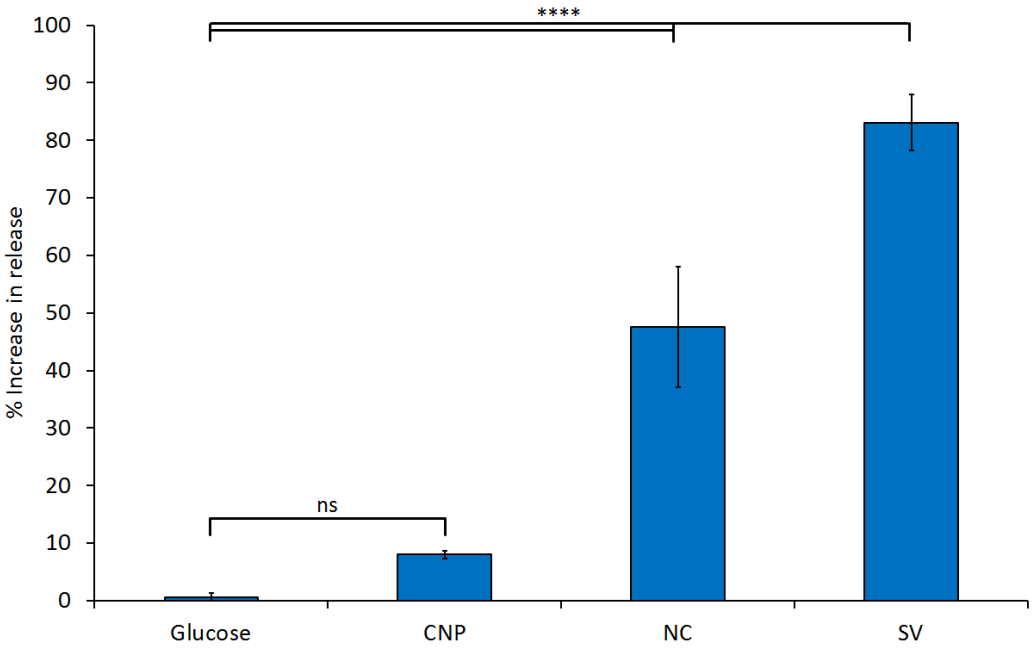

(b) *1.614 MHz*

Figure 5.5: *Luciferin release from DSPE liposomes using (a) 0.5 MHz, 1.5 MPa and (b) 1.614 MHz, 4 MPa therapeutic ultrasound exposure of 10 minutes with or without the addition of CNP, NCs LB3, or SV. Percentage increase in release compared with no ultrasound exposure shown. One-way ANOVA with Tukey for significance, **** $p < 0.0001$, * $p < 0.05$, ns = non-significant, n=3, standard deviation shown.*

5.3 Correlation between cavitation and release from liposomes using cavicatalytic nanoparticles

Although the input parameters can be used to control release, as indicated by varying frequency, pressure and exposure period, another advantage of cavitation controlled drug release, is that there is the possibility to monitor cavitation as a marker for drug release non-invasively.

Broadband energy associated with cavitation events showed different relationships for the two classes of cavitation nuclei, SV and cavicatalytic nanoparticles (Figure 5.6). A trend between increasing broadband energy and increasing payload release is seen for NCs and CNPs, however liposomal release was achieved at much lower broadband energies when SV cavitation nuclei were used. The same trends were observed at 0.5 MHz as they were at 1.614 MHz.

At 0.5 MHz, a n=1 SV control was used at 90 seconds to compare with previous experiments and is shown in Figure 5.6 (a). This additional point shows that with increased broadband energy received by the PCD, there is an increase in payload release, within the SV test group.

Another measure of cavitation activity is maximum power received over the exposure period which might be an indicator of the maximum violence (i.e. maximum bubble wall speed) and number of events occurring at a given time in the phantom holder. Figure 5.7 shows a threshold behaviour independent of cavitation nuclei type. Higher maximum power values corresponded with higher payload release until a maximum in release was reached at approximately 3 μWatts at 0.5 MHz. At 1.614 MHz, the relationship is not as clear, as liposomal release was higher in the presence of SV compared with NC even though the maximum power recorded from NC was slightly higher than with SV. Despite this observation, there is a trend of increasing payload release with increasing maximum power associated with acoustic emissions received by the PCD with 83.1 % release observed with SV at approximately 1.4 μWatts.

To illustrate more clearly the threshold observed when using maximum power as an indicator of cavitation events causing payload release, data from experiments using 90 sec-

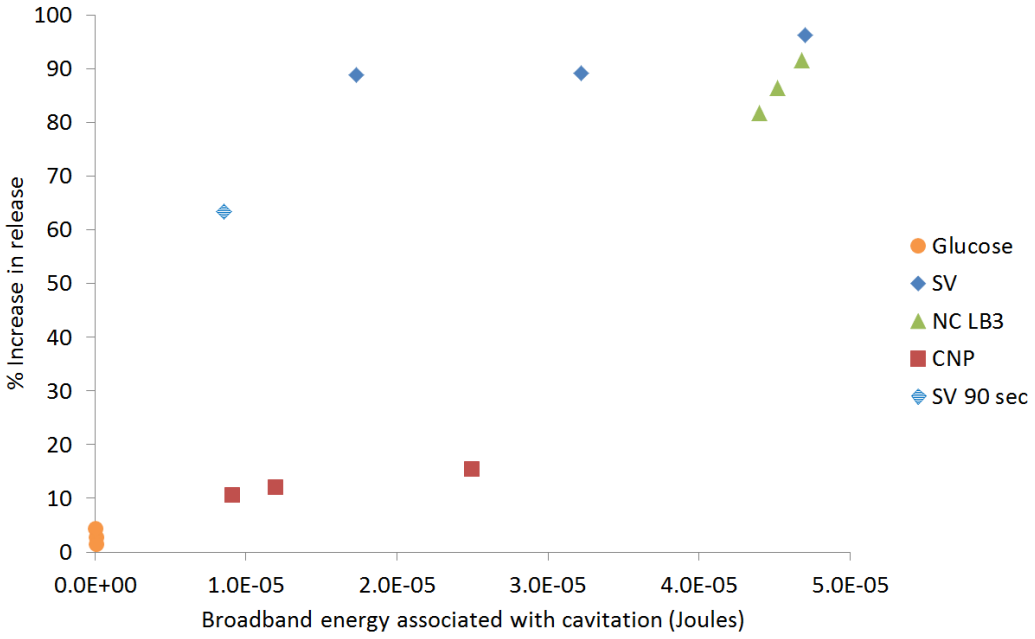

(a) *0.5 MHz*

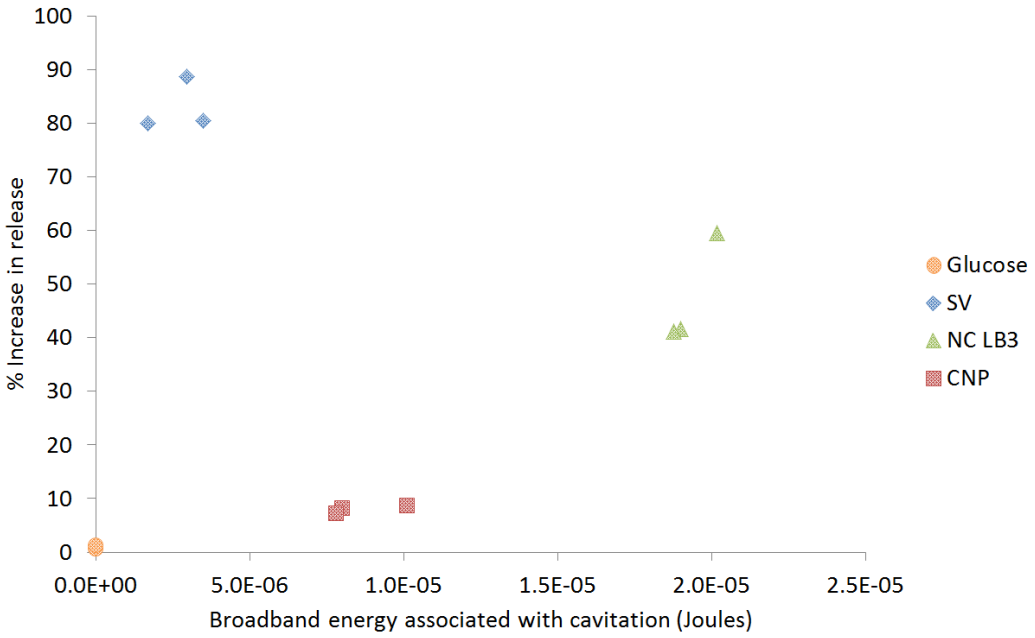

(b) *1.614 MHz*

Figure 5.6: ***Broadband energy versus drug release****. Luciferin release from DSPE liposomes using a (a) 0.5 MHz, 1.5 MPa and (b) 1.614 MHz, 4MPa therapeutic ultrasound exposure of 10 minutes with or without the addition of SV, CNPs or NCs (LB3) shown against total broadband energy associated with cavitation over the 10 minute exposure.*

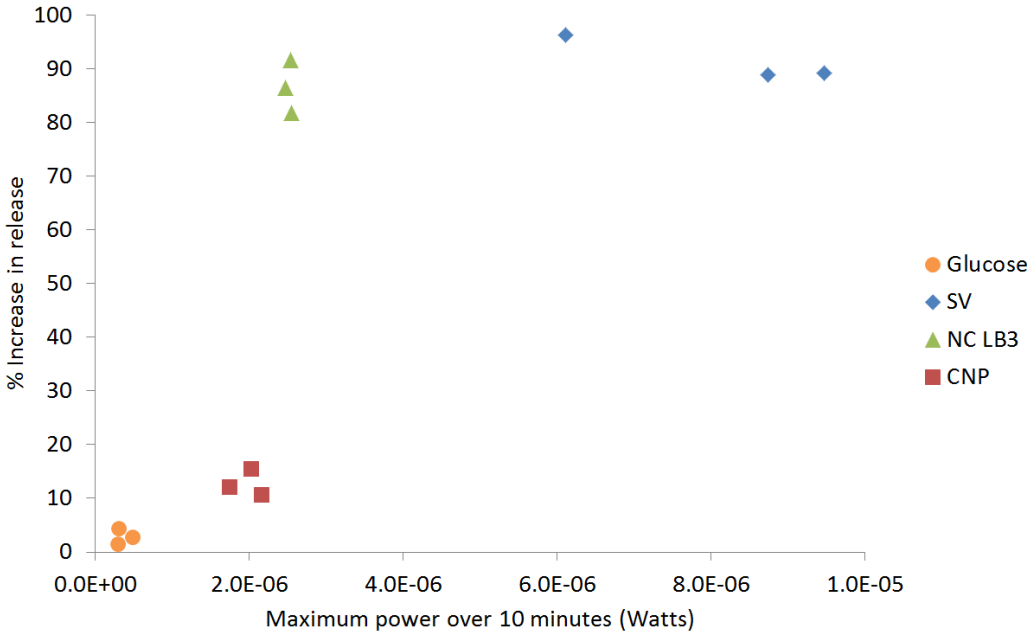

(a) *0.5 MHz*

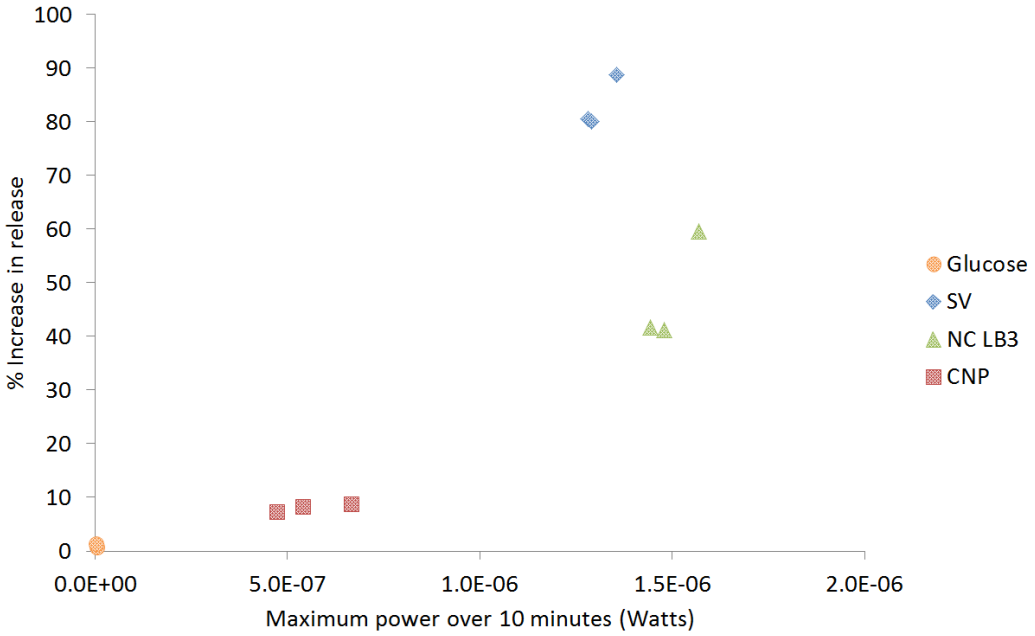

(b) *1.614 MHz*

Figure 5.7: ***Maximum power threshold for drug release.*** *Luciferin release from DSPE liposomes using a (a) 0.5 MHz, 1.5 MPa and (b) 1.614 MHz, 4MPa therapeutic ultrasound exposure of 10 minutes with or without the addition of SV, CNPs or NCs (LB3) shown against maximum power over the 10 minute exposure.*

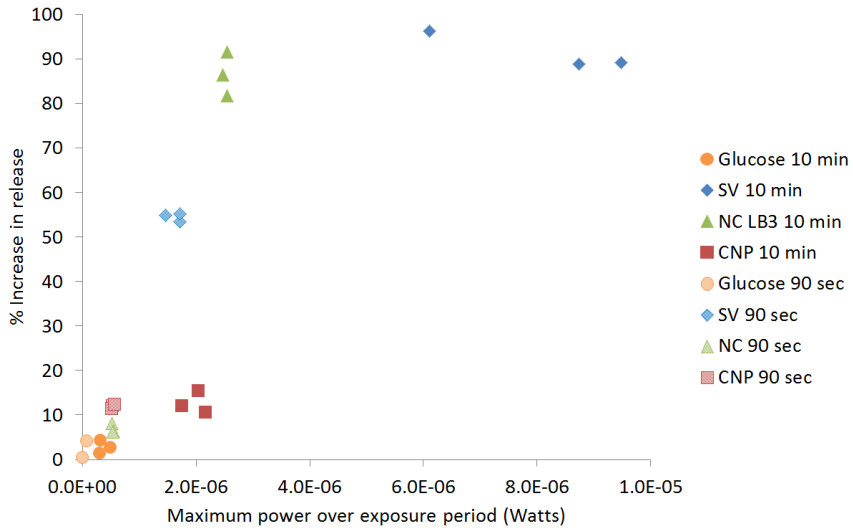

Figure 5.8: *Luciferin release from DSPE liposomes using a 0.5 MHz therapeutic ultrasound exposure of 90 seconds (shaded shapes) or 10 minutes (solid shapes) at 1.5 MPa with or without the addition of SV, CNPs or NCs (LB3) increases with increasing maximum power. n=3 shown.*

ond and 10 minute exposure periods was collated (Figure 5.8). The threshold is observed across cavitation nuclei types and across treatment times. Therefore, maximum power associated with cavitation may be used as an indicator for drug release from cavitation sensitive liposomes in this experimental set-up used.

5.4 Discussion of potential mechanisms of cavitation mediated release from liposomes

When hypothesising the mechanisms involved in liposomal destruction, parallels are able to be drawn between human cells, a lipid bilayer vesicle, and the liposomes used in these experiments. This comparison is useful in that a substantial amount of research has been conducted on the use of ultrasound for cell membrane perturbation also known as sonoporation. Here, the possible mechanisms acting to cause liposomal destruction by cavitation are discussed. The most likely mechanism of liposomal release according to the results observed is a high bubble wall speed which translates to a high shear stress causing a breakage of the lipid bilayer as described below.

5.4.1 Mechanisms of cavitation mediated release from liposomes

Five possible mechanisms for cavitation mediated release from liposomes were considered, having been observed as important in the breaking of lipid bilayers in the literature: shear stress applied to the liposomal bilayer from an adjacent cavitating bubble [195]; streaming from a bubble near but not necessarily in contact with a liposome [129]; shock wave formation from inertial cavitation events [28]; jetting produced by inertial cavitation [28]; and a less likely mechanism of bubble entrapment inside the liposome [41].

Physically, the mechanism of liposome destruction is likely to be the mechanical disruption of liposomal bilayers when in contact with an oscillating bubble creating a shear stress sufficient to rupture the bilayer. In an experiment conducted by Zhou et al. microbubbles were used as cavitation nuclei for human cell disruption. Using 1.5 MPa, 1.5 MHz driving ultrasound conditions, a shear stress of approximately 5 Pa and a shear rate of 2 x 10^4 sec^{-1} was calculated for successful cell disruption [195]. The equation for shear rate is shown in Equation 5.1:

$$\dot{\gamma} = \frac{v}{h} \tag{5.1}$$

where $\dot{\gamma}$ is the shear rate, v is the bubble wall velocity, and h is the distance between the liposomal wall and the microbubble wall. The shear rate can then be used to calculate the corresponding shear stress as shown in Equation 5.2:

$$\tau_w = \dot{\gamma}\mu \tag{5.2}$$

where τ_w is the bubble wall shear stress and μ is the dynamic viscosity of the fluid.

Experimentally, drug release was correlated with maximum power of acoustic emissions as summarised in Figure 5.8. Physically, a larger bubble wall excursion (R_{max}/R_0, where R_0 is the initial bubble radius, and R_{max} is the maximum bubble radius) in a given time period correlates with increasing power of acoustic emissions [190]. By maximising R_{max}/R_0, bubble wall velocity is also maximised. As such, the hypothesis that shear stress is the dominant mechanism for drug release from liposomes, is supported by these results.

Modelling of bubble cavitation from cavicatalytic nanoparticles as discussed in Section

3.4.2 is able to estimate the maximum bubble radius and maximum wall speed. For a bubble of initial diameter of 237 nm (which corresponds to the approximate cavity size of the NC LB3) and at the ultrasound exposure conditions used in drug release studies, the following values were estimated as shown in Table 5.1:

Table 5.1: *Bubble cavitation modelling at 0.5 MHz and 1.6 MHz. Initial, R_0, and maximum bubble radius, R_{max}, with corresponding maximum wall velocity are shown for a bubble insonated by a 10 cycle ultrasound pulse. Data derived from a modified Rayleigh-Plesset model (personal communication, Dr James Kwan, 2014).*

Frequency (MHz)	0.5	1.6
PRFP (MPa)	1.5	4
Initial bubble radius (R_0) (μm)	0.118	0.119
Maximum bubble radius (R_{max}) (μm)	24.9	14.4
Maximum wall velocity (m/sec)	-1823	-1654

This modelled data indicates that the shear stress from bubbles insonated at 0.5 MHz, 1.5 MPa is greater than that from bubbles insonated at 1.614 MHz, 4 MPa. This data gives a possible explanation for the higher liposomal release observed at 0.5 MHz compared with 1.614 MHz in the presence of NCs.

To calculate the shear rate, and therefore shear stress, for each of these conditions, the distance between the bubble wall and the liposome, h, is required. The distance between particles, and therefore the value of shear rate, is inversely proportional to the concentration of both particles, and is discussed further below.

5.4.2 Cavitation nuclei concentration

One difference between the two cavicatalytic nanoparticles tested in this release study was particle concentration. CNPs were produced at 0.2 mg/mL, a maximum concentration allowing for reliable stability, and NCs were produced at 0.6 mg/mL to match the likely concentration to be tested in the blood stream *in vivo*.

These *in vitro* drug release studies show that CNPs did not produce strong cavitation signals as measured by maximum power over the exposure period, and were therefore unable to cause significant payload release when compared with NCs. Increasing concentration of cavitation nuclei is correlated with increasing energy of cavitation as shown in Figure 3.25 which may contribute to the lower release observed in the presence of CNPs. In addition

to an increase in energy associated with cavitation however, there is also the decrease in distance between cavitation nuclei and drug carrying liposomes. With an increase in concentration of either cavitation nuclei or liposomes, or both, it is predicted that increased release would be observed due to increase in stress on the liposomal bilayer, which was previously observed by Zhou et al. showing cell membrane lysis increases as the distance between a bubble and the cell decrease [195]. As such this correlation between concentration and energy is important in relation to drug release. At these concentrations used, energy from cavitation events instigated by NCs is substantially higher than from CNPs. In this way, CNPs are limited by their stability at increasing concentrations, and therefore if stability was improved, higher CNP concentrations could yield higher payload release from liposomes when exposed to ultrasound. This concentration effect illustrates another advantage of non invasive monitoring where reduced cavitation signals due to lower concentrations is able to be correlated with decreased drug release without the requirement to directly measure the concentration of cavitation nuclei.

5.4.3 In vitro phantom considerations

One limitation of this experiment is that there is a pressure gradient over the phantom holder. With each pulse, the volume of cavitation nuclei and liposomes experience different pressures. Within the volume, some particles will experience the stated peak rarefactive pressure (1.5 MPa at 0.5 MHz and 4 MPa at 1.614 MHz respectively), while at the edges of the phantom holder, particles will experience approximately half that pressure. In this way, with each pulse, even if 100% of liposomes are destroyed and release their full payload at the focus (maximum pressure), liposomes outside the region of maximum cavitation may remain intact. To achieve 100% release when assayed (taking a representative portion of the exposed volume) the sample requires mixing such that liposomes and cavitation nuclei which have not been exposed to the maximum pressure are then pushed into the centre of the sample holder. In addition, the focal volume at 0.5 MHz is approximately 3 times larger than that at 1.614 MHz, exposing more cavitation nuclei and liposomes, further biasing increased drug release to the lower driving frequency.

A consideration related to this limitation is amount of sample mixing. Based on the

original bubble size, SV has greater potential to provide stronger streaming effects within the sample holder, when compared with NCs or CNPs, as it is larger and closer to resonance [13]. This mixing will enable more of the sample to be exposed to cavitation events which are able to cause drug release. This difference between the cavitation nuclei might explain why at 1.614 MHz, although NC produce a higher maximum power, SV shows more release from DSPE liposomes (Figure 5.7 (b)).

5.5 Conclusions

One challenge in targeted drug delivery is developing a release system, and another is developing a release system which will work *in vivo*. One challenge in *in vivo* environments is that blood vessels are on the micro-scale, whereas gaps between endothelial cells supplying the tumour tissue are on the nano-scale. This size difference means that microbubbles are restricted to the blood vessels where as nano-scale particles may be able to penetrate deeper into the tumour tissue. This decrease in size of cavitation nuclei capable of causing drug release was the motivation for this chapter's work.

Cavitation at the micron scale was shown to cause release of drug from liposomes in Chapter 4. In this chapter, release triggered by cavitation nucleated from cavicatalytic nanoparticles has been demonstrated. This development ensures that the effector agent, the cavicatalytic nanoparticle, and the drug carrier, the liposome, are all at the same size scale. This size matching enables potential co-localization to improve the chances of drug release in a complex environment such as *in vivo*.

To conclude, over a 10 minute ultrasound exposure, release from liposomes in the presence of SV and NC at both 0.5 MHz, 1.5 MPa (91.5% and 86.6% increase in release respectively) and 1.614 MHz, 4 MPa (83.1% and 47.5% increase in release respectively) was both substantial (31.8- and, 33.6-fold increase at 0.5 MHz; 94.5- and 165.4-fold increase at 1.614 MHz) and significantly greater ($p < 0.0001$ for each) than that in the absence of cavitation nuclei. Liposomes in the presence of CNPs at both 0.5 MHz and 1.614 MHz over 10 minutes of ultrasound exposure yielded a 12.6% and 8% increase in release respectively. These release results were correlated with maximum power of acoustic emissions received

remotely by a PCD which was able to be used as a remote indicator for release.

To summarize, the following conclusions can be drawn. Firstly, cavitation sensitive liposomes previously found to be stable to ultrasound alone over 30 second exposures were also stable to ultrasound alone over 10 minute exposures at both 0.5 MHz and 1.614 MHz. Secondly, cavitation sensitive liposomes were found to be stable in the presence of all cavitation nuclei tested in the absence of ultrasound exposure. Thirdly, triggered drug release can be achieved using cavitation from cavicatalytic nanoparticles, and this release is of a similar payload percentage to that achieved using microbubbles. Fourthly, release could be correlated with maximum power of cavitation for the frequencies tested and cavitation nuclei used. The correlation suggests that there may be a maximum power threshold for liposomal release. This trend was clearer at 0.5 MHz than 1.614 MHz and may be an area for future investigation. Finally, release at 0.5 MHz was notably higher than that at 1.614 MHz with each cavitation nuclei tested (SV: ns, NC: $p < 0.01$, and CNP: $p < 0.05$), and may be an area for future investigation if using higher frequency clinical ultrasound probes to replace the driving transducer.

Chapter 6

In vivo assessment of drug release using cavicatalytic nanoparticles

The drug delivery system that has been developed in this thesis so far is ultimately designed for use in living creatures. There are many differences between *in vitro* and *in vivo* systems, with key factors explored below. The majority of the chapter however details *in vivo* experiments both to test cavitation activity and drug release in a murine model. This chapter builds on the development and characterisation of cavicatalytic nanoparticles in Chapter 3, the demonstration of drug release from cavitation sensitive liposomes using microbubbles in Chapter 4, and the demonstration of drug release using cavicatalytic nanoparticles in Chapter 5.

6.1 Method and materials adjustments

Liposomes were formulated and tested *in vitro* before use *in vivo*. Liposomal encapsulation was tested using the luciferin-luciferase assay, confirming a background free luciferin percentage of 18.3% for liposomes prepared for *in vivo* use and verified as cavitation sensitive *in vitro*. Before *in vivo* studies were conducted, liposomes were re-purified on a PD10 column reducing the background free luciferin percentage to 14.3% with a total luciferin concentration of 287.3 μg/100 μL and a free luciferin concentration of 41 μg per 100 μL.

6.2 Mimicking in vivo environments

To test cavitation dynamics and characteristics of nanoparticles *in vivo*, particles were first validated using *in vitro* phantoms which simulated the *in vivo* environment. Specifically the affect of the *in vivo* environment on particle stability and cavitation response was tested.

One of the key principles of ethical treatment of animals is that of the '3Rs' - Replacement, Reduction and Refinement, as coined by Russell and Burch [154]. The first option of 'Replacement' is necessary in understanding cavitation behaviour in an environment as similar as possible to a live animal whilst allowing for a more controlled environment, decreased cost and reduced animal usage.

To mimic the in vivo environment, three major factors were considered: blood flow, blood components, and exposure volume:

1. **Blood flow:** Blood flow could effect cavitation dynamics in several potential ways. As the blood is flowing, particles travelling in the blood will only transiently be in the focus of the ultrasound transducer. This situation is in contrast to the in vitro testing in Section 3.4 where particles were tested in an enclosed phantom holder. If particles behave differently on the first pulse compared with subsequent pulses, this will not be observed in a flow scenario (depending on the PRF relative to flow rate).

2. **Blood proteins:** The surrounding liquid has the potential to alter cavitation events significantly. Firstly, the surrounding proteins may interact with the bubble as it forms and affect the magnitude of the radial oscillations (as shell properties have been shown to be important in bubble dynamics [126]). Secondly, the proteins present may adsorb onto the surface of the particle affecting the way in which gases adsorb to the surface of the particle.

3. **Exposure volume:** The volume considered in the static phantom holder was 6.8 mL. Within that volume the -6dB focal zone of the therapeutic ultrasound was 670 μL. The approximate total blood volume of a mouse is 1.5 mL (7-8% of mouse weight e.g. 20 g), and the maximum IV injectable dose of 1% body weight in mL was set, 200 μL, was set [164]. The possible sample volume which can be exposed by ultrasound therefore is greatly reduced. To account for this volume change, the sample volume

exposed at one time in the flow phantom was reduced using a thin channel.

With any *in vitro* model, there are limitations that reduce the accuracy of representation. Factors that are important but were not incorporated into the flow phantom include:

1. **Particle accumulation:** The enhanced permeability and retention effect is greatest at 24-48 hours. The initial *in vivo* experiments planned are to expose the area to ultrasound and inject the cavitation nuclei simultaneously, thereby not allowing for accumulation. This effect however could be important to look at in future studies as passive accumulation of nanoparticles in tumours is hypothesised to enhance the cavitation response.

2. **Pulsatile flow:** The heart rate of an anaesthetised mouse is approximately 400 bpm. This rapid heart rate is difficult to model in a flow phantom, and so was not incorporated. Instead, a constant flow rate was used.

6.2.1 Effect of blood proteins on size of cavicatalytic particles in vitro

Stability of cavicatalytic particles in the blood stream is important in determining whether the particles will remain 'nano' sized by the time they reach the tumour site. To test this stability, particles were mixed with human plasma (10%), incubated for 10 minutes and sized by DLS.

Both CNPs and NC LB3s were mixed with plasma and sized by DLS (Figure 6.1). Plasma alone have size peaks at approximately 13 nm, 240 nm, and 3940 nm. In plasma from a healthy individual, the largest proteins should be approximately 10 nm in diameter [59], these two larger peaks at 240 nm and 3940 nm therefore are likely to be due to agglomeration during heat treatment of the plasma before use [177] or fibrin clots. There is an overlap between the middle peak corresponding (240 nm) and the CNPs in water, making it challenging to distinguish between the two. In addition, the largest micron sized peak could either be attributed to cavitation nuclei particle agglomeration or simply to the larger protein agglomerate/clot peak. It is therefore difficult to determine, using this technique, whether the plasma proteins have caused agglomeration of the particles after

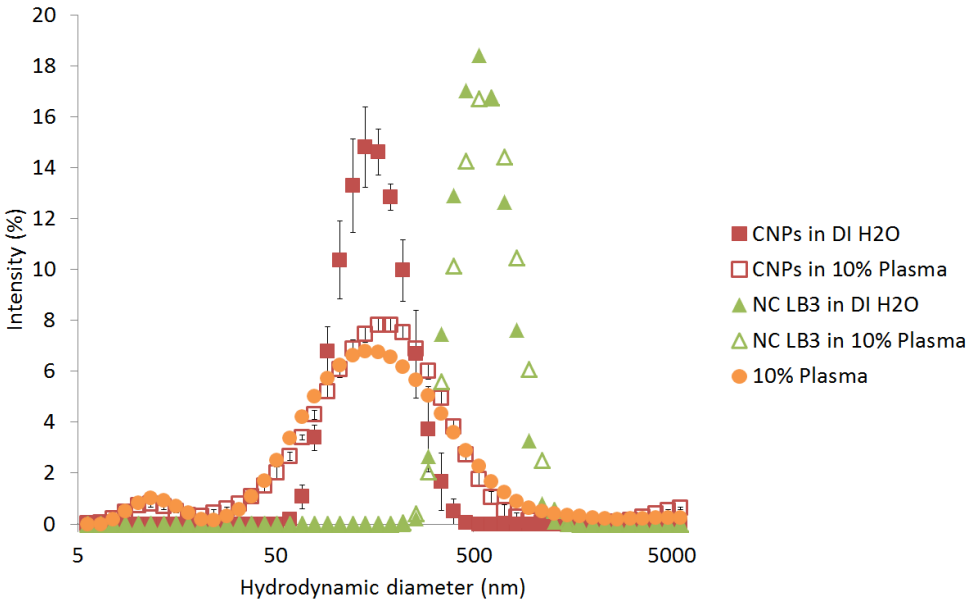

Figure 6.1: *Size of cavicatalytic nanoparticles in plasma. CNPs in water (solid red squares) or 10% human plasma (hollow red squares) n=3; NC LB3 in water (solid green triangles) or 10% human plasma (hollow green triangles) n=1; and 10% human plasma alone (orange circles) n=1. Standard deviation shown.*

mixing. Nonetheless, the shift to increasing size of the CNP peak and NC peak was 39 nm and 48 nm respectively. This slight size increase could be caused by the adsorption of proteins onto the surface or simply a slowing of particle Brownian motion in solution increasing the apparent size of the particle. However, the magnitude of the size increases, which are significantly smaller than double the cavicatalytic particle size, suggest that these particles are stable in plasma despite some level of protein interaction.

Dobrovolskaia et al. [56] observed that gold nanoparticles in solution agglomerated in PBS but were stable in plasma, even when subsequently being resuspended in PBS. This result was attributed to stabilisation of the particles by steric hindrance. This same effect is likely here, whereby even though CNPs and NCs are not stable in salt containing solutions, they are stable in human plasma.

6.2.2 Effects of blood proteins on cavitation in vitro

CNPs when suspended in human plasma do not show any 'priming' or sustained cavitation response as they do in water. Instead a decay in cavitation energy over time is observed (Figure 6.2). This decay in energy over time can be explained by plasma proteins stabilising

gas bubbles removed from the surface of the carbon during nucleation, or plasma proteins adsorbing to the surface of the CNPs preventing any re-adsorption of gas to the surface of the particles. In this way, the maximum power received from cavitation of acoustic emissions in water and in plasma is comparable. However, the total energy of cavitation over a given period is reduced due to the decay in cavitation response.

Cavitation dynamics of shelled microbubbles have been assessed in the literature where above a certain MI, bubbles enter into a 'destructive' zone [24]. The MI required for this 'destructive' zone as observed optically by Bouakaz et al. was above 0.6. Conditions used to instigate inertial cavitation and test cavitation dynamics as shown in Figure 6.2, had a MI of 1.7, well above the 'destructive' parameters determined by Bouakaz et al. The predicted destructive behaviour was observed by a decay in power of cavitation from SV bubbles in plasma (Figure 6.2). Decay to background power of cavitation was over approximately two to three minutes. Bubble destruction in the literature occurs on the scale of milliseconds, however this observation is for a single bubble. Approximately 234 million bubbles were injected into the static phantom holder used to study cavitation dynamics. With each pulse, bubbles would be destroyed, as well as mixing of the fluid to replenish the focal volume with bubbles which have not yet been destroyed. Decay of power signal follows a smooth reduction in power of acoustic emissions over the first 1.5 minutes after which there is a short period of variable power of cavitation before returning to background cavitation power. Although clearance of SV from the liver for example may take up to 6 minutes [191], bubbles are destroyed by cavitation before reaching that clearance limit.

NC and CNP particles however have a very different decay profile to SV. Both NC and CNP show an extended cavitation response in plasma compared with SV. Compared with the decay observed in water (Figure 3.24), decay in plasma occurs far more rapidly for both CNPs and NC LB3. One consideration in these comparisons is that the number concentration of NCs and CNPs is substantially higher than that of SV microbubbles as discussed in Section 3.3.3, which may bias extended decay times towards the nanoparticles in this study. Cavitation dynamics were tested over 10 minutes, and within that time frame, power from cavitation events persists for both solid particles again confirming their 'catalytic' properties in an environment more similar to *in vivo* conditions. Although the strict definition of a

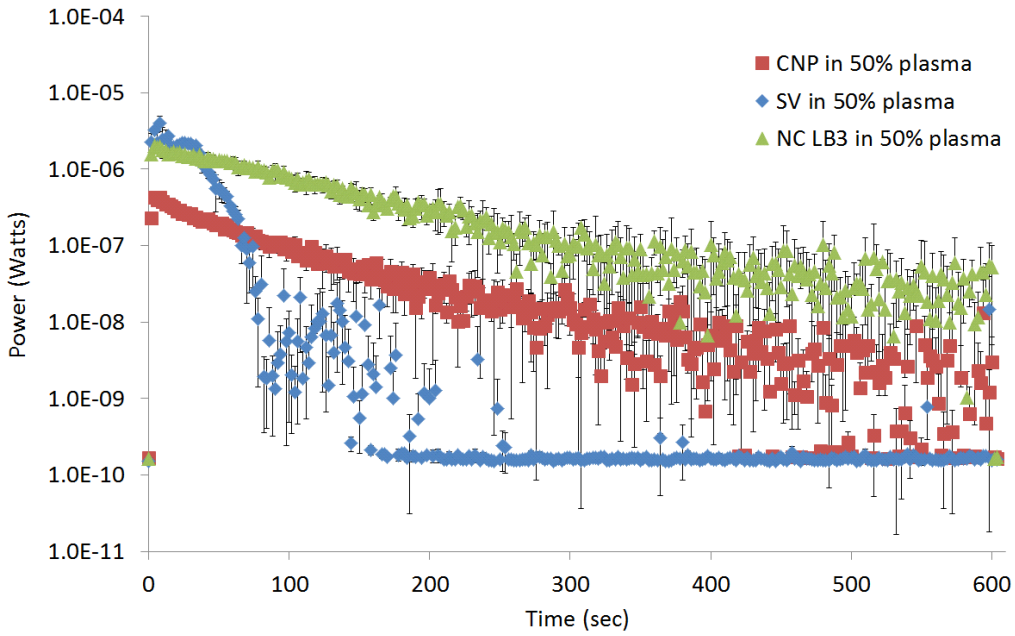

Figure 6.2: *Cavitation dynamics of SonoVue (50%), CNPs (0.1 mg/mL), and NC LB3s (0.3 mg/mL) in human plasma (50%) showing power of acoustic emissions associated with cavitation over the exposure period. Samples were insonated in the static phantom holder at 0.5 MHz, 0.5 Hz PRF, at 1.2 MPa for 10 minutes. N=3, standard deviation shown.*

catalyst implies that the catalyst is not 'used up', in practice, deactivation or decay of catalysts is typically observed over varying time periods [18]. Importantly, good catalysts should remain active for sufficiently long times so that replenishment is not impractical. For the purpose of therapy *in vivo*, and observing substantial drug release over 90 second periods in a protein-free environment (Figure 5.5), 10 minutes is considered a long time period. Based on these results, if these cavicatalytic particles are able to penetrate into tumour tissue and remain sufficiently active to trigger drug release, such release may potentially be extended both over time and deeper into the tumour tissue.

To investigate the effect of plasma proteins on the cavitation threshold of cavitation nuclei, cavitation response was assessed at 5 pressures near the cavitation threshold observed in the absence of proteins. The cavitation thresholds were defined in Chapter 3 as the pressure required to achieve a gain of 20 dB in the presence of cavitation nuclei over background media alone. According to this criterion, the cavitation thresholds in plasma were observed to be between 0.14 MPa and 0.5 MPa for SV, between 0.5 MPa and 0.8 MPa for NC LB3, and between 1.2 MPa and 1.5 MPa for CNPs. It should be noted that each of the thresholds observed in plasma has shifted higher than in water as reported in

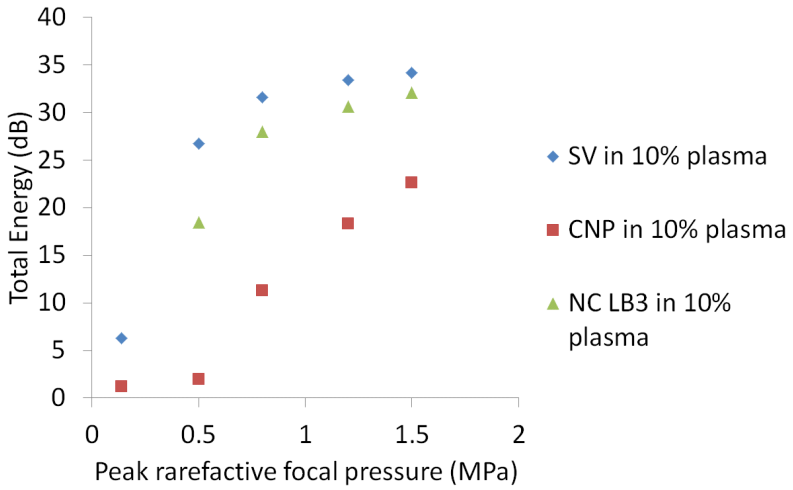

Figure 6.3: *Cavitation threshold of SV, NC LB3s, and CNPs in human plasma (10%). Samples suspended in human plasma (10%) were insonated for 30 seconds at each pressure to 0.5 MHz driving frequency, 0.5 Hz PRF and 5% DC. Individual samples were used for each pressure measurement, n=1. Energy shown as dB above plasma (10%)*

Section 3.4.1. Each pressure threshold is however lower than that used to test drug release using cavicatalytic nanoparticles *in vitro* (1.5 MPa). The absolute energy associated with background cavitation in plasma was lower than in water, and as such the relative gain over background energy is correspondingly lower. The shift in cavitation threshold, therefore, was not considered substantial.

To mimic the *in vivo* environment as closely as possible, cavitation nuclei were suspended in human plasma and flowed through an agar flow phantom (Figure 6.4). The cavitation response is sustained due to the flow and replenishment of cavitation nuclei, however reduced due to the presence of plasma proteins for both SV and CNPs. The reduction in total energy over the 30 second exposure period due to the presence of plasma was 45.8% and 59.8% for SV and CNPs respectively. This reduction in power of acoustic emissions suggests that either a higher concentration of cavitation nuclei, or higher pressure of driving ultrasound, would be required to yield the same percentage of drug release from liposomes as that observed *in vitro*. Importantly to note, as the volume of cavitation nuclei in the ultrasound focus is greatly reduced in the flow phantom, the signal to noise ratio is also greatly reduced and is particularly evident in the case of CNPs flowing in plasma (Figure 6.4 (b)). This low signal to noise ratio observed in this phantom helps to explain the preliminary *in vivo* results as discussed in Section 6.4.

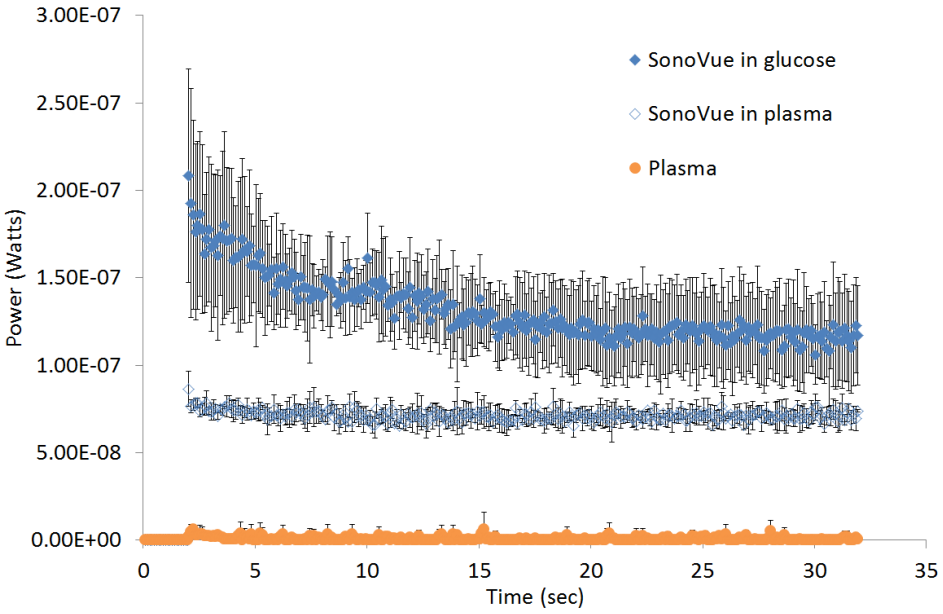

(a) *SonoVue in plasma*

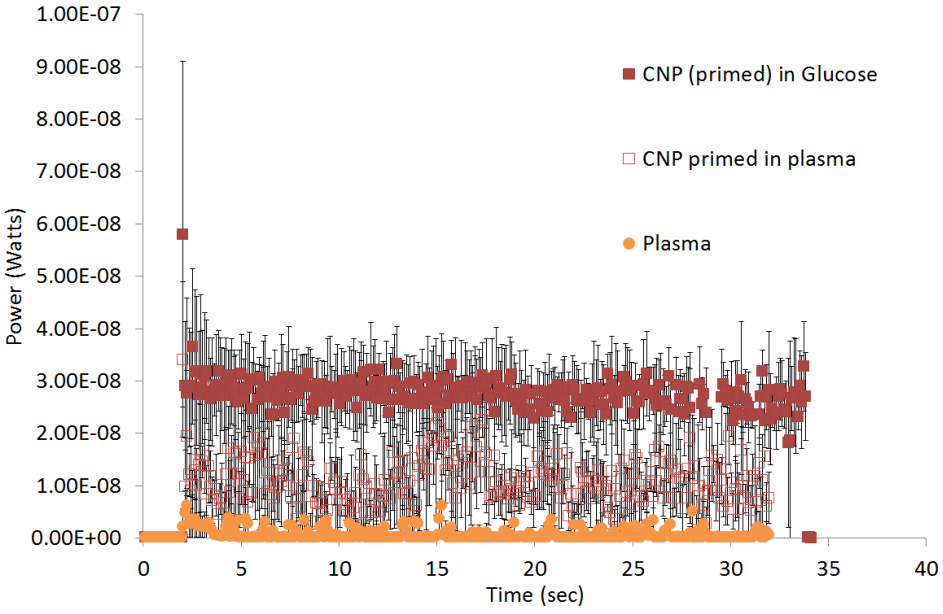

(b) *CNP in plasma*

Figure 6.4: *Power of cavitation in the presence and absence of plasma proteins in an agar flow phantom. a) SonoVue and b) CNPs were diluted by 50% into either DI H_2O or human plasma. Samples were flowed continuously and exposed for 30 seconds at a PRFP of 1.2 MPa, with a driving frequency of 0.5 MHz, and 10 Hz PRF. N=3, standard deviation shown.*

6.3 Pharmacokinetics of cavicatalytic nanoparticles

Before understanding the effect of the *particles* on the body, i.e. pharmacodynamics, the effect of the *body* on the particles, i.e. pharmacokinetics, must first be understood. In order to track particles to assess routes of clearance and longevity in the body, particles need to be labelled in some way. NC particles can be easily labelled with FITC fluorescent polymers during the production process. CNP particles however are more challenging to label. Modifying the surface chemistry in order to attach a fluorescent label, and using radioactive carbon as a starting material were both considered. Due to the complexity of these methods, they were not pursued. For these reasons, pharmacokinetic studies were performed using NC particles, and not CNPs.

6.3.1 Organ distribution

Organ distribution studies (performed using fluorescently labelled NC injected IV into female BALB/C mice with CT-26 tumours, see methods in Section 2.9.2) showed that a majority of particles were likely processed in the liver and kidney within 5 minutes (Figure 6.5). After 120 minutes, 0.022 mg remained in the blood stream which corresponds to 3.53% of the original injected dose with 8.56% of the dose remaining in the liver (Figure 6.6). Urine analysis suggests that the remainder of the particles had been cleared through the kidneys and passed into the urine as discussed in Section 6.3.3.

At the two time points tested, 5 minutes and 120 minutes, no appreciable concentration of NC particles was detected in the tumour. Accumulation of nanoparticles in tumours via the EPR effect typically reaches a maximum at 24 to 48 hours [73] and so particles need to remain circulating in the blood stream for at least this period of time for accumulation via the EPR effect to occur. As only 23.09% of the NCs remained in the blood stream after 5 minutes, and only 3.53% of the dose remained after 120 minutes, any accumulation in the tumour via the EPR effect would be limited. Additionally, with such a rapid clearance, no accumulation in the lungs, spleen, kidney or heart was observed, which suggests a decreased risk of potential toxicity to these organs.

These studies suggest that although the ideal nanoparticle drug release and delivery

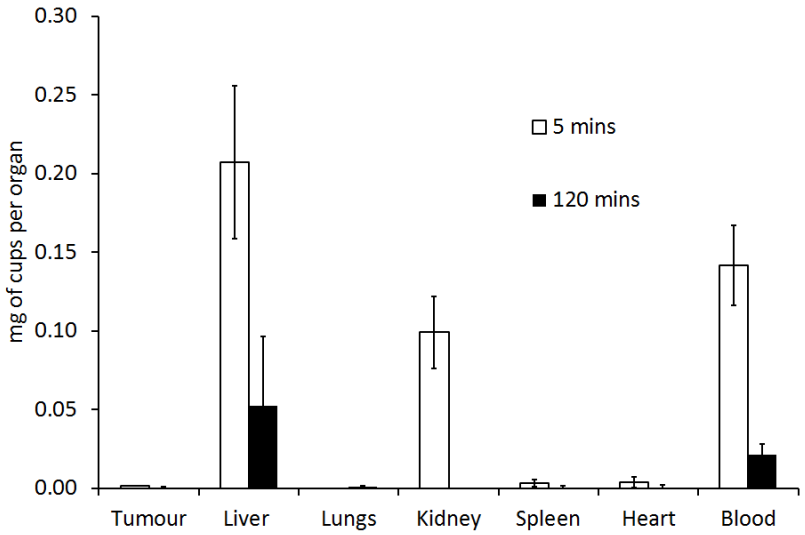

Figure 6.5: *Mass distribution of NCs in organs. 0.61 mg NC injection (100 µL, 6.1 mg/mL) where animals were culled at either 5 minutes (n=4) or 120 minutes (n=3), standard deviation shown.*

system would utilize the EPR, the NC particles developed do not circulate for long enough to take advantage of this potential effect. Modifications to the surface of the particle may be possible to extend the circulation time and thus increase the chances of tumour accumulation via the EPR effect. With the current system, it is likely that the NC particles are constrained to the vasculature or to the excretion pathways for the first two hours after injection. This result suggests that *in vivo* assessment of cavitation activity and effect should be conducted by commencing ultrasound exposure immediately after injection before the particles are cleared from the tumour and body vasculature.

6.3.2 Plasma

Clearance of the particles from the blood stream over time follows a similar trend with each particle concentration. With increasing particle concentrations injected, an increased dose remained in the blood stream at any time point (Figure 6.7). However, the concentration which yielded the highest retention of particles in the blood stream as a percentage of the original dose was 1.2 mg/mL (Figure 6.8, n=1). Increasing the concentration further increased the particle mass in the blood stream at a decreasing rate (Figure 6.9 a)), in other words, it yielded lower retention as a percentage of the injected dose (Figure 6.9 b)).

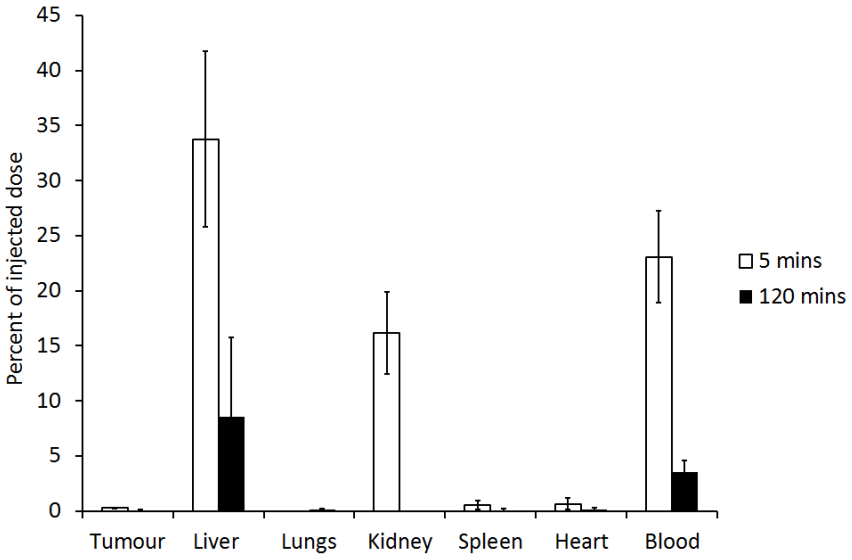

Figure 6.6: *Percentage of initial dose distribution of NCs in organs. 0.61 mg NC injection (100 µL, 6.1 mg/mL) where animals were culled at either 5 minutes (n=3) or 120 minutes (n=4), standard deviation shown.*

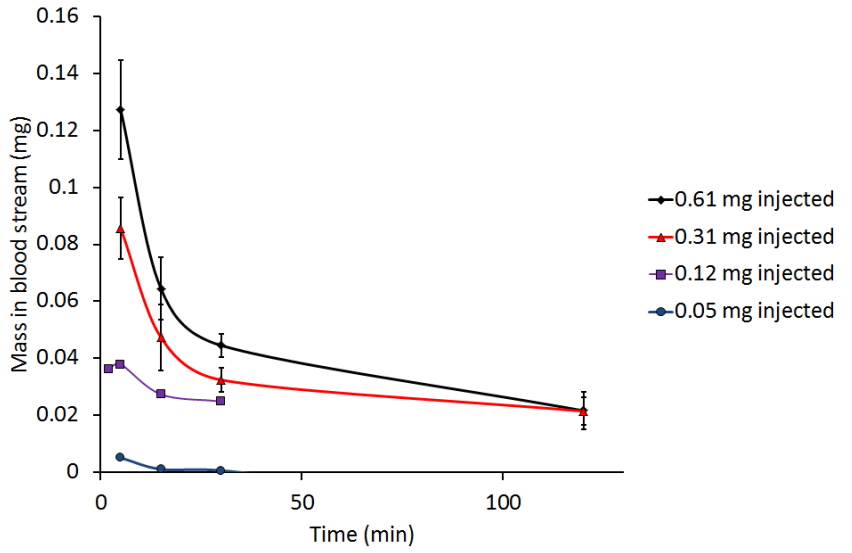

Figure 6.7: *Circulation kinetics of NCs in the blood stream represented by mass of NCs at a range of injected concentrations. NC injections of 0.61 mg (black), 0.31 mg (red), 0.12 mg (purple), and 0.05 mg (blue) were made and blood samples taken at 5, 15, 30, and 120 minutes after injection for each concentration except after the injection of 0.12 mg where sampling occurred at 2, 5, 15 and 30 minutes. n=4 (0.61 mg), n=3 (0.31 mg), n=1 (0.12 mg), n=1 (0.05 mg), standard deviation shown where applicable.*

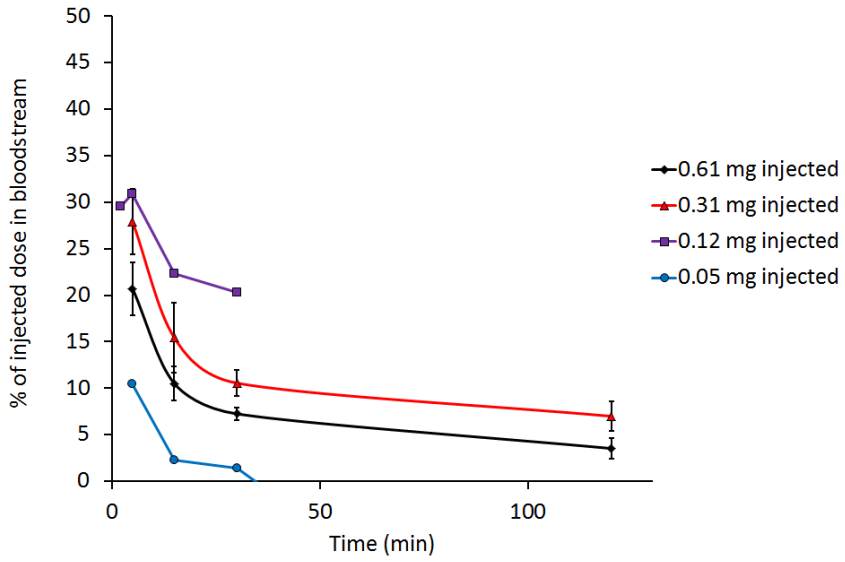

Figure 6.8: *Circulation kinetics of NCs in the blood stream represented by percent of remaining dose of NC circulating after injection of a range of NC concentrations. Highest percent dose remaining was achieved by injection of 0.12 mg NC followed by 0.31 mg, 0.61 mg and 0.05 mg. n=4 (0.61 mg), n=3 (0.31 mg), n=1 (0.12 mg), n=1 (0.05 mg), standard deviation shown where applicable.*

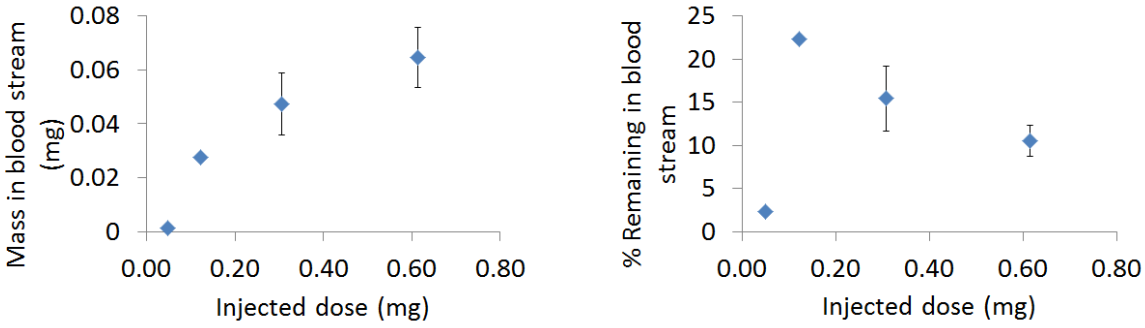

(a) *Mass* **(b)** *Percent remaining*

Figure 6.9: *NC particles in plasma after injections of increasing dose (0.5 mg/mL n=1, 1.2 mg/mL n=1, 3.1 mg/mL n=4, 6.1 mg/mL n=4) shown as a) mass of particles in the blood stream or b) percent of injected dose remaining in the blood stream at 15 minutes after I.V. injection. Standard deviation shown.*

6.3.3 Urine

From the organ distribution and plasma studies, the decrease of NC concentration in plasma and presence in liver and kidney suggest that NC particles are cleared from the body via either liver or kidney or both. Urine samples were obtained from mice if they urinated at the time points used for blood sampling. Fluorescence in the urine increased over the first 30 minutes after injection and reduced thereafter (Figure 6.10).

Plate reader measurements (Figure 6.10 (a)) show fluorescence of the sample and are independent of particle size. Flow cytometer measurements (Figure 6.10 (b)) however only record fluorescence when a particle is detected. In this way, it measures fluorescence associated with particles with a lower size limit of 500 nm. As the upper size limit observed in the literature for particles cleared through the kidney is approximately 8 - 9 nm [37, 120], it is unlikely that these particles cleared through the kidney as particles. A possible explanation is that NCs were broken down in the liver into polymer chains which then re-entered the blood stream and were cleared as polymer chains through the kidney. The polymer chains may then have formed aggregates in the bladder. However it is hard to align the speed with which this process occurs and the time needed for liver capture, degradation, biliary excretion and reabsorption and renal excretion.

Factors contributing to fluorescence intensity in the urine include: 1) concentration of NCs injected; 2) amount of NCs processed by the liver; 3) glomerular filtration rate; 4) volume of urine in the bladder at time of injection; 5) volume of urine in the bladder at time of urine collection. It is clear that these preliminary studies do not form the basis for solid assertions to be made about the process or extent of renal excretion. Metabolic studies using radio-labelled polymer may help define these aspect more precisely.

Faecal samples were also analysed and showed no fluorescence however this lack of fluorescence may have been due to the difficulty in observing fluorescence in an opaque sample and was not necessarily indicative of no particle accumulation.

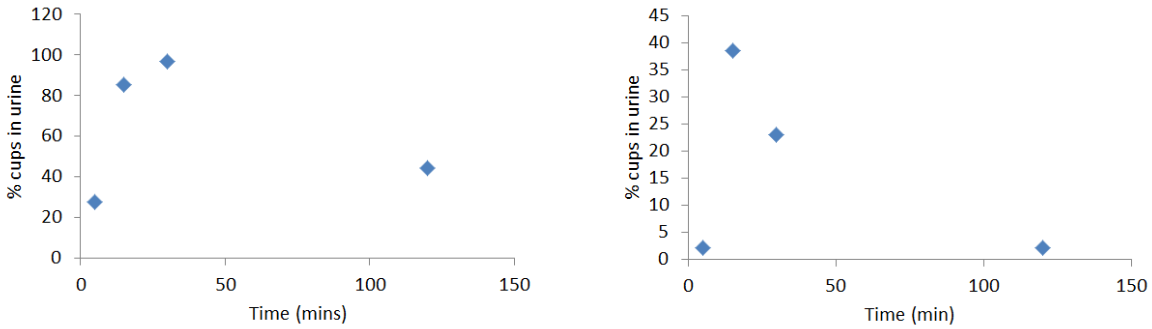

(a) *Plate reader* **(b)** *Flow cytometer*

Figure 6.10: *A comparison between detection methods of NC particles in urine after 3.1 mg/mL 100 µL injection. n=1. NC in the urine as a percentage of the injected dose was measured by fluoresecence using (a) plate reader technology, independent of particle size, and (b) flow cytometer technology which only records fluorescence of particles with a minimum size limit of 500 nm.*

6.4 Preliminary studies of nano cavitation nuclei in vivo

Preliminary *in vivo* studies were conducted with both CNPs and NCs. Mice were injected intravenously with 0.2 mg/mL CNPs in 5% glucose and 0.56 mg/mL NC in 5% glucose during exposure to 0.5 MHz therapeutic ultrasound at 1.2 MPa and 1.5 MPa PRFP (n=3 mice in each treatment group, 12 mice total). Each mouse was exposed to ultrasound focused at two locations within the tumour. When aligned at each position, each mouse was administered with a total of 150 µL of cavitation nuclei in two separate injections of 75 µL. No substantial increase in cavitation signal was observed above background noise that could be attributed to injection of cavitation nuclei. Based on the results from this preliminary study the null hypothesis could not be rejected. This lack of difference between background cavitation energy and that achieved upon injection of CNPs and NCs was attributed to the low concentration of cavitation nuclei injected and therefore circulating in the blood. Assuming a blood volume of 1.5 mL, final concentrations of cavitation nuclei in the blood stream were 10% of the injected concentration, i.e. 0.02 mg/mL CNP and 0.056 mg/mL NC. Even if cavitation events were occurring, at this concentration the signal from these events would not be of sufficient magnitude to be detected by the PCD above background energy.

These preliminary experiments showed that at these concentrations of injected cavitation nuclei (0.2 mg/mL CNP and 0.56 mg/mL NC), no cavitation signal can be detected above background cavitation. Based on these results, concentrations of cavitation nuclei were

increased for *in vivo* drug release experiments.

6.5 Drug release using cavitation in vivo

NC were tagged with FITC to enable assessment of accumulation of NC in the tumour and plasma. Studies were conducted in female C57Bl/6 mice bearing B16 F10 - LUC tumours (n=4).

6.5.1 NC distribution in vivo with ultrasound

Fluorescence from NC-FITC particles was detected in the tumour with a 2.5-fold ($p < 0.05$) and 3.5-fold ($p < 0.001$) increase above background fluorescence intensity for low concentration (6.14 mg/mL) and high concentration (25.75 mg/mL) injections respectively. When calibrated however, the mass of NCs in the tumour was almost negligible with less than 0.001% of the injected dose present (Figure 6.11 (a) and (b)). The lower concentration of NCs showed a higher concentration in the tumour as a percent of injected dose, with 0.0009% injected dose in the tumour (NC 6.14 mg/mL) compared with 0.0004% at the higher concentration of NCs injected (25.75 mg/mL) (Figure 6.11 (b)).

With the 4.2-fold increase in concentration of NCs between the two groups in the absence of ultrasound, a corresponding 4.7-fold increase ($p < 0.001$) in fluorescence from NCs was observed in the plasma between the low- (6.14 mg/mL) and high- (25.75 mg/mL) concentration of NCs. However, this same increase was not observed in the tumour, where only a 1.9-fold increase (ns) was observed. NCs used in these studies were approximately 500 nm in diameter and therefore are not able to permeate easily into tissue. As the EPR effect takes hours to days to reach a maximum effect, the passive accumulation which could be expected here would be via the increase of NCs in the blood supply to the tumour, or through limited accumulation into the tissue via the EPR effect. Active accumulation of NCs in the tumour could be achieved by micro-streaming and radiation force after cavitation has been initiated on the surface of the NCs. All these potential mechanisms to achieve accumulation in the tumour in combination showed an increase of NCs in the tumour which did not scale 1:1 with increasing NC concentration, with only a 1.9-fold increase of NCs in tumour when a

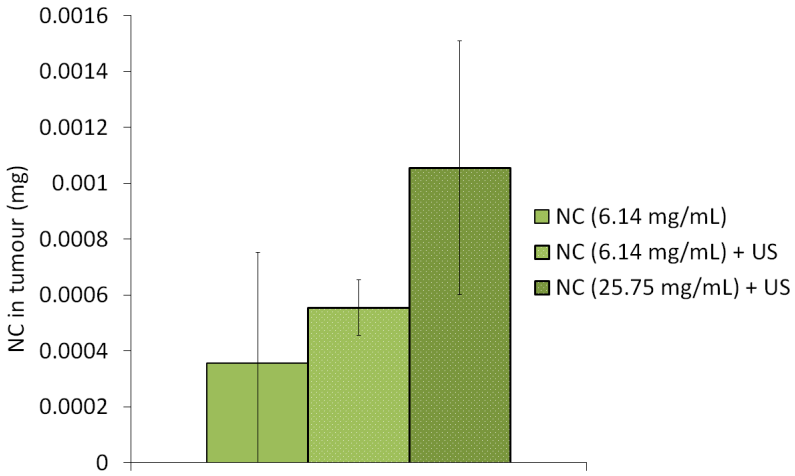

(a) *Tumour*

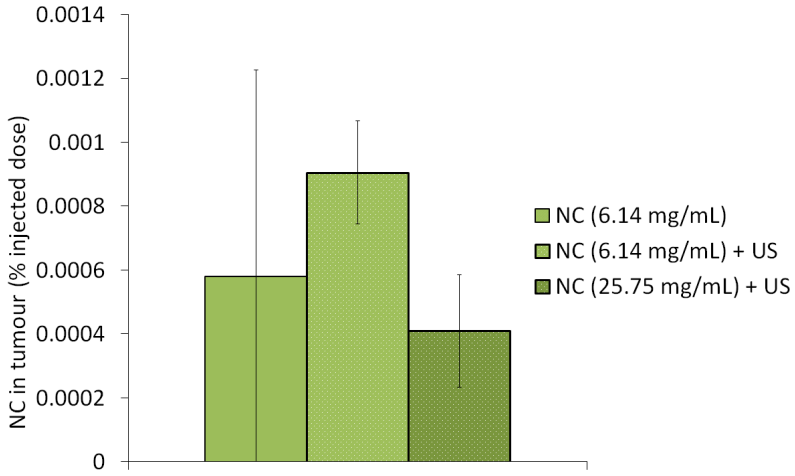

(b) *Tumour*

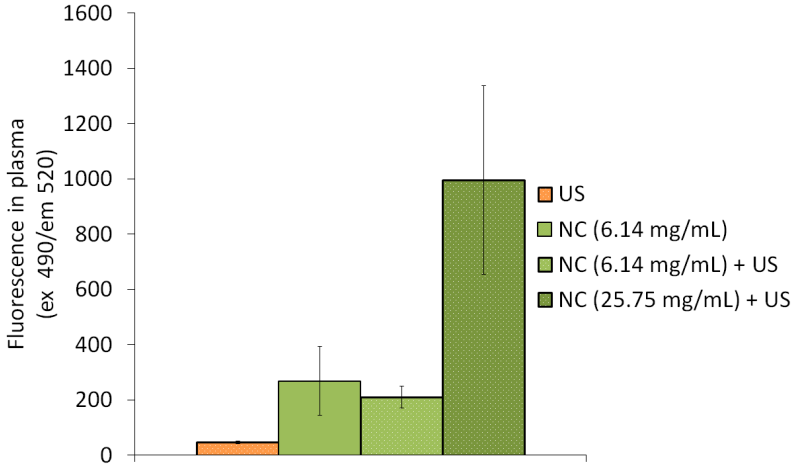

(c) *Plasma*

Figure 6.11: *Pharmacokinetics of NC in tumour with and without ultrasound exposure. (a) Mass and (b) percent of injected dose of fluorescent NC-FITC particles in tumour after background subtraction and (c) fluorescence intensity in plasma is shown for mice injected with DSPE liposomes treated with therapeutic ultrasound (US) alone (spotted orange), NC (6.14 mg/mL) alone (solid pale green), or a combination of NC (6.14 mg/mL) and therapeutic ultrasound (spotted pale green) or NC (25.75 mg/mL) and therapeutic ultrasound (spotted dark green). N = 4, standard deviation shown, one-way ANOVA for significance, *** $p < 0.001$, ns = non significant.*

4.2-fold increase in dose was used.

A 1.6 fold increase in NCs (6.14 mg/mL) in the tumour was observed when ultrasound was applied (ns, one-way ANOVA). A corresponding 1.3-fold decrease of fluorescence from NC in the plasma was observed (Figure 6.11). However, this decrease was once again not statistically significant (ns, one-way ANOVA).

6.5.2 Cavitation response of nuclei in vivo

Up to this point, the cavicatalytic properties of nanoparticles had not been confirmed *in vivo*. The following section demonstrates that NC particles can provide levels of cavitation activity comparable to those from SV microbubbles *in vivo*.

6.5.2.1 Effect of different nuclei on cavitation activity in vivo

Cavitation response of nuclei *in vivo* can be quantified in many ways. Maximum power of acoustic emissions has been used to quantify cavitation in other chapters, and is shown here for each cavitation nuclei treatment group in Figure 6.12.

The key observations which can be drawn from Figure 6.12 are: 1) injection of NC particles causes a substantial increase in the maximum power associated with acoustic emissions above background; 2) within one location in the tumour, SV achieves a higher maximum power of acoustic emissions, however the emissions from NC are more sustained; 3) upon moving to a new position within the tumour following a NC injection, cavitation activity is renewed, which is in contrast to SV which decays to background with no renewal; 4) concentration of NC injection has no obvious scaling in the amount of cavitation activity as measured by maximum power, however the effect of concentration on other measures of cavitation activity is discussed Section 6.5.2.3.

In vivo variation has also been observed to be substantial and so in addition to mean values shown, individual data sets are represented for each mouse in Figure 6.13 where each mouse is represented by a different coloured line. As an example of *in vivo* variability, one of the four mice (purple line) in the low concentration NC group (Figure 6.13 (c)) showed a strong background cavitation signal even before injection of DSPE liposomes and did not show as strong a response to NC injection following any of the three injections

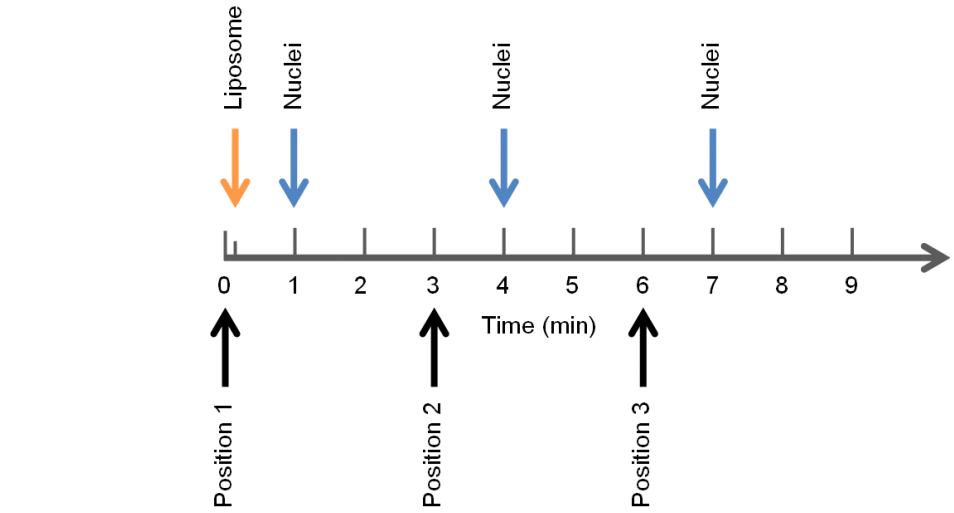

(a) *Treatment protocol*

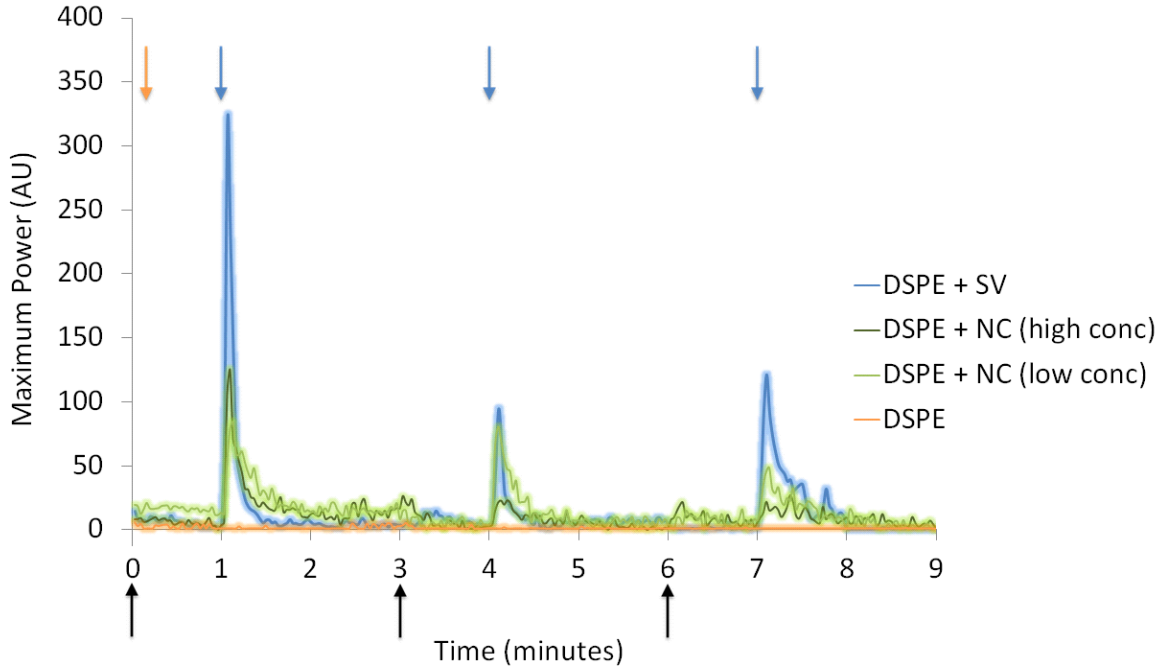

(b) *Cavitation response*

Figure 6.12: *In vivo cavitation response during drug delivery. (a) Schematic outlining the injections of DSPE liposomes (100 µL) (orange arrows, 10 seconds) and cavitation nuclei (33.3 µL each) (blue arrows, 1, 4, and 7 minutes), as well as the times when the focus of the transducer was moved to a previously non-exposed position in the tumour (black arrows, 0, 3 and 6 minutes) during the 9 minute ultrasound exposure. (b) C57 Bl 6 mice were exposed for 9 minutes to 0.5 MHz (H-107-B-10; Sonic Concepts), 1.75 MPa PRFP, 0.5 Hz PRF ultrasound. Each mouse was injected with 100 µL DSPE liposomes after 10 seconds (orange arrow) followed by 33.3 µL injections of cavitation nuclei (blue arrows) every 3 minutes totalling 100 µL. Cavitation nuclei tested were: 1) glucose 5% (orange line), 2) NC at low concentration (6.14 mg/mL) (pale green line), 3) NC at high concentration (25.75 mg/mL) (dark green line), and 4) SV at 200% stock concentration. Ultrasound focus was aligned in the tumour exposing 3 areas, with movement of the focus indicated by black arrows. n=4, average values shown, standard deviation omitted for clarity.*

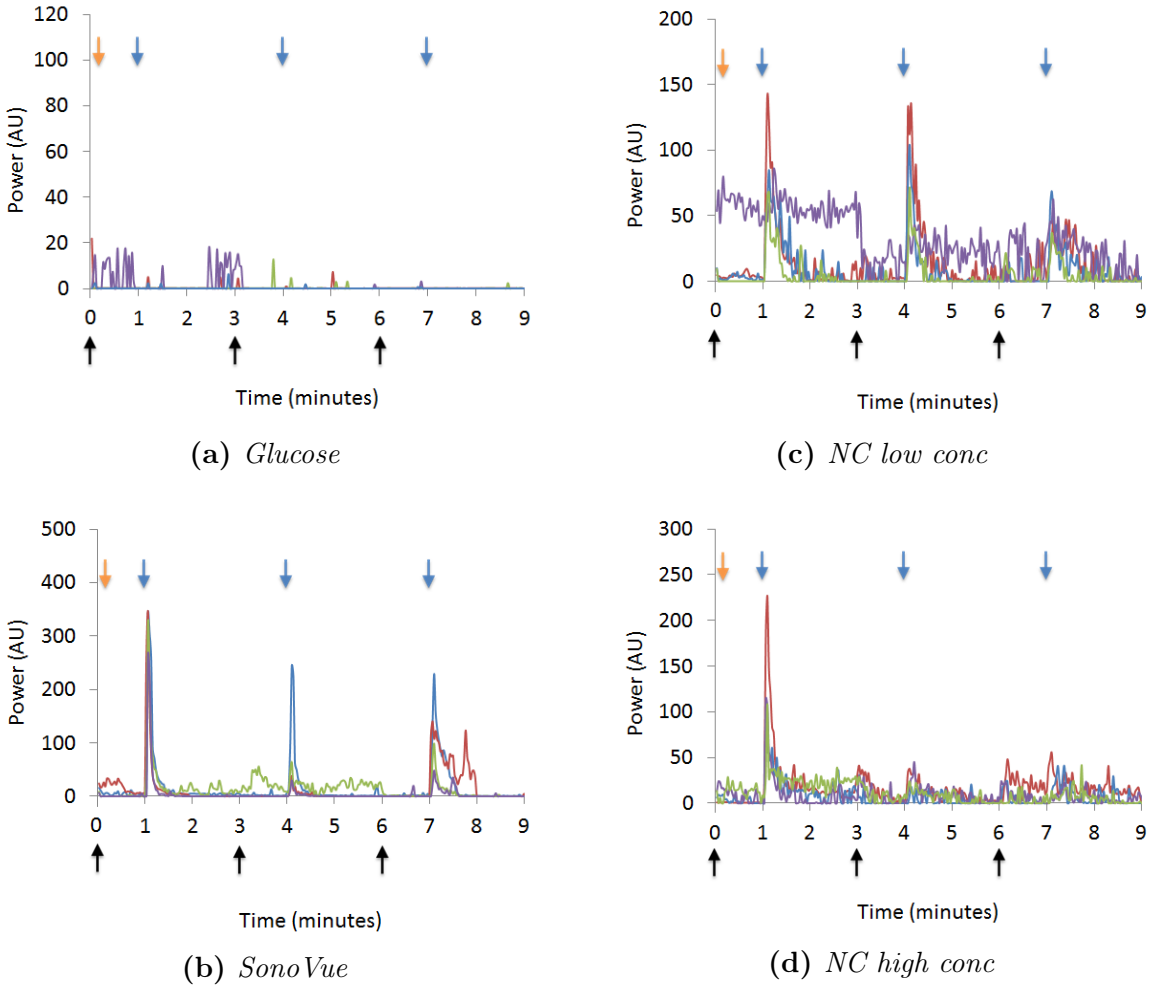

(a) *Glucose* **(c)** *NC low conc*

(b) *SonoVue* **(d)** *NC high conc*

Figure 6.13: *In vivo cavitation response upon injection of (a) glucose, (b) SonoVue (200%), (c) NC at 6.14 mg/mL, and (d) NC at 25.75 mg/mL. C57 Bl 6 mice were exposed for 9 minutes to 0.5 MHz (H-107-B-10; Sonic Concepts), 1.75 MPa PRFP, 0.5 Hz PRF ultrasound. Each mouse was injected with 100 µL DSPE liposomes after 10 seconds (orange arrow) followed by 33.3 µL injections of cavitation nuclei (blue arrows) every 3 minutes totalling 100 µL. The maximum power over time for each mouse is represented as an individual line, n=4 mice.*

when compared with the other three mice. A possible reason for this outlier in cavitation response was a high concentration of existing cavitation nuclei in the tumour tissue resulting in high background energy, and limited vascular supply to the tumour resulting in a marginal response following NC injection.

The cavitation activity following glucose injections alone is very low (Figure 6.13 (a)), with the 'spikes' in cavitation occurring in a random manner, confirming that glucose alone caused no increase in cavitation response. In contrast, injection of SV (as indicated by the blue arrows) provides clear increases in maximum power of acoustic emissions above background noise (Figure 6.13 (b)). With each SV injection, a peak in the maximum power of acoustic emissions is observed followed by a rapid decay in the signal over 30 to

60 seconds. Movement to a new position, as indicated by the black arrows, has no effect on maximum power. The increase in maximum power following a position change in the mouse represented by the green line can be explained by tumour variability. An increase in maximum power was observed after the first move, and a decrease in cavitation power after the second move, most likely due to moving to areas of the tumour which had more and fewer native cavitation nuclei respectively.

Cavitation activity following NC injections, at both concentrations tested (Figure 6.13 (c and d)), was notably different to SV. At the lower concentration of NC (6.14 mg/mL) (Figure 6.13 (c)), clear increases in cavitation were observed following the first, second and third injections of NCs (blue arrows). At the higher concentration of NC however (Figure 6.13 (d)), the cavitation response following the second and third injections of NC was substantially decreased in all four of the mice tested. Decay of the signal following NC injections occurred over 30 to 60 seconds, with a slightly higher maximum power response during that decay compared with SV. Unlike SV however, a renewed power of cavitation activity was observed when moving the focus to a previously unexposed position (black arrows). An increase in maximum power from cavitation was observed at 4 of the 6 position changes at the lower concentration (excluding the outlier mouse), and 5 of the 8 position changes at the higher concentration. These observations at both concentrations demonstrate the sustained cavitation response achieved *in vivo* following NC injections.

The maximum power of acoustic emissions in response to SV injections is substantially higher than that observed following either concentration of NC injections. However, it is likely that the cavitation activity from SV is dominated by stable cavitation and that the cavitation activity from NC is dominated by inertial cavitation as observed in Section 3.4.1.

6.5.2.2 Correlation of cavitation activity with pharmacokinetics

The sustained power of acoustic emissions observed following NC injections in contrast to SV can be explained by examining the pharmacokinetics of NC particles. The increase in cavitation response following NC injection at a new position could either be explained by the remaining circulating dose of NC in the blood vessels supplying the tumour in the focal volume, or by an accumulation of NC in the tumour tissue. Both of these mechanisms assume

that both the concentration and the maintained activity of the NC are sufficient to show a response. The pharmacokinetic studies carried out in Section 6.3 show that NC particles are cleared rapidly from the bloodstream with approximately 20% of the dose circulating after 5 minutes with negligible a concentration of NC in the tumour. Based on concentration decrease alone, a response of approximately 20% that of the response following injection could be expected at the move in position which occurred 2 minutes after injection of NC. The increase in maximum power of acoustic emissions observed ranged between 10 and 18% of the response following injection immediately preceding that move. This cavitation activity power is in accordance with the predicted power of circulating NC with a slight reduction in activity potentially due to some NC being deactivated (gas pockets removed) or trapped in a previous area of the tumour. This sustained cavitation activity observed *in vivo* is in keeping with the cavitation dynamics test *in vitro* shown in Figure 6.2.

6.5.2.3 Spatio-temporal characterisation of cavitation activity in vivo

To illustrate the amount of cavitation and where it occurred in the tumour, B-mode images were taken for each tumour, and registered with passive acoustic maps with power summed over each frame to give a total energy map. Assessment of the energy of cavitation inside the tumour volume as compared with outside, was performed using a masking algorithm developed by Calum Crake. A mask was drawn over the B-mode image around the tumour and then applied to the PAM image after registration as shown in Figure 6.14.

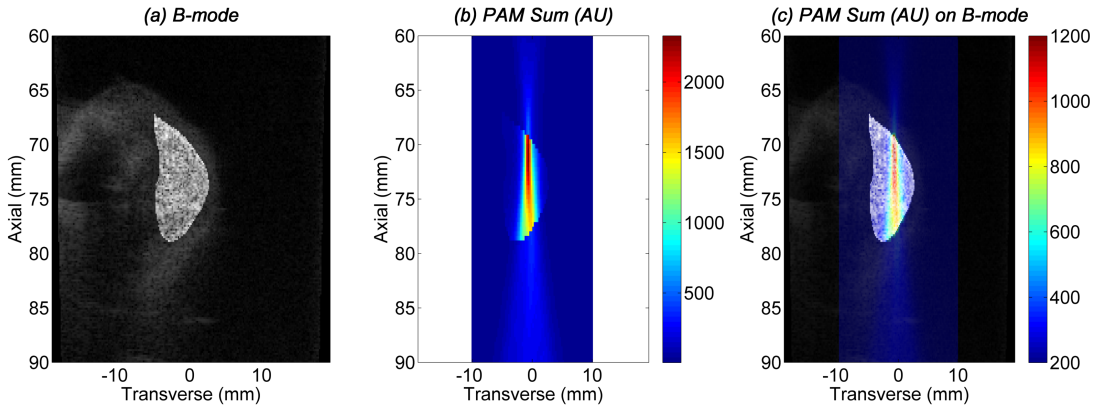

Figure 6.14: *Method for creating a mask around the tumour volume (a) on the B-mode image, (b) applying that mask to the sum of all PAM frames and (c) registering the data into a combined map. Code developed by Calum Crake.*

The theoretical transverse, Δx_{-3dB}, and axial, Δz_{-3dB}, resolutions of the linear array used for B-mode imaging and PAM acquisition are governed by Equations 6.1 and 6.2 [83].

$$\Delta x_{-3dB} = 0.89 f_{\#} \lambda \tag{6.1}$$

$$\Delta z_{-3dB} = 6.95 f_{\#}^2 \lambda \tag{6.2}$$

where the f-number, $f_{\#}$, is equal to z/D, where z is the focal length, D is the transducer aperture, and λ is the mean wavelength of the transducer. The linear array used here had an approximate transverse resolution of 0.3 mm, and axial resolution of 5.1 mm. The axial resolution limits the ability to discern whether cavitation is occurring inside or outside the tumour in the axial imaging direction, however the fine resolution in the transverse plane is able to provide more detail over the width of the tumour.

PAM images overlaid on B-mode images (Figure 6.15) show that the majority of the signal from cavitation was in the tumour in each group of cavitation nuclei tested. The focus of the driving transducer was set to a couple of millimeters within the skin on the proximal side of the tumour. This position was chosen to avoid the potentially necrotic core of the tumour where cavitation nuclei may not be present due to reduced vascular supply. The transducer was moved in the elevational plane and so the focus remained stationary in the axial/transverse plane which is displayed in the B-mode images. As such, the PAM displayed in Figure 6.15 is a sum of cavitation over the entire exposure.

To further illustrate the benefit of real-time PAM imaging, Supplementary Video 2 shows the cavitation response to injection of cavitation nuclei and to the movement to a new position. Compared to Figure 6.13 which shows the maximum power in each frame over time, Supplementary Video 2 is able to show the full passive acoustic map overlaid over the B-mode images over time. This feature of being able to attain real-time feedback allowed the pressure setting to be chosen based on *in vivo* observations rather than relying on *in vitro* observations alone. Before treatment of mice began, two mice were exposed to ultrasound using pressure ramps. Tumours were exposed at three positions, with a pressure ramp conducted at each position from 1.2 MPa to 2 MPa before and after NC injections.

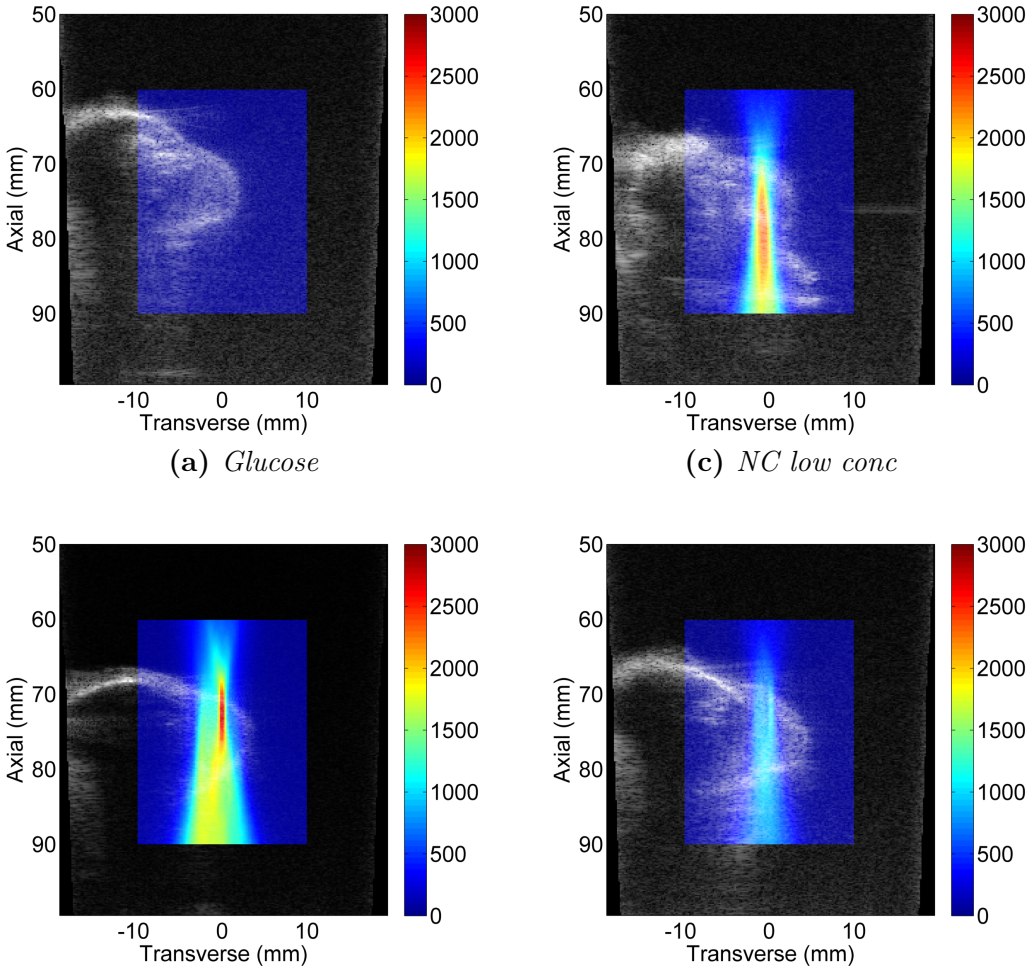

(a) *Glucose* **(c)** *NC low conc*

(b) *SonoVue* **(d)** *NC high conc*

Figure 6.15: *In vivo cavitation signal represented as the sum of all PAM frames registered to the B-mode image of the tumour during exposure. Tumours were injected with (a) glucose, showing no cavitation signal, (b) SV (200%), (c) NC (6.14 mg/mL) and (d) NC (25.75 mg/mL) each showing a cavitation response inside the tumour. B-mode images were acquired at 0.5 Hz (L-11-4v, 128 element linear array, Verasonics) with the first frame represented here. Tumours chosen were those showing highest release from DSPE liposomes in each treatment group of n=4.*

In real-time, the highest pressure which did not cause a noticeable increase in background but showed substantial increases in power with the injection of NC was chosen. Based on this study on two mice, the pressure of 1.75 MPa was chosen to expose all other mice.

Assessment of cavitation inside the tumour volume using masking showed that nearly all energy associated with acoustic emissions was contained within the tumour volume. Total energy associated with cavitation decreases when the mask is applied (Figure 6.16), however the maximum power (Figure 6.17) and number of frames above background energy (Figure 6.18) show no substantial change after the mask is applied. This combination of results suggest that the mask cuts a substantial amount of energy from the signal which is not

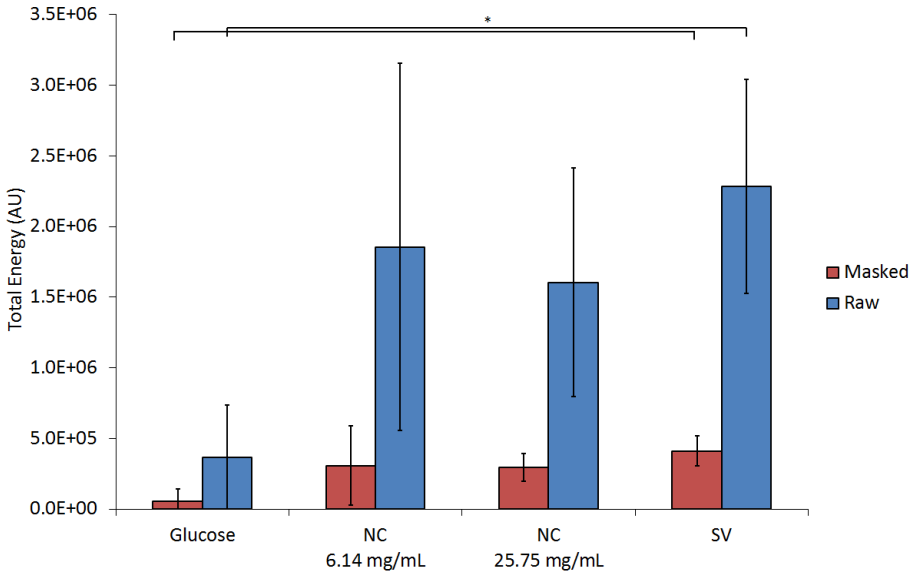

Figure 6.16: *Total energy associated with cavitation over all frames during ultrasound treatment over the entire mapping region (raw = blue) or only over the tumour region (masked = red). Low (6.14 mg/mL) and high (25.75 mg/mL) concentration of NC showed no statistical increase in total energy over glucose background controls. SV showed an increase of statistical significance ($p < 0.05$) over glucose, of both masked and raw data. n=4, standard deviation shown, ANOVA for significance.*

associated with the cavitation events above background noise. As the mask introduces error due to the assessment of the tumour boundary, and provides no added benefit of removing signal associated with above-background cavitation events occurring outside the tumour volume, the total PAM volume was considered for calculations associated with drug release.

Maximum power achieved by injections of SV was substantially higher than that of NC (25.75 mg/mL) (Figure 6.17) (2.3-fold increase, $p < 0.001$). However, the total number of frames above background was lower (1.3-fold decrease, ns) following SV injections than NC (25.75 mg/mL) injections (Figure 6.18). This observation is in accordance with the observations from Figures 6.13 and 6.12, where NC at both concentrations tested showed an increase in cavitation signal when the focus of the transducer was moved to a different position within the tumour, raising the amount of time that cavitation events occurred at energies above background.

With the 4.2-fold increase in concentration of NC between the two NC groups, only a marginal increase in maximum power of cavitation (Figure 6.17), and time above background energy (Figure 6.18) was observed. When comparing the total energy of cavitation over the entire exposure period, no increase was observed with increasing concentration (Figure

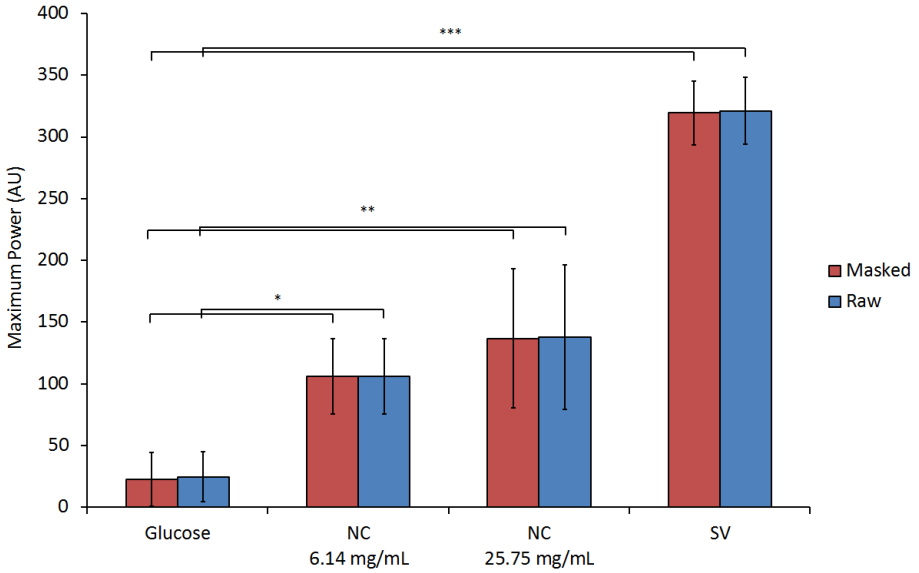

Figure 6.17: *Maximum power achieved from cavitation over the entire ultrasound exposure period and volume. Values from masked (red) and raw (blue) data are shown for each treatment group. Increase in maximum power over that following glucose injections alone was achieved for low concentration NC (6.14 mg/mL) ($p < 0.05$), high concentration NC (25.75 mg/mL) ($p < 0.01$) and SV (200%) ($p < 0.001$). N=4, standard deviation shown, one-way ANOVA for significance.*

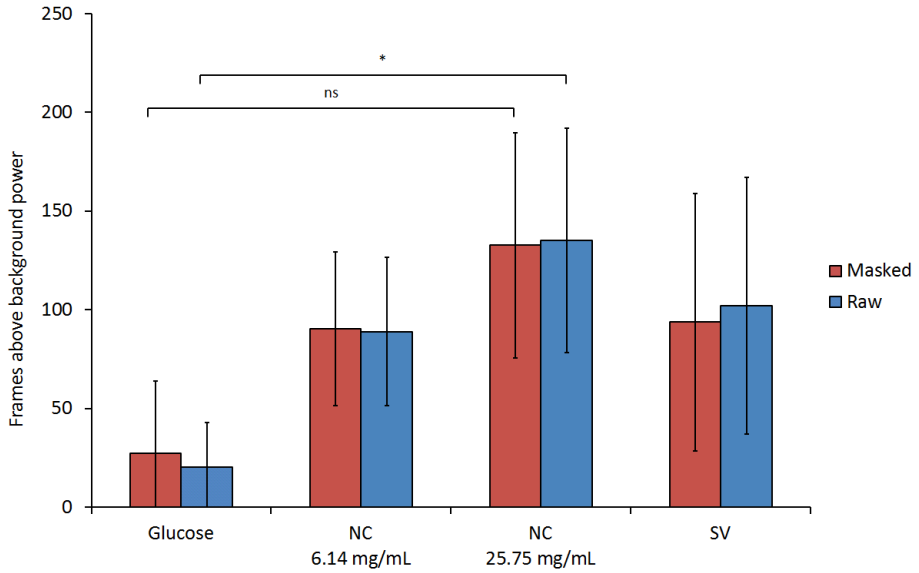

Figure 6.18: *Number of frames recorded with power above the background energy are shown for each treatment group. Background power was measured as the average of the first 25 frames (i.e. 50 seconds). All frames which recorded a power above the background energy for the individual mouse were recorded considering the entire treatment area (blue) or only the masked tumour area (red). Low concentration of NC (6.14 mg/mL) and SV (200%) showed an increase above background that was not statistically significant. High concentration of NC (25.75 mg/mL) showed a statistically significant increase above glucose alone on raw data ($p < 0.05$) but not statistically significant on masked data (ns = non significant). N=4, standard deviation shown, one-way ANOVA for significance.*

6.16). These observations may be explained by the discussion above, on why at the increased concentration, a decrease in power of cavitation following the first injection was observed.

6.5.2.4 Monitoring of adverse side effects in vivo

Photos were taken of mice before and after treatments to assess any damage caused by cavitation instigated from cavitation nuclei. Specifically, bruising and ulceration are two side effects that have been reported in literature when using ultrasound induced cavitation in mice at high intensities [131]. Although intensities used in this experiment were substantially lower than that reported by Miller et al. [131], the use of artificial cavitation nuclei, even at lower intensities, has the potential to also cause tissue damage. No tissue damage was observed in any mouse treated with ultrasound alone, NC alone, NC with ultrasound at 6.14 mg/mL, or NC with ultrasound at 25.75 mg/mL. However, ulceration on the tumour surface was observed in one mouse, on the skin distal to the ultrasound transducer, when SV microbubbles were used as cavitation nuclei. It should also be noted that although histological analysis was not conducted here, as all organs collected were homogenised for drug and particle analysis, histological analysis should be included in future studies to better characterise micro-scale damage to the tissue.

6.5.3 Drug release using cavitation nuclei in vivo

6.5.3.1 Characterisation of liposomes for in vivo drug release study

Substantial variability has been observed in the loading and purification efficiency during liposome preparation. For this reason, free and total luciferin concentrations were calculated for each batch tested and liposome batches were excluded if loading or purification failed. In addition, variability in release has been observed with different liposomal batches. Liposomes used in the *in vivo* drug release study were chosen as the best of three batches in terms of loading efficiency and purity.

To confirm cavitation sensitivity, liposomes were tested *in vitro* before *in vivo* studies (Figure 6.19). Release triggered by cavitation events was observed when compared with glucose controls, however the release profile was not in accordance with previously tested liposomes as shown in Figure 5.5. SV microbubbles and ultrasound yielded a substantially

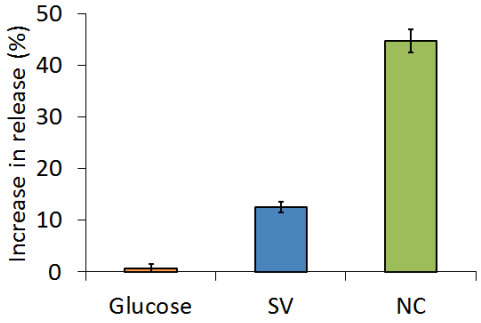

Figure 6.19: *In vitro release of luciferin from DSPE liposomes before testing in vivo. Samples exposed to 1.5 MPa, 0.5 MHz ultrasound for 10 minutes. N=3, standard deviation shown.*

lower percentage of release than observed in Figure 5.5 (12.5% compared with 91.5%). This variability in results may be due to experimental variability in preparation and batch variability of SV. It may also be due to variability in liposome preparation, although the identical process was carried out to produce both batches of liposomes. NC and ultrasound also yielded substantially lower percentage of release than observed in Figure 5.5 (44.8% compared with 86.6%).

Despite the lower release profile as compared with Figure 5.5, the increase in release observed in the presence of NC, was still higher than that observed in the presence of SV when tested *in vitro* before *in vivo* drug release studies described by Graham et al. [79].

Based on these results, these liposomes were deemed to be sufficiently cavitation sensitive to yield a detectable luciferin release response *in vivo*. To further quantify the expected luminescence intensity based on the recorded percentage of release, luciferin at known concentrations was incubated with the B16-F10-LUC cells which were implanted into the mice. This study revealed that the amount of luciferin released observed *in vitro* in Figure 6.19 would produce detectable luminescence *in vivo*.

6.5.3.2 Quantification of release in vivo

A mean 4.6-fold and 52.4-fold increase in free luciferin delivered to the tumour was observed for SV and NC (25.75 mg/mL) respectively, when exposed to ultrasound. However, the results of this drug release study *in vivo* using SV and NC cavitation nuclei showed no statistically significant increases in luciferin in the tumour in the treatment groups as compared with the glucose control (one-way ANOVA for significance). Figure 6.20 represents the amount of luciferin in the tumour after DSPE liposomes were injected and exposed to therapeutic ultrasound at 1.75 MPa for 9 minutes with the injection of glucose (orange bar),

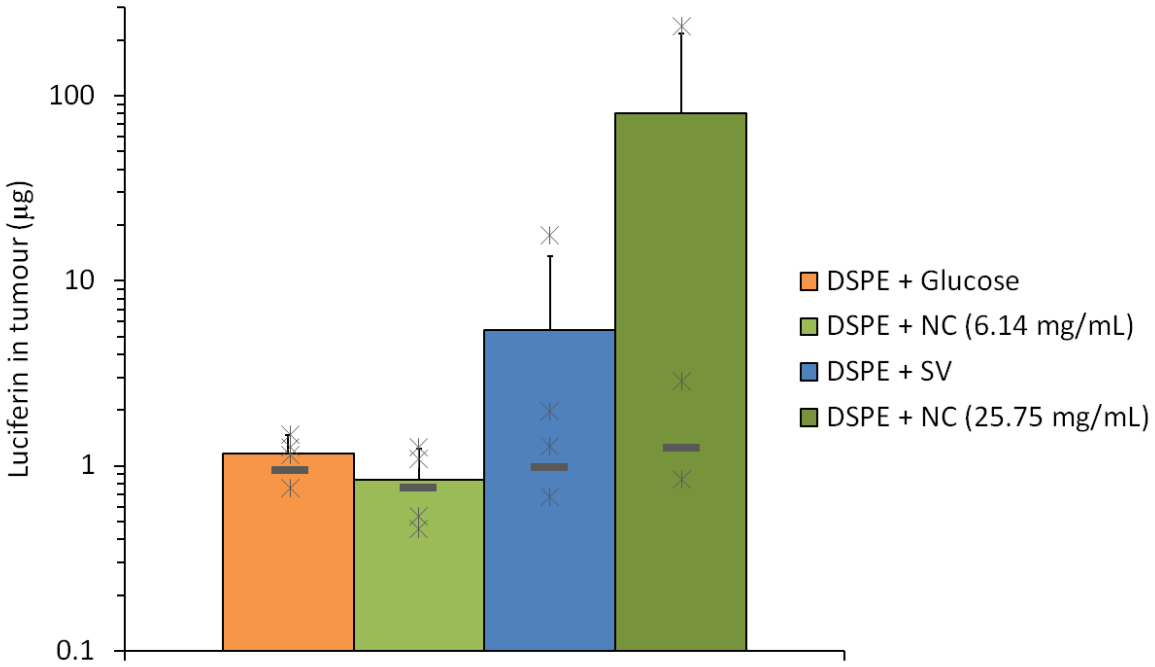

Figure 6.20: *In vivo payload release from liposomes. C57 Bl 6 mice bearing B16 F10 - luc tumours were exposed to 0.5 MHz driving frequency, 1.75 MPa PRFP, 0.5 Hz PRF ultrasound for 9 minutes. Coloured bars represent luciferin release (µg) in the tumour after injection of DSPE - luciferin containing liposomes and one type of cavitation nuclei or control: glucose (orange); NC (6.14 mg/mL) (aqua); SV (200%) (blue); or NC (25.75 mg/mL) (green). Grey stars represent individual data points for each group. Grey horizontal lines represent the average free luciferin estimated in the tumour due to non-purified free luciferin in the DSPE liposome sample. One-way ANOVA for significance, each cavitation nuclei shows a non-significant difference in luciferin compared with the glucose control. n=4 for each group apart from DSPE + NC (25.75 mg/mL) which is n=3, average and standard deviation shown.*

low concentration of NC (6.14 mg/mL) (pale green bar), SV (200%) (blue bar), or a high concentration of NC (25.75 mg/mL) (dark green bar). Individual data points from each mouse are plotted as gray stars on top of each bar. The estimated average free luciferin in the tumour due to non-purified free luciferin in the liposome sample is represented by gray horizontal lines for each treatment group. The results from this study are discussed in detail below.

The method for calculating the amount of luciferin in the tumour was based on the IVIS images taken of the mouse while alive and the known doses of luciferin injected into each mouse 2 days before the release study was conducted as described above. IVIS was chosen as the most accurate measure compared with all other measurements taken and is discussed in Section 6.5.3.3.

After IVIS imaging of each mouse, blood samples were taken for plasma analysis and each mouse was euthanized and tumours were then sectioned and re-imaged, firstly in the same orientation as the live mouse was imaged (dorsal orientation) and secondly with the body-facing side upwards (frontal orientation). The results from the dorsal orientation were similar to those acquired with the mouse alive, and the results from the frontal orientation showed a higher signal in general with a substantially higher variation than either the live or dorsal results. This increase in signal is most likely due to the lack of attenuation from the skin. In addition to the signal strength changing, the distribution of luminescence signal changed from being uneven to more evenly distributed over the tumour when imaged in the frontal orientation. This observation is likely due to the mixing of luciferin and luciferase in the blood on the surface of the sectioned side of the tumour and is unlikely to represent a more even distribution of drug release nearer the body of the mouse. As time passes between drug release and luminescence imaging, luciferin is being deactivated by luciferase produced in the tumour with light being emitted. This deactivation leads to a decrease in signal strength which depending on the amount of luciferase expression in each tumour, may decrease at varying rates between mice. In addition to data acquired using the IVIS measuring the luminescence due to luciferase produced by the tumour reacting with free luciferin, tumours were homogenized and tested with the luciferin-luciferase assay in a plate reader where additional luciferase and ATP was added to each sample. This measurement was conducted to act as a confirmation of results seen using the IVIS however it has increased error associated with it. The first error introduced is discussed above where with the passing of time, luciferin is deactivated by the remaining luciferase in the sample. In addition, if any luciferase remained active in the sample, and if luciferase expression varied between tumours, this would add to the set amount of luciferase being added to each sample, further increasing the error of the measurement. Despite these limitations, the results acquired from the post-cull homogenisation analysis correlated well with those acquired using the IVIS. Based on these findings, results from the IVIS on live mice were used for all drug release calculations.

Stability of DSPE liposomes to ultrasound alone was confirmed by injecting glucose instead of cavitation nuclei during the therapeutic ultrasound exposure. Glucose alone

yielded no increase in cavitation maximum power above pre-injection background power (Figure 6.13(a)) and showed no events on the summed PAM images (Figure 6.15 (a)). The amount of luciferin measured in the tumour was approximately equal to the calculated amount of background free luciferin in the delivered dose (see orange bar compared to grey line for 'glucose' sample in Figure 6.20) indicating that there was no release of luciferin from liposomes in the absence of cavitation nuclei.

NC at the lower concentration tested (6.14 mg/mL) showed substantial increases in maximum power of acoustic emissions with each injection of NC (Figure 6.13(c)), which was also observed as high energies on the summed PAM images (Figure 6.15 (c)), however no increase in release was observed above the estimated background (see pale green bar compared to grey line for 'NC (6.14 mg/mL)' sample in Figure 6.20).

SV microbubbles showed substantial increases in maximum power of acoustic emissions with each injection (Figure 6.13(b)), and a strong cavitation signal on the summed PAM images (Figure 6.15 (b)). In two of the four mice tested, the amount of luciferin measured was approximately equal to the background amount of luciferin estimated for that treatment group (see blue bar compared to grey line for 'SV' sample in Figure 6.20). The other two mice each showed increases in free luciferin compared with the estimated background. One mouse showed a 2-fold increase and the other showed an 18-fold increase from the estimated background amount of free luciferin. When considering all mice in the treatment group, a mean 4.6-fold increase in luciferin delivered to the tumour was observed when SV was injected in the presence of ultrasound compared with glucose.

NC at the higher concentration tested (25.75 mg/mL) showed substantial increases in maximum power of acoustic emissions with each injection of NC (Figure 6.13(d)), and also showed a cavitation signal on the summed PAM images (Figure 6.15 (d)). One mouse from this group was excluded from drug release analysis as it did not receive the full dose of DSPE liposomes due to a breakage of the tubing leading to the injection needle. Of the three mice which were included in analysis, one mouse showed no increase in the amount of luciferin in the tumour (see gray star on dark green bar compared to grey line for 'NC (25.75 mg/mL)' sample in Figure 6.20). Of the two mice which did show an increase in amount of free luciferin, one showed a 3-fold increase and the other showed a 221-fold increase in the

amount of free luciferin in the tumour. When considering the three mice used in the analysis together, a mean 52.4-fold increase in luciferin delivered to the tumour was observed when NC (25.75 mg/mL) was injected in the presence of ultrasound compared with glucose.

Although these results do not show a statistically significant increase from either NC or SV above glucose, the increases that are observed from SV and NC (25.75 mg/mL) reflect the same trend of increased release observed from the same batch of liposomes tested *in vitro* (Figure 6.19) before this current *in vivo* study.

6.5.3.3 Discussion of in vivo drug release results

There are several reasons that the percentage of release observed *in vivo* was not as pronounced or consistent as that observed *in vitro*. The two main issues discussed here are: 1) the high luciferin background in the injected liposome sample; and 2) the limited dynamic range of this luciferin-luciferase assay *in vivo*.

The amount of free luciferin in the DSPE liposomes used for *in vivo* studies to previously show release using SV as cavitation nuclei was 5% [79] which was substantially lower than the free luciferin of 14.3% used in this present study. Potential reasons for batch variability may include: lipid concentration variation; temperature during encapsulation which is conducted at 'room temperature'; and variability in efficiency of PD10 column during purification. To accommodate for this batch variability in encapsulation efficiency and free luciferin percentage, the luciferin-luciferase assay was used to quantify total and free luciferin concentrations. This information was then used to aid in the interpretation of results. The high background of free luciferin could explain why the effect observed was not as marked as the effect seen previously. The background luminescence of the control group previously [79] was below the detection limit of the IVIS machine (approximately 20 μg as shown here), whereas the background luminescence of the control group in this present study was above the detection limit of the IVIS machine. Any fold increase in luminescence is therefore not as substantial.

Another difference between the two studies is the passage number of the B16-F10 luciferase expressing melanoma cells. Although the same cell line was used, a higher passage number was used in this present study. A loss of luciferase expression has been observed dur-

ing cell culture with increasing passage number. A lower amount of luciferase in the tumour could lead to a decreased luminescence signal for a given amount of free luciferin available if the lucifease is saturated. This would effectively reduce the dynamic range of detection, possibly below that of the highest luciferin concentration. To test this possibility, tumours were frozen after IVIS imaging and homogenised before testing using the luciferin-luciferase assay, adding both luciferase and ATP to the samples to ensure the reaction can go to completion. The results of these experiments yielded similar results to those acquired using the IVIS on live animals and therefore did not support the hypothesis that luminescence was capped due to insufficient luciferase expression *in vivo*.

One of the hypotheses of this drug release experiment was that by triggering drug release from a liposome using cavitation nuclei that is also on the nanoscale, a more even drug release profile could be achieved across the tumour than compared with the use of cavitation nuclei on the microscale. The uneven drug release observed when using SV microbubbles as cavitation nuclei for drug release from liposomes as seen by Graham et al. [79] was discussed in the context of the irregular vasculature found in tumours. Variability in power of inertial cavitation at different positions within the tumour may have been due to a lack of SV microbubbles in different tumour regions due to this irregular vasculature. One hypothesis of this drug release experiment using cavicatalytic nanoparticles was that the nanoscale cavitation nuclei would be able to penetrate further into the tumour tissue while circulating and/or during ultrasound exposure. Assuming the liposomes were also able to penetrate deeper into the tumour, the trigger for drug release would be more evenly distributed over the tumour leading to a more even drug release over the tumour.

The *in vivo* experiments described here were designed to compare SV and NC thereby allowing this hypothesis to be addressed. However, due to the high background luminescence intensity and the low amount of triggered release achieved in mice treated with ultrasound and either SV or NC this hypothesis was difficult to address. Nevertheless, IVIS images of tumours showing a slight increase in release due to SV and NC cavitation nuclei were compared in Figure 6.21. Distribution of luminescence signal from tumours exposed to ultrasound in the presence of SV or NC was uneven in both cases.

Free luciferin was injected into all mice 2 days before drug release experiments were

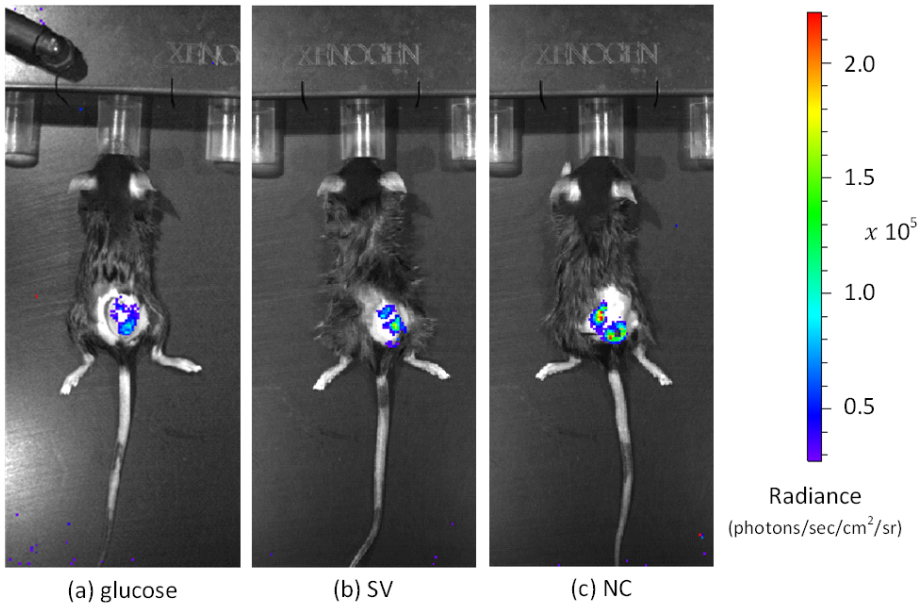

Figure 6.21: *Luminescence in vivo representing free luciferin after ultrasound exposure in the presence of (a) glucose, (b) SV or (c) NC 25.75 mg/mL. Scale bar is the same for all images. Mice represented showed the second highest release of each group with similar luminescence amounts for comparison.*

conducted and were imaged using the IVIS system (see methods in Section 2.9.5) to measure luminescence of known quantities of luciferin in each mouse. These measurements were made to account for the difference in tumours between mice that may lead to variations in luminescence. 5 μg was injected into 5 mice all showing no signal as measured by IVIS. 20 μg was injected into 1 mouse which also showed no signal as measured by IVIS. This amount of luciferin (20 μg) was assumed to be undetectable in every mouse based on this initial study. On this basis, all mice were injected intraperitoneally with 50 μg and 200 μg luciferin 4 hours later, and a standard curve with log fit was prepared including the assumed 20 μg zero luminescence point. The mass of luciferin in the tumour for each standard curve was calculated by normalising the luminescence at each known quantity of luciferin injected by the total mouse weight and multiplying by the tumour weight which was determined after sectioning. This calculation assumes that the injected luciferin distributed equally throughout the body of the mouse over the 11 minutes between injection and luminescence measurement.

The amount of free luciferin as a percentage of the total luciferin circulating (encapsulated and free) is shown in Figure 6.22. This free luciferin percentage was quantified using the luciferin-luciferase assay where one sample of plasma was heated to 100°C to release

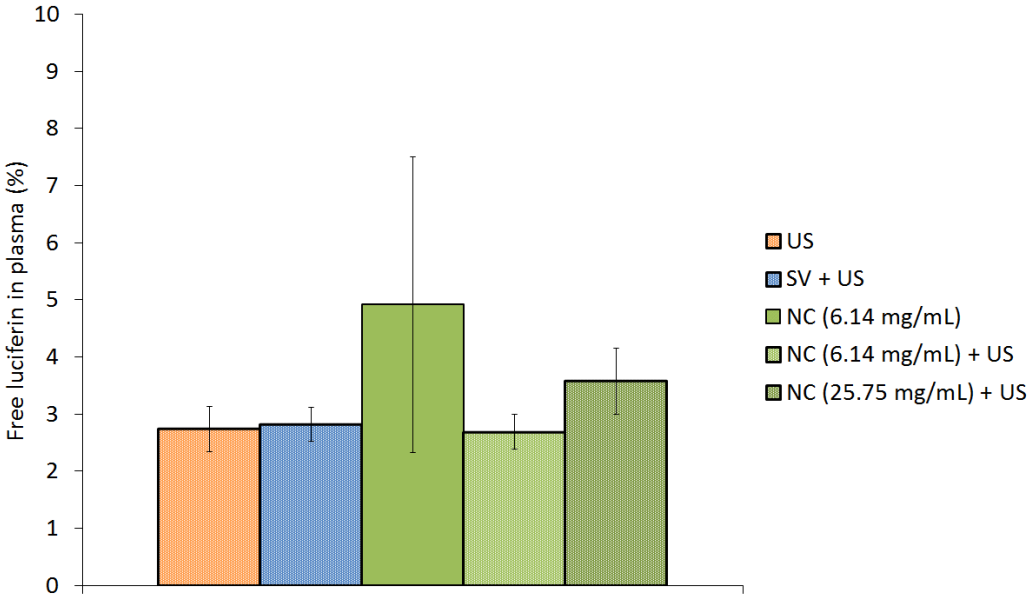

Figure 6.22: *Percentage free luciferin of total luciferin circulating in plasma after treatment. One mouse excluded from therapeutic ultrasound (US) alone (orange spotted) due to difficulty obtaining blood sample. All other groups n=4, standard deviation shown.*

all luciferin from liposomes, and the other kept at 4°C. The quantified percentage of free luciferin in the DSPE liposome sample before injection was 14.3% of the total luciferin in the sample, and the percentage of free luciferin in the plasma samples after treatment in all treatment groups was approximately 3% of the total administered. This percentage of free luciferin was observed across all treatment groups and controls with 2 outliers in the NC control group at 6% and 8%. The decrease in free luciferin in the plasma compared with the injected luciferin sample can be explained by luciferin, as a small, membrane-permeable molecule, being taken up into all tissues by diffusion. This observation also helps to explain the high background luminescence in the tumours of the control groups. Assuming the free portion of luciferin injected into each mouse (41 μg) diffuses equally throughout the body, the mass which would be present in the tumour was plotted as grey horizontal bars as averages for each treatment group on Figure 6.20. This level represents a background luminescence intensity due only to the luminescence of the free injected dose.

Although this experiment was limited by the high background amount of free luciferin, and the limited dynamic range of the luciferin-luciferase assay *in vivo* some observations relating to the correlation between release and cavitation activity can be made.

6.5.3.4 Discussion on cavitation mapping for drug release quantification

Correlation between cavitation activity and drug release *in vitro* was discussed in Chapters 4 and 5. Total energy associated with cavitation as well as maximum power of cavitation showed good correlation with release *in vitro*. These results suggested that non-invasive passive acoustic mapping might be able to be used to quantify release *in vivo*.

This hypothesis was not able to be tested fully as there were not enough treatments which yielded a substantially higher luciferin release compared with background amounts. Nonetheless, free luciferin in the tumour was compared with both total energy (Figure 6.23 (a)) and maximum power (Figure 6.23 (b)) over the exposure period. Across all three treatment groups there was no correlation between luciferin amount in the tumour and level of cavitation. Within the two groups which showed increased release, NC (25.75 mg/mL) and SV, tenuous correlations can be observed. Mice treated with NC (25.75 mg/mL) in the presence of ultrasound showed a linear increase in luciferin in the tumour with increasing total energy and a near linear, however very steep correlation with increasing maximum power. Mice treated with SV in the presence of ultrasound showed an increase in luciferin in the tumour with increasing maximum power (with one outlier) but showed no correlation with total energy.

Various other markers of cavitation were also assessed for correlation with release, but no improved correlation was observed. Markers which were analysed included: the number of frames with power of cavitation above an arbitrary threshold; the number of frames above background cavitation energy calculated for each individual mouse; and number of frames above a percentage of the maximum cavitation power for each mouse.

Increase in release was observed in mice treated with a high concentration of NC (25.75 mg/mL) but not at the lower concentration of NC (6.14 mg/mL). This observation is despite there being no increase in total energy associated with acoustic emissions, and only a marginal increase in maximum power associated with acoustic emissions. The largest difference associated with acoustic emissions was length of time above background power. In Chapter 5, exposure time was explored at 90 seconds and 10 minutes. At 90 seconds exposure, only a marginal increase in release was observed in the presence of NC. At 10 minutes however, substantial release was observed. This same dependency on duration of

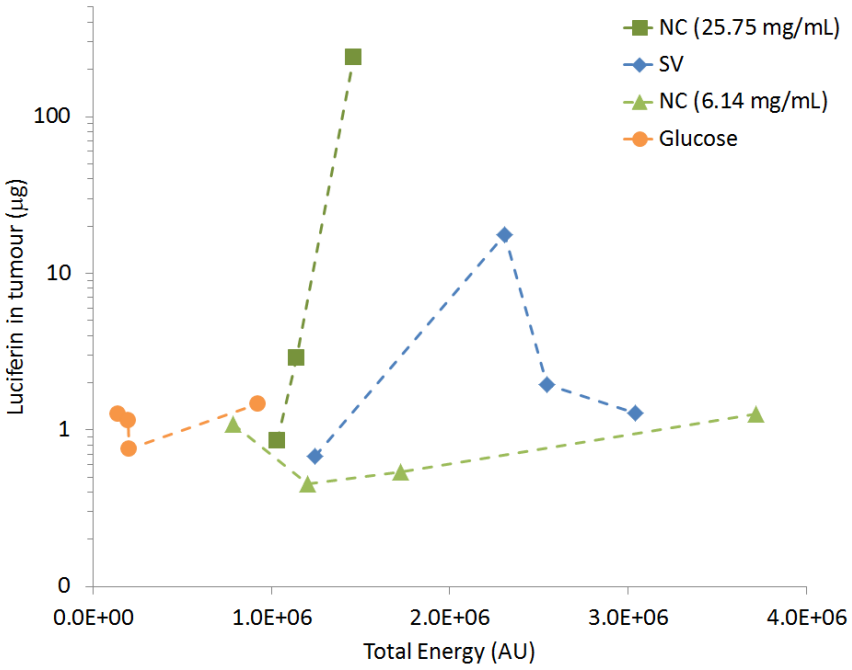

(a) *Total Energy*

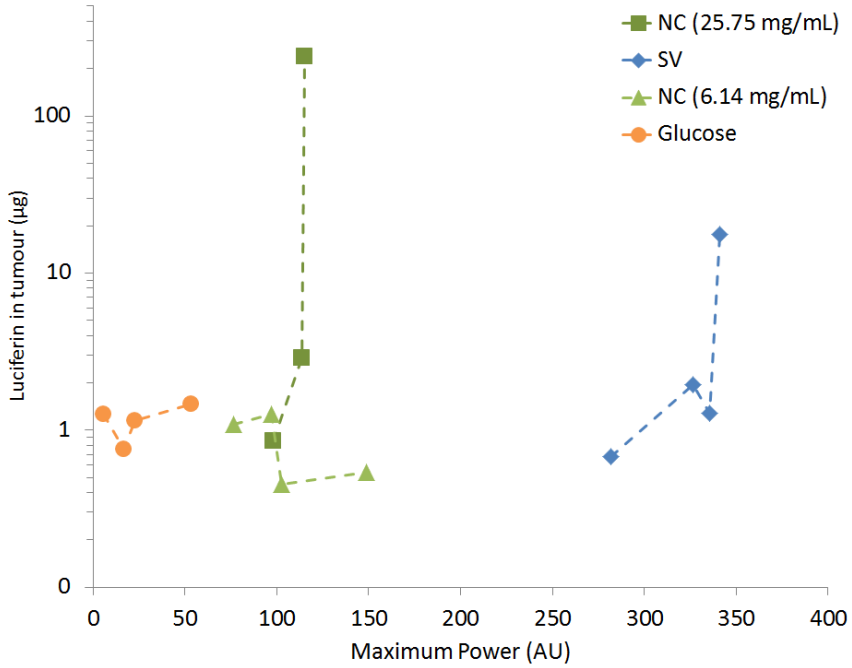

(b) *Maximum Power*

Figure 6.23: *Investigation of the correlation between drug release observed and cavitation measurements recorded for each mouse. The mass of luciferin detected in the tumour is compared with (a) the unmasked total energy associated with cavitation over the entire exposure period and (b) the unmasked maximum power of cavitation achieved in each mouse. Each mouse is represented by a marker with adjoining lines connecting points in order of increasing energy and power respectfully. Correlation for each of glucose (orange), NC (6.14 mg/mL) (pale green), SV (blue), and NC (25.75 mg/mL) (dark green), is not clear. One mouse was excluded from the high concentration NC (25.75 mg/mL) treatment group as it did not receive the full dose of DSPE liposomes. For each other group, n=4.*

cavitation response may be responsible for the increased release observed in two of the mice treated with the higher concentration of NC.

As such, this data set was not sufficient to determine whether passive acoustic mapping can be used to quantify the amount of drug release *in vivo*. To increase the likelihood of being able to address this question, the background luminescence intensity due to the free luciferin in the DSPE liposome sample and the moderate power of cavitation achieved from NC when compared with SV *in vivo* should be addressed. Further purification of the DSPE liposome sample would yield a lower free luciferin background concentration in the sample which may increase the dynamic range over which release can be observed. Additionally, altering the NC structure and/or concentration for optimisation *in vivo* would potentially yield a stronger cavitation response. As increasing the NC concentration did not achieve a substantial increase in cavitation as observed over the parameters measured, using infusion instead of a bolus injection may improve the cavitation response from both the NC and SV cavitation nuclei by extending the period over which cavitation occurs.

To further improve the likelihood of correlation between cavitation from cavicatalytic nanoparticles and release from liposomes, modification to the dual particle system could be made. Encapsulating the cavicatalytic nanoparticle inside the liposome might increase the likelihood of liposome destruction upon cavitation. NC LB3 particles (∼500 nm) would be too large for this configuration however NC LB1 (∼150 nm) or CNPs (∼180 nm) would both be potential candidates for co-encapsulation with a drug inside a liposome. Another configuration which would increase the correlation between cavitation and release would be to tether the cavicatalytic nanoparticle to the surface of the liposome. This method would be able to be applied to each of the sizes of particles however chemical modification to the surface of the cavicatalytic particles, possibly via a PEG linker, may reduce the cavicatalytic properties of the particles.

6.6 Conclusions

The motivation behind the work of this thesis is to target drugs to tumour tissue, while leaving healthy tissue unaffected, to reduce the side effects of potent chemotherapeutics. A system for drug release from cavitation sensitive liposomes using cavitation nuclei at the nanoscale has been developed *in vitro* in Chapters 3, 4, and 5. In this chapter, this drug release system was tested *in vivo*.

Even though the same trend in drug release was identified *in vivo* as anticipated *in vitro*, the results were not statistically significant. A high background of luciferin reduced the ability to observe an increase in release from liposomes in the presence of cavitation.

The increased variability observed in these *in vivo* studies compared to the *in vitro* studies reported in Chapter 5 is likely due to the increased complexity and dynamic nature of biological systems, and tumours in particular. While *in vitro* studies were planned to match particle concentrations, plasma components and flow rates within the phantoms used to those potentially present within tumours, it is clear that all of these factors may vary dramatically between regions of the same tumour as well as between tumours on different mice. Progress in this field would therefore benefit from more complex *in vitro* models and a more complete understanding of the exact flow and accumulation, as well as the activity, of cavicatalytic particles within tumours.

This chapter's results were however able to confirm that NC maintain their cavitation nucleating potential *in vivo* and showed a sustained response with ultrasound exposure. In addition, release results, although not statistically significant, showed a mean 4.6-fold increase in luciferin in the tumour in the presence of SV and ultrasound, and a mean 52.4-fold increase in luciferin in the tumour in the presence of NC (25.75 mg/mL) and ultrasound.

These results warrant further research in this area to optimise the delivery system developed here. Future work based on these *in vivo* studies could include: modification of the NC particle surface to extend blood circulation time to increase the likelihood of tumour accumulation via the EPR effect, without hindering the cavitation response of the particles; improvement of release from liposomes, by co-location of liposomes and cavitation nuclei either by encapsulating cavitation nuclei inside liposomes or by tethering cavitation nuclei to the surface of liposomes; and optimising ultrasound exposure parameters for the *in vivo*

environment.

The results presented and discussed in this chapter allow the following conclusions to be drawn. Firstly, CNP and NC particles were shown to be stable in plasma samples *in vitro* and were able to maintain a strong cavitation response over time compared with SV. Secondly, a strong cavitation response was observed *in vivo* using passive acoustic mapping following injections of SV at 200% concentration and NC at 6.14 mg/mL and 25.75 mg/mL when activated by ultrasound at 0.5 MHz, 1.75 MPa PRFP, 0.5 Hz. Thirdly, cavitation from NC particles showed extended cavitation responses *in vivo* as well as a renewed cavitation response when the focus of the transducer was moved to a previously non-exposed region of the tumour, which was not observed when SV was used. This extended cavitation response may indicate a difference in the clearance or distribution of nuclei in the tumour, between NC and SV. Fourthly, an increase in release of luciferin from DSPE liposomes was observed *in vivo* under ultrasound exposure in the presence of SV and NC (25.75 mg/mL), compared to the use of ultrasound alone, however the increases observed were not statistically significant. Finally, correlations between cavitation activity and drug release were discussed, with future work needed to improve understanding of potential correlations *in vivo*.

Chapter 7

Conclusions and future work

This thesis was motivated by the compelling requirement to improve the efficiency and decrease the side effects of current chemotherapeutics. A drug targeting system was developed to release drugs in a triggered fashion in tumour tissues. This approach was taken in order that it may restrict the toxic effects of the encapsulated drugs to only cancer tissue while leaving healthy tissue unaffected. Triggered drug release was achieved from liposomes using nanoscale cavitation nuclei and was tested both *in vitro* and *in vivo*. The conclusions from this thesis, and future work which could develop this system further are discussed below.

7.1 Conclusions

The major novel accomplishments of this thesis which are discussed here are:

1. Development and validation of cavitation nuclei at the nanoscale
2. Drug release from cavitation sensitive liposomes using both micro- and nano-scale cavitation nuclei
3. Assessment of drug release from liposomes *in vivo* using nanoscale cavitation nuclei

7.1.1 Development of cavitation nuclei at the nanoscale

In the development and characterization of cavitation nuclei at the nanoscale, two particle types were explored. The first, a rough, irregularly shaped carbon nanoparticle (CNP), the

second, a smooth, regularly shaped polymeric nano-cup (NC) particle. Both particle types were solid particles found to be size stable in de-ionized water and glucose (5%) which is an FDA approved injectate. Both particle types were shown to reduce the cavitation threshold of water and human plasma at both 0.5 MHz and 1.614 MHz. The cavitation response that both of these particle types instigated was compared with that of SonoVue® (SV), a clinically approved microbubble formulation. Two distinguishing features were identified with regard to SV. The first is that at all pressures tested, energy associated with nanoparticle induced cavitation was dominated by broadband energy which is associated with inertial cavitation. This observation is in contrast to SV microbubbles which at low insonation pressures emit harmonic energy dominated cavitation signals associated with stable cavitation. The second distinguishing feature of these solid nanoparticles is that cavitation activity was maintained over much longer periods than with SV microbubbles in both water and plasma (from 2 minutes to more than 10 minutes). In water, CNPs showed a slower cavitation decay than NCs. However in plasma the power of cavitation from both CNPs and NCs decayed at the same rate.

Two possible explanations for this extended cavitation response compared with free microbubbles are that: 1) gas on the surface of the solid particle is removed from the surface during the rarefactional pressure cycle, expands as a free bubble, and collapses violently before re-stabilising on the particle surface or 2) given the size of the particles, the number concentration of particles is high compared with the number concentration of microbubbles tested providing more cavitation nuclei in the focal volume thus taking longer for them to be destroyed. Testing of the size distribution of both CNPs and NCs before and after ultrasound exposure showed no substantial change, suggesting that their hydrodynamic radius is not substantially altered by ultrasound excitation. Due to these features of instigating cavitation and not being greatly affected by the cavitation events themselves, these particles were classified as cavicatalytic.

7.1.2 Drug release from cavitation sensitive liposomes using both micro- and nano-scale cavitation nuclei

To address the issue of chemotherapeutics acting on non-target tissues a cavitation sensitive liposome was developed and tested. Liposome composition was found to be critical in determining cavitation sensitivity. DSPE-based liposomes were found to be cavitation sensitive, whereas HSPC-based liposomes were not cavitation sensitive to all conditions tested. Triggered release would allow a higher proportion of drug to be released within the target, thereby lowering the amount in non-target organs. Three distinguishing features of these liposomes were ultrasound stability, thermal stability and cavitation sensitivity. Previous nano-sized liposomes used for triggered drug release have been either ultrasound sensitive [62] or thermally sensitive [57], whereas these liposomes developed were demonstrated to only be sensitive to cavitation events. The triggered drug release mechanism was initially proven using SV microbubbles as cavitation nuclei with results published in the Journal of Controlled Release [79].

This work was further developed to demonstrate payload release from liposomes using cavicatalytic nanoparticles. This development may allow for improved co-localisation of effector agent (cavicatalytic nanoparticle) and drug carrier (cavitation sensitive liposome) in tumour tissue based on their similar size distributions. The extent of drug release was demonstrated to be correlated with the power of cavitation activity. Cavitation activity arising from all three nuclei types (SV, CNP and NC) was quantified both in terms of the total energy of acoustic emissions, which is indicative of the extent of cavitation activity, and the peak power of emissions, which is indicative of the violence of inertial cavitation events. No correlation could be found between the energy of acoustic emissions and payload release across all nuclei tested, but a threshold value for the peak power of emissions could clearly be identified, beyond which liposomal release was always observed.

7.1.3 Assessment of drug release from liposomes in vivo using nanoscale cavitation nuclei

Drug release *in vivo* was assessed in tumour bearing mice. This first required the pharmacokinetics and bio-distribution of the cavitation nuclei to be characterised. NC particles were cleared rapidly from the body through the liver and kidneys with less than 5% of the dose remaining in the blood stream after 2 hours (0.61 mg injected). This rapid clearance limits the extent of the EPR effect that these particles might have experienced in the tumour tissue. When tumours were exposed to ultrasound following NC injections, a non-statistically-significant increase in NC in the tumour and corresponding decrease in the plasma was observed. Further studies with larger sample groups may reveal whether cavitation events can drive the NC from the bloodstream and into tumours.

The cavitation response of NC following intravenous injection was of the same order of magnitude as that following SV injections. One distinguishing feature of the cavitation response from NC *in vivo* was a sustained power of cavitation activity. The cavitation signal from both SV and NC decayed over 30 to 60 seconds, however when the transducer focus was moved to a previously unexposed region in the tumour, a substantial increase in cavitation power was observed following NC injections, whereas no response was observed from mice injected with SV. This observation suggests that active NC are still present in either the blood stream or tumour which is in contrast to SV which is completely destroyed during the initial ultrasound exposure.

Assessment of drug release from liposomes following cavitation instigated by either NC or SV was achieved in a luciferase expressing tumour cell line grown subcutaneously in mice with luciferin encapsulated in the liposome. Differences in drug release from this *in vivo* study were not statistically significant due to high background signal and high variability in response, however some observations were still made. Cavitation instigated by SV caused a mean 4.6-fold increase and by NC caused a mean 52.4-fold increase in luciferin in the tumour. These increases in release were not able to be correlated well to cavitation activity as measured non-invasively using passive acoustic mapping (PAM). However, PAM was found to be a highly useful tool in identifying successful targeting of the tumour and successful activation of the nanoparticles at the target site.

7.2 Future work

This work has established a novel ultrasound triggered platform for drug release at the nanoscale. There are many areas for development that would help in the translation of this work from the laboratory to the clinic. Future work includes development of the drug delivery system as well as more in depth testing.

Efficacy study in vivo would provide insight into the desired effect (rather than simply using cavitation or drug concentration as a marker). Tumour response to therapy should be assessed, in addition to drug delivery, to ensure that the delivered dose is sufficient to show a therapeutic outcome. This approach will require marker molecules to be substituted with a suitable drug for therapy. Correlating the occurrence or non-occurrence of tumour shrinkage following cavitation-mediated liposomal drug delivery with the presence or absence of cavitation activity at the same location using passive acoustic mapping would enable a more definitive demonstration of the value of real-time monitoring during drug delivery.

Whole organ targeted drug delivery may be possible using this cavitation dependent release platform. Enhancing targeting of particles would enable the use of an unfocused ultrasound field to instigate cavitation only in areas where cavitation nuclei were present. This development would expand the capability of this system to treat micro-metastatic tumour deposits where the certainty of the exact location of the tumour is low. A system using a diagnostic probe could then be developed to sweep over a whole organ while only causing cavitation where cavicatalytic nanoparticles were present, therefore only causing a triggered drug release in tumour areas, leaving healthy tissue intact.

Optimisation of cavicatalytic particle composition would improve *in vivo* cavitaiton responses. Testing of cavicatalytic properties of varying polymers and organic compounds with similar size and morphology is a logical extension to this work. Testing of effect of PEGylation on cavicatalytic properties would be highly beneficial. PEG modification may be able to extend the circulation time of NC or CNP particles such that accumulation via the EPR effect may be utilised. In addition, PEG modification would allow for further particle functionalisation.

Modifying the cavicatalytic particle - drug carrier interaction could result in improved drug release. By co-localising the drug carrier (liposome) with the effector agent (cavicat-

alytic nanoparticle), an improved likelihood of release may be achieved. There are several ways that this modification could be achieved, with two possibilities being: to tether the drug carrying liposome to the cavicatalytic particle using a PEG linker; or to further develop an encased system where the drug carrier also contains the cavicatalytic nanoparticle. The latter approach requires that the cavicatalytic nanoparticle is sufficiently small to be fully encapsulated.

Probing deeper into the mechanism for drug release would allow for more efficient optimisation of this drug delivery system. The use of high speed photography to capture cavitation and drug release events may yield a better understanding of the mechanical events occurring. In addition, encapsulated dyes could be used to model drug release. Using these techniques, studies could be conducted to determine the proximity of particles required for drug release. Further developing a shear stress model to simulate shear stresses at the liposome wall would greatly improve understanding of this system. A capillary model with moving sides could be developed to create shear stresses mimicking those potentially induced by cavitation events.

These future developments may be able to improve both understanding and impact of the work in this thesis. This novel ultrasound triggered platform for drug release at the nanoscale has only been demonstrated with a limited number and type of particles and drug carriers, and has potential to be explored in many ways. Any future work would add to the body of knowledge and ultimately move towards the larger goal of improved drug delivery for cancer therapy.

Bibliography

[1] Agarwal, A., Lvov, Y., Sawant, R., and Torchilin, V. Stable nanocolloids of poorly soluble drugs with high drug content prepared using the combination of sonication and layer-by-layer technology. *Journal of Controlled Release 128*, 3 (June 2008), 255–260.

[2] Alexis, F., Pridgen, E., Molnar, L. K., and Farokhzad, O. C. Factors affecting the clearance and biodistribution of polymeric nanoparticles. *Molecular Pharmaceutics 5*, 4 (Aug. 2008), 505–515.

[3] Aliabadi, H. M., Maranchuk, R., Kucharski, C., Mahdipoor, P., Hugh, J., and Uludag, H. Effective response of doxorubicin-sensitive and -resistant breast cancer cells to combinational siRNA therapy. *Journal of Controlled Release 172*, 1 (Aug. 2013).

[4] Apfel, R. E., and Holland, C. K. Gauging the likelihood of cavitation from short-pulse, low-duty cycle diagnostic ultrasound. *Ultrasound in Medicine and Biology 17*, 2 (1991), 179–185.

[5] Arora, M., Ohl, C. D., and Morch, K. A. Cavitation inception on microparticles: A self-propelled particle accelerator. *Physical Review Letters 92*, 17 (Apr. 2004).

[6] Arvanitis, C. D., Bazan-Peregrino, M., Rifai, B., Seymour, L. W., and Coussios, C. C. Cavitation-Enhanced extravasation for drug delivery. *Ultrasound in Medicine and Biology 37*, 11 (Nov. 2011), 1838–1852.

[7] Atchley, A. The blake threshold of a cavitation nucleus having a radius-dependent surface-tension. *Journal of the Acoustical Society of America 85*, 1 (Jan. 1989), 152–157.

[8] Atchley, A., and Prosperetti, A. The crevice model of bubble nucleation. *Journal of the Acoustical Society of America 86*, 3 (Sept. 1989), 1065–1084.

[9] Avanti Polar Lipids. 18:0 pe 1,2-distearoyl-sn-glycero-3-phosphoethanolamine. Available online.

[10] Avanti Polar Lipids. Dspe-peg(2000) amine 1,2-distearoyl-sn-glycero-3-phosphoethanolamine-n-[amino(polyethylene glycol)-2000] (ammonium salt). Available online.

[11] Avanti Polar Lipids. Hydro soy pc l-alpha-phosphatidylcholine, hydrogenated (soy). Available online.

[12] Avanti Polar Lipids. Lipids for liposome formation. Available online.

[13] Bader, K. B., Gruber, M. J., and Holland, C. K. Shaken and stirred: mechanisms of ultrasound-enhanced thrombolysis. *Ultrasound in Medicine and Biology 41*, 1 (Jan. 2015), 187–196.

[14] Bader, K. B., and Holland, C. K. Gauging the likelihood of stable cavitation from ultrasound contrast agents. *Physics in Medicine and Biology 58*, 1 (Jan. 2013), 127–144.

[15] Bae, Y. Drug targeting and tumor heterogeneity. *Journal of Controlled Release 133* (2009), 2–3.

[16] Bae, Y., Nishiyama, N., Fukushima, S., Koyama, H., Yasuhiro, M., and Kataoka, K. Preparation and biological characterization of polymeric micelle drug carriers with intracellular pH-triggered drug release property: Tumor permeability, controlled subcellular drug distribution, and enhanced in vivo antitumor efficacy. *Bioconjugate Chemistry 16*, 1 (Feb. 2005), 122–130.

[17] Barenholz, Y. Doxil - the first FDA-approved nano-drug: Lessons learned. *Journal of Controlled Release 160*, 2 (June 2012), 117–134.

[18] Bartholomew, C. H. Mechanisms of catalyst deactivation. *Applied Catalysis a-General 212*, 1-2 (Apr. 2001), 17–60.

[19] Bazan-Peregrino, M., Arvanitis, C. D., Rifai, B., Seymour, L. W., and Coussios, C. Ultrasound-induced cavitation enhances the delivery and therapeutic efficacy of an oncolytic virus in an in vitro model. *Journal of Controlled Release 157*, 2 (Jan. 2012), 235–242.

[20] Bazan-Peregrino, M., Rifai, B., Carlisle, R. C., Choi, J., Arvanitis, C. D., Seymour, L. W., and Coussios, C. C. Cavitation-enhanced delivery of a replicating oncolytic adenovirus to tumors using focused ultrasound. *Journal of Controlled Release 169*, 1-2 (July 2013), 40–47.

[21] Bazile, D., Prudhomme, C., Bassoullet, M., Marlard, M., Spenlehauer, G., and Veillard, M. Stealth me.peg-pla nanoparticles avoid uptake by the mononuclear phagocytes system. *Journal of Pharmaceutical Sciences 84*, 4 (Apr. 1995), 493–498.

[22] Bergers, G., and Benjamin, L. E. Tumorigenesis and the angiogenic switch. *Nature Reviews Cancer 3*, 6 (June 2003), 401–410.

[23] Binaschi, M., Bigioni, M., Cipollone, A., Rossi, C., Goso, C., Maggi, C. A., Capranico, G., and Animati, F. Anthracyclines: Selected new developments. *Current Medicinal Chemistry - Anti-Cancer Agents 1*, 2 (Aug. 2001), 113–130.

[24] Bouakaz, A., Versluis, M., and de Jong, N. High-speed optical observations of contrast agent destruction. *Ultrasound in Medicine and Biology 31*, 3 (Mar. 2005), 391–399.

[25] Braet, F., and Wisse, E. Structural and functional aspects of liver sinusoidal endothelial cell fenestrae: a review. *Comparative Hepatology 1* (Aug. 2002), 1.

[26] Brahmer, J. R., Tykodi, S. S., Chow, L. Q., Hwu, W.-J., Topalian, S. L., Hwu, P., Drake, C. G., Camacho, L. H., Kauh, J., Odunsi, K., Pitot, H. C., Hamid, O., Bhatia, S., Martins, R., Eaton, K., Chen, S., Salay, T. M., Alaparthy, S., Grosso, J. F., Korman, A. J., Parker, S. M., Agrawal, S., Goldberg, S. M., Pardoll, D. M., Gupta, A., and Wigginton, J. M. Safety and activity of antiPD-l1 antibody in patients with advanced cancer. *New England Journal of Medicine 366*, 26 (June 2012), 2455–2465.

[27] Brennen, C. E. *Cavitation and Bubble Dynamics*. No. 44 in Oxford Engineering Science Series. Oxford University Press, 1995.

[28] Brujan, E. A., Ikeda, T., and Matsumoto, Y. Jet formation and shock wave emission during collapse of ultrasound-induced cavitation bubbles and their role in the therapeutic applications of high-intensity focused ultrasound. *Physics in Medicine and Biology 50*, 20 (Oct. 2005), 4797–4809.

[29] Cabral, H., Matsumoto, Y., Mizuno, K., Chen, Q., Murakami, M., Kimura, M., Terada, Y., Kano, M. R., Miyazono, K., Uesaka, M., Nishiyama, N., and Kataoka, K. Accumulation of sub-100 nm polymeric micelles in poorly permeable tumours depends on size. *Nature Nanotechnology 6*, 12 (Dec. 2011), 815–823.

[30] Cancer Research UK. Lifetime risk of cancer, 2012. Available online.

[31] Carlisle, R., Seymour, L. W., and Coussios, C. C. Targeting of liposomes via PSGL1 for enhanced tumor accumulation. *Pharmaceutical Research 30*, 2 (Feb. 2013), 352–361.

[32] Caruso, F., and Mohwald, H. Preparation and characterization of ordered nanoparticle and polymer composite multilayers on colloids RID a-9587-2011. *Langmuir 15*, 23 (Nov. 1999), 8276–8281.

[33] Cedervall, T., Lynch, I., Lindman, S., Berggard, T., Thulin, E., Nilsson, H., Dawson, K. A., and Linse, S. Understanding the nanoparticle-protein corona using methods to quantify exchange rates and affinities of proteins for nanoparticles.

Proceedings of the National Academy of Sciences of the United States of America 104, 7 (Feb. 2007), 2050–2055.

[34] Chakravarty, P., Qian, W., El-Sayed, M. A., and Prausnitz, M. R. Delivery of molecules into cells using carbon nanoparticles activated by femtosecond laser pulses. *Nature Nanotechnology 5*, 8 (Aug. 2010), 607–611.

[35] Chames, P., Van Regenmortel, M., Weiss, E., and Baty, D. Therapeutic antibodies: successes, limitations and hopes for the future. *British Journal of Pharmacology 157*, 2 (May 2009), 220–233.

[36] Chen, W. S., Matula, T. J., Brayman, A. A., and Crum, L. A. A comparison of the fragmentation thresholds and inertial cavitation doses of different ultrasound contrast agents. *Journal of the Acoustical Society of America 113*, 1 (Jan. 2003), 643–651.

[37] Choi, H. S., Liu, W., Misra, P., Tanaka, E., Zimmer, J. P., Ipe, B. I., Bawendi, M. G., and Frangioni, J. V. Renal clearance of nanoparticles. *Nature biotechnology 25*, 10 (Oct. 2007), 1165–1170.

[38] Choi, J. J., Carlisle, R. C., Coviello, C., Seymour, L., and Coussios, C.-C. Non-invasive and real-time passive acoustic mapping of ultrasound-mediated drug delivery. *Physics in Medicine and Biology 59*, 17 (Sept. 2014), 4861.

[39] Church, C. C. Spontaneous homogeneous nucleation, inertial cavitation and the safety of diagnostic ultrasound. *Ultrasound in Medicine and Biology 28*, 10 (Oct. 2002), 1349–1364.

[40] Church, C. C. Frequency, pulse length, and the mechanical index. *Acoustics Research Letters Online 6*, 3 (2005), 162.

[41] Church, C. C., and Miller, M. W. The kinetics and mechanics of ultrasonically-induced cell lysis produced by non-trapped bubbles in a rotating culture tube. *Ultrasound in Medicine and Biology 9*, 4 (July 1983), 385–393.

[42] Cochran, M. C., Eisenbrey, J., Ouma, R. O., Soulen, M., and Wheatley, M. A. Doxorubicin and paclitaxel loaded microbubbles for ultrasound triggered drug delivery. *International Journal of Pharmaceutics 414*, 1-2 (July 2011), 161–170.

[43] Costigan, S. The toxicology of nanoparticles used in healthcare products. *Comittee on Human Medicines, MHRA* (2006).

[44] Coukell, A. J., and Spencer, C. M. Polyethylene glycol-liposomal doxorubicin - a review of its pharmacodynamic and pharmacokinetic properties, and therapeutic efficacy in the management of AIDS-related kaposi's sarcoma. *Drugs 53*, 3 (Mar. 1997), 520–538.

[45] Coussios, C.-C., Holland, C. K., Jakubowska, L., Huang, S.-L., MacDonald, R. C., Nagaraj, A., and McPherson, D. D. In vitro characterization of liposomes and Optison by acoustic scattering at 3.5 MHz. *Ultrasound in Medicine and Biology 30*, 2 (Feb. 2004), 181–190.

[46] Danhier, F., Feron, O., and Preat, V. To exploit the tumor microenvironment: Passive and active tumor targeting of nanocarriers for anti-cancer drug delivery. *Journal of Controlled Release 148*, 2 (Dec. 2010), 135–146.

[47] Datta, S., Coussios, C., Ammi, A. Y., Mast, T. D., de Courten-Myers, G. M., and Holland, C. K. Ultrasound-Enhanced thrombolysis using definity as a cavitation nucleation agent. *Ultrasound in Medicine and Biology 34*, 9 (Sept. 2008), 1421–1433.

[48] de Boer-Dennert, M., de Wit, R., Schmitz, P., Djontono, J., v Beurden, V., Stoter, G., and Verweij, J. Patient perceptions of the side-effects of chemotherapy: the influence of 5HT3 antagonists. *British Journal of Cancer 76*, 8 (Oct. 1997), 1055–1061.

[49] De Cock, L. J., De Koker, S., De Geest, B. G., Grooten, J., Vervaet, C., Remon, J. P., Sukhorukov, G. B., and Antipina, M. N. Polymeric multilayer capsules in drug delivery. *Angewandte Chemie-International Edition 49*, 39 (2010), 6954–6973.

[50] Dean, M., Fojo, T., and Bates, S. Tumour stem cells and drug resistance. *Nature Reviews Cancer 5*, 4 (Apr. 2005), 275–284.

[51] Decher, G., Hong, J., and Schmitt, J. Buildup of ultrathin multilayer films by a self-assembly process: III consecutively alternating adsorption of anionic and cationic polyelectrolytes on charged surfaces. *Thin Solid Films 210*, 1-2 (Apr. 1992), 831–835.

[52] Delon-Martin, C., Vogt, C., Chignier, E., Guers, C., Chapelon, J. Y., and Cathignol, D. Venous thrombosis generation by means of high-intensity focused ultrasound. *Ultrasound in Medicine and Biology 21*, 1 (1995), 113–119.

[53] Deng, C. X., Xu, Q. H., Apfel, R. E., and Holland, C. K. Inertial cavitation produced by pulsed ultrasound in controlled host media. *Journal of the Acoustical Society of America 100*, 2 (Aug. 1996), 1199–1208. WOS:A1996VB16600052.

[54] Desai, M. P., Labhasetwar, V., Amidon, G. L., and Levy, R. J. Gastrointestinal uptake of biodegradable microparticles: Effect of particle size. *Pharmaceutical Research 13*, 12 (Dec. 1996), 1838–1845.

[55] Desai, M. P., Labhasetwar, V., Walter, E., Levy, R. J., and Amidon, G. L. The mechanism of uptake of biodegradable microparticles in caco-2 cells is size dependent. *Pharmaceutical Research 14*, 11 (Nov. 1997), 1568–1573.

[56] Dobrovolskaia, M. A., Patri, A. K., Zheng, J., Clogston, J. D., Ayub, N., Aggarwal, P., Neun, B. W., Hall, J. B., and McNeil, S. E. Interaction of colloidal gold nanoparticles with human blood: effects on particle size and analysis of plasma protein binding profiles. *Nanomedicine-Nanotechnology Biology and Medicine 5*, 2 (June 2009), 106–117.

[57] Dromi, S., Frenkel, V., Luk, A., Traughber, B., Angstadt, M., Bur, M., Poff, J., Xie, J., Libutti, S. K., Li, K. C. P., and Wood, B. J. Pulsed-high intensity focused ultrasound and low temperature sensitive liposomes for enhanced targeted drug delivery and antitumor effect. *Clinical Cancer Research 13*, 9 (May 2007), 2722–2727.

[58] Ebeling, D., van den Ende, D., and Mugele, F. Electrostatic interaction forces in aqueous salt solutions of variable concentration and valency. *Nanotechnology 22*, 30 (July 2011).

[59] Erickson, H. P. Size and shape of protein molecules at the nanometer level determined by sedimentation, gel filtration, and electron microscopy. *Biological Procedures Online 11*, 1 (Dec. 2009), 32–51.

[60] Escoffre, J.-M., Mannaris, C., Geers, B., Novell, A., Lentacker, I., Averkiou, M., and Bouakaz, A. Doxorubicin liposome-loaded microbubbles for contrast imaging and ultrasound-triggered drug delivery. *IEEE transactions on ultrasonics, ferroelectrics, and frequency control 60*, 1 (Jan. 2013), 78–87.

[61] Etheridge, M. L., Campbell, S. A., Erdman, A. G., Haynes, C. L., Wolf, S. M., and McCullough, J. The big picture on nanomedicine: the state of investigational and approved nanomedicine products. *Nanomedicine-Nanotechnology Biology and Medicine 9*, 1 (Jan. 2013), 1–14.

[62] Evjen, T. J., Hagtvet, E., Moussatov, A., Rognvaldsson, S., Mestas, J.-L., Fowler, R. A., Lafon, C., and Nilssen, E. A. In vivo monitoring of liposomal release in tumours following ultrasound stimulation. *European Journal of Pharmaceutics and Biopharmaceutics 84*, 3 (Aug. 2013), 526–531.

[63] Evjen, T. J., Nilssen, E. A., Barnert, S., Schubert, R., Brandl, M., and Fossheim, S. L. Ultrasound-mediated destabilization and drug release from liposomes comprising dioleoylphosphatidylethanolamine. *European Journal of Pharmaceutical Sciences 42*, 4 (Mar. 2011), 380–386.

[64] Evjen, T. J., Nilssen, E. A., Rognvaldsson, S., Brandl, M., and Fossheim, S. L. Distearoylphosphatidylethanolamine-based liposomes for ultrasound-mediated drug delivery. *European Journal of Pharmaceutics and Biopharmaceutics 75*, 3 (Aug. 2010), 327–333.

[65] Fakhrullin, R. F., and Lvov, Y. M. Face-lifting and make-up for microorganisms: Layer-by-Layer polyelectrolyte nanocoating. *ACS Nano* (2012).

[66] Fletcher, J. I., Haber, M., Henderson, M. J., and Norris, M. D. ABC transporters in cancer: more than just drug efflux pumps. *Nature Reviews Cancer 10*, 2 (Feb. 2010), 147–156.

[67] Flynn, H. Cavitation dynamics 1: Mathematical formulation. *Journal of the Acoustical Society of America 57*, 6 (1975), 1379–1396.

[68] Flynn, H. G. Generation of transient cavities in liquids by microsecond pulses of ultrasound. *The Journal of the Acoustical Society of America 72*, 6 (Dec. 1982), 1926–1932.

[69] Food and Drug Administration. Guidance for industry and FDA staff: Information for manufacturers seeking marketing clearance of diagnostic ultrasound systems and transducers. Available online.

[70] Food and Drug Administration. Guidances - considering whether an FDA-regulated product involves the application of nanotechnology. Guidance for Industry: Considering Whether an FDA-Regulated Product Involves the Application of Nanotechnology. Available online.

[71] Food and Drug Administration. Draft guidance for industry: Safety of nanomaterials in cosmetic products, April 2012. Available online.

[72] Fowler, R. A., Fossheim, S. L., Mestas, J.-L., Ngo, J., Canet-Soulas, E., and Lafon, C. Non-invasive magnetic resonance imaging follow-up of sono-sensitive liposome tumor delivery and controlled release after high-intensity focused ultrasound. *Ultrasound in Medicine and Biology 39*, 12 (Dec. 2013), 2342–2350.

[73] Gabizon, A. Liposome circulation time and tumor targeting - implications for cancer-chemotherapy. *Advanced Drug Delivery Reviews 16*, 2-3 (Sept. 1995), 285–294.

[74] Gasselhuber, A., Dreher, M. R., Negussie, A., Wood, B. J., Rattay, F., and Haemmerich, D. Mathematical spatio-temporal model of drug delivery from low temperature sensitive liposomes during radiofrequency tumour ablation. *International Journal of Hyperthermia 26*, 5 (2010), 499–513.

[75] Gerweck, L., and Seetharaman, K. Cellular ph gradient in tumor versus normal tissue: Potential exploitation for the treatment of cancer. *Cancer Res 56* (1996), 1194–1198.

[76] Gillies, R., Raghunand, N., Karczmar, G., and Bhujwalla, Z. Mri of the tumor microenvironment. *Journal of Magnetic Resonance Imaging 16* (2002), 430–450.

[77] Goldenbogen, B., Brodersen, N., Gramatica, A., Loew, M., Liebscher, J., Herrmann, A., Egger, H., Budde, B., and Arbuzova, A. Reduction-sensitive liposomes from a multifunctional lipid conjugate and natural phospholipids: Reduction and release kinetics and cellular uptake. *Langmuir 27*, 17 (Sept. 2011), 10820–10829.

[78] Gradishar, W., Tjulandin, S., Davidson, N., Shaw, H., Desai, N., Bhar, P., Hawkins, M., and O'Shaughnessy, J. Phase III trial of nanoparticle albumin-bound paclitaxel compared with polyethylated castor oil-based paclitaxel in women with breast cancer. *Journal of Clinical Oncology 23*, 31 (Nov. 2005), 7794–7803.

[79] Graham, S. M., Carlisle, R., Choi, J. J., Stevenson, M., Shah, A. R., Myers, R. S., Fisher, K., Peregrino, M.-B., Seymour, L., and Coussios, C. C. Inertial cavitation to non-invasively trigger and monitor intratumoral release of drug from intravenously delivered liposomes. *Journal of Controlled Release 178* (Mar. 2014), 101–107.

[80] Graham, S. M., Myers, R. S., Choi, J., Bazan-Peregrino, M., Seymour, L., Carlisle, R., and Coussios, C. C. Use of micro- and nano-sized inertial cavitation nuclei to trigger and map drug release from cavitation-sensitive liposomes. *The Journal of the Acoustical Society of America 134*, 5 (Nov. 2013), 4050.

[81] Guo, X., Li, Q., Zhang, Z., Zhang, D., and Tu, J. Investigation on the inertial cavitation threshold and shell properties of commercialized ultrasound contrast agent microbubbles. *The Journal of the Acoustical Society of America 134*, 2 (Aug. 2013).

[82] Guttenberg, Z., Rathgeber, A., Keller, S., Radler, J. O., Wixforth, A., Kostur, M., Schindler, M., and Talkner, P. Flow profiling of a surface-acoustic-wave nanopump. *Physical Review E 70*, 5 (Nov. 2004).

[83] Gyongy, M., and Coussios, C. Passive cavitation mapping for localization and tracking of bubble dynamics. *The Journal of the Acoustical Society of America 128*, 4 (2010), EL175.

[84] Gyongy, M., and Coussios, C. Passive spatial mapping of inertial cavitation during HIFU exposure. *IEEE Transactions on Bio-Medical Engineering 57*, 1 (Jan. 2010), 48–56.

[85] Harrison, G. H., Balcerkubiczek, E. K., and Eddy, H. A. Potentiation of chemotherapy by low-level ultrasound. *International Journal of Radiation Biology 59*, 6 (June 1991), 1453–1466.

[86] Haworth, K. J., Mast, T. D., Radhakrishnan, K., Burgess, M. T., Kopechek, J. A., Huang, S.-L., McPherson, D. D., and Holland, C. K. Passive imaging with pulsed ultrasound insonations. *The Journal of the Acoustical Society of America 132*, 1 (July 2012), 544–553.

[87] Heath, J. K., White, S. J., Johnstone, C. N., Catimel, B., Simpson, R. J., Moritz, R. L., Tu, G. F., Ji, H., Whitehead, R. H., Groenen, L. C., Scott, A. M., Ritter, G., Cohen, L., Welt, S., Old, L. J., Nice, E. C., and Burgess, A. W. The human a33 antigen is a transmembrane glycoprotein and a novel member of the immunoglobulin superfamily. *Proceedings of the National Academy of Sciences of the United States of America 94*, 2 (Jan. 1997), 469–474.

[88] Heldin, CH Rubin, K. P. K. O. A. High interstitial fluid pressure - an obstacle in cancer therapy. *Nature Reviews Cancer 4* (2004), 806–813.

[89] Hill, C., Bamber, J., and ter Haar, G. *Physical Principles of Medical Ultrasonics*, second edition ed. Wiley, 2004.

[90] Hobbs, S. K., Monsky, W. L., Yuan, F., Roberts, W. G., Griffith, L., Torchilin, V. P., and Jain, R. K. Regulation of transport pathways in tumor vessels: Role of tumor type and microenvironment. *Proceedings of the National Academy of Sciences of the United States of America 95*, 8 (Apr. 1998), 4607–4612.

[91] Holland, C., and Apfel, R. An improved theory for the prediction of microcavitation thresholds. *IEEE Transactions on Ultrasonics Ferroelectrics and Frequency Control 36*, 2 (Mar. 1989), 204–208.

[92] Holland, C. K., Deng, C. X., Apfel, R. E., Alderman, J. L., Fernandez, L. A., and Taylor, K. J. Direct evidence of cavitation in vivo from diagnostic ultrasound. *Ultrasound in Medicine and Biology 22*, 7 (1996), 917–925.

[93] Howles, G. P., Bing, K. F., Qi, Y., Rosenzweig, S. J., Nightingale, K. R., and Johnson, G. A. Contrast enhanced in vivo magnetic resonance microscopy of the mouse brain enabled by noninvasive opening of the blood brain barrier with ultrasound. *Magnetic Resonance in Medicine 64*, 4 (Oct. 2010), 995–1004.

[94] Huang, S., McPherson, D. B., and MacDonald, R. C. A method to co-encapsulate gas and drugs in liposomes for ultrasound-controlled drug delivery. *Ultrasound in Medicine and Biology 34*, 8 (Aug. 2008), 1272–1280.

[95] Hynynen, K., Colucci, V., Chung, A., and Jolesz, F. Noninvasive arterial occlusion using MRI-guided focused ultrasound. *Ultrasound in Medicine and Biology 22*, 8 (1996), 1071–1077.

[96] Ibsen, S., Benchimol, M., Simberg, D., Schutt, C., Steiner, J., and Esener, S. A novel nested liposome drug delivery vehicle capable of ultrasound triggered release of its payload. *Journal of Controlled Release 155*, 3 (Nov. 2011), 358–366.

[97] Ibsen, S., Schutt, C. E., and Esener, S. Microbubble-mediated ultrasound therapy: a review of its potential in cancer treatment. *Drug Design Development and Therapy 7* (2013), 375–388.

[98] Iler, R. Multilayers of colloidal particles. *Journal of Colloid and Interface Science 21*, 6 (1966), 569–&.

[99] Instruments, M. Dynamic light scattering: An introduction in 30 minutes. Enigma Musiness Park Grovewood Road Malvern Worcestershire.

[100] Jensen, C., Ritchie, R., Gyongy, M., Collin, J., Leslie, T., and Coussios, C. Spatiotemporal monitoring of high-intensity focused ultrasound therapy with passive acoustic mapping. *Radiology 262* (2012), 252–261.

[101] Johnston, A. P. R., Cortez, C., Angelatos, A. S., and Caruso, F. Layer-by-layer engineered capsules and their applications RID a-9254-2011 RID a-9587-2011. *Current Opinion in Colloid and Interface Science 11*, 4 (Oct. 2006), 203–209.

[102] Johnston, A. P. R., Such, G. K., Ng, S. L., and Caruso, F. Challenges facing colloidal delivery systems: From synthesis to the clinic RID a-9254-2011 RID b-1157-2011 RID a-9587-2011. *Current Opinion in Colloid and Interface Science 16*, 3 (June 2011), 171–181.

[103] Kamphuis, M. M. J., Johnston, A. P. R., Such, G. K., Dam, H. H., Evans, R. A., Scott, A. M., Nice, E. C., Heath, J. K., and Caruso, F. Targeting of cancer cells using Click-Functionalized polymer capsules. *Journal of the American Chemical Society 132*, 45 (Nov. 2010), 15881–15883.

[104] Karanth, H., and Murthy, R. S. R. pH-sensitive liposomes - principle and application in cancer therapy. *Journal of Pharmacy and Pharmacology 59*, 4 (Apr. 2007), 469–483.

[105] Kastantin, M., Ananthanarayanan, B., Karmali, P., Ruoslahti, E., and Tirrell, M. Effect of the lipid chain melting transition on the stability of DSPE-PEG(2000) micelles. *Langmuir : the ACS journal of surfaces and colloids 25*, 13 (July 2009), 7279–7286.

[106] Kaufman, H. L., and Bines, S. D. OPTIM trial: a phase III trial of an oncolytic herpes virus encoding GM-CSF for unresectable stage III or IV melanoma. *Future Oncology 6*, 6 (June 2010), 941–949.

[107] Kim, D., Lee, E. S., Park, K., Kwon, I. C., and Bae, Y. H. Doxorubicin loaded pH-sensitive micelle: Antitumoral efficacy against ovarian A2780/DOX(R) tumor. *Pharmaceutical Research 25*, 9 (Sept. 2008), 2074–2082.

[108] Kirpotin, D. B., Drummond, D. C., Shao, Y., Shalaby, M. R., Hong, K., Nielsen, U. B., Marks, J. D., Benz, C. C., and Park, J. W. Antibody targeting of Long-Circulating lipidic nanoparticles does not increase tumor localization but does increase internalization in animal models. *Cancer Research 66*, 13 (July 2006), 6732 –6740.

[109] Kopechek, J. A., Abruzzo, T. M., Wang, B., Chrzanowski, S. M., Smith, D. A. B., Kee, P. H., Huang, S., Collier, J. H., McPherson, D. D., and Holland, C. K. Ultrasound-mediated release of hydrophilic and lipophilic agents from echogenic liposomes. *Journal of Ultrasound in Medicine 27*, 11 (Nov. 2008), 1597–1606.

[110] Kopechek, Jonathan A.; Haworth, K. J. R. K. H. S.-L. K. M. E. M. D. D. H. C. K. The impact of bubbles on measurement of drug release from echogenic liposomes. *Ultrasonics Sonochemistry 20* (2013), 1121–1130.

[111] Kreft, O., Georgieva, R., Baumler, H., Steup, M., Muller-Rober, B., Sukhorukov, G., and Mohwald, H. Red blood cell templated polyelectrolyte capsules: A novel vehicle for the stable encapsulation of DNA and proteins. *Macromolecular Rapid Communications 27*, 6 (Mar. 2006), 435–440.

[112] Kyriakou, Z., Ignasi Corral-Baques, M., Amat, A., and Coussios, C.-C. Hifu-induced cavitation and heating in ex vivo porcine subcutaneous fat. *Ultrasound in Medicine and Biology 37*, 4 (Apr. 2011), 568–579.

[113] Lafon, C., Somaglino, L., Bouchoux, G., Chesnais, S., Mestas, J., Matias, A., and Chapelon, J. Developpement d'un dispositif experimental ultrasonore pour le largage cible et controle d'une chimiotherapie encapsulee. *IRBM 30*, 4 (Sept. 2009), 171–173.

[114] Laginha, K., Verwoert, S., Charrois, G., and Allen, T. Determination of doxorubicin levels in whole tumor and tumor nuclei inmurine breast cancer tumors. *Clinical Cancer Research 11* (2005), 6944–6949.

[115] Larina, I. V., Evers, B. M., Ashitkov, T. V., Bartels, C., Larin, K. V., and Esenaliev, R. O. Enhancement of drug delivery in tumors by using interaction of nanoparticles with ultrasound radiation. *Technology in Cancer Research and Treatment 4*, 2 (Apr. 2005), 217–226.

[116] Larina, I. V., Evers, B. M., and Esenaliev, R. O. Optimal drug and gene delivery in cancer cells by ultrasound-induced cavitation. *Anticancer Research 25*, 1A (Feb. 2005), 149–156.

[117] Leighton, T. G. *The Acoustic Bubble*. Elsevier, 1994.

[118] Leu, A., Berk, D., Lymboussaki, A., Alitalo, K., and Jain, R. Absence of functional lymphatics within a murine sarcoma: A molecular and functional evaluation. *Cancer Research 60* (2000), 4324–4327.

[119] Liberman, A., Martinez, H. P., Ta, C. N., Barback, C. V., Mattrey, R. F., Kono, Y., Blair, S. L., Trogler, W. C., Kummel, A. C., and Wu, Z. Hollow silica and silica-boron nano/microparticles for contrast-enhanced ultrasound to detect small tumors. *Biomaterials 33*, 20 (July 2012), 5124–5129.

[120] Longmire, M., Choyke, P. L., and Kobayashi, H. Clearance properties of nano-sized particles and molecules as imaging agents: Considerations and caveats. *Nanomedicine (London, England) 3*, 5 (Oct. 2008), 703–717.

[121] Longva, K. E., Pedersen, N. M., Haslekas, C., Stang, E., and Madshus, I. H. Herceptin-induced inhibition of ErbB2 signaling involves reduced phosphorylation of akt but not endocytic down-regulation of ErbB2. *International Journal of Cancer 116*, 3 (Sept. 2005), 359–367.

[122] Lv, H., Lin, Q., Zhang, K., Yu, K., Yao, T., Zhang, X., Zhang, J., and Yang, B. Facile fabrication of monodisperse polymer hollow spheres. *Langmuir 24*, 23 (Dec. 2008), 13736–13741.

[123] Ma, P., and Mumper, R. J. Anthracycline nano-delivery systems to overcome multiple drug resistance: A comprehensive review. *Nano Today 8*, 3 (June 2013), 313–331.

[124] Maeda, H., Wu, J., Sawa, T., Matsumura, Y., and Hori, K. Tumor vascular permeability and the EPR effect in macromolecular therapeutics: a review. *Journal of Controlled Release 65*, 1-2 (Mar. 2000), 271–284.

[125] Mannaris, C., Efthymiou, E., Meyre, M.-E., and Averkiou, M. A. In vitro localized release of thermosensitive liposomes with ultrasound-induced hyperthermia. *Ultrasound in Medicine and Biology 39*, 11 (Nov. 2013), 2011–2020.

[126] Marmottant, P., van der Meer, S., Emmer, M., Versluis, M., de Jong, N., Hilgenfeldt, S., and Lohse, D. A model for large amplitude oscillations of coated bubbles accounting for buckling and rupture. *Journal of the Acoustical Society of America 118*, 6 (Dec. 2005), 3499–3505.

[127] McGill, S. L., Cuylear, C. L., Adolphi, N. L., Osinski, M., and Smyth, H. D. C. Magnetically responsive nanoparticles for drug delivery applications using low magnetic field strengths. *IEEE Transactions on Nanobioscience 8*, 1 (Mar. 2009), 33–42.

[128] Mestas, J.-L., Fowler, R. A., Evjen, T. J., Somaglino, L., Moussatov, A., Ngo, J., Chesnais, S., Rognvaldsson, S., Fossheim, S. L., Nilssen, E. A., and Lafon, C. Therapeutic efficacy of the combination of doxorubicin-loaded liposomes with inertial cavitation generated by confocal ultrasound in AT2 dunning rat tumour model. *Journal of Drug Targeting 22*, 8 (Apr. 2014), 688–697.

[129] Miller, D. A review of the ultrasonic bioeffects of microsonation, gas-body activation, and related cavitation-like phenomena. *Ultrasound in Medicine and Biology 13*, 8 (Aug. 1987), 443–470.

[130] Miller, D. L., Dou, C., and Song, J. Lithotripter shockwave-induced enhancement of mouse melanoma lung metastasis: dependence on cavitation nucleation. *Journal of Endourology / Endourological Society 18*, 9 (Nov. 2004), 925–929.

[131] Miller, D. L., and Song, J. M. Tumor growth reduction and DNA transfer by cavitation-enhanced high-intensity focused ultrasound in vivo. *Ultrasound in Medicine and Biology 29*, 6 (June 2003), 887–893.

[132] Minotti, G., Menna, P., Salvatorelli, E., Cairo, G., and Gianni, L. Anthracyclines: Molecular advances and pharmacologic developments in antitumor activity and cardiotoxicity. *Pharmacological Reviews 56*, 2 (June 2004), 185–229.

[133] Moghimi, S. M., Hunter, A. C., and Murray, J. C. Long-circulating and target-specific nanoparticles: Theory to practice. *Pharmacological Reviews 53*, 2 (June 2001), 283–318.

[134] Mylonopoulou, E., Arvanitis, C. D., Bazan-Peregrino, M., Arora, M., and Coussios, C. C. Ultrasonic activation of thermally sensitive liposomes. In *9th International Symposium on Therapeutic Ultrasound*, K. Hynynen and J. Souquet, Eds., vol. 1215. Amer Inst Physics, Melville, 2010, pp. 83–87.

[135] Mylonopoulou, E., BazÃ¡n-Peregrino, M., Arvanitis, C. D., and Coussios, C. C. A non-exothermic cell-embedding tissue-mimicking material for studies of ultrasound-induced hyperthermia and drug release. *International Journal of Hyperthermia 29*, 2 (Mar. 2013), 133–144.

[136] Nandlall, S. D., Jackson, E., and Coussios, C. Real-Time passive acoustic monitoring of HIFU-Induced tissue damage. *Ultrasound in Medicine and Biology 37*, 6 (June 2011), 922–934.

[137] Netti, P. A., Hamberg, L. M., Babich, J. W., Kierstead, D., Graham, W., Hunter, G. J., Wolf, G. L., Fischman, A., Boucher, Y., and Jain, R. K. Enhancement of fluid filtration across tumor vessels: Implication for delivery of macromolecules. *Proceedings of the National Academy of Sciences 96* (1999), 3137–3142.

[138] Nishiyama, N., Okazaki, S., Cabral, H., Miyamoto, M., Kato, Y., Sugiyama, Y., Nishio, K., Matsumura, Y., and Kataoka, K. Novel cisplatin-

incorporated polymeric micelles can eradicate solid tumors in mice. *Cancer Research 63*, 24 (Dec. 2003), 8977–8983.

[139] Northfelt, D., Dezube, B., Thommes, J., Miller, B., Fischl, M., Friedman-Kien, A., Kaplan, L., Du Mond, C., Mamelok, R., and Henry, D. Pegylated-liposomal doxorubicin versus doxorubicin, bleomycin, and vincristine in the treatment of AIDS-related kaposi's sarcoma: Results of a randomized phase III clinical trial. *Journal of Clinical Oncology 16*, 7 (July 1998), 2445–2451.

[140] Oxford University Press. Oxford english dictionary, 2014. Available online.

[141] Ozpolat, B., Sood, A. K., and Lopez-Berestein, G. Nanomedicine based approaches for the delivery of siRNA in cancer. *Journal of Internal Medicine 267*, 1 (Jan. 2010), 44–53.

[142] Parato, K. A., Senger, D., Forsyth, P. a. J., and Bell, J. C. Recent progress in the battle between oncolytic viruses and tumours. *Nature Reviews Cancer 5*, 12 (Dec. 2005), 965–976.

[143] Peer, D., Karp, J. M., Hong, S., Farokhzad, O. C., Margalit, R., and Langer, R. Nanocarriers as an emerging platform for cancer therapy. *Nature Nanotechnology 2*, 12 (Dec. 2007), 751–760.

[144] Peiris, P. M., Bauer, L., Toy, R., Tran, E., Pansky, J., Doolittle, E., Schmidt, E., Hayden, E., Mayer, A., Keri, R. A., Griswold, M. A., and Karathanasis, E. Enhanced delivery of chemotherapy to tumors using a multicomponent nanochain with Radio-Frequency-Tunable drug release. *ACS Nano 6*, 5 (May 2012), 4157–4168.

[145] Pernodet, N., Maaloum, M., and Tinland, B. Pore size of agarose gels by atomic force microscopy. *Electrophoresis 18*, 1 (Jan. 1997), 55–58.

[146] Poon, Z., Chang, D., Zhao, X., and Hammond, P. T. Layer-by-layer nanoparticles with a pH-Sheddable layer for in vivo targeting of tumor hypoxia. *ACS Nano 5*, 6 (June 2011), 4284–4292.

[147] Potocnik, J. Commission recommendation of 18 October 2011 on the definition of nanomaterial. *Official Journal of the European Union* (20 October 2011).

[148] Prokop, A. F., Soltani, A., and Roy, R. A. Cavitational mechanisms in Ultrasound-Accelerated fibrinolysis. *Ultrasound in Medicine and Biology 33*, 6 (June 2007), 924–933.

[149] Radhakrishnan, K., Bader, K. B., Haworth, K. J., Kopechek, J. A., Raymond, J. L., Huang, S.-L., McPherson, D. D., and Holland, C. K. Relationship between cavitation and loss of echogenicity from ultrasound contrast agents. *Physics in medicine and biology 58*, 18 (Sept. 2013).

[150] Rapoport, N., Gao, Z., and Kennedy, A. Multifunctional nanoparticles for combining ultrasonic tumor imaging and targeted chemotherapy. *Journal of the National Cancer Institute 99*, 14 (July 2007), 1095–1106.

[151] Ross, J. S., and Fletcher, J. A. The HER-2/neu oncogene in breast cancer: Prognostic factor, predictive factor, and target for therapy. *Stem Cells 16*, 6 (1998), 413–428.

[152] Ross, J. S., Schenkein, D. P., Pietrusko, R., Rolfe, M., Linette, G. P., Stec, J., Stagliano, N. E., Ginsburg, G. S., Symmans, W. F., Pusztai, L., and Hortobagyi, G. N. Targeted therapies for cancer 2004. *American Journal of Clinical Pathology 122*, 4 (Oct. 2004), 598 –609.

[153] Roy, R. A., Madanshetty, S. I., and Apfel, R. E. An acoustic backscattering technique for the detection of transient cavitation produced by microsecond pulses of ultrasound. *The Journal of the Acoustical Society of America 87*, 6 (June 1990), 2451–2458.

[154] Russell, W.M.S. Burch, R. *The Principles of Humane Experimental Technique*. Wheathampstead: Universities Federation for Animal Welfare, 1959. Reprinted 1992.

[155] Sarkar, K., Katiyar, A., and Jain, P. Growth and dissolution of an encapsulated contrast microbubble: Effects. *Ultrasound in Medicine and Biology 35*, 8 (Aug. 2009), 1385–1396.

[156] Schlicher, R. K. Radhakrishna, H. T. T. P. A. R. P. Z. V. P. M. R. Mechanism of intracellular delivery by acoustic cavitation. *Ultrasound in Medicine and Biology 32*, 6 (June 2006), 915–924.

[157] Schlicher, Robyn K. Hutcheson, J. D. R. H. A. R. P. P. M. R. Changes in cell morphology due to plasma membrane wounding by acoustic cavitation. *Ultrasound in Medicine and Biology 36*, 4 (Apr. 2010), 677–692.

[158] Schneider, G., and Decher, G. Functional core/shell nanoparticles via layer-by-layer assembly. investigation of the experimental parameters for controlling particle aggregation and for enhancing dispersion stability. *Langmuir 24*, 5 (Mar. 2008), 1778–1789.

[159] Schroeder, A., Goldberg, M. S., Kastrup, C., Wang, Y., Jiang, S., Joseph, B. J., Levins, C. G., Kannan, S. T., Langer, R., and Anderson, D. G. Remotely activated protein-producing nanoparticles. *Nano Letters 12*, 6 (June 2012), 2685–2689.

[160] Seddon, J. R. T., Zandvliet, H. J. W., and Lohse, D. Knudsen gas provides nanobubble stability. *Physical Review Letters 107*, 11 (Sept. 2011).

[161] Seynhaeve, A. L. B., Dicheva, B. M., Hoving, S., Koning, G. A., and Ten Hagen, T. L. M. Intact doxil is taken up intracellularly and released doxorubicin sequesters in the lysosome: Evaluated by in vitro/in vivo live cell imaging. *Journal of controlled release 172*, 1 (Sept. 2013).

[162] Shaffer, S. A., Baker-Lee, C., Kennedy, J., Lai, M. S., de Vries, P., Buhler, K., and Singer, J. W. In vitro and in vivo metabolism of paclitaxel poliglumex: identification of metabolites and active proteases. *Cancer Chemotherapy and Pharmacology 59*, 4 (Mar. 2007), 537–548.

[163] Shaw, G. J., Meunier, J. M., Huang, S.-L., Lindsell, C. J., McPherson, D. D., and Holland, C. K. Ultrasound-enhanced thrombolysis with tPA-loaded echogenic liposomes. *Thrombosis research 124*, 3 (July 2009), 306–310.

[164] Shimizu, S. Chapter 32 - routes of administration. In *The Laboratory Mouse*, P. H. J. H. G. Bullock, Ed. Academic Press, London, 2004, pp. 527–542.

[165] Sivendran, S., Pan, M., Kaufman, H. L., and Saenger, Y. Herpes simplex virus oncolytic vaccine therapy in melanoma. *Expert Opinion on Biological Therapy 10*, 7 (July 2010), 1145–1153.

[166] Smith, D. A. B., Porter, T. M., Martinez, J., Huang, S., MacDonald, R. C., McPherson, D. D., and Holland, C. K. Destruction thresholds of echogenic liposomes with clinical diagnostic ultrasound. *Ultrasound in Medicine and Biology 33*, 5 (May 2007), 797–809.

[167] Society, T. B. M. U. Statement on the safe use, and potential hazards of diagnostic ultrasound, 2012. Available online.

[168] Somaglino, L., Bouchoux, G., Mestas, J.-L., and Lafon, C. Validation of an acoustic cavitation dose with hydroxyl radical production generated by inertial cavitation in pulsed mode: Application to in vitro drug release from liposomes. *Ultrasonics Sonochemistry 18*, 2 (Mar. 2011), 577–588.

[169] Sorace, A. G., Warram, J. M., Umphrey, H., and Hoyt, K. Microbubble-mediated ultrasonic techniques for improved chemotherapeutic delivery in cancer. *Journal of Drug Targeting 20*, 1 (Jan. 2012), 43–54.

[170] Starnes, C. Coley toxins in perspective. *Nature 357*, 6373 (May 1992), 11–12.

[171] Stephens, D., Ming Lu, X.and Proulx, T., Walters, W., Dayton, P., Tartis, M., Kruse, D., Lum, A., Kitano, T., Stieger, S., and Ferrara, K. Multi-frequency array development for drug delivery therapies: characterization and first use of a triple row ultrasound probe. *2006 IEEE Ultrasonics Symposium (IEEE Cat. No.06CH37777)* (2006), 4 pp.

[172] Strebhardt, K., and Ullrich, A. Paul ehrlich's magic bullet concept: 100 years of progress. *Nature Reviews Cancer 8* (2008), 473–480.

[173] Suchkova, V., Siddiqi, F. N., Carstensen, E. L., Dalecki, D., Child, S., and Francis, C. W. Enhancement of fibrinolysis with 40-kHz ultrasound. *Circulation 98*, 10 (Sept. 1998), 1030–1035.

[174] Sutton, J. T., Haworth, K. J., Pyne-Geithman, G., and Holland, C. K. Ultrasound-mediated drug delivery for cardiovascular disease. *Expert Opinion on Drug Delivery 10*, 5 (May 2013), 573–592.

[175] Tailor, T., Hanna, G., Yarmolenko, P., Dreher, M., Betof, A., Nixon, A., Spasojevic, I., and Dewhirst, M. Effect of pazopanib on tumor microenvironment and liposome delivery. *Molecular Cancer Therapeutics 9* (2010), 1798–1808.

[176] ter Haar, G., and Coussios, C. High intensity focused ultrasound: Physical principles and devices. *International Journal of Hyperthermia 23*, 2 (Jan. 2007), 89–104.

[177] Thomas, K., McGrath, K., Taylor, M., Young, I., Herrington, R., and Schiff, P. Effect of virucidal heat treatment on proteins in human factor VIII concentrates. *Transfusion 28*, 1 (1988), 8–13.

[178] Trédan, O., Galmarini, C., Patel, K., and Tannock, I. Drug resistance and the solid tumor microenvironment. *J Natl Cancer Inst 99* (2007), 1441–1454.

[179] Tu, Juan; Guan, J. Q. Y. M. T. J. Estimating the shell parameters of sonovue microbubbles using light scattering. *Journal of the Acoustical Society of America 126* (Dec 2009), 2954–2962.

[180] Uster, P., Working, P., and Vaage, J. Pegylated liposomal doxorubicin (doxil (r), caelyx (r)) distribution in tumour models observed with confocal laser scanning microscopy. *International journal of pharmaceutics 162* (1998), 77–86.

[181] Vaage, J., Donovan, D., Uster, P., and Working, P. Tumour uptake of doxorubicin in polyethylene glycol-coated liposomes and therapeutic effect against a xenografted human pancreatic carcinoma. *British Journal of Cancer 75*, 4 (1997), 482–486.

[182] Vaupel, P., Kallinowski, F., and Okunieff, P. Blood flow, oxygen and nutrient supply, and metabolic microenvironment of human tumors: a review. *Cancer Research 49*, 23 (Dec. 1989), 6449–6465.

[183] von Maltzahn, G., Park, J., Lin, K. Y., Singh, N., Schwoppe, C., Mesters, R., Berdel, W. E., Ruoslahti, E., Sailor, M. J., and Bhatia, S. N. Nanoparticles that communicate in vivo to amplify tumour targeting. *Nature Materials advance online publication* (June 2011).

[184] Vonhoff, D., Layard, M., Basa, P., Davis, H., Vonhoff, A., Rozencweig, M., and Muggia, F. Risk-factors for doxorubicin-induced congestive heart-failure. *Annals of Internal Medicine 91*, 5 (1979), 710–717.

[185] Wagstaffe, S. J., Arora, M., Coussios, C.-C., and Schiffter, H. A. Sonosensitive nanoparticle formulations for cavitation-mediated ultrasonic enhancement of local drug delivery. *MRS Online Proceedings Library 1316* (2011), null–null.

[186] Walkey, C. D., Olsen, J. B., Guo, H., Emili, A., and Chan, W. C. W. Nanoparticle size and surface chemistry determine serum protein adsorption and macrophage uptake. *Journal of the American Chemical Society 134*, 4 (Feb. 2012), 2139–2147.

[187] Walton, A., and Reynolds, G. Sonoluminescence. *Advances in Physics 33*, 6 (1984), 595–660.

[188] Wang, Y., and Caruso, F. Mesoporous silica spheres as supports for enzyme immobilization and encapsulation RID c-6394-2008 RID a-9587-2011. *Chemistry of Materials 17*, 5 (Mar. 2005), 953–961.

[189] Webb, I. R. *Acoustic Cavitation in Tissue during Ultrasound-Induced Heating*. PhD thesis, University of Oxford, 2010.

[190] Webb, I. R., Payne, S. J., and Coussios, C.-C. The effect of temperature and viscoelasticity on cavitation dynamics during ultrasonic ablation. *The Journal of the Acoustical Society of America 130*, 5 (Nov. 2011), 3458–3466.

[191] Westwood, M., Joore, M., Grutters, J., Redekop, K., Armstrong, N., Lee, K., Gloy, V., Raatz, H., Misso, K., Severens, J., and Kleijnen, J. Contrast-enhanced ultrasound using SonoVue® (sulphur hexafluoride microbubbles) compared with contrast-enhanced computed tomography and contrast-enhanced magnetic resonance imaging for the characterisation of focal liver lesions and detection of liver metastases: a systematic review and cost-effectiveness analysis. *Health Technology Assessment 17*, 16 (Apr. 2013).

[192] Yu, Yuan; von Gottberg, F. Coagulation kinetics of surface modified pigment particles. In *NIP18: International Conference on Digital Printing Technologies* (2002), pp. 383–387.

[193] Zhang, P., and Porter, T. An in vitro study of a phase-shift nanoemulsion: A potential nucleation agent for bubble-enhanced hifu tumor ablation. *Ultrasound in Medicine and Biology 36*, 11 (Nov. 2010), 1856–1866.

[194] Zhang, X., Harrison, G. H., and Balcer-Kubiczek, E. K. Exposimetry of unfocused pulsed ultrasound. *IEEE Transactions on Ultrasonics, Ferroelectrics and Frequency Control 41*, 1 (Jan. 1994), 80–83.

[195] Zhou, Y., Yang, K., Cui, J., Ye, J. Y., and Deng, C. X. Controlled permeation of cell membrane by single bubble acoustic cavitation. *Journal of Controlled Release 157*, 1 (Jan. 2012), 103–111.

Appendix A

Preliminary study

A.1 Development of cavicatalytic nanoparticles

Based on the intended therapeutic application of these cavicatalytic particles, desired properties include: i) ease of manufacture at the nanoscale, whereby particles can be reproducibly manufactured in monodisperse solutions of particles smaller than 500 nm in diameter such that they may be able to take advantage of the EPR effect; ii) ability to instigate cavitation, preferably inertial cavitation only and ideally over prolonged periods of time; and iii) biocompatibility for potential use *in vivo*. In the sections below, these concepts are explored to develop cavicatalytic nanoparticles.

A.1.1 Non-cavicatalytic nanoparticles

A series of mesoporous silica particles were tested for cavicatalytic properties. Many of them showed no substantial increase in cavitation energy above water background. The samples tested which showed no cavitation response included: 200 nm silica particles with 4 nm pore size (748161-5G); mesostructured silica with 2.31 cm^3/g pore volume (560979-10G); 200 nm propylamine functionalized silica with 4 nm pore size (749265-5G); 200 nm propylcarboxylic acid functionalized silica, FITC labelled, with 4 nm pore size (749664-5G); and 200 nm propylcarboxylic acid functionalized silica with 4 nm pore size (749710-1G), all purchased from Sigma. These particles were tested using an insonation frequency of 0.5 MHz, 0.5 Hz PRF at a range of pressures up to 1.5 MPa. No response was observed and

it was concluded that the pore size of these particles (4 nm) was too small to entrap gas capable of responding to the ultrasound used in the study.

A.1.2 Cavicatalytic micro-carbon particles

Initially, mesoporous carbon (699632, Sigma) micro-particles were tested as candidates for cavitation nuclei. Freeze drying was carried out in order to dry particle solutions while maintaining a similar size distribution. Before freeze drying, particle solutions were mixed in a 1:2 ratio with 10% trehalose (D-(+)-Trehalose dihydrate, T9531-100G, Sigma). Trehalose was used as a cryoprotectant and lyoprotectant, stabilising the particles during freezing and resuspension. Samples were loaded into glass vials with rubber stoppers and placed in a freeze dryer (VirTis Advantage Plus, SP Industries) following the protocol in Table A.1. Freeze dried particles were resuspended in DI water (220 nm filtered) with the aim of entrapping air on the surface of the particles during re-suspension. Particles were freeze dried following the method outlined in Table A.1.

Table A.1: *Freeze drying protocol*

Stage	Shelf Temperature Set Point (°C)	Time per step (min)	Accumulative time (min)	Vacuum (mTorr)
Freeze	20	5	5	
	5	15	20	
	5	10	30	
	-5	10	40	
	-5	10	50	
	-40	35	85	
	-40	60	145	
Primary Drying	-40	5	150	100
	-20	40	190	100
	-20	2160	2350	100
	20	160	2510	100
Secondary Drying	20	720	3230	100

Carbon particles were prepared in three size ranges at a concentration of 1mg/mL by either A) shaking by hand to resuspend, B) shaking by hand followed by 10 min sonicator bath, or C) shaking by hand, followed by 10 min sonicator bath, followed by 5 x 30 second

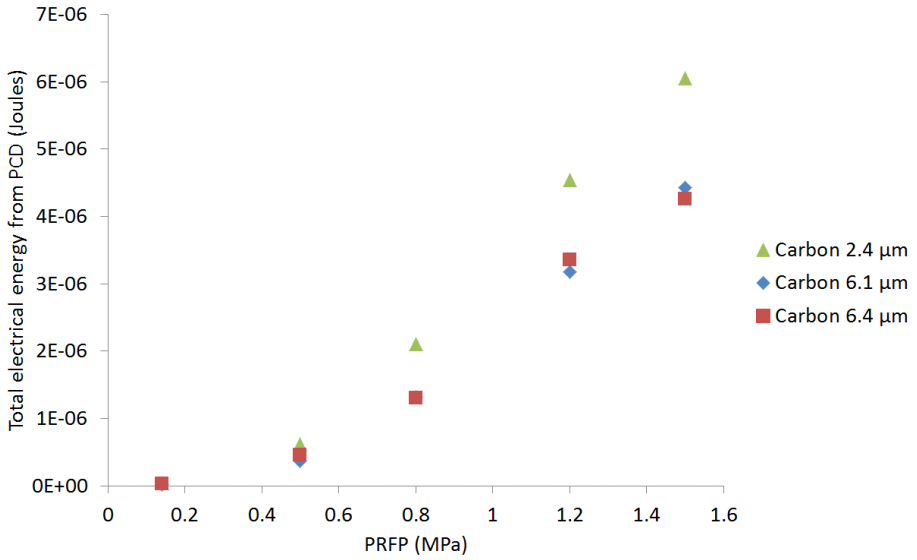

Figure A.1: *Cavitation energy received from the PCD for carbon particles of diameter 6.1 µm, 6.4 µm, and 2.4 µm. Particles were insonated at 0.5 MHz driving frequency, 0.5 Hz PRF, 5% DC over a pressure range 0.14 MPa to 1.5 MPa for 30 seconds each. N=1.*

sonic probe at 15 Watts (22.5 kHz, Microson™ Ultrasonic Cell Disrupter, Misonix). Samples were freeze dried in trehalose to a final carbon concentration of 0.3 mg/mL using the protocol in Table A.1. Size before freeze drying (by DLS) and after freeze drying (by master sizer) is shown in Table A.2. Freeze dried particles were resuspended in DI water to a concentration of 0.2 mg/mL before cavitation testing in the static chamber.

Table A.2: *Carbon particle size before freeze drying (FD) by DLS, and after FD by Master Sizer. N=1.*

Sample	Production method	Before FD (nm)	After FD (nm)
A	Shake	8915	6092
B	Shake + sonic bath	5484	6472
C	Shake + sonic bath + sonic probe	398.6	2361

A.1.3 Cavicatalytic nano-carbon particles

Once it was established that carbon particles were cavicatalytic at the micro-scale, development started to produce similar particles at the nano-scale. During development of the manufacturing method for carbon nanoparticles (CNPs), particles of various sizes and cavitation responses were produced. The methods used during development are shown diagrammatically in Figure A.2 indicating both the size of the particles produced, and whether

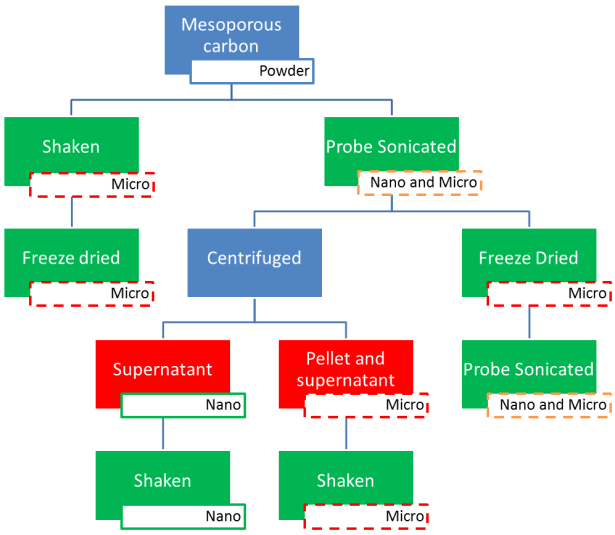

Figure A.2: *Carbon nanoparticle production process. Particles were sized and tested for their cavicatalytic behaviour. Green boxes (large) represent particles which showed cavicatalytic behaviours. Red boxes (large) represent particles which showed no cavicatalytic behaviour. Particles were characterised as either micro-sized (red, dashed), nano-sized (green) or as mixed populations (orange dashed) as indicated in the smaller white-filled boxes. Sonication = 5 × 30 seconds at 22 kHz, 15 Watts; Shaken = hand shaken vigorously for 10 seconds; Freeze drying was performed using the protocol given in Table A.1; and Supernatant = leaving 10 mL pellet + solution.*

or not they were cavicatalytic. The particles were deemed nano-sized as defined in Section 2.3.1. In this experiment, particles were deemed to be cavicatalytic if the power of cavitation received by the PCD during ultrasound exposure (0.5 MHz, 5% DC, 0.5 Hz PRF) was at least 10 dB higher than that of water exposed to ultrasound using the same conditions.

Figure A.2 illustrates key features necessary to convey cavicatalytic properties to a particle. Firstly, mesoporous carbon particles resuspended from a dry powder, with or without subsequent freeze drying, were cavicatalytic. Sonication was able to achieve a nano subpopulation of particles, and the mixture of micro- and nano-sized particles was also cavicatalytic. Centrifugation was successfully used to size-separate the particle solution, however the process of centrifugation also removed the cavicatalytic properties (independent of the size population tested). Shaking the suspension post-sonication was able to restore the cavitation response to both micro- and nano-particle populations. Based on this exploratory study, CNPs were developed to be both nano-sized and cavicatalytic.

A.1.3.1 Effect of surface area variation

During development, three particle populations were prepared with a size range 2.4 - 6.4 μm. At the same weight concentration, smaller particles (2.4 μm diameter) had a stronger cavitation signal than the larger particles (6.1 - 6.4 μm diameter) shown in Figure A.1. This may be the result of the increased available surface area on which gas bubbles are able to stabilize accounting for the increase in energy associated with cavitation. As the three populations were prepared using the same weight concentration of carbon, the only factor that is different between the groups is the size of the particles, and therefore number of particles and total surface area. As the size decreases, the number and surface area of the particles increases. Assuming the mass is the same in each sample (Equation A.1), and the shape of the particle remains the same (Equation A.2), and it is only the size of the particle that changes, the 2.4 μm particles have a surface area 2.67 times greater than that of the 6.4 μm particles.

$$n_1 \times \frac{4}{3}\pi r_1^3 \times \rho = n_2 \times \frac{4}{3}\pi r_2^3 \times \rho \tag{A.1}$$

$$\frac{SA_1}{SA_2} = \frac{n_1 \times 4\pi r_1^2}{n_2 \times 4\pi r_2^2} \tag{A.2}$$

No appreciable change in cavitation response over the pressure range 0.14 MPa to 0.8 MPa was observed indicating that the size of the gas nuclei trapped on the surface are likely similar on each of the particle sets. The energy associated with cavitation on the particles with higher surface area however was substantially increased at increasing pressures with a 1.39 fold increase at 1.5 MPa which compared to the 2.67 fold increase in surface area indicates that the effect of increased cavitation energy does not scale linearly with increasing surface area.

To test this theory further, mesoporous carbon with two different surface areas according to the manufacturer was purchased. High surface area CNPs (699632, Sigma) had a surface area of 216 m^2/g while low surface area CNPs (699624, Sigma) had a surface area of 80 m^2/g. Both were prepared using the standard CNP preparation technique (0.2 mg/mL in water) yielding similar size populations (Figure A.3) and thus a similar increase in surface area,

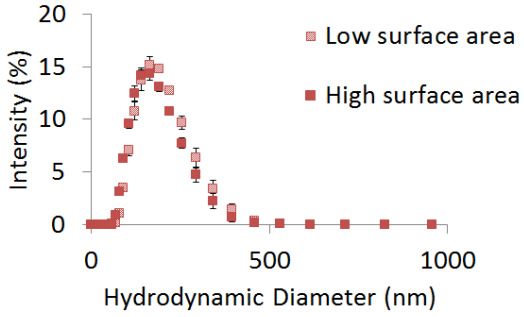

Figure A.3: *Size distributions of low surface area (shaded red) and high surface area (solid red) CNPs. N=4, standard deviation shown.*

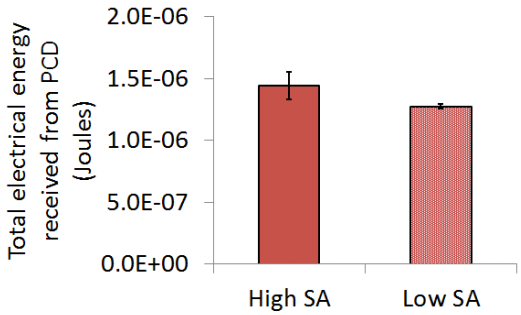

Figure A.4: *Cavitation energy from CNPs with high and low surface areas (SA). N=3, standard deviation shown.*

2.7 times, when compared to the micron-sized carbon particles discussed above. Slightly more energy was received from high surface area (SA) CNPs compared with low SA particles (1.13-fold increase) however this difference was not significantly different ($p > 0.05$, Student's t-test). Based on this, the high surface area particles were used for all other experiments.

These two experiments at the micro- and nano-scale suggest that increasing surface area and increasing number of particles play roles in increasing cavitation response but their effects do not scale linearly.

A.1.4 Types of cavicatalytic nanoparticles

After validation that cavicatalytic particles could be manufactured on the nanoscale, while maintaining the same ability to instigate cavitation as was observed on the micro-scale, other particle types were explored. Dr James Kwan developed the polymeric nanocup (NC) as described in the methods (Section 2.1.3), which also showed cavicatalytic properties at the nanoscale. Within this particle type, three size ranges were prepared utilising the varying size of starting bead (~100, ~300, and ~500 nm). The three particle size ranges in increasing order are referred to as NC LB1, NC LB3, and NC LB5. A particular point of interest in these two particle types is the vast differences in morphology, yet similar ability to instigate cavitation. For this reason, both particle types were explored.

Appendix B

Matlab scripts

B.1 analyse_smg_autoget.m

```
% analyse data from the DAQ card

% Susan M Graham
% 22/10/12
% updated 17/07/13
% updated 30/10/13 to account for variable pulse lengths and acquistion
% updated 28/01/13 validated against Jamie Collin's code
% 11/03/14 SMG validated against a sin wave  - was correct :-) ; ...
   updated Wtf
% 17/03/14 SMG updated Energy trapz integrating over t_plot instead of
% assuming it captured every pulse integrating with unit spacing.
% also accounted for different phantoms ie diff earliest cav point

% for code which collects 1 trace per pulse or continuous

% functions it calls:
% spectrogram_smg_optimised; bbandharm_smg; calculations_smg
```

```
clc
clear variables
close all

TEST = 0; % 0 = not a test; 1 = test mode

% pc mac conversions
% change all \ to / for mac
% addpath (switch)
% dirs (switch)

% initialise variables
% ****************************************
% **** Enter Values for each of these ****
Fs = 100e6; % sampling frequency
Fdrive = input('Driving Frequency in MHz eg 0.5 \n');
Fdrive = Fdrive*1e6;
%Fdrive = 0.5e6; % (Hz)  Fdrive = driving frequency of the HIFU

% Acuisition settings
cont=0;
%cont= input('0 = 1 trace per pulse; 1= continuous \n');
%cont=0; % cont = 1 if collecting traces continuously
        % cont = 0 if collecting 1 trace per pulse

% HIFU settings
PRF = input('Enter the PRF used (Hz) e.g. 0.5 \n'); %eg 0.5 Hz % ...
   pulse repetition frequency (Hz)
dc = 0.05; % duty cycle in i.e. 0.05 = 5%

% ****************************************
```

```
% calculations
T = 1/Fdrive; % period (sec)
pulse = dc/PRF; % pulse length (sec)
cycles = pulse * Fdrive; % number of cycles per pulse
% load on PCD
Res = 50; % load that the PCD is plugged into = 50 Ohms
% Time range you are interested in from your voltage trace
% change to capture from earliest possible point at focus to only ...
   get pulse on time.
Flow = input('Flow = 1, Static = 0 \n');
% 20 mm static holder: first point = 79e-6
% channel flow phantoms: first point = 90e-6
if Flow ==1
    tstart = 90e-6; % micro secs
else
    tstart = 79e-6; % micro secs  (ignore first part of 'zero' ...
       response)
end
tend = 240e-6; % micro secs

% calculate the width of the harmonic peaks (based on the width of the
% fft hamming window)
% ** NB ** this may need to change when the window size or shape ...
   changes!
notchwidth = 96000; % Hz  i.e. 96 kHz
% scaling the energy (when calculated) depending on acquisition mode
AcquWait = 15e-3; % 15 msec; minimum wait between acquisition (on ...
   trigger)
PulsePeriod = pulse/dc; % pulse period

% to only capture 'pulse' and not 'off time' for a single pulse
```

```
if pulse<= (tend-tstart) % if the pulse is shorter than the ...
   captured segment
    tend = tstart + pulse; % cut the captured segment to the pulse ...
       length
end

if cont ==1 & pulse>=AcquWait % if in continuous acquisition mode ...
   AND the pulse is longer than the wait
    EnAdj = 1; % Adjust energy by extrappolating out over the time ...
       between traces (assuming each trace represents the time till ...
       the next trace)
else % if acquiring 1 trace per pulse
    EnAdj = (pulse/PulsePeriod); % multiply by DC to account for ...
       on-time
end

% Background time period
tbstart = 10e-6; % 10 micro secs
tbend = 40e-6; % 40 micro secs

% Frequency range you are interested in (for plotting)
Fhigh = 15; % MHz highest bound of frequency range interested in

% Add folders to path so export_fig works
addpath(genpath('C:\SMG\Susan Graham Thesis\Programs ...
   _matlab_C_etc\SMG\14_03_11_FFT PSD BB Harm analysis with Test ...
   Code\Plot tools from random dude'))
% addpath(genpath('/Users/susan/Desktop/FFT PSD BB Harm ...
   analysis_0_5MHz Edit Correct FFT'))

if TEST == 1
    [Zfiles, timestamps] = testing(T,Fs,PRF);
```

```
    ProcFolder = uigetdir('Pick TEST Processed results directory');
    dirs = ProcFolder;
    % SRS amp amplification — no amp for test data
    SRSamp=1;
else

% Setup Folder Structure

% FIND Folder
% dialogue prompt for picking binary data directory
StartFolder = ...
   'Z:\netshares\bubldata3\SonoSensitiveNanoParticles3\SMG ...
   Results\14_02_01_RawData_Flow_Plasma_SV_CNPs_Cups';
RawFolder = uigetdir(StartFolder,'Pick binary data directory')

% SAVE Folder
% dialogue prompt for picking directory for processed results
FinishFolder = 'C:\SMG\Susan Graham ...
   Thesis\Results_Processed\14_02_01_FLOW_injectables_Plasma_SV_CNPs_Cups\Anal
   NEW TESTED FFT';
ProcFolder = uigetdir(FinishFolder,'Pick processed results directory');

% get folder structure and save as dirs
% regular expressions: ^ beginning of line ; or : separator * match any
% number of that in the braket
dirs = regexp(genpath(RawFolder),['[^;]*'],'match'); % pc
% dirs = regexp(genpath(RawFolder),['[^:]*'],'match'); % mac

% SRS amp amplification; 5 or 25 times
SRSamp=5;
end
```

```
a = 1; % start counter for folder structure
char_top = length(char(dirs(1))); % number of characters in the ...
   full folder length

while a<=length(dirs)
    Sdir = dirs(a); % chose folder at strucutre level 'a'
    Sdir = char(Sdir); % conver to character array
    % getting the data
    if TEST == 1
        Yfiles = Zfiles;
        Nfiles = length(Zfiles(1,:));
    else
        Yfiles = dir(strcat(Sdir, '\', '*.bin' )); % get struct ...
           array of .bin files
        Nfiles = length(Yfiles); % number of data files
    end


    if Nfiles==0

    else % if the folder contains .bin files

        % ************************************************
        % collect data and make the spectrogram
        [Yfftcut, fc, t_plot,Lfft,PSD,PowerMS, ...
           EnergyMS]=spectrogram_smg_optimised(Fs, Fdrive, tstart, ...
           tend, tbstart, tbend, Fhigh, Sdir, Yfiles, SRSamp, ...
           Res,pulse, PulsePeriod, T, Nfiles,AcquWait,TEST,PRF);

        % apply a comb filter to the data
        [Yfftbb,BBPSD] = bbandharm_smg(Yfftcut, Fdrive, Fs, fc, ...
           t_plot, Fhigh, Res,Lfft);
```

```
% Do calculations and plots to find ratios etc
[Power,Energy,PowerBB,EnergyBB,PowerHarm,EnergyHarm,harmbbpow,harmbben
   = calculations_smg (t_plot, EnAdj,Lfft,Fs,PSD,BBPSD);
PowMax = max(Power);
bbb=[Energy,EnergyBB,EnergyHarm,harmbbenergyrat,PowMax]; % ...
   useful variable
% ************************************************
% NOTE: when saving files they will save over all previous ...
   files without
% warning!!

% save all the processed data
ending = Sdir((char_top + 1) :  end); % sub folder ...
   characters only
name = strrep(ending,' ','_'); % replace all spaces with ...
   underscores
name = strrep(name,'\','_'); % replace folder segments \ ...
   with underscores to make a file name
name=strcat('S',name); % the name for the data file

folderending = ending(2:end);
mkdir(ProcFolder,folderending) % make the folder structure ...
   (won't do it if it already exists)
save(strcat(ProcFolder, ending, '\', name)) % save the data ...
   in the folder created

% save the figures
h=sort(get(0,'children')); % get the number of figures in ...
   the order they were made
for i=1:length(h)
```

```
            saveas(h(i),[ProcFolder,ending, '/', name 'fig' ...
                num2str(i), get(h(i),'Name')], 'fig');
        end
        export_fig(1,[ProcFolder, ending, '/', 'PSD.png'], '-m2', ...
            '-nocrop', '-transparent') % export the first figure, ...
            i.e. PSD as a .png
        export_fig(6,[ProcFolder, ending, '/', 'Power.png'], '-m2', ...
            '-nocrop', '-transparent') % export the 6th figure, i.e. ...
            Power as a .png

    end

    clearvars -except a dirs char_top ProcFolder Fs Fdrive cont PRF ...
        dc SRSamp T pulse cycles Res tstart tend notchwidth AcquWait ...
        PulsePeriod EnAdj tbstart tbend Fhigh TEST
    close all % close all figures
    a = a + 1; % move counter forwards by 1, go to next folder
end
```

B.2 spectrogram_smg_optimised.m

```
function[Yfftcut, fc, t_plot,Lfft,PSD,PowerMS, ...
    EnergyMS]=spectrogram_smg_optimised(Fs, Fdrive, tstart, tend, ...
    tbstart, tbend, Fhigh, Sdir, Yfiles, SRSamp, Res,pulse, ...
    PulsePeriod, T, Nfiles,AcquWait,TEST,PRF)
% spectrogram
% to take data from a set of voltage traces, take the fft and then plot
% them along time to give a spectrogram
% the output is a matrix of the FFT and the frequency range it is
% calculated over
```

```
% Susan M Graham
% 26/9/12

% this function will be called by analyse_smg

timestamps = zeros(Nfiles,1);

if TEST == 1
[Zfiles, timestamps] = testing(T,Fs,PRF);
t_plot=timestamps;
else
    for I = 1:Nfiles
    timestamps(I)=sscanf(Yfiles(I).name,'%f');
    % times in seconds corresponding to timestamps
    t_plot = timestamps * 1e-6; % time in seconds of all the traces
    end

end



% load e.g. 5th data point as an example trace
if PulsePeriod>=AcquWait
    tracenum = round(2/PulsePeriod + 4); % a trace 4 past the 2 ...
       second delay
else
    tracenum = round(2/AcquWait + 4);
end

if TEST == 1
    data = Zfiles(:,5);
else
```

```
    [data Ndata R_t B1channel] = ...
       load_file(Sdir,timestamps(tracenum)); % load data
end

yorig = squeeze(data(:,1)); % take the first channel
yorig = yorig./SRSamp; % divide by the SRS amp level
Lorig = length(yorig); % total time of trace
torig = (0:Lorig-1)/Fs;                % Time of each voltage trace

% to minimise the leakage in the fft, the data region selected ...
   should be a
% multiple of the number of cycles (i.e. don't take part of a cycle)
cycles = round((tend-tstart)/T);
tend1 = cycles*T+tstart;
y5 = yorig(round(tstart*Fs):round(tend1*Fs)); % voltage data in ...
   interested region
L5 = length(y5); %  samples/trace
t5 = tstart:1/Fs:tend1;
t5 = [t5,tend1,tend1]; % buffer with t=lasts incase of rounding error
ypts = size(y5);
t5=t5(1:ypts(1));
% remove the DC bias
bias = mean(yorig(round(tbstart*Fs):round(tbend*Fs))); % mean value ...
   of the background signal
y5adj = y5-bias; % remove the bias from the windowed signal

%NFFT has been removed as padding with zeros will not improve the ...
   ability
%to detect frequencies because we already know what frequencies we are
%looking for

% Important  note on Matlab FFT
```

```
% Matlab FFT does not divide by N, this needs to be included.

% Discrete Fourier transform
% X(m) = 1/N sum x(n)e^(-j2pinm/N)

% apply a window to the data so that the fft has less leakage
Window = 1; % do the windowing?
if Window == 1
    Wtf = 0.6305; % weighting factor for the Hamming window
else
    Wtf = 1;
end


% take fft of data selection and put in a matrix
for i = 1:Nfiles %i.e. all the voltage trace files
    if TEST ==1
         data=Zfiles(:,i);
    else
    [data Ndata R_t B1channel] = load_file(Sdir,timestamps(i)); % ...
       i.e. steps through all the data
    end

    y = squeeze(data(1:end,1));
    y = y./SRSamp; % divide by the SRS amp level

    %calculate DC bias
    bias = mean(y(round(tbstart*Fs):round(tbend*Fs))); % mean value ...
       of the background signal

    % window data
```

```
    y = y(round(tstart*Fs):round(tend1*Fs)); % voltage data in ...
       interested region
    L = length(y); % total time pts of windowed trace

    % remove the DC bias
    yadj = (y-bias); % remove the bias from the windowed signal

    if Window ==1
    % apply a window to the data so that the fft has less leakage
    hamwin = window(@hamming,L); % a hamming window same lenth as data
    yham = hamwin.*yadj; % apply the window to the data
    else
        yham=yadj;
    end

    PowerMS(i) = sum(yham.^2)/(Res*Wtf^2*L); % checker for time ...
       domain data

    % calculate fft
   % NFFT = 2^nextpow2(L); %number of points;  Next power of 2 from ...
      length of y
    Y = fft(yham)./Wtf; % fft of current voltage trace adjusted for ...
       weighting factor

    %store data in matrix and adjust for hamming window
    Yfft(:,i)=abs(Y); % matrix of data

end

% check energy from voltage trace (not FFT)
EnergyMS = PulsePeriod*trapz(PowerMS)*pulse/(PulsePeriod);
```

```
Lfft = length(Yfft); % full length of FFT
numfpts = size(Yfft,1);
f = Fs/2*linspace(0,1,numfpts/2+1); % frequency (Hz) vector from 0 ...
   to Fs/2 (i.e. the Nyquist freq) in steps of 1 Hz

% double sided FFT to single sided FFT ---- but actually just taking ...
   0-15
% MHz
% cut the FFT matrix down to 0-Fhigh to save memory
fplace = find(f>=(Fhigh*1e6),1);
fc = f(1:fplace); % cut the frequency vector to range to Fhigh
Yfftcut = Yfft(1:length(fc),:);

clear Yfft

% Power Spectral Density
% power makes it independent of time, i.e. only relating to the ...
   amplitude
% multiply by 2 because taking half of the frequencies
% square to get power
% (Yfft/N)^2 / (Fs/N) i.e. Yfft^2/(N*Fs)
% divide by length of the FFT - scaling for the FFT
% divide by sampling frequency - scaling for the FFT
% divide by resistance (Ohms) of the PCD to convert from V^2/(Hz*R) to
% Watts/Hz
% multiply by 2 because we are taking half (but dividing by the whole
% length)
% assuming there is no power between Fhigh (15 MHz) and the Nyquist ...
   frequency
% (note resistence of the transducer is frequency dependent so this ...
   is only
% partialy correct)
```

```
% Don't need to multiply with complex conjugate because already ...
   taken abs
% therefore can just square.

PSD = (2.*(Yfftcut(1:length(fc),:)).^2)/(Res*Lfft*Fs); % Units Watts/Hz

% plot the power spectral density
f=figure('Name','PSD');
g=imagesc(t_plot,fc/1e6,PSD);
ylabel('Frequency (MHz)','FontSize',20)
xlabel('Time (sec)','FontSize',20)
ylim([0 Fhigh]) % only plot between y = 0 and y = Fhigh
colorbar
caxis([0, 1E-13]) % set the colour bar scale
c = colorbar;
ylabel(c,'Power (Watts/Hz)','FontSize',20)
set(findall(f,'Type','text'),'FontSize', 20)
set(findall(g,'Type','text'),'FontSize', 20)
a =  get(gca,'XTickLabel');
set(gca,'fontsize',20)
position = [100, 100];
sizefig = [600, 450];
set(f, 'Position',[position, position+sizefig])


% plot the power spectral density in black and white
f=figure('Name','PSD_BW');
g=imagesc(t_plot,fc/1e6,PSD) ;
ylabel('Frequency (MHz)','FontSize',20)
xlabel('Time (sec)','FontSize',20)
%title('Power Spectral Density','FontSize',16)
ylim([0 Fhigh]) % only plot between y = 0 and y = Fhigh
```

```
colorbar
caxis([0 1E-13]) % set the colour bar scale
c = colorbar;
ylabel(c,'Power (Watts/Hz)','FontSize',20)
colormap(flipud(gray));
set(findall(f,'Type','text'),'FontSize', 20)
set(findall(g,'Type','text'),'FontSize', 20)
a =  get(gca,'XTickLabel');
set(gca,'fontsize',20)
position = [100, 100];
sizefig = [600, 450];
set(f, 'Position',[position, position+sizefig])

% % plots for debugging ***************************
%plot the e.g. 5th trace of the original data
f=figure('Name','5thVoltageTrace');
plot(torig*1E6, yorig,'r')
hold on
g=plot(t5*1E6,y5adj,'b');
xlabel('Time (\musec)')
ylabel('Volatge (V)')
set(findall(f,'Type','text'),'FontSize', 20)
set(findall(g,'Type','text'),'FontSize', 20)
a =  get(gca,'XTickLabel');
set(gca,'fontsize',20)
position = [100, 100];
sizefig = [600, 450];
set(f, 'Position',[position, position+sizefig])

TotalOfTrace5FromVoltageTrace=sum(y5adj);
%
```

```
% plot the fft of the 5th trace
f=figure('Name','FFT5');
g=plot(fc/1e6, (2.*Yfftcut(1:length(fc),5))/(Lfft));
xlabel('Frequency (MHz)','FontSize',16)
ylabel('Voltage (V)','FontSize',16)
set(findall(f,'Type','text'),'FontSize', 20)
set(findall(g,'Type','text'),'FontSize', 20)
a =  get(gca,'XTickLabel');
set(gca,'fontsize',20)
position = [100, 100];
sizefig = [600, 450];
set(f, 'Position',[position, position+sizefig])

TotalofTrace5FromFFT = sum(2.*Yfftcut(1:length(fc),5))/(Lfft);
%
% % plot the fft of the hamming window
% figure
% plot(f/1e6,Winfft(1:length(f)))
% title ('FFT of a Hamming window')
% xlabel('Frequency (MHz)')
% ylabel('Voltage')
%
% % plot the fft of all traces
% figure
% plot(fc/1e6, 2.*Yfftcut(1:length(fc),:))
% title('FFT of all traces')
% xlabel('Frequency (MHz)')
% ylabel('Voltage')
%
% % % plot the voltage spectrogram
% figure('Name','Spectrogram')
% imagesc(t_plot,fc/1e6,Yfftcut(1:length(fc),:))
```

```
% ylabel('Frequency (MHz)','FontSize',16)
% xlabel('Time (sec)','FontSize',16)
% %title('Frequency spectrogram magnitude','FontSize',16)
% ylim([0 Fhigh]) % only plot between y = 0 and y = Fhigh
% colorbar
% caxis([0 0.1]) % set the colour bar scale
% c = colorbar;
% ylabel(c,'Voltage (V)','FontSize',16)
```

B.3 bbandharm_smg.m

```
function [Yfftbb, BBPSD] = bbandharm_smg(Yfftcut, Fdrive, Fs, fc, ...
   t_plot, Fhigh, Res,Lfft)
% BBANDHARM calculates the amount of broadband and harmonic ...
   emissions that are
% in the signal.  It also calculates the relative intensity of the two.

% this function will be called by analyse_smg

% Susan M Graham
% 22/10/12

% notch filter to isolate braodband components

Yfftbb=Yfftcut;
[~, ntraces] = size(Yfftcut);
for i =1:ntraces
    for j=1:Fs/(2*Fdrive)-1 % from 1 to total number of notches (at ...
       multiples of the driving frequency)
        notprevplus = find(fc>=(Fdrive*(j-1)+48e3),1);
        notptmin = find(fc>=(Fdrive*j-48e3),1);
```

```
        notptplus = find(fc>=(Fdrive*j+48e3),1);
        Yfftbkg = mean(Yfftcut(notprevplus:notptmin,i)); % assume ...
           the broad band background signal is the mean of the ...
           signal between notches.
        % check that the 'broadband background' is lower than the
        % 'harmonics' window otherwise we are adding signal
        if Yfftbkg<=mean(Yfftcut(notptmin:notptplus,i))
            % everything is ok
        else
            Yfftbkg = mean(Yfftcut(notptmin:notptplus,i));
        end

        Yfftbb(notptmin:notptplus, i)=Yfftbkg; % set values
    end
end

% Broad Band Power Spectral Density
% PSD with energy attributed to harmonics remove
BBPSD = (2.*(Yfftbb(1:length(fc),:)).^2)/(Res*Lfft*Fs);% units Watts/Hz

% plot the BroadBandPSD
f=figure('Name','BBPSD');
g=imagesc(t_plot,fc/1e6,(BBPSD));
ylabel('Frequency (MHz)','FontSize',20)
xlabel('Time (sec)','FontSize',20)
ylim([0 Fhigh])
colorbar
caxis([0, 1E-13])
c = colorbar;
ylabel(c,'Power (Watts/Hz)','FontSize',20)
set(findall(f,'Type','text'),'FontSize', 20)
set(findall(g,'Type','text'),'FontSize', 20)
```

```
a =  get(gca,'XTickLabel');
set(gca,'fontsize',20)
position = [100, 100];
sizefig = [600, 450];
set(f, 'Position',[position, position+sizefig])
```

B.4 calculations_smg.m

```
function[Power,Energy,PowerBB,EnergyBB,PowerHarm,EnergyHarm,harmbbpow,harmbben
   = calculations_smg (t_plot, EnAdj,Lfft,Fs,PSD,BBPSD)
% Calculates the voltage and power from the fft over time.  Also ...
   looks at
% the ratios of harmonic to broadband emissions

% Susan M Graham
% 22/10/12

% looking from 0 to Fhigh (frequency range of interest), calculate the
% total energy associated with each and thus the relative broadband and
% harmonic components

% P = V^2/R (P=IV and V=IR)
% square all values to get in terms of power ... ish
% integrate power over frequency to get power plotted over time
% integrate power over frequency and time to get energy

% Total power (Watts) (integrate over frequency)
Power = trapz(PSD)*(Fs/Lfft); % units Watts; multiply by FS and ...
   divide by LFFT to account for bin size during integration
% Total energy (Joules) (integrate over time)
```

```
Energy = EnAdj*trapz(t_plot,Power); % units Joules; integrate over ...
   time, multiply by DC

% Broadband power
PowerBB = trapz(BBPSD)*(Fs./Lfft);
% Broadband energy
EnergyBB = EnAdj*trapz(t_plot,PowerBB);

% Harmonic power
PowerHarm = Power - PowerBB;
% Harmonic energy
EnergyHarm = Energy - EnergyBB;

% calculate semi useful ratios :-)
harmbbpow = PowerHarm./PowerBB;
harmbbenergyrat = EnergyHarm/EnergyBB;

% plot the sums over time
f=figure('Name','Power');
g=plot(t_plot,Power,'b');
hold on
plot(t_plot,PowerBB,'r')
plot(t_plot,PowerHarm,'g')
h=legend ('Total','Broadband','Harmonics');
set(h,'FontSize',12);
xlabel('Time (seconds)','FontSize',16)
ylabel('Power (Watts)','FontSize',16)
set(findall(f,'Type','text'),'FontSize', 20)
set(findall(g,'Type','text'),'FontSize', 20)
a =  get(gca,'XTickLabel');
set(gca,'fontsize',20)
position = [100, 100];
```

```
sizefig = [600, 450];
set(f, 'Position',[position, position+sizefig])
%
%
% % plot the ratio over time
% figure('Name','EnergyRatio')
% plot(t_plot,harmbbenergy)
% xlabel('Time (seconds)','FontSize',16)
% ylabel('Harmonic:Broadband Ratio','FontSize',16)
% ylim([0 1]);
```

Appendix C

List of publications and presentations

C.1 Peer reviewed publications

- [79] Susan M. Graham, Robert Carlisle, James J. Choi, Mark Stevenson, Apurva R. Shah, Rachel S. Myers, Kerry Fisher, Miriam-Bazan Peregrino, Len Seymour, and Constantin C. Coussios. Inertial cavitation to non-invasively trigger and monitor intratumoral release of drug from intravenously delivered liposomes. Journal of Controlled Release, 178:101-107, March 2014.

C.2 Presentations

- Susan Graham, Rachel Myers, James Choi, Miriam Bazan-Peregrino, Len Seymour, Robert Carlisle, Constantin Coussios. "Use of micro- and nano- sized inertial cavitation nuclei to trigger and map drug release from cavitation-sensitive liposomes", *166th Meeting of the Acoustical Society of America, San Francisco, 2nd-6th December 2013 [Presentation]*

- Susan Graham and Rachel Myers. "Carbon nanoparticles as cavitation nuclei for targeted drug delivery", *Wellcome Trust Presentations 2013, Rosemary Rue, Oxford, 2nd July 2013 [Presentation].*

- Susan Graham, Rachel Myers, James Choi, Miriam Bazan-Peregrino, Leonard Seymour, Constantin Coussios, Robert Carlisle. "Inertial cavitation to trigger and mon-

itor drug release from liposomes and the future of nano-scale cavitation nuclei", *UK Therapeutic Ultrasound Interest Group (THUGS), Richard Doll, Oxford, 1st July 2013 [Presentation].*

- Susan Graham. "The Immune Bomb", *CDT Symposium 2013, Richard Doll, Oxford, 22nd March 2013 [Presentation].*

C.3 Posters

- Susan Graham, Rachel Myers, Caroline Harfield, Robert Carlisle, Constantin Coussios. "Carbon nanoparticles as cavitation nuclei for targeted drug delivery to tumors", *Engineering Sciences Graduate Lunch, Information Engineering Building, Oxford, 4th October 2013 [Poster].*

- Susan M Graham, Rachel E Myers, Robert Carlisle, Constantin Coussios. "Carbon nanoparticles as cavitation nuclei for targeted drug delivery to tumors", *Medical Engineering Initiative Conference 2013, Ascott, 3-4th September 2013 [Poster] (Won Best Poster Award in the Cancer Therapeutics Category).*

- Susan Graham, Rachel Myers, Heiko Schiffter, Constantin Coussios. "Sonosensitive nanoparticles for targeted drug delivery and release in cancer therapy", *CDT Symposium 2013, Richard Doll, Oxford, 12th March 2012 [Poster].*

Appendix D

Abbreviations

- CNP: Carbon nanoparticle. A rough surfaced nanoparticle made of carbon
- DC: Duty cycle. A measure of ultrasound 'on' time to 'off' time expressed as a percent (%)
- DLS: Dynamic light scattering
- EPR: Enhanced permeability and retention effect
- FDA: Food and Drug Administration
- FFT: Fast Fourier transform. The analysis of a voltage trace in the frequency domain.
- HIFU: High Intensity Focused Ultrasound
- I_{SPTP}: Spatial peak, temporal peak intensity
- I_{SPPA}: Spatial peak, pulse average intensity
- I_{SATA}: Spatial average, temporal average intensity
- I_{SPTA}: Spatial peak, temporal average intensity
- LB1: Polymeric nano cup with cup size approximately 100 nm
- LB3: Polymeric nano cup with cup size approximately 300 nm
- LB5: Polymeric nano cup with cup size approximately 500 nm

- NC: Polymeric nano cup. A polymeric nanoparticle in the shape of a smooth cup
- PAM: Passive Acoustic Mapping. Using an array transducer to passively detect ultrasound signals from cavitation events over 2 dimensional space.
- PCD: Passive Cavitation Detector. A transducer used to passively receive ultrasound signals from cavitation events
- PRF: Pulse repetiton frequency. The number of ultrasound pulses per second (Hz).
- PRFP: Peak rarefactive focal pressure. The peak negative pressure of an ultrasound wave (MPa)
- PSD: Power spectral density. The analysis of a voltage trace plotted as power over frequency, and plotted over time if multiple traces were acquired. Units Watts/Hz or V^2/Hz.
- SV: SonoVue® is microbubble with an approximate diameter of 3 μm [179] (Bracco Diagnostics Inc., Geneva, Switzerland)
- TEM: Transmission electron microscopy
- UCA: Ultrasound contrast agent